TYPE-2 FUZZY LOGIC CONTROLLERS FOR RENEWABLE ENERGY SYSTEMS

Ph.D. THESIS

by

S KRISHNAMA RAJU

DEPARTMENT OF ELECTRICAL ENGINEERING
INDIAN INSTITUTE OF TECHNOLOGY ROORKEE
ROORKEE - 247667 (INDIA)

MAY, 2016

TYPE-2 FUZZY LOGIC CONTROLLERS FOR RENEWABLE ENERGY SYSTEMS

A THESIS

Submitted in partial fulfilment of the

requirements for the award of the degree

of

DOCTOR OF PHILOSOPHY

in

ELECTRICAL ENGINEERING

by

S KRISHNAMA RAJU

DEPARTMENT OF ELECTRICAL ENGINEERING
INDIAN INSTITUTE OF TECHNOLOGY ROORKEE
ROORKEE - 247667 (INDIA)

MAR, 2016

INDIAN INSTITUTE OF TECHNOLOGY ROORKEE
ROORKEE

CANDIDATE'S DECLARATION

I hereby certify that the work which is being presented in the thesis entitled TYPE-2 FUZZY LOGIC CONTROLLERS FOR RENEWABLE ENERGY SYSTEMS in partial fulfilment of the requirements for the award of the Degree of Doctor of Philosophy and submitted in the Department of Electrical Engineering of the Indian Institute of Technology Roorkee, Roorkee is an authentic record of my own work carried out during a period from Jan, 2013 to Mar, 2016 under the supervision of Dr. Gopinath Pillai, Professor, Department of Electrical Engineering , Indian Institute of Technology Roorkee, Roorkee.
The matter presented in this thesis has not been submitted by me for the award of any other degree of this or any other Institute/University.

(S Krishnama Raju)

This is to certify that the above statement made by the candidate is correct to the best of my knowledge.

Date: (Gopinath Pillai)

Supervisor

ACKNOWLEDGEMENT

First of all, I praise Godhead Sri Krishna, the almighty, merciful and compassionate for providing me this opportunity and granting me the capability to proceed successfully in this course. The thesis appears in its current form due to the assistance and guidance of several people. I would like to offer my sincere thanks to all of them.

I express my deepest sense of gratitude towards my supervisor Dr. G. N. Pillai, Professor, Department of Electrical Engineering, Indian Institute of Technology Roorkee, for his patience, inspirational guidance, constant encouragement, moral support and keen interest in my work. I am very much thankful to him for creating a nice and tension free atmosphere, adequate laboratory facility that is suitable for research work. I am thankful to him for introducing me to the area of Type-2 fuzzy logic systems.

I express my sincere thanks to Dr. B. Tyagi, Department of Electrical Engineering, Prof. N. Sukavanam, Department of Mathematics and Prof. N. P. Padhy, Department of Electrical Engineering for their valuable comments and suggestions on my work in various presentations during my research work tenure.

I am thankful to Dr. Premlata Jena, Department of Electrical Engineering, Faculty In-charge, RTDS Lab for her cooperation and help provided during the course of research work. Also I am thankful to Mr. Anil Agarwal, Lab Assistant, Control and Robotics Lab , IIT Roorkee who always provided all types of help required during my research work.

I am grateful to the reviewers whose constructive suggestions and invaluable advices improved the quality of my publication derived from this work. I am highly obliged to owe my sincere thanks to the technical and administrative staff of the EED, especially to Sri Mohan Singh and Sri Rishabh, who helped me in all possible ways during the work. I also have been lucky to have some of research fellows like Dr.Manoj Panda, Mr. Y Srinivass Rao, Mr. Hari Krishna, Dr. Asutosh Nandi, Mr. Sanjeev Pannala and Dr. Venkat Ramana who never hesitated to render their help at the time of some difficulties and spared their time whenever required. I express my thanks for their help in need.

I thank my fellow lab-mates in for the stimulating discussions, for the sleepless nights we were working together before deadlines, and for all the fun we have had in the last four years. Also I thank my friends in the following institutions Dr.J Ganeswara Rao, IIT Kharagpur, Dr. Kaushik Das, DTU, Denmark, Dr.Dilip Kumar, Hyderabad and Mr. Manjunath Yadav, Indian Railways, Mr. Uma Maheswar Rao, Consultant, Civil Engineering, Visakhapatnam, Mr.Mahaboob Basha, AE, SPDCL, Tirupati for their grate support during some challenging times.

I am also grateful to all the members of Bhakti Vedanta Academy for Culture and Education, Roorkee, for their invaluable moral support and spiritual guidance during my research work. My sincere thanks to the Government of India for providing me the timely scholarship and opportunity for pursuing Ph.D program at IIT Roorkee.

I owe a debt of gratitude to my parents, my uncles SG Nagaraj and B Subramanyam Raju, who are always an inspiration for me in my life for their consistent support and encouragement. I am especially thankful to my wife Swapna for her unfailing support and patience towards completion of this thesis.

Last but not the least, I am also thankful to my sister Ashwini, brother Janardhan, daughters Poojya and Vaishnavi and other family members for their utmost moral support, love and care in all the aspects of my life.

(S Krishnama Raju)

Abstract

The uncertainty in the availability of wind speed and solar radiation is a bottleneck, to export bulk amount of power from the wind and solar energy systems to the utility grid. For reliable grid operation, the modern grid codes demand fault ride through (FRT) capability from the distributed generation sources. Designing a robust control strategy for effective power sharing, fault ride through and grid interacted operation is a challenging task to the control engineers due to uncertainty in the operating conditions.

In response to this challenge, this thesis, proposes a novel control strategy with interval type-2 fuzzy sets (IT-2 FSs), for handling the uncertainties in network operating conditions. The IT-2 FSs, with its third dimension and foot print of uncertainty (FOU) in the membership functions (MFs) offers an additional degree of freedom in the controller design to take the uncertainties into account. The type-2 fuzzy logic controllers (FLCs) are designed for the wind energy system with varying levels of complexity of the plant model. The feasibility of the controller for real-time applications is investigated through the simulations on Real time digital simulator (RTDS). The controller is implemented on a digital signal processor (DSP) based DSPACE 1104 module, interfaced through RTDS in the Hardware-in-loop (HIL) environment.

The main focus of this thesis is to investigate the applicability of type-2 fuzzy logic for real-time wind energy systems through designing controllers for the power electronic converters of doubly fed induction generator (DFIG), with varying network operating conditions. The core objectives of this research work are formulated as

- Preliminary study on applicability of type-2 FSs for wind energy systems and optimization of its parameters with MATLAB based simulations
- Design and performance analysis of Type-2 FLC, for a grid connected DFIG under the uncertainties of grid faults and load changes
- Performance analysis of Type-2 FLC with an IEEE-34 bus distributed network, connected with DFIG based wind energy system
- Design and analysis of type-2 FLC for a microgrid, connected with DFIG, PV system and battery storage system.

The type-2 FSs have been recognized as a suitable tool for modeling the numerical and linguistic uncertainties. In order to establish its applicability for renewable energy systems,

type-2 FLC is designed and tested under various possible contingencies. As a preliminary study, type-2 FLC is designed for grid connected DFIG and comparative performance analysis is done with the type-1 FLC. Tuning the control parameters of type-2 FLC is a challenging task, because the plant model is complex and sensitive. To get the optimal controller parameters, a constrained optimization problem is formulated, and solved using an evolutionary optimization method i.e. genetic algorithm. In order to study the effect of FOU, the performance is evaluated with perturbed parameters.

Doubly fed induction generator is very sensitive to voltage variations in the grid, which pose limitations for wind power plants during the grid integrated operation. Handling the uncertainty in wind speed and grid faults is a major challenge to compliant with the modern grid code requirements. This work proposes a new control strategy for rotor side converter using interval type-2 fuzzy sets which can counter the effects of fluctuations in wind speed and low voltage during severe grid fault conditions. A 2 MW DFIG connected to the grid is modeled in simulation software RSCAD and interfaced with real time digital simulator (RTDS) to perform the analysis with real-time simulations . The RTDS platform is considered by many research laboratories as real-time testing module for controller prototyping and also for hardware in the loop (HIL) applications. The controller performance is evaluated in HIL configuration, by performing the real-time simulations under various parameter uncertainties. The proposed controller can improve the low voltage ride through capability of DFIG compared to that of proportional integral (PI) and type-1 fuzzy controller.

Distributed generation (DG) systems based on renewable energy sources are seen as a reliable and alternative to the conventional energy sources such as coal and oil. Designing an effective control strategy for DGs is a challenging task, if the distribution network comprises unbalanced loads and variable network parameters. The presence of third dimension in the type-2 membership function offers an additional degree of freedom in the design of the proposed controller to contribute to power oscillations damping and voltage recovery following disturbances in the network. The vector control with proposed strategy for DFIG is able to handle uncertainties in the operating conditions in the network like faults, load changes and wind speed. The performance of the controller is evaluated through real time simulations on IEEE 34-bus distribution network with various network uncertainties. The real time simulations carried out on RTDS shows that the proposed strategy outperformed the type-1 FLC and PI counterparts. The results presented in this work are more realistic, since the computational delays and signal conversion delays are taken into account.This work distribution proposes using the and implementation design of a novel DFIG strat-

egy intervalcontrol fuzzy type-2reliable sets for grid interaction of, when connected to an network unbalanced .

Accurate power sharing in a microgrid with DGs is a challenging task due to various uncertainties in the network operating conditions. This work proposes a new control scheme for power sharing in a microgrid comprising DFIG based wind energy system, photo voltaic (PV) system and battery storage, operating in both grid connected and islanding conditions. A robust intelligent controller is designed for power sharing to counter the effects of nonlinearities in the model and uncertainties in the operating conditions. The special features of the type-2 fuzzy sets are explored, to ascertain its suitability to handle the uncertainties associated with the rules and MFs. The performance of the proposed scheme is verified through a comparative analysis with the conventional PI controller, considering the IEEE 34 bus system as a microgrid, under various network disturbances. Further the feasibility of the controller for real-time applications is demonstrated through hardware-in-loop simulations in the RTDS environment.

Contents

List of Abbreviations

AC	Alternate Curent
ADC	Anaalog to Digiital Convortor
DAC	Digiital to Anaalog Convertor
ddc	Direct dc Current
DFIG	Doubly Fed Induction Generator
DG	Distributed Generation
DSP	Digital Signal Processor
EMT	Electro Magnetic Transient
FACTS	Flexible Alternating Current Transmission System
FLC	Fuzzy Logic Controlerl
FOU	Footprint Of Uncertainty
FS	Fuzzy Set
FRT	Fault Ride Through
GA	Genetic Algorithm
GSC	Grid Side Converter
GTAI	Gigabit Transceiver Analog Input
GTAO	Gigabit Transceiver Analog Output
HIL	Hardware In Loop
IT-2 FLC	Interval Fuzzy Type-2 Logic Controller
IT2-FLS	Interval Logic type-2 Fuzzy system
IT-2 FSs	Interval Sets Fuzzy Type-2
LMF	Lower Membership Function
LVRT	Low Voltage Ride Through
MF	Membership Function
MG	Microgrid
MPPT	Maximum Power Point Tracking
PCC	Point of Common Coupling
PI	Proportional Integral
PID	Proportional Integral Derivative
PLL	Phase Lock Loop
PMSG	Permanent Magnet Synchronous Generator

PSO	Particle Swarm Optimization
PV	Photo Voltaic
PWM	Pulse Width Modulation
RTDS	Real Time Digital Simulator
UMF	Upper Membership Function
VSC	Voltage Source Converter
WECS	Wind Energy Conversion System
RSC	Rotor Side Converter

List of Symbols

x	Primary variable of type-2 fuzzy MF
u	Secondary Variable of type-2 fuzzy MF
$\mu_{\tilde{A}}(x,u)$	membership Secondary function
X	Domain of primary function membership
J_x	Domain of secondary membership function
$\underline{\mu}_{A_k}(x)$	Lower MF
$\overline{\mu}_{A_k}(x)$	Upper MF
J	Inertia constant
$\Delta\omega$	Rotor speed deviation
P	Active power
Q	Reactive power
P_m	Mechanical generator power input to
P_e	Electrical output of the power generator
ω_s	Stator electrical frequency
V_T	Terminal voltage of generator
δ	rotor angle of generator
I_d	d-axis component of current
I_q	q-axis component of current
T_e	Electromagnetic torque
V_{qs}	q-axis stator voltage
i_{qs}	q-axis stator current
V_{ds}	d-axis stator voltage
i_ds	d-axis stator current
R_s	Stator resistance
L_{ls}	Stator leakage inductance
ω_m	Angular velocity of rotor
θ_m	Rotor angular position
$\bigcup$	Union operation
$\bigcap$	Intersection operation
L_{ss}	Self-inductances of stator
L_{rr}	Self- inductance of rotor

L_m Mutual inductance

L_{ls} inductance of Leakagee stator

L_{lr} inductancee Leakage of rotor

R_s Statorr resistance

R_r Rotor resistance

λ_s Stator flux linkage

λ_r Rotor flux linkage

d Direct axis

q Quadrature axis

ω_r Rotor electrical frequency

List of Figures

List of Tables

Chapter 1

Introduction

The fossil fuels being a major energy supplier, recognized as a major cause of environmental pollution posing severe challenge to the majority of the nations in the world. To address the ever increasing energy demands and depletion of fossil fuels, the research community is always striving for an efficient alternative energy sources. The necessity of bulk energy production combined with the interest in clean technologies yields in an increased development of power generation systems using renewable energy sources. As per the recent statistics from the Paris climate change agreement, India has committed to produce 37000 Mw,from renewable energy , which is 15% of the total power capacity in the country. The quantity of renewable energy produced in European union nations has increased overall by 84.4 % between 2003 and 2013, equivalent to an average increase of 6.3 % per year [67].

Among the renewable energy sources, wind and solar are emerged as the suitable sources for bulk energy production. The main drawback of these sources is the uncertainty in solar radiation and wind speed leads to unpredictable behavior and uncontrolled output of energy conversion units. Moreover, grid integration, controllability, reliability and power quality are the other challenges in using these sources with the utility grid. The recent advancements in power electronics could grant a relief to some of these challenges that gives rise to many topologies in the energy conversion units. However, the control strategies recommended for power electronic converters needs a rigorous analysis and design to effectively interact with the grid [80].

1.1 Motivation

In many countries, wind energy has become a major source of renewable energy generation due to the many advantages [169, 62]. In the preliminary days, wind energy conversion systems with fixed speed induction generators have contributed a significant portion in the renewable share of energy production. Recently, the use of doubly fed induction generators in wind power generation has received an increasing attention, because of its ability to control active and reactive powers and also support variable speed operation. Other advantages of the DFIG topology are the power electronic converters required are rated at

only 20 % to 30% of the generator rated power, and efficient power capture is possible with reduced mechanical stresses [70].

The drawback of the DFIG based wind turbine is that, it is very sensitive to voltage variations, which are caused by grid faults and other network disturbances. In earlier stages of grid integration, for the safety of the converter system, the wind generators have been designed to get disconnected fast from the grid if a grid fault causes a large voltage drop [35]. However, sudden disconnection during the faults, poses serious challenges in terms of reliability and stability of the grid, when the penetration levels of wind farms are very high. Therefore, for reliable and stable operation of the grid, the recent grid standards require that during the faults, the wind generators should remain connected to the grid. To enable the wind turbines fault ride through compliant, the control strategies meant for these systems should be capable of handling the uncertainties in operating conditions [123]. Further, the controllers should react fast enough to change in wind speed conditions, to maintain the grid stability.

In the literature, PI controllers are widely used to control the power electronic converters and grid interactive inverters [25, 51, 58]. However, the PI controllers are not robust enough to perform under uncertainties in operating conditions. Using PI controller with fixed gains for a determined operating point provides an acceptable performance, but poor transient performance is often obtained when the inverter operation point varies continuously because of changing dynamics of the plant [15]. Operating points of the grid interactive inverters vary with the natural conditions such as solar radiation or wind speed. Moreover, grid specifications such as grid voltage, frequency and impedance might change during operation of inverter [144]. The other drawbacks of the PI controllers are listed as follows.

- Modeling the power system networks and DFIG, is complex and highly nonlinear whereas the best performance with the PI controller, is observed only with linear models [40].

- It is generally implemented using operational amplifier circuits whose parameters are adjusted for an operating point based on a piece wise linear model of the nonlinear system. To obtain an acceptable performance with system dynamics, these circuits require frequent tuning of its parameters [52].

- To address the grid connectivity issues, many variations for PI have been proposed in the power electronics literature (modified PI) including the addition of a grid voltage feedforward path, multiple-state feedback and increasing the proportional

gain etc. Generally, these variations can expand the PI controller bandwidth but, unfortunately, they also push the systems towards their stability limits [59, 153].

- In most of the existing schemes, the PI controller is designed for a specific objective, like Fault Ride through (FRT), handling unbalanced grid voltages, reactive power control, or maximum power point tracking (MPPT) etc., and none of these schemes are tested for robustness [121, 173].

- For severe disturbances such as three phase short circuit fault and sudden change in wind speed, the linearized models do not predict the behavior of the system correctly. This shows that the PI based control strategies are not robust enough to deal with uncertainty in operating conditions [153].

To address the above issues, controllers based on conventional Fuzzy logic sets (Type-1) are proposed in literature [7, 62, 158]. The fuzzy logic controller (FLC) circumvents the problem of modeling using knowledge and experience of the field experts. Moreover, in contrast to conventional PI compensator the control surface of the FLC can be shaped to define appropriate sensitivity for each operating point. The FLCs used for power electronic converters have shown a better performance in terms of tracking error and transient overshoots compared to that of conventional PI controller [61].

In general, the uncertainties related to inputs and outputs are modeled by using type-1 FSs, with precise and crisp membership functions. Once the type-1 membership functions have been chosen, the fact that the actual degree of membership itself is uncertain which is no longer modelled in type-1 fuzzy sets. It is assumed that a given input results in a precise and single value of membership [49]. However, the uncertainties associated with the rules and membership functions causes difficulty in determining the exact and precise antecedents and consequents membership functions during the FLC design.

As a consequence, the designed type-1 fuzzy system cannot give an optimal performance, when the parameters and operating conditions are uncertain. In order to deal with the uncertainties of the system with type-1 fuzzy sets needs to be frequently retuned, which results in wastage of resources. This shows the inability of type-1 FSs to represent linguistic and numerical uncertainties and need for new techniques to address the issues. Hence, it is argued that type-1 FSs with its two dimensional structure in MFs, cannot provide a good approximation to the uncertainties in rules and MFs [122, 167].

The existing literatures reveal that the interval type-2 fuzzy logic controllers (IT-2 FLCs) are generally more robust than their type-1 counterparts especially in dealing with

the uncertainties [8, 48, 64] . With the unique structure in membership functions, type-2 FSs can effectively model the uncertainties in rules and MFs. It has also been reported that the IT2-FLC has a smoother control surface around the steady state in comparison to type-1 FLC. Thus, it is envisaged, if the special features of IT-2 FSs are properly explored, might result in potentially more robust controllers that can behave like a variable gain PI controller [89].

In the renewable energy field, very few applications of type-2 FSs are reported till date, which is a great motivation factor to utilize the theory of type-2 FSs to address the issues of wind energy systems. In this work, an attempt has been made to apply the type-2 FSs for handling the uncertainties in wind energy systems. Further, to validate the feasibility of type-2 FLC for real-time applications, the controller is tested in hardware in loop environment.

1.2 Type-1 fuzzy logic control system

Conventional fuzzy logic sets also known as type-1 fuzzy sets were introduced by Zadeh in 1965, and its application has been the subject of debate for many years. Basically, the fuzzy sets are intended to mathematically represent the vagueness, ambiguity, imprecise and uncertainty in the information using linguistic variables. In recent years, it has found many applications in a variety of fields. Among the most successful applications of this theory has been in the area of fuzzy logic control, initiated by the work of Mamdani and Assilian [85].

Fuzzy logic control is a technique to embody human like thinking into a control system. A fuzzy controller can be designed to emulate human deductive thinking to infer conclusions from the past experience. To satisfy the control objectives, the decision making process of controller is designed based on fuzzy rule base, structured as a if $< situation >$ then $< action >$ where both situation and action have suitable fuzzy representation. It suits the control problems that are complex and cannot be easily represented by mathematical models.

Thus the performance of an FLC depends on human expertise about the system and the knowledge acquisition techniques to convert human expertise to appropriate fuzzy rules as well as proper fuzzy MFs for each fuzzy variable [11]. There are some important advantages of fuzzy controller like (i) FLC is tolerant of imprecise data (ii) can model nonlinear functions of arbitrary complexity (iii) can be blended with conventional control techniques

(iv) good qualitative understanding of plant or process operation. However it cant fully handle or accommodate the linguistic and numerical uncertainties associated with dynamic unstructured environments. Poor performance is often reported, where there is a difficulty in determining an exact MF for a fuzzy set.

Type-1 fuzzy systems, whose membership functions are crisp sets, do not provide sufficient support for many kinds of uncertainty that appears in subjectively expressed knowledge of experts. Hence, it is argued that type-1 representation does not provide a good approximation to meaning in representation of words and does not allow computing with words within a richer platform by considering the uncertainty in the definition of the membership functions [21].

The application of Fuzzy logic controllers are reported in almost all the areas of engineering, some of those are listed as follows:

- Power system control [138]
- Power system protection and Relaying [86]
- Economic load dispatch
- Stability Analysis [103]
- Inverted Pendulum system
- Magnetic levitation system
- Classification problem
- Robotic path planning
- Load forecasting
- Ball and beam system

1.3 Type-2 fuzzy logic control system

Type-2 Fuzzy sets let us model the uncertainties that are inherent in words as well as other uncertainties in a better way than type-1 FSs. Type-2 fuzzy systems (also known as general type-2 FSs) are introduced as a new tool with three dimensional fuzzy sets and foot print of uncertainty. The membership grade for each element of this set is a fuzzy set in [0, 1] - the primary membership; and corresponding to each primary membership

there is a secondary membership (also in [0 1]) [116]. The controller structure consists of three stages, fuzzification, inference engine and defuzzification, which is similar to that of type-1 FLC ; in addition, type reduction operation is required for various computations on type-2 FSs. The third dimension in MFs and the footprint of uncertainty together provides additional degrees of freedom to the controller, which enables it to model and handle the uncertainties. Hence, the type-2 FSs can be exploited to address the limitations of type-1 FSs in the applications where the uncertainty in the system parameters is a serious concern.

1.4 Interval type-2 fuzzy logic control system

The type-reduction operation in the general type-2 FLC, makes it computationally very intensive. Because it includes a large number of embedded type-1 fuzzy sets to deal with different uncertainties [60]. In order to avoid the computational complexity, the interval type-2 fuzzy sets (IT-2 FSs) are derived with the secondary memberships made as either zero or one. All the studies in this work, considers the IT-2 FSs, for design and analysis of the controller. When the secondary MFs are interval sets, we call the type-2 FSs as interval type-2 FSs. The explicit discussions on the use of IT-2 FSs can be found in chapter 2. Some of the successful applications with IT2 FLC, from wide variety of engineering fields are reported below.

- Control of flexible joint manipulator [93]
- IT2F sliding mode controller for a buck DC-DC converter [101]
- IT2FC for magnetic levitation system [167]
- IT2FLC for thyristor controlled series compensator (TCSC) for improving power system stability
- Handling uncertainty in controllers using interval type-2 fuzzy logic [20]
- Solar power prediction [64]
- Traffic forecasting [95]
- Genetic algorithm tuned IT2FLC to control a liquid level process [109]
- IT2FLC for the desulphurization process of a real steel industry
- Shunt active filter for harmonic analysis [118]

- IT2FLC for medical applications [92]
- Control of ambient intelligent environments [20]
- To address the congestion control for video streaming across internet protocol (IP) network
- Load forecasting [84]
- Equalization of nonlinear time-varying channels [100]

1.5 Real Time Digital Simulator (RTDS)

The RTDS simulator consists of custom hardware and software, specifically designed to perform real-time Electro Magnetic Transient (EMT) simulations. It operates continuously in real time while providing accurate results over a frequency range from DC to 3 kHz. This range provides a greater depth of analysis on power systems than traditional stability or load flow programs which study phenomenon within a very limited frequency range.

Figure 1.1: RTDS with racks

The RTDS simulator's fully digital parallel processing hardware is capable of simulating complex networks using a typical time step of 50 μs. The simulator also allows for small time step subnetworks that operate with time steps in the range of 1-4 μs for simulation of fast switching power electronic devices. The hardware is bundled into modular units called racks that allow easy expansion of the simulator's computing capability as required. Using the RTDS simulator, analytical studies can be performed must faster than with offline EMT simulation programs.

The parallel processing required by the RTDS simulator is carried out by processor cards. These cards are mounted in card cages, knows as racks, which are housed in cubicles. As the simulation demands of a user increase, processor cards can be added to the racks. As the racks are filled, more cubicles can be acquired, and many different racks can be involved in a given simulation. RTDS simulator cubicles include standard rails for the installation of I/O cards and other components. The I/O cards are used for closed loop testing of protective relay and control systems, power hardware in the loop studies, and much more.

RTDS Technologies proprietary software, designed specifically for interfacing to the RTDS simulator hardware, is called RSCASD. RSCAD is a user friendly interface, intended to create a working environment familiar to the power system engineer. RSCAD is an all-in-one package, containing all facilities that the user needs to prepare and run simulations, and to view and analyze results. Since the RTDS simulator operates in continuous real time, the simulated power system can be operated in a manner similar to a real power system. As simulation parameters are modified and contingencies are applied, the user can watch the power system respond in real time.

RSCAD represents a family of software tools consisting of individual modules that accomplish the different tasks involved in operating the simulator. Through RSCAD, the user has the ability to organize and share simulation projects and cases; assemble circuit diagrams using predefined or user-defined power and control system component models; automate or interact with simulator operation; and analyze and post-process simulation results.

1.6 The problems under study

Renewable energy and distributed generation systems have attracted special attention all over the world as an alternative to the conventional fossil fuel based energy sources. Wind

and solar are the two feasible sources for bulk energy production. The main drawback of these sources is uncontrollable meteorological conditions. In consequence, their connection to the utility grid will lead to instability or even failure of the grid if they are not properly controlled. The recent grid codes also demands certain features like, fault ride through(FRT) capability, frequency control and voltage regulation of the local grid which makes the control strategies of renewable sources an important topic for research and analysis.

From the literature survey, it is reported that PI controllers are not robust enough to deal with the uncertainties and type-2 FSs have been recognized as the suitable tool for modeling the system uncertainties. To investigate its applicability to renewable energy systems, in this work, DFIG based wind energy system is considered with varying network operating conditions. Type-2 FLC is designed for power electronic converters of DFIG, and tested under all possible contingencies. The control problems considered in this work are as follows:

- Design and optimization of type-2 FLC for grid connected DFIG using MATLAB based simulations
- Design and Implementation of Type-2 FLC for grid connected DFIG using real-time simulations
- Design and Implementation of Type-2 FLC for DFIG-based wind energy Systems in distribution networks
- Type-2 Fuzzy Logic based robust control strategy for power sharing in Microgrids

1.6.1 Design and Optimization of Type-2 FLC for grid connected DFIG using MATLAB based simulations

The type-2 FSs have been recognized as suitable tool for modeling the uncertainties in system parameters. As a preliminary study,to investigate its applicability to wind energy systems, a type-2 FLC is designed for grid connected DFIG and the performance is compared with that of type-1 FLC. A small improvement in the transient response has been observed with type-2 FLC. It is analyzed that, tuning the parameters of type-2 FLC is a tedious job, when the model is complex and sensitive. To get the optimal controller parameters, a constrained optimization problem is formulated, and solved via an evolutionary optimization tool based on genetic algorithm. To reduce the computational complexity a

linearized model of the power electronic inverter is considered as plant and integral square error as cost function. In order to realize the effect of FOU, the performance of the controller is evaluated under perturbed parameters.

1.6.2 Design and Real time implementation of Type-2 FLC for grid connected DFIG

The DFIG is the most commonly used configuration for variable speed wind turbines that are connected to the grid. In general, for the safety of converters, the generator unit is disconnected if a fault causes a large voltage drop in the grid. For reliable operation of the grid, the recent grid codes require that the wind turbines should remain connected to the grid during and after the fault. Further, to maintain the voltage stability, reactive power support is expected from the wind turbines throughout the period of interconnection. To meet the above requirements, in recent years, the conventional crowbar systems are used, however they do not fulfill the requirement of reactive power support. In this objective, a new control strategy is proposed with type-2 FLC that fulfills the FRT requirement eliminating the use of the crowbar. To validate the proposed control strategy, a case study of a 2 MW DFIG supplying an infinite bus is carried out by real-time simulations on RTDS environment. The performance of the controller is analyzed for three phase fault, unbalanced fault and also with varying wind speed conditions.

1.6.3 Design and implementation of Type-2 FLC for DFIG-based Wind energy systems in Distribution Networks

As the penetration levels of wind energy into the utility grid increases, the stability and reliability of the grid becomes a major challenge for the power transmission operators. In recent times, DFIG topology is widely being used for variable speed wind turbines due to many advantages. Since the grid codes demands, voltage control, reactive power and frequency control and FRT capability, various control strategies are reported for grid connection of DFIGs. The operating conditions of the wind energy systems are highly uncertain due to unpredictable inputs of wind speed. The control strategies to date have concentrated mainly on accurate tracking of power references, voltage and reactive power control etc., under a specific operating condition and no attempt has been made to address the issues of uncertainty in operating conditions.

In this objective, a robust vector control strategy using type-2 FLC is recommended for

DFIG, to deal with various uncertainties in generator system as well as in the distribution network. In order to validate the applicability of controller for real time applications, a standard IEEE -34 bus system connected with DFIG, is considered for real time simulations. The controller is implemented on a digital platform and tested with RTDS in a hardware-in-loop environment. The performance of the proposed controller is analyzed by comparing with that of standard type-1 FLC with all possible contingencies.

1.6.4 Type-2 FLC based Robust control strategy for Power sharing in Microgrids

The concept of microgrid (MG) and distributed generation (DG) are the two subjects that appear very frequently in recent times, in the power systems research. The rising concerns about energy independence and global warming issues, makes the microgrids a fascinating topic for researchers around the world. The microgrid generally comprises hybrid renewable sources like PV, wind, fuel cells and energy storage devices, intended to operate in both grid connected and islanded modes. Besides the uncertainty in solar radiation and wind speed, grid integration, controllability, reliability and power quality are the main challenges to use the renewable sources in microgrid (MG) [81]. Further, the DG units are low inertia sources and highly sensitive to disturbances. The power system networks with such sources are prone to various uncertainties which affect the operating points, stability and reliability leading to frequent islanding. Therefore, for effective power sharing the designed control schemes should be capable of handling the disturbances that arise as a result of uncertainties in load changes and other network transient conditions. In this work, a microgrid model is designed using IEEE-34 bus system, connected with wind farm , PV system and battery storage system. Type-2 FLC is designed and tested under grid connected as well as islanded conditions, with all possible contingencies.

1.7 Contribution of Thesis

The contribution of this work can be seen in the following objectives. From the literature review, it has been found that uncertainty in operating conditions is the major challenge in using the renewable energy sources with the utility grid. The conventional PI controllers are model dependent and not robust enough to perform in variable operating conditions. It is also found that type-2 FSs with its special features in MFs, can effectively model and handle

the uncertainties. An attempt has been made to explore the possibility of using the theory of interval type-2 fuzzy sets as type-2 FLC for renewable energy applications, especially for DFIG based wind energy systems. Also the feasibility of the controller for real-time applications has been verified with hardware-in-loop simulations in RTDS environment. The design objectives are framed as follows:

- Design and Real time Implementation of Type-2 FLC for FRT of DFIG based Wind Generators.

  In this objective, at first, the mathematical modeling of the DFIG and other power electronic converters is derived. Type-2 FLC is designed for rotor side converter of the DFIG. The performance of controller is verified for a three phase fault and load changes. Further to realize the effect of FOU, an optimization problem is formulated using Genetic algorithm and the performance is compared with that of other counterparts. Secondly, the controller performance is evaluated with real-time simulations. Since, many researchers have considered the RTDS as real-time platform for controller prototyping and hardware in loop simulations, in this work the DFIG model is implemented in RSCAD for execution in RTDS. The controller is implemented on a DSP based Dspace 1104 module and interfaced with the RTDS through hardware-in-loop. The performance is verified for all the possible contingencies that have been considered in the Matlab simulations.

- Design and Implementation of Type-2 FLC for DFIG-Based Wind Energy Systems in Distribution Networks

  In the previous objective the controller performance is verified with the DFIG model connected to an infinite bus. To evaluate the controller performance under unbalanced voltages and other uncertainties in the distributed networks, the IEEE-34 bus system is considered in the plant model which has been used in the previous objective. The controller parameters are tuned based on the observations from extensive simulation results. In order to verify the robustness of the controller, all the possible uncertainties in the distributed networks are considered for testing cases. Further to ascertain the feasibility of the controller for renewable energy applications, the performance is compared with that of type-1 FLC.

- Type-2 FLC based Robust Control Strategy for Power Sharing in Microgrids

  In the previous objectives the controller performance is analyzed with a single wind

farm connected to the utility grid. In order to verify the effectiveness of type-2 FLC in the presence of multiple DGs, in this work, the type-2 FLC is designed for power sharing in a microgrid comprising a PV system, DFIG and a battery storage system under grid uncertainties. The IEEE-34 bus system is modeled in RSCAD as a microgrid. The conventional droop control strategy is used for generating the reference powers to the controllers. The real time simulations are carried out on RTDS, considering the grid connected as well as islanded conditions. The performance of the proposed strategy is evaluated by comparing with that of PI controller under various possible contingencies.

1.8 Organization of Thesis

The work done in this thesis for the investigation of application of type-2 fuzzy sets for renewable energy systems has been presented in six different chapters. The description about each research objective is included in the introduction section of each chapter.

Chapter-1 discusses the need for intelligent control methodology for the renewable energy systems. The research gaps found in the literature survey are discussed in the motivation section. A brief note on type-1 FSs and IT-2 FSs and their applications in power and control engineering are discussed. A small introduction about the control problems that are considered for type-2 FLC design is explained. Finally the contribution of this thesis work is presented.

Chapter-2 provides a brief review on mathematical analysis of interval type-2 fuzzy logic systems. The structure of the interval type-2 fuzzy logic controller is presented and discussed with examples. The comparative features of Type-1 FSs and the IT-2 FSs are also elaborated.Various operations on type-2 Fuzzy sets are explained with possible examples.

Chapter-3 details the mathematical modeling of the DFIG and the design of type-2 FLC for fault ride through of DFIG based wind generators. The optimization problem for tuning the controller parameters is analyzed with genetic algorithm. The performance of the proposed strategy is compared with the type-1 FLC under various possible contingencies. The robustness of the proposed controller is also discussed with real time simulations.

Chapter-4 includes design and analysis of type-2 FLC for distributed networks connected with DFIG. The IEEE-34 bus system, model implementation in RSCAD and the controller design on Dspace 1104 module are presented. The performance analysis of the real-time simulation results is discussed. The robustness analysis is done by comparing the

performance with type-1 FLC under various uncertainties of the distributed work.

Chapter-5 presents the modelling of PV system and design of type-2 FLC for power sharing in microgrid comprising PV, wind and battery storage system. The controller design steps based on droop control strategy and type-2 FLC are discussed. The performance of type-2 FLC in the presence of multiple DG sources with uncertainties in PV system is elaborately discussed. The details of hardware in loop simulations and interfacing with RTDS are presented.

Chapter-6 compiles the salient conclusions of the present study regarding the design of interval type-2 fuzzy logic controller for renewable energy systems and the recommended directions for further investigations.

Chapter 2

A review on type-2 fuzzy logic system

2.1 Introduction

The concept of type-2 fuzzy set (FS) was introduced by Zadeh [175] as an extension to the traditional type-1 fuzzy set. In type-1 FS, the membership grade is a crisp number in [0 1], where as in type-2 FS, the membership grades themselves are type-1 FSs. This feature of type-2 FS is very useful in circumstances where it is difficult to determine exact membership grade for fuzzy set and also for incorporating uncertainties. This chapter provides an overview of type-2 fuzzy logic sets and its characteristics. The aim of this chapter is to provide a background on several aspects related to type-2 FSs and also various set operations with examples.

2.2 Type-2 Fuzzy logic system

Generally, in a fuzzy logic system (FLS) the uncertainties related to inputs and outputs are modeled by using type-1 FSs, with precise and crisp membership functions (MFs). Once the type-1 MFs have been chosen, the fact that the actual degree of membership itself is uncertain is no longer modeled in type-1 FSs. It is assumed that a given input results in a precise and single value of membership grade [73]. Quite often, the knowledge used to design the FLS ignores the uncertainties in rules, spread of MFs, membership grade etc., and such systems cannot guarantee the optimal performance when it is subjected to the contingencies.

For example: 1) A fuzzy logic modulation classifier described in [159] centers type-1 Gaussian MFs at constellation points on the in-phase/quadrature plane. In practice, the constellation points drift. This is analogous to the situation of a Gaussian membership function (MF) with an uncertain mean. A type-2 formulation can capture this drift. 2) In most of the forecasting problems the noise in training data is ignored, which leads to uncertainty in both the antecedents and consequents. If the information about the level of uncertainty is known, it can be taken into account by designing the system with type-2 FSs [95]. 3) The fuzzy rules are decided by knowledge and experience of field experts, which

varies from case to case; this leads to statistical uncertainties about locations and spread of antecedent and consequent fuzzy sets. Such uncertainties can be easily modeled and accounted into the descriptions of these sets using type-2 MFs [2].

In addition, experts often give different answers to the same rule-question; this results in rules that have the same antecedents but different consequents. In such a case, it is also possible to represent the output of the FLS built from these rules as a fuzzy set rather than a crisp number. This can also be achieved within the type-2 framework. Type-2 fuzzy logic seems to be as fundamental to the design of systems that include linguistic and/or numerical uncertainties [48]. Just as one can work with higher than second order moments in probabilistic modeling, we can also use higher than type-2 sets in fuzzy modeling; but, as we go on to higher types, the complexity of the system increases rapidly [60]. So, in this work we analyze just with type-2 sets and its features. A fuzzy relation of higher type (e.g., type-2) has been regarded as one way to increase the fuzziness of a relation and, according to [53], increased fuzziness in a description means increased ability to handle inexact information in a logically correct manner. Detailed description of algebraic structure of type-2 sets are given in [116].

From literature survey, it is found that type-2 FSs have been successfully applied in many science and engineering applications [100, 99, 112]. In data process applications, the system with type-2 FSs seem to be more promising method than the type-1 counterpart in processing of noisy data with uncertainties [64]. Type-2 FSs have been applied in decision making [118], survey processing [92], solving fuzzy relation equations [113] and function approximation [165] by comparing the performance with its type-1 counterparts. In real world applications which exhibit measurement noise and parameter uncertainties, type-2 fuzzy logic controllers are better option than type-1 fuzzy logic controllers [55]. If the parameters are tuned properly, type-2 FSs have better ability to predict the time series compared to type-1 FSs [117]. The controllers with type-2 FSs have shown better tracking capability in real time mobile robots for indoor and outdoor environments [109]. In [57], the VLSI implementation of type-2 FSs and the increasing the speed of inference engine has been discussed. Recently, many power system applications have adopted the type-2 FSs as an alternative for handling the uncertainties in operating conditions [101]. It is believed that other promising areas in which type-2 FSs may be advantageous over type-1 FSs include mobile communications, communication networks, pattern recognition, renewable energy systems and robust control, because frequently the information to be processed in these areas is uncertain.

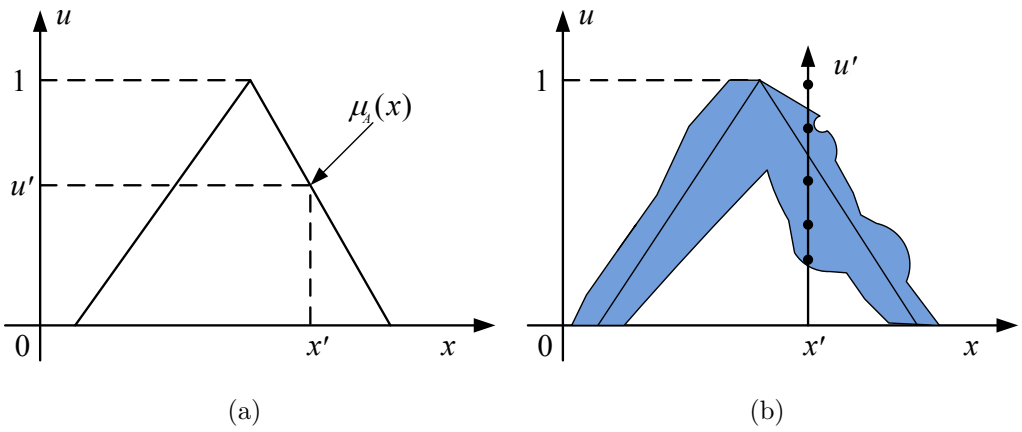

(a) (b)

Figure 2.1: Example of (a) Type-1 FS (b) blurred type-1 FS

2.3 Mathematical analysis on type-2 FSs

In this section, the detailed information about the concept of type-2 fuzzy set is explained. The MF of a standard type-1 FS is shown in Figure 2.1(a) , with a crisp membership grade varying in [0 1]. The type-2 MF can be imagined as a blurred type-1 MF as shown in Figure 2.1(b). At a specific point of x , say x' , the type-1 MF is having a single value of membership grade u' where as in type-2 case, it takes on values wherever the vertical line intersects the blur. The weights of these intersection points need not be the same, and amplitude distribution may be applied to have a valid representation. Doing this for all $x \in X$, a three dimensional membership function or a type-2 membership function can be created which characterises a type-2 fuzzy set.

A type-2 fuzzy set, denoted A, is characterized by a type-2 membership function $\mu_A(x, u)$ is represented as

$$A = \{(x, u), \mu_A(x, u)\} \qquad \forall x \in X,\ \forall u \in J_x \subseteq [0, 1] \tag{2.1}$$

where μ_A varies in $0 \leq \mu_A(x, u) \leq 1$. The set A can also be expressed as

$$A = \int_{x \in X} \int_{u \in J_x} \mu_A(x, u)/(x, u) \qquad J_x \subseteq [0, 1] \tag{2.2}$$

$$= \int_{x \in X} \left[\int_{u \in J_x} \mu_A(x, u)/u \right] \Big/ x \tag{2.3}$$

where

x :primary variable

u :primary membership grade

$\mu_A(x, u)$: secondary membership grade (amplitude of secondary membership function)

X : domain of primary membership function

J_x : domain of secondary membership function and

$\int\int$ denotes union over all admissible x and u [168].

The graphical representation of type-2 FS with discrete universe is shown in Figure 2.2. The axis u represents the domain of the primary MF and μ_A represents the secondary MF. The secondary MF is also represented as vertical slice of the axis μ_A. J_x is the domain of the secondary MF also called the primary membership of x, varies in the range of [0 1].

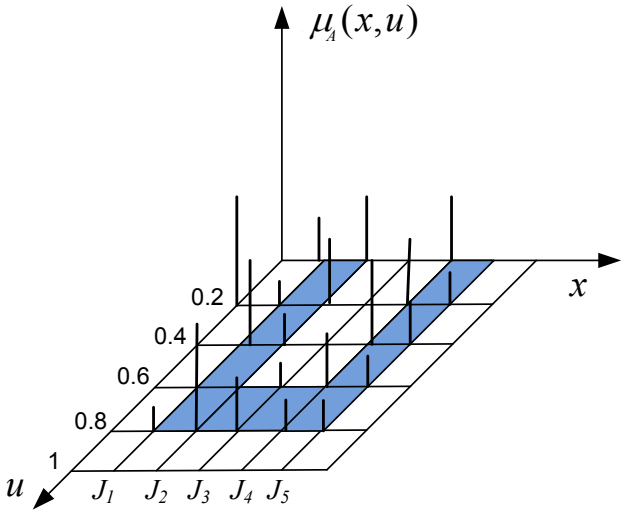

Figure 2.2: Example of a Type-2 FS

The uncertainty in the primary memberships consists of a bounded region, known as footprint of uncertainty (FOU), shown as shaded region in Figure 2.2. The FOU is derived as the union of all primary memberships, i.e.,

$$FOU(A) = \bigcup_{x \in X} J_x \tag{2.4}$$

The term foot print of uncertainty draws a special attention towards type-2 FSs, because it is framed to represent the uncertainties inherent in a specific type-2 MF and its shape is direct consequence of the nature of these uncertainties. The type-2 FSs are represented in three dimensional nature which causes difficulty in depicting them graphically. The FOU lets us two dimensional graphical representation of type-2 MF providing a convenient verbal description of the domain of the secondary membership grades. The distribution that sits on the shaded FOU is known as the third dimension of the type-2 FSs, which depends upon the choice of the secondary grades.

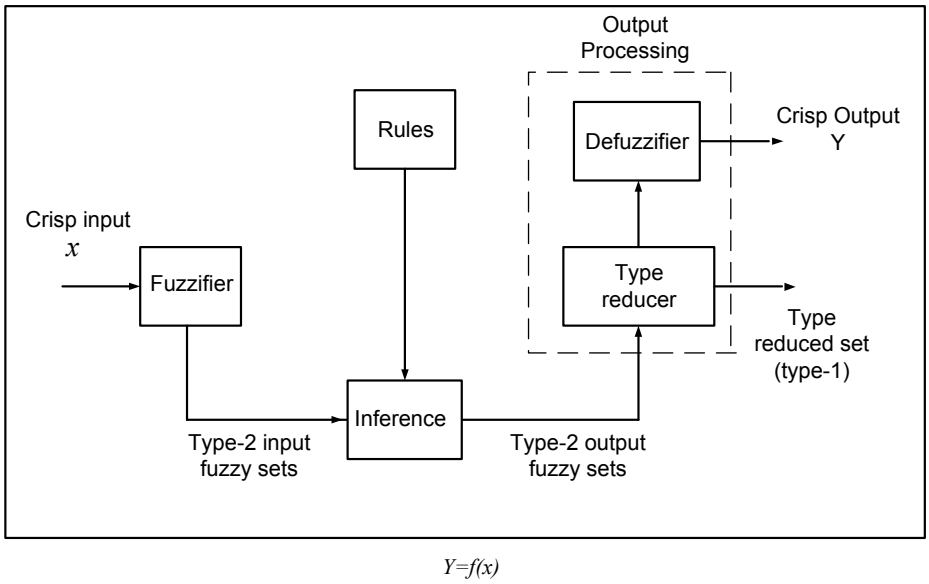

Figure 2.3: The structure of type-2 FLS

2.3.1 Structure of Type-2 FLS

The structure of the type-2 FLS is shown in Figure 2.3. It is very similar to type-1 FLS except the output processing block.

Fuzzifier

The fuzzifier maps the crisp input into a type-2 fuzzy set. This operation can be done by choosing the appropriate type-2 FSs in the range of the input variable. The challenge here lies in the definition of membership grade fuzziness. Clearly the primary and secondary MFs should be formulated in such a way that it reduces the problem of complexity as much as possible.

Rules

The rules are framed based on "IF THEN" logic , where the l^{th} rule has the form
R^l: IF x_1 is F_1^1 and x_2 is F_2^l ...and x_p is F_p^l THEN y is G^l
where x_is are inputs, F_i^ls are antecedent sets (i=1,....p); y is the output; and G^ls are consequent sets.
Although the type-1 and type-2 MFs are distinct in structure, the rule formation is not dependent on the nature of MF; hence, the structure of the rules in type-2 FLS remains exactly same as in type-1 case, the only difference being that now some or all of the sets involved are of type-2.

Inference Engine

The inference engine maps the input and output fuzzy sets by combining the rules. Multiple antecedents in rules are connected by the t-norm which can be obtained through the intersection operation of type-2 sets. Super star compositions are used for combining the membership grades of input and output sets. The t- conorm, obtained through union operation of sets, is used for combining the multiple rules. To do this one needs to find unions and intersections of type-2 sets, as well as compositions of type-2 relations which is explained in the following section.

Type Reduction

In a type-1 FLS, the output corresponding to each fired rule is a type-1 set in the output space. The crisp output is obtained by combining all the fired rules through a defuzzifier using some fuzzy relations. Most of the defuzzifiers discretize the combined output space into type-1 sets and use the centroid method for calculating the combined crisp output. In contrast, in type-2 FLS, the output set corresponding to the each fired rule is a type-2 set, on which the centroid method cannot be applied directly. In order to calculate the crisp output the type-2 sets are combined in some way to get the type-1 form known as type reduction operation. In this operation the combined output space is discretized into various samples and every combination of these samples is combined through t- norm to generate a set A'. The set A' has the same domain as A and is known as an embedded type-1 set in A. The detailed description on type reduction can be found in [74, 129].

For example, an embedded type-2 set A_e has N elements, where A_e contains exactly one element from J_{x_1},J_{x_2},....,J_{x_N} namely u_1,u_2,....,u_N, each with its associated secondary grade, namely $f_{x_1}(u_1)$,$f_{x_2}(u_2)$,.....$f_{x_N}(u_N)$, i.e.

$$A_e = \sum_{i=1}^{N} [f_{x_i}(u_i)/u_i]/x_i \qquad u_i \in J_{x_i} \subseteq U = [0,1] \tag{2.5}$$

Some of the popular type reduction methods are - centroid type reduction, height type reduction and center- of- sets type reduction.

Defuzzification

The output of the type reduction block results in type-1 form of combined space. The simple way to get a crisp output is through finding the centroid of all the type-1 sets embedded in type-2 FLS. The other way of doing this operation is by choosing the highest

membership point in the type-reduced set. For example, if the type reduced set Y for an input x is discretized into N points, then the centroid is expressed as

$$C_y(x) = \frac{\sum_{k=1}^{N} y_k \mu_Y(y_k)}{\sum_{k=1}^{N} \mu_Y(y_k)} \tag{2.6}$$

where $\mu_Y(y_k)$ represents the membership grade.

2.3.2 Centroid type reduction using Karnik-Mendel Algorithm

As explained in [45], the centroid defuzzifier combines the output type-1 sets using a t-conorm and then finds the centroid of this set. If B is a composite output fuzzy set, then centroid defuzzifier output is given as shown in 2.6. The centroid type reducer combines all the output type-2 sets by finding their union.The membership grade of $y \in Y$ is given as

$$\mu_{\tilde{B}}(y) = \coprod_{l=1}^{M} \mu_{\tilde{B}^l}(y) \tag{2.7}$$

where $\mu_{\tilde{B}^l}(y)$ is the minimum t-norm corresponding to the l^{th} rule. The expression for the output of centroid type reducer is written as an extension of equation 2.6, i.e.,

$$Y_c(x) = \int_{\theta_1} ... \int_{\theta_N} [\mu_{D_1}(\theta_1) * ... * \mu_{D_N}(\theta_N)] / \frac{\sum_{i=1}^{N} y_i \theta_i}{\sum_{i=1}^{N} \theta_i} \tag{2.8}$$

where $D_i = \mu_{\tilde{B}}(y_i)$ and $\theta_i \in \mu_{\tilde{B}}(y_i) (i = 1, ..., N)$. Let

$$a \triangleq \frac{\sum_{i=1}^{N} y_i \theta_i}{\sum_{i=1}^{N} \theta_i} \tag{2.9}$$

$$b \triangleq \mu_{D_1}(\theta_1) * ... * \mu_{D_N}(\theta_N) \tag{2.10}$$

The computation of $Y_c(x)$ involves computing the tuple (a, b) many times. The sequence of computations in Karnik-Mendel algorithm to obtain $Y_c(x)$ is as follows.

- Compute the combined output set using 2.7.
- Discretize the output space Y into N points, $y_1, ..., y_N$.
- Discretize the domain of each $\mu_{\tilde{B}}(y_i)$ $(i = 1, ..., N)$ into a suitable number of points.

- Enumerate all the embedded sets.For example, if each $\mu_{\tilde{B}}(y_i)$ is discretized into M_i points, there will be $\prod_{j=1}^{N} M_j$ embedded sets.

- Compute the centroid type-reduced set using 2.8, i.e., compute the tuples $(a_i, b_i), i = 1, 2..... \prod_{j=1}^{N} M_j$

In step 5, the centroid and membership computation has to be repeated $\prod_{j=1}^{N} M_j$ times and so, in general, will involve an enormous amount of computation. Computational complexity and ways to reduce it are discussed in the following section.

2.4 Interval type-2 Fuzzy sets

In order to reduce the computational complexity of general type-2 FSs, the concept of interval type-2 fuzzy sets (IT-2 FSs) were introduced. An Interval type-2 set $\tilde{A}$, is characterized as

$$\tilde{A} = \int_{x \in X} \int_{u \in J_x} 1/(x, u), \qquad J_x \subseteq [0, 1] \tag{2.11}$$

$$= \int_{x \in X} [\int_{u \in J_x} 1/u]/x \tag{2.12}$$

$\tilde{A} : X \to \{[a, b] : 0 \leq a \leq b \leq 1\}$. Structurally, the membership function of both type-2 FSs and IT-2 FSs are three dimensional with only difference of secondary merbership grades of IT-2 FSs are always 1. Figure 2.4 shows the interval type-2 gaussian membership function in which the secondary membership grade is highlighted. Uncertainty about $\tilde{A}$ is conveyed by the union of all the primary memberships, which is called the footprint of uncertainty (FOU) of $\tilde{A}$, i.e.

$$FOU(\tilde{A}) = \cup_{\forall x \in X} J_x = \{(x, u) : u \in J_x \subseteq [0, 1]\} \tag{2.13}$$

As shown in Figure 2.5, the upper membership function (UMF) and lower membership function (LMF) of $\tilde{A}$ are two type-1 MFs that bound the FOU. The UMF is associated with the upper bound of $FOU(\tilde{A})$ and is denoted $\bar{\mu}_{\tilde{A}}(x), \forall x \in X$ and the LMF is associated with the lower bound of $FOU(\tilde{A})$ and is denoted by $\underline{\mu}_{\tilde{A}}(x)$ i.e. $FOU(\tilde{A})$ in 2.13 can also be expressed as

$$FOU(\tilde{A}) = \bigcup_{\forall x \in X} [\underline{\mu}_{\tilde{A}}(x), \bar{\mu}_{\tilde{A}}(x)] \tag{2.14}$$

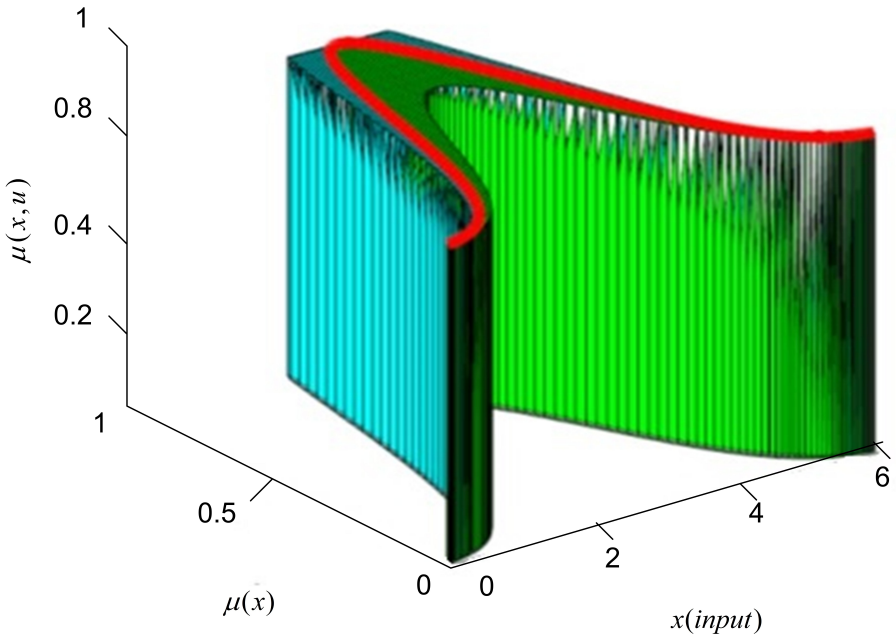

Figure 2.4: Type-2 fuzzy set with FOU and embedded FS

For continuous universe of discourse X and u an embedded IT-2 fuzzy set $\tilde{A}_e$ is

$$\tilde{A}_e = \int_{x \in X} [1/u]/x, \quad u \in J_x \tag{2.15}$$

note that (2.15) means $\tilde{A}_e : X \to \{u : 0 \leq u \leq 1\}$, the set $\tilde{A}_e$ is embedded in $\tilde{A}$ such that at each x it only has one secondary variable (i.e. one primary membership whose secondary grade equals 1). Examples of $\tilde{A}_e$ are represented as $1/\bar{\mu}_{\tilde{A}}(x)$ and $1/\underline{\mu}_{\tilde{A}}(x)$, $\forall x \in X$.

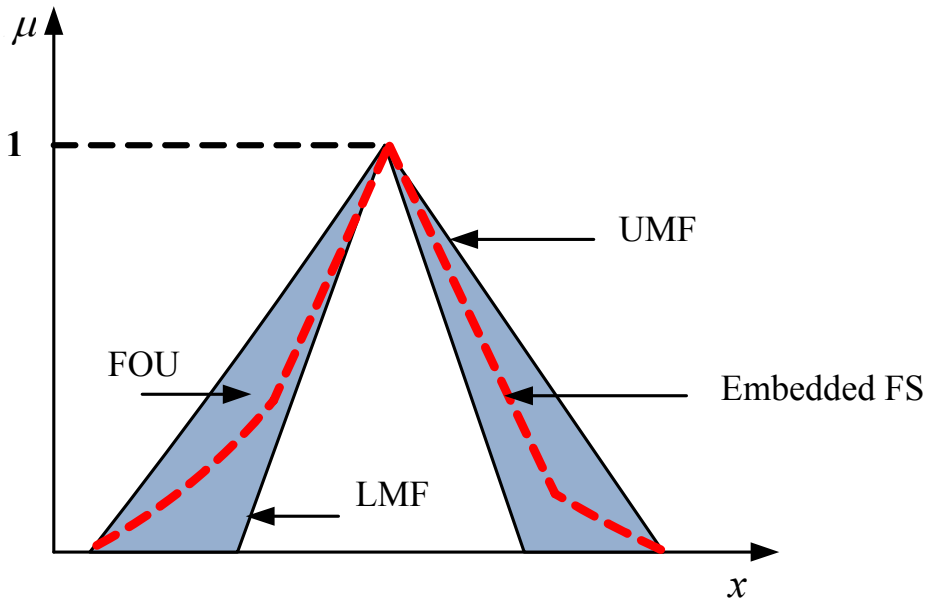

Figure 2.5: Type-2 fuzzy set with FOU and embedded FS

The detailed analysis of embedded IT-2 FSs are given in [112]. Referring to [115], for discrete universes of discourse X and U, in which x has been discretized into N values

and at each of these values u has been discretized into Mi values; an embedded IT-2 FS $\tilde{A}_e$ has N elements, where $\tilde{A}_e$ contains exactly one element from $J_{x1}, J_{x2}, ..., J_{xN}$, namely $u_1, u_2, ..., u_N$, each with a secondary grade equal to 1, i.e.,

$\tilde{A}_e = \sum_{i=1}^{N} [1/u_i]/x_i \quad$ where $u_i \in J_{x_i}$.

If $\tilde{A}_e$ is embedded in $\tilde{A}$ and there are a total of $\prod_{i=1}^{N} M_i \tilde{A}_e$.

An embedded type-1 FS A_e is associated with each $\tilde{A}_e$, where

$$A_e = \int_{x \in X} u/x, \qquad u_i \in J_x \tag{2.16}$$

Here the equation (2.16) means: $A_e : X \to \{u : 0 \leq u \leq 1\}$. The set A_e, which acts as the domain for $\tilde{A}_e$, is the union of all the primary membership of the set $\tilde{A}_e$ in the equation (2.15). Examples of A_e are $\bar{\mu}_{\tilde{A}}(x)$ and $\underline{\mu}_{\tilde{A}}(x)$, $\forall x \in X$. As the universes of discourse X and U are continuous then there is an uncountable number of embedded IT-2 FSs ($\tilde{A}_e$) and embedded type-1 FSs (A_e) in $\tilde{A}$. Such sets are only used for theoretical analysis and not for computational purpose.

For discrete universes of discourse X and U, a new representation theorem was derived in [73]. Here a general type-2 FS is expressed as the union of all of its embedded fuzzy sets, i.e.

$$\tilde{A} = \bigcup_{i=1}^{n_A} \tilde{A}_e^j \tag{2.17}$$

where $n_A = \prod_{i=1}^{N} M_i$.

This representation theorem is applicable to the IT-2 FSs, since they are a special case of the more general type-2 FSs, and is also applicable to continuous universes of discourse. Therefore, the type-2 FS representation theorem specialized to an IT-2 FS is defined as follows:

For an IT-2 FS, for which X and U are discrete, the domain of $\tilde{A}$ is equal to the union of all of its embedded type-1 FSs, so that $\tilde{A}$ can be expressed as [115]

$$\tilde{A} = 1 \Big/ FOU\left(\tilde{A}\right) = 1 \Big/ \bigcup_{j=1}^{n_A} A_e^j \tag{2.18}$$

where $A_e^j = \sum_{i=1}^{N} u_i^j / x_i$ and $u_i^j \in J_{x_i} \subseteq U = [0, 1]$. Therefore

$$FOU\left(\tilde{A}\right) = \sum_{j=1}^{n_A} A_e^j = \{\underline{\mu}_{\tilde{A}}(x), ..., \bar{\mu}_{\tilde{A}}(x)\}, \qquad \forall x \in X_d \tag{2.19}$$

$$= [\underline{\mu}_{\tilde{A}}(x), \bar{\mu}_{\tilde{A}}(x)], \qquad \forall x \in X \tag{2.20}$$

The equation (2.19) is for a discrete universe of discourse, X_d , and contains n_A elements, where $n_A = \prod_{i=1}^{N} M_i$. Here M_i denotes the discretization levels of secondary variable u_i^j at each of the N_{x_i}. And the equation 2.20 is for a continuous universe of discourse and is an interval set of functions, means it contains an uncountable number of functions that completely fills the space between $\bar{\mu}_{\tilde{A}}(x) - \underline{\mu}_{\tilde{A}}(x)$,$\forall x \in X$ [167].

2.5 Set operations on Interval type-2 FSs

The set theoretic operations of interval type-2 fuzzy sets are widely used in an IT-2 FLS design. The operations like union, intersection and complement are very popular and used for fuzzy inferencing. Most of these operations on type-1 FSs are based on the extension principle [175], alpha-cuts or interval arithmetic [45, 82]. The same operations on IT-2 FSs use the representation theorem 1, as explained below.

Theorem: (i) The union of two IT-2 FSs $\tilde{A}$ and $\tilde{B}$ is

$$\tilde{A} \cup \tilde{B} = 1/[\underline{\mu}_{\tilde{A}}(x) \vee \underline{\mu}_{\tilde{B}}(x), \bar{\mu}_{\tilde{A}}(x) \vee \bar{\mu}_{\tilde{B}}(x)], \quad \forall x \in X \tag{2.21}$$

(ii) The intersection of two IT-2 FSs $\tilde{A}$ and $\tilde{B}$ is

$$\tilde{A} \cap \tilde{B} = [\underline{\mu}_{\tilde{A}}(x) \wedge \underline{\mu}_{\tilde{B}}(x), \bar{\mu}_{\tilde{A}}(x) \wedge \bar{\mu}_{\tilde{B}}(x)] \tag{2.22}$$

(iii) The complement of IT-2 FS $\tilde{A}$ is

$$\bar{\tilde{A}} = 1/[1 - \bar{\mu}_{\tilde{A}}(x), 1 - \underline{\mu}_{\tilde{A}}(x)] \tag{2.23}$$

Proof (i): Lets consider two IT-2 FSs $\tilde{A}$ and $\tilde{B}$. From representation theorem, it is known that an interval type-2 fuzzy set $\tilde{A}$ for which X and U are discrete can be expressed as the union of all of its embedded IT-2 FSs

$$\tilde{A} = \sum_{j=1}^{n_A} \tilde{A}_e^j \tag{2.24}$$

From (2.19) and (2.20),

$$\tilde{A} \cup \tilde{B} = \sum_{j=1}^{n_A} \tilde{A}_e^j \cup \sum_{i=1}^{n_B} \tilde{B}_e^i = \sum_{j=1}^{n_A} \sum_{i=1}^{n_B} \tilde{A}_e^j \cup \tilde{B}_e^i = 1 \Big/ FOU\left(\tilde{A} \cup \tilde{B}\right) \tag{2.25}$$

where n_A and n_B represents the number of embedded IT-2 FSs that are associated with $\tilde{A}$ and $\tilde{B}$ respectively. Referring to the equation (2.19)

$$FOU\left(\tilde{A} \cup \tilde{B}\right) = \sum_{j=1}^{n_A} \sum_{i=1}^{n_B} \tilde{A}_e^j \cup \tilde{B}_e^i \tag{2.26}$$

Now we have to compute the union of the $n_A \times n_B$ pairs of the embedded type-1 FSs $\tilde{A}_e^j$ and $\tilde{B}_e^j$. Since the union of the two type-1 FSs is a function,

$$A_e^j \cup B_e^j = \max\left\{\mu_{A_e^j}(x_k), \mu_{B_e^i}(x_k)\right\}, \quad k = 1, 2.....N \tag{2.27}$$

Therefore the equation (2.26) is a collection of $n_A \times n_B$ functions that contain a lower bounding function and an upper bounding function because both $\mu_{A_e^j}(x_k)$ and $\mu_{B_e^j}(x_k)$ are bounded for all values of x_k .

It is to be recalled that the upper and lower membership functions for IT-2 FS are also embedded type-1 FSs. For $\tilde{A}$, $\bar{\mu}_{\tilde{A}}(x)$ and $\underline{\mu}_{\tilde{A}}(x)$ represents its upper and lower MF respectively, whereas for $\tilde{B}$, $\bar{\mu}_{\tilde{B}}(x)$ and $\underline{\mu}_{\tilde{B}}(x)$ denotes its equivalent quantities. Therefore, it is true that

$$\sup_{\forall j,i} \max\left\{\mu_{A_e^j}(x_k), \mu_{B_e^i}(x_k)\right\} = \max\left\{\bar{\mu}_{\tilde{A}}(x), \bar{\mu}_{\tilde{B}}(x)\right\}$$

$$= \bar{\mu}_{\tilde{A}}(x) \vee \bar{\mu}_{\tilde{B}}(x), \quad \forall x \in X \tag{2.28}$$

and $\inf_{\forall j,i} \max\left\{\mu_{A_e^j}(x_k), \mu_{B_e^i}(x_k)\right\} = max\{\underline{\mu}_{\tilde{A}}(x), \underline{\mu}_{\tilde{B}}(x)\}$

$$= \underline{\mu}_{\tilde{A}}(x) \vee \underline{\mu}_{\tilde{B}}(x), \quad \forall x \in X \tag{2.29}$$

From equation (2.21)-(2.25), it is concluded that

$$\tilde{A} \cup \tilde{B} = 1 \Big/ \sum_{j=1}^{n_A} \sum_{i=1}^{n_B} \tilde{A}_e^j \cup \tilde{B}_e^i$$

$$= 1/[\underline{\mu}_{\tilde{A}}(x) \vee \underline{\mu}_{\tilde{B}}(x), \bar{\mu}_{\tilde{A}}(x) \vee \bar{\mu}_{\tilde{B}}(x)] \tag{2.30}$$

Proof (ii): Similar to proof (i) applying equation (2.16) and (2.20),

$$\tilde{A} \cap \tilde{B} = \sum_{j=1}^{n_A} \tilde{A}_e^j \cap \sum_{i=1}^{n_B} \tilde{B}_e^i = \sum_{j=1}^{n_A} \sum_{i=1}^{n_B} \tilde{A}_e^j \cap \tilde{B}_e^i = 1 \Big/ FOU\left(\tilde{A} \cap \tilde{B}\right) \tag{2.31}$$

where n_A and n_B represents the number of embedded IT-2 FSs that are associated with $\tilde{A}$ and $\tilde{B}$ respectively. Referring to the equation (2.16)

$$FOU\left(\tilde{A} \cap \tilde{B}\right) = \sum_{j=1}^{n_A} \sum_{i=1}^{n_B} \tilde{A}_e^j \cap \tilde{B}_e^i \tag{2.32}$$

Now we have to compute the intersection of the $n_A \times n_B$ pairs of embedded type-1 FSs in $\tilde{A}_e^j$ and $\tilde{B}_e^j$. Since the intersection of two type-1 FSs is a function,

$$A_e^j \cap B_e^j = \min\left\{\mu_{A_e^j}(x_k), \mu_{B_e^i}(x_k)\right\}, \quad k = 1, 2, ...N \tag{2.33}$$

Therefore, the equation (2.28) is a collection of $n_A \times n_B$ functions, that contain a lower bounding function and an upper bounding function because both $\mu_{A_e^j}(x_k)$ and $\mu_{B_e^j}(x_k)$ are bounded for all values of x_k . It is to be recalled that the upper and lower membership functions for the IT-2 FS are also embedded type-1 FSs. For the type-2 fuzzy set $\tilde{A}$, $\bar{\mu}_{\tilde{A}}(x)$ and $\underline{\mu}_{\tilde{A}}(x)$ represents its upper and lower MF respectively, whereas for $\tilde{B}$, $\bar{\mu}_{\tilde{B}}(x)$ and $\underline{\mu}_{\tilde{B}}(x)$ denotes its equivalent quantities. Therefore it is true that

$$\sup_{\forall j,i} \min\left\{\mu_{A_e^j}(x_k), \mu_{B_e^i}(x_k)\right\} = \min\left\{\bar{\mu}_{\tilde{A}}(x), \bar{\mu}_{\tilde{B}}(x)\right\}$$

$$= \bar{\mu}_{\tilde{A}}(x) \wedge \bar{\mu}_{\tilde{B}}(x), \forall x \in X \tag{2.34}$$

and if $\inf_{\forall j,i} \min\left\{\mu_{A_e^j}(x_k), \mu_{B_e^i}(x_k)\right\} = \min\{\underline{\mu}_{\tilde{A}}(x), \underline{\mu}_{\tilde{B}}(x)\}$

$$= \underline{\mu}_{\tilde{A}}(x) \wedge \underline{\mu}_{\tilde{B}}(x), \quad \forall x \in X \tag{2.35}$$

From equations (2.27)-(2.31),it is concluded that

$$\tilde{A} \cap \tilde{B} = 1 \Big/ \sum_{j=1}^{n_A} \sum_{i=1}^{n_B} \tilde{A}_e^j \cup \tilde{B}_e^i$$

$$= 1/[\underline{\mu}_{\tilde{A}}(x) \wedge \underline{\mu}_{\tilde{B}}(x), \bar{\mu}_{\tilde{A}}(x) \wedge \bar{\mu}_{\tilde{B}}(x)] \tag{2.36}$$

Proof (iii) Applying the equation (2.16) and (2.20),

$$\bar{\tilde{A}} = \overline{\sum_{j=1}^{n_A} \tilde{A}_e^j} = \sum_{j=1}^{n_A} \overline{\tilde{A}_e^j} = 1/FOU\left(\bar{\tilde{A}}\right) \tag{2.37}$$

where

$$FOU\left(\bar{\tilde{A}}\right) = \sum_{j=1}^{n_A} \overline{A}_e^j = [\underline{\mu}_{\bar{\tilde{A}}}(x), \bar{\mu}_{\bar{\tilde{A}}(x)}] \qquad \forall x \in X \tag{2.38}$$

As the MF of the complement of type-1 FS is $1 - \mu_A(x)$, it follows that

$$\mu_{\overline{A_e^j}}(x) = 1 - \mu_{A_e^j}(x) \tag{2.39}$$

The equation (2.34) is a collection of functions that has a lower bounding and upper bounding function, therefore

$$\bar{\mu}_{\bar{\tilde{A}}}(x) = \sup_{\forall j}\left[1 - \mu_{A_e^j}(x_k)\right]$$

$$= 1 - \underline{\mu}_{\tilde{A}}(x), \quad \forall x \in X \tag{2.40}$$

$$\bar{\mu}_{\bar{\tilde{A}}}(x) = \inf_{\forall j}\left[1 - \mu_{A_e^j}(x_k)\right]$$

$$= 1 - \bar{\mu}_{\tilde{A}}(x), \quad \forall x \in X \tag{2.41}$$

The right hand parts of the equation (2.36) and (2.37) are obtained by assuming the facts that $\bar{\mu}_{\tilde{A}}(x) \geq \underline{\mu}_{\tilde{A}}(x)$ is always true; therefore it is always true that $1 - \underline{\mu}_{\tilde{A}}(x) \geq 1 - \bar{\mu}_{\tilde{A}}(x)$. From the equations (2.33), (2.34), (2.36) and (2.37), it is concluded that

$$\bar{\bar{A}} = 1 \Big/ \sum_{j=1}^{n_A} \overline{A}_e^j = 1/[1 - \bar{\mu}_{\tilde{A}}(x), 1 - \underline{\mu}_{\tilde{A}}(x)], \qquad \forall x \in X \tag{2.42}$$

An example with all the above set operations is explained as follows.

Example:

Let $\tilde{A}$ and $\tilde{B}$ are the two type-2 fuzzy sets given by

$\tilde{A}$ = (0.5/0.4+0.9/0.7+0.7/0.9)/1+ (0.5/0.6+0.9/0.8+1/0.9)/2+ (0.5/0.3+0.9/0.5+0.7/0.8)/3

$\tilde{B}$= (0.9/0.3)/1+ (0.5/0.4+0.9/0.8)/2+ (0.9/0.6+0.5/0.9)/3

for $x = 1$

$\mu_{\tilde{A}\cup\tilde{B}}(1) = (0.5 \wedge 0.9)/(0.4 \vee 0.3) + (0.9 \wedge 0.9)/(0.7 \vee 0.3) + (0.7 \wedge 0.9)/(0.9 \vee 0.3)$

$= 0.5/0.4+0.9/0.7+0.7/0.9$

for $x = 2$

$\mu_{\tilde{A}\cup\tilde{B}}(2) = (0.5 \wedge 0.5)/(0.6 \vee 0.4) + (0.5 \wedge 0.9)/(0.6 \vee 0.8) + (0.9 \wedge 0.5)/(0.8 \vee 0.4)+$
$(0.9 \wedge 0.9)/(0.8 \vee 0.8) + (1 \wedge 0.5)/(0.9 \vee 0.4) + (1 \wedge 0.9)/(0.9 \vee 0.8)$

$= 0.5/0.6+0.5/0.8+0.5/0.8+0.9/0.8+0.5/0.9+0.9/0.9$

$= 0.5/0.6+\max(0.5, 0.5, 0.9)/0.8+\max(0.5, 0.9)/0.9$

$= 0.5/0.6+0.9/0.8+0.9/0.9$

for $x = 3$

$\mu_{\tilde{A}\cup\tilde{B}}(3) = (0.5 \wedge 0.9)/(0.3 \vee 0.6) + (0.5 \wedge 0.5)/(0.3 \vee 0.9) + (0.9 \wedge 0.9)/(0.5 \vee 0.6)+$
$(0.9 \wedge 0.5)/(0.5 \vee 0.9) + (0.7 \wedge 0.9)/(0.8 \vee 0.6) + (0.7 \wedge 0.5)/(0.8 \vee 0.9)$

$= 0.5/0.6+0.5/0.9+0.9/0.6+0.5/0.9+0.7/0.8+0.5/0.9$

$= \max(0.5, 0.9)/0.6+0.7/0.8+\max(0.5, 0.5, 0.5)/0.9$

$=0.9/0.6+0.7/0.8+0.5/0.9$

Therefore the union of the two given type-2 fuzzy sets can be expressed as the sum of all the three MFs,

$\tilde{A}\cup\tilde{B}$=(0.5/0.4+0.9/0.7+0.7/0.9)/1+(0.5/0.6+0.9/0.8+0.9/0.9)/2+(0.9/0.6+0.7/0.8+0.5/0.9)/3

If the given two type-2 fuzzy sets are IT-2 FSs i.e, all the secondary membership grades will be equal to 1,then

$\tilde{A} \cup \tilde{B}$ = (1/0.4+1/0.7+1/0.9)/1+(1/0.6+1/0.8+1/0.9)/2+(1/0.6+1/0.8+1/0.9)/3

for $x = 1$

$\mu_{\tilde{A}\cap\tilde{B}}(1) = (0.5 \wedge 0.9)/(0.4 \wedge 0.3) + (0.9 \wedge 0.9)/(0.7 \wedge 0.3) + (0.7 \wedge 0.9)/(0.9 \wedge 0.3)$

$= 0.5/0.3+0.9/0.3+0.7/0.3$

$=$ max (0.5, 0.9, 0.7)/0.3

$=0.9/0.3$

for $x = 2$

$\mu_{\tilde{A}\cap\tilde{B}}(2) = (0.5 \wedge 0.5)/(0.6 \wedge 0.4) + (0.5 \wedge 0.9)/(0.6 \wedge 0.8) + (0.9 \wedge 0.5)/(0.8 \wedge 0.4)+$
$(0.9 \wedge 0.9)/(0.8 \wedge 0.8) + (1 \wedge 0.5)/(0.9 \wedge 0.4) + (1 \wedge 0.9)/(0.9 \wedge 0.8)$

$= 0.5/0.4+0.5/0.6+0.5/0.4+0.9/0.8+0.5/0.4+0.9/0.8$

$=$ max (0.5, 0.5, 0.5)/0.4+0.5/0.6+max (0.9, 0.9)/0.8

$= 0.5/0.4+0.5/0.6+0.9/0.8$

for $x = 3$

$\mu_{\tilde{A}\cap\tilde{B}}(3) = (0.5 \wedge 0.9)/(0.3 \wedge 0.6) + (0.5 \wedge 0.5)/(0.3 \wedge 0.9) + (0.9 \wedge 0.9)/(0.5 \wedge 0.6)$
$+(0.9 \wedge 0.5)/(0.5 \wedge 9) + (0.7 \wedge 0.9)/(0.8 \wedge 0.6) + (0.7 \wedge 0.5)/(0.8 \wedge 0.9)$

$=0.5/0.3+0.5/0.3+0.9/0.5+0.5/0.5+0.7/0.6+0.5/0.8$

$=$ max (0.5, 0.5)/0.3+max (0.9, 0.5)/0.5+0.7/0.6+0.5/0.8

$= 0.5/0.3 +0.9/0.5+0.7/0.6+0.5/0.8$

So, the intersection of $\tilde{A}$ and $\tilde{B}$ is

$\tilde{A} \cap \tilde{B}$= (0.9/0.3)/1+(0.5/0.4+0.5/0.6+0.9/0.8)/2+(0.5/0.3 +0.9/0.5+0.7/0.6+0.5/0.8)/3

If the given two type-2 fuzzy sets are IT-2, then

$\tilde{A} \cap \tilde{B} = (1/0.3)/1+ (1/0.4+1/0.6+1/0.8)/2+ (1/0.3 +1/0.5+1/0.6+1/0.8)/3$

Let the membership function of the type-2 fuzzy set $\tilde{A}$ is given by

$\mu_{\tilde{A}}(x) = 0.3/0.4+0.6/0.7+1/0.8,$ then its complement will be

$\mu_{\overline{\tilde{A}}}(x) = 0.3/(1\text{-}0.4)+0.6/(1\text{-}0.7)+1/(1\text{-}0.8)$

$= 0.3/0.6+0.6/0.3+1/0.2$

Similarly if $\mu_{\tilde{A}}(x) = 1/0.5+1/0.7+1/0.8$ i.e MF of IT-2 FS then

$\mu_{\overline{\tilde{A}}}(x) = 1/0.5+1/0.3+1/0.2$

2.6 Conclusion

This chapter gives an insight into the interval type-2 fuzzy logic system. A brief introduction on type-2 fuzzy sets is presented followed by a description on interval type-2 fuzzy sets. Different operation on interval type-2 fuzzy sets like union, intersection and complement are discussed with suitable examples. The structure of the interval type-2 fuzzy logic controller is presented and the roles of individual blocks used in the structure are discussed thoroughly.

Chapter 3

Design and Implementation of Type-2 FLC for grid connected DFIG

3.1 Introduction

The increasing concerns about the energy demands, fossil fuel reserves and environmental pollution draw a special attention towards alternate energy sources, especially to renewable energy field. In many countries, wind energy has become a major source of renewable energy generation due to the many advantages [62, 169].

In the preliminary days, wind energy conversion systems with fixed speed induction generators have contributed a significant portion in the renewable share of energy production. Recently, the use of doubly fed induction generators (DFIGs) in wind power generation has received an increasing attention, because of its ability to control active and reactive powers and also support variable speed operation. Other advantages of the doubly fed induction generator (DFIG) topology are the converters required are rated at only 20 % to 30 % of the generator rated power, efficient power capture and reduced mechanical stresses [70].

The schematic diagram of wind turbine coupled to a DFIG system is shown in Figure3.1. The turbine is coupled to a gear box to attain the rated speed of the generator. Unlike a conventional fixed speed induction generator, the DFIG delivers power to the grid from stator as well as rotor. The stator is directly connected to the grid through a transformer and delivers major portion of the electric power converted from wind. The rotor is connected through a frequency converter, which comprises two self commutated pulse width modulation (PWM) converters known as rotor side converter (RSC) and grid side converter (GSC). The capacitor acts as a dc voltage source, decoupling the operation of the two converters. The rotor side converter controls the rotor voltages to track the reference power inputs and the grid side converter is used for maintaining the dc link voltage at constant level. The DFIG output parameters such as torque, speed, stator real/reactive power and rotor real/reactive power can be controlled by controlling the back-to-back converters independently through a defined vector control approach [59].

The drawback of DFIG in wind energy systems is that, it is very sensitive to voltage variations, generally caused by grid faults, load changes and other disturbances in the

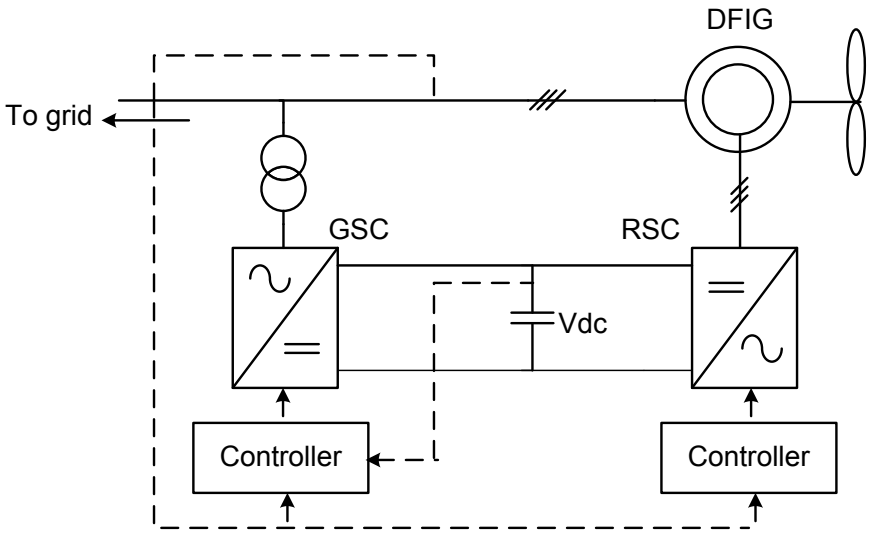

Figure 3.1: Schematic diagram of the DFIG and converters

network. The network faults cause a voltage dip at the connection point, which leads to an increased current in the stator windings. The magnetic coupling between stator and rotor reflects the stator current in the rotor windings that leads to damage of the rotor side converter and DC link capacitor. In general, for the safety of the converter system, the wind generators have been designed to get disconnected fast from the grid if a grid fault causes a large voltage drop. However, the sudden disconnection from the grid, poses many challenges in terms of reliability and stability when the penetration levels of wind farms are very high [47]. This chapter introduces the basic concepts of application of type-2 fuzzy logic for DFIG operation, which lays the background for better understanding of materials in the subsequent chapters.

3.1.1 Problem Description

For reliable and stable operation of the grid, the recent grid codes demand fault ride through (FRT) capability from the wind turbines. Therefore, for effective grid interaction, the wind power generators must be able to withstand network disturbances that are successfully eliminated. In the literature, distinct control schemes are suggested for FRT of variable speed wind generators [51, 63, 96, 171]. In [157, 178], the converters are controlled by employing direct feedback of torque and power in the cascaded control loops for enhancing the reliability of grid operation. The problem of reactive power control during grid faults is addressed using different energy storage devices and by varying the number of control loop parameters [125]. Application of FACTS devices for enhancing the LVRT capability has been investigated in [124]. Most of these control schemes are based on either stator

flux or voltage oriented control and uses conventional PI controllers accessing, references from the stator and rotor parameters. However, in all the above schemes, tuning the PI gains is a challenging task when the plant is nonlinear and parameters are uncertain, also requires the knowledge of dynamic modelling and behaviour of the DFIG.

Recent reviewing studies on DFIG shows that type-1 fuzzy logic controllers presents a better performance than the traditional PI controllers in terms of tracking terminal voltage, active and reactive power in the presence of network disturbances [35, 138]. In general, the rules and membership functions of FLC are chosen based on experience and knowledge of experts. However, the type-1 fuzzy sets cannot take account of uncertainty in membership functions and rules which vary from case to case.

Acknowledging the limitations of conventional PI and type-1 fuzzy controllers, this chapter proposes a new control strategy with type-2 fuzzy sets which can address the above issues. The type-2 fuzzy sets with its third dimension in membership function and foot print of uncertainty (FOU) offers an extra degree of freedom in the design of the controller. By choosing an appropriate FOU, a smooth control surface can be generated that enables the controller to handle the network faults. The special features of the type-2 FLC can avoid frequent retuning of the controller parameters when there is an uncertainty in the operating conditions [19, 118].

In this chapter, at first, mathematical model of the DFIG is presented. As a preliminary study, the initial designs of the controller and simulation models are developed in MATLAB/Simulink. This study mainly focuses on design of type-2 FLC, to investigate whether the special features of the type-2 FLC are useful in dealing with the uncertainties in the plant model. Type-2 FLC is designed with minimum parameters and the performance is compared with that of type-1 FLC. In order to realize the effect of FOU on the output performance, an optimization problem is formed to optimize the MF parameters using genetic algorithm. The system model shown in Figure 3.1 is considered for all the simulations and analysis.

Secondly, for the analysis with real time simulations, the same system model in Figure 3.1 is considered for implementing in RSCAD software. Afterwards, the type-2 FLC is designed and implemented for the rotor side converter (RSC) of DFIG. To evaluate the feasibility of the controller for real-time applications, at first, the error signals in RSCAD model are converted to analogue signals as controller input, then processed through type-2 FLC with HIL configuration, and fed back to the RTDS as an actuating input. The performance of the type-2 FLC is compared with that of PI and type-1 FLC for a three phase

short circuit fault. Further, the validity of the proposed controller for parameter uncertainties is confirmed by analyzing the performances of an unbalanced fault and variable wind speed conditions.

3.2 Modeling of DFIG

The mathematical modelling equations of DFIG, expressed in the space vector form, referring to arbitrary reference frame, results in [136, 162]

$$\begin{cases} \vec{v}_s = R_s\vec{i}_s + j\omega_s\vec{\lambda}_s + \frac{d\vec{\lambda}_s}{dt} \\ \vec{v}_r = R_r\vec{i}_r + j(\omega_s - \omega_r)\vec{\lambda}_r + \frac{d\lambda_r}{dt} \end{cases} \tag{3.1}$$

where $\vec{v}_s$ and $\vec{i}_s$ are the stator voltage(V) and current (A) vectors; R_s and R_r are the stator and rotor resistances (Ω); ω_s and ω_r are the stator and rotor electrical frequencies (rad/s); $\vec{\lambda}_s$ and $\vec{\lambda}_r$ are the stator and rotor flux linkage vectors (Wb), respectively.

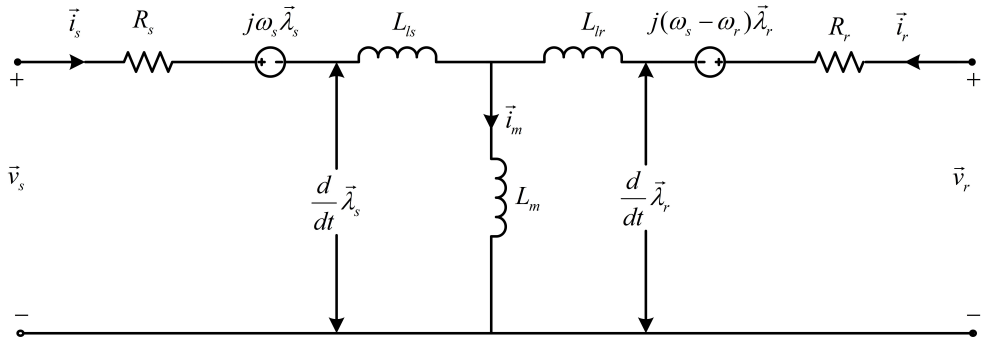

Figure 3.2: Space vector equivalent circuit of induction generator

The flux linkages $\vec{\lambda}_s$ and $\vec{\lambda}_r$ can be expressed as

$$\begin{cases} \vec{\lambda}_s = (L_{ls} + L_m)\vec{i}_s + L_m\vec{i}_r = L_{ss}\vec{i}_s + L_m\vec{i}_r \\ \vec{\lambda}_r = (L_{lr} + L_m)\vec{i}_r + L_m\vec{i}_s = L_{rr}\vec{i}_r + L_m\vec{i}_s \end{cases} \tag{3.2}$$

where L_{ss} , L_{rr}, are the self-inductances of stator and rotor(H); L_m is the mutual inductance(H); L_{ls} , L_{lr} are the leakage inductances of stator and rotor(H). The above equations constitute the space-vector model of the induction generator, whose equivalent circuit representation is given in Figure 3.2. Since the synchronous reference frame model is widely used for control analysis, the above model is transformed to synchronous reference frame and the resulted equations are as follows . The *dq*- axis model can be derived as

$$\begin{cases} \vec{v}_s = v_{ds} + jv_{qs}; \vec{i}_s = i_{ds} + ji_{qs}; \vec{\lambda}_s = \lambda_{ds} + j\lambda_{qs} \\ \vec{v}_r = v_{dr} + jv_{qr}; \vec{i}_r = i_{dr} + ji_{qr}; \vec{\lambda}_r = \lambda_{dr} + j\lambda_{qr} \end{cases} \tag{3.3}$$

Substituting the equation (3.3) in equation (3.1) and (3.2), the dq-axis components of the voltages and flux are obtained as

$$\begin{cases} v_{ds} = R_s i_{ds} - \omega_s \lambda_{qs} + \frac{d\lambda_{ds}}{dt} \\ v_{qs} = R_s i_{ds} + \omega_s \lambda_{ds} + \frac{d\lambda_{qs}}{dt} \end{cases} \tag{3.4}$$

$$\begin{cases} v_{dr} = R_r i_{dr} - (\omega_s - \omega_r)\lambda_{qr} + \frac{d\lambda_{dr}}{dt} \\ v_{qr} = R_r i_{qr} + (\omega_s - \omega_r)\lambda_{dr} + \frac{d\lambda_{qr}}{dt} \end{cases} \tag{3.5}$$

$$\begin{cases} \lambda_{ds} = L_{ss} i_{ds} + L_m i_{dr} \\ \lambda_{qs} = L_{ss} i_{qs} + L_m i_{qr} \end{cases} \tag{3.6}$$

$$\begin{cases} \lambda_{dr} = L_{rr} i_{dr} + L_m i_{ds} \\ \lambda_{qr} = L_{rr} i_{qr} + L_m i_{qs} \end{cases} \tag{3.7}$$

The subscripts d and q denote the direct and quadrature axis components of the reference frame. From the above equations the stator currents are calculated as

$$\begin{cases} i_{ds} = \frac{\lambda_{ds} - L_m i_{dr}}{L_{ss}} \\ i_{qs} = \frac{\lambda_{qs} - L_m i_{qr}}{L_{ss}} \end{cases} \tag{3.8}$$

The swing equation describes the dynamic behavior of the machine which provides state variables for rotor parameters. To analyze the mechanical behavior of the system, it is necessary to describe the relation of electrical voltages and currents with swing equation. It is derived as

$$\frac{d\omega_r}{dt} = \frac{1}{J}(T_m - T_e) \tag{3.9}$$

where T_m and T_e are mechanical and electro - magnetic torques (N-m) respectively, and J is the moment of the inertia ($kg - m^2$). The electromagnetic torque in terms of voltage and current variables is expressed as

$$T_e = \frac{3P}{2}(i_{qs}\lambda_{ds} - i_{ds}\lambda_{qs}) \tag{3.10}$$

where P is the number of pole pairs. Substituting (3.8) into (3.10) yields

$$T_e = \frac{3PL_m}{2L_{ss}}(-i_{qr}\lambda_{ds} + i_{dr}\lambda_{qs}) \tag{3.11}$$

Equation 3.11 indicates that the electromagnetic torque is a function of stator flux and rotor current. The stator and rotor, active and reactive powers can be derived as, [170]

$$\begin{cases} P_s = \frac{3}{2}(v_{ds} i_{ds} + v_{qs} i_{qs}) \\ Q_s = \frac{3}{2}(v_{qs} i_{ds} - v_{ds} i_{qs}) \end{cases} \tag{3.12}$$

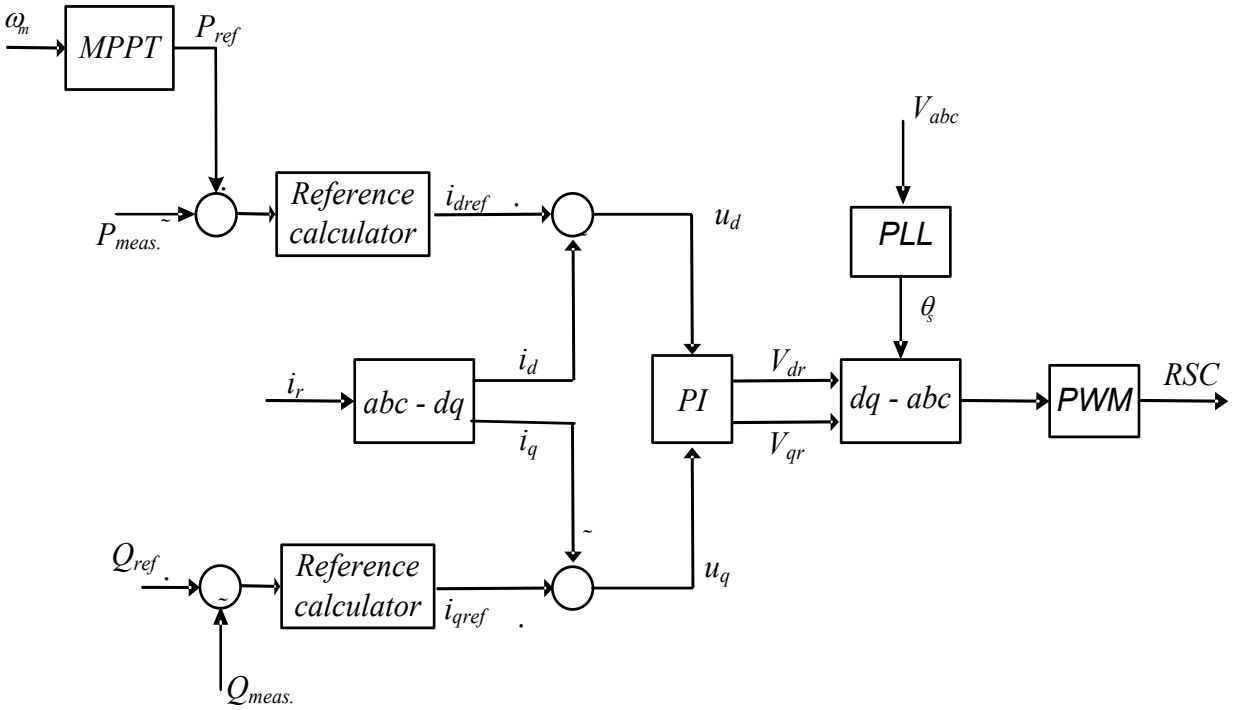

Figure 3.3: Control scheme for RSC with PI controller

$$\begin{cases} P_r = \frac{3}{2}(v_{dr}i_{dr} + v_{qr}i_{qr}) \\ Q_r = \frac{3}{2}(v_{qr}i_{dr} - v_{dr}i_{qr}) \end{cases} \tag{3.13}$$

In the stator voltage oriented control the $v_{qs} = 0$, which simplifies the output powers as

$$\begin{cases} P_s = \frac{3}{2}(v_{ds}i_{ds}) \\ Q_s = \frac{3}{2}(-v_{ds}i_{qs}) \end{cases} \tag{3.14}$$

Substituting the equation (3.8) into equation (3.14), the final expressions after simplification are obtained as

$$\begin{cases} i_{dr} = -\frac{2L_{ss}}{3v_{ds}L_m}P_s\lambda_{ds} + \frac{1}{L_m}\lambda_{ds} \\ i_{qr} = \frac{2L_{ss}}{3v_{ds}L_m}Q_s + \frac{1}{L_m}\lambda_{qs} \end{cases} \tag{3.15}$$

By substituting the expression of flux linkages from (3.6), the equation (3.15) can be further simplified as

$$\begin{cases} i_{dr} = -\frac{2L_{ss}}{3v_{ds}L_m}P_s \\ i_{qr} = \frac{2L_{ss}}{3v_{ds}L_m}Q_s - \frac{v_{ds}}{\omega_s L_m} \end{cases} \tag{3.16}$$

From the above expression it is clear that for a given stator voltage, the output powers P_s and Q_s can be controlled by controlling the rotor currents.

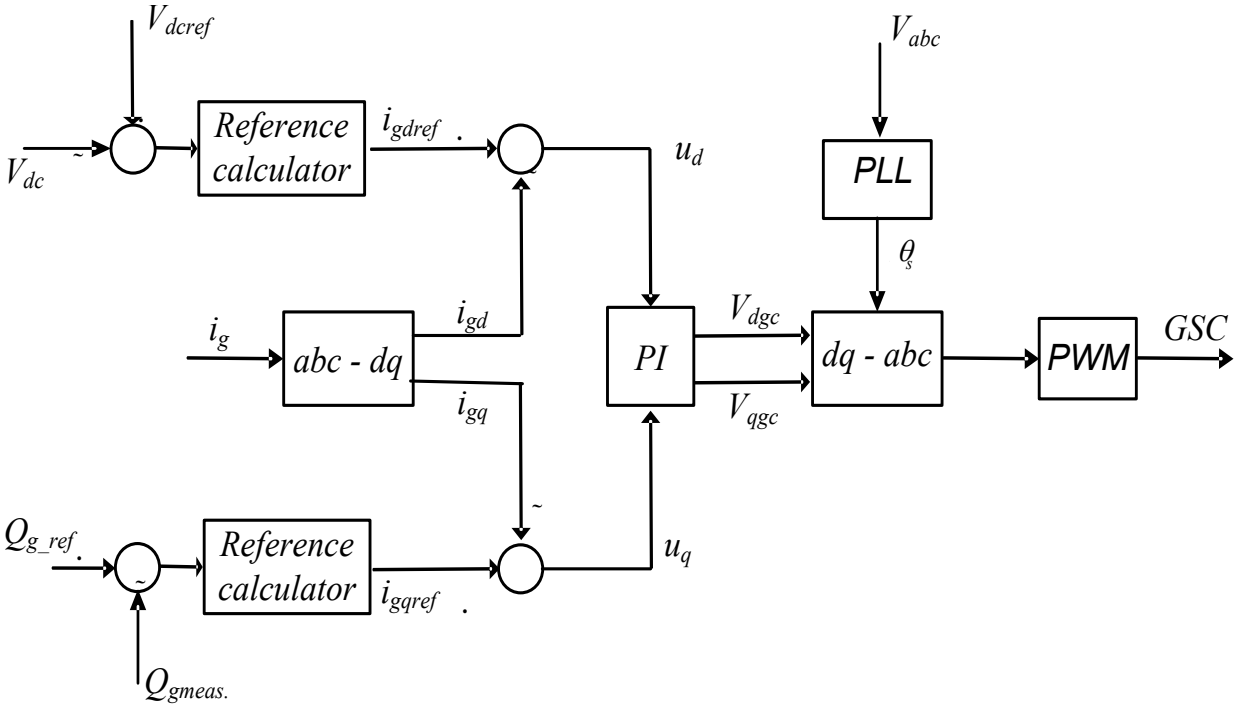

Figure 3.4: Control scheme for GSC with PI controller

3.3 Conventional PI Controller

In order to control the DFIG output powers the rotor currents are considered as controlling variables. The control objectives can be carried out through the RSC, by generating the appropriate firing pulses to its switches. The most popular approach to control the converters is $d-q$ vector control, which uses the cascaded feedback loops to track the given references. The control strategy with stator voltage oriented scheme using PI controllers is shown in Figure 3.3. The RSC generally uses a two stage controller consisting of active power controller and reactive power controller.

At first, the voltages and currents in *abc* stationary reference frame are transformed to *dq* synchronous reference frame. A three phase, phase lock loop (PLL) is used to generate the voltage angle , which is required for transformation from *abc* to *dq* and vice-versa. For a given wind speed the MPPT algorithm generates the reference active power, which is compared with the measured active power to generate a *d*-axis reference current (i_d) to the PI controller. Similarly the reactive power reference is compared with the measured power to generate the *q*-axis reference current. The reference *dq*- axis currents are compared to the measured current values, and the resulted errors are fed as input to the current controllers. The controller outputs v_{dr}, v_{qr} are the rotor voltage references in synchronous frame, which are transformed into stationary frame using *dq* to *abc* transformation. The rotor voltages

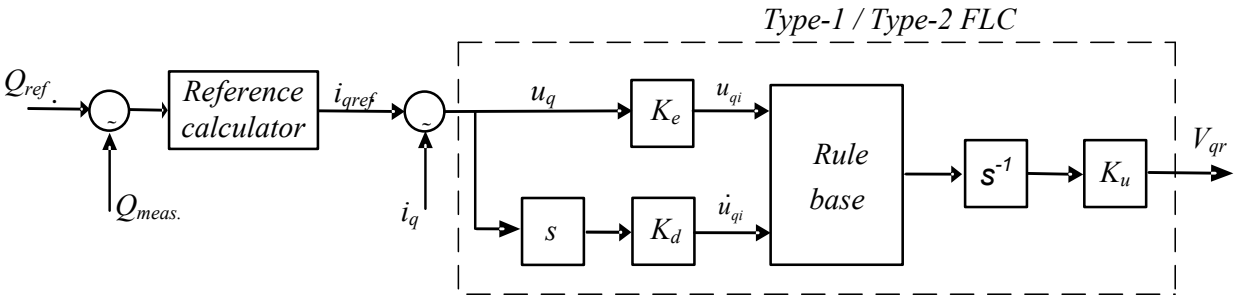

Figure 3.5: Prposed control scheme with type-1 and type-2 FLC

can serve as the three phase modulating waveforms to the Pulse width modulator, which generates the IGBT gate control pulses to drive the rotor side converter.

The grid side converter is controlled to maintain the DC link voltage at a constant level and also to control the reactive power when required. The control system of the GSC is shown in Figure 3.4. The *abc* quatities are transformed to *dq* components using a reference frame oriented to stator voltage. The dc voltage is controlled through the i_{dc} reference and the reactive power is controlled through the i_{qc} reference.

3.4 Preliminary analysis with MATLAB based simulations

The proposed control structure for reactive power control, with type-1 and type-2 FLC is shown in Figure 3.5. At first the rotor currents are converted to per unit values and then converted to a rotating reference frame to quasi DC quantities. The rotating reference frame in this case, is computed from the difference between the position of the stator flux vector and the physical rotor direct axis. This difference is generally changing and is referred to as the slip angle. By decoupling the d and q rotor currents, the electrical torque and rotor excitation current can be controlled independently. The reference value for V_{dr} is generated from the optimal power reference algorithm, which decides the optimal power output for the turbine from available wind speed, and the same for V_{qr} is defined from the set point value of the reactive power/voltage. The analysis of the current controller is explained as follows. The error signals are derived as

$$u_d = i_{dref} - i_{dr} \tag{3.17}$$

$$u_q = i_{qref} - i_{qr} \tag{3.18}$$

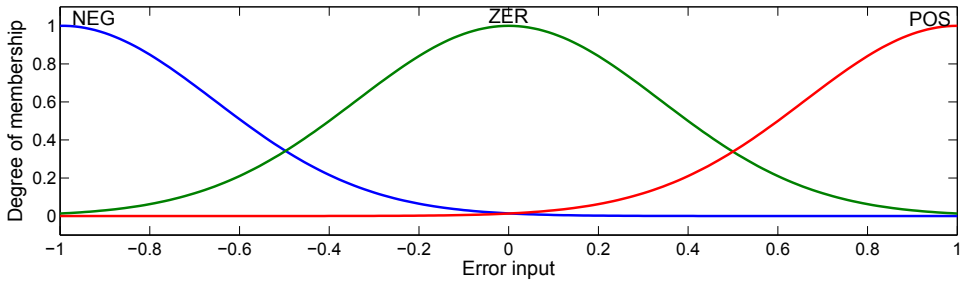

(a)

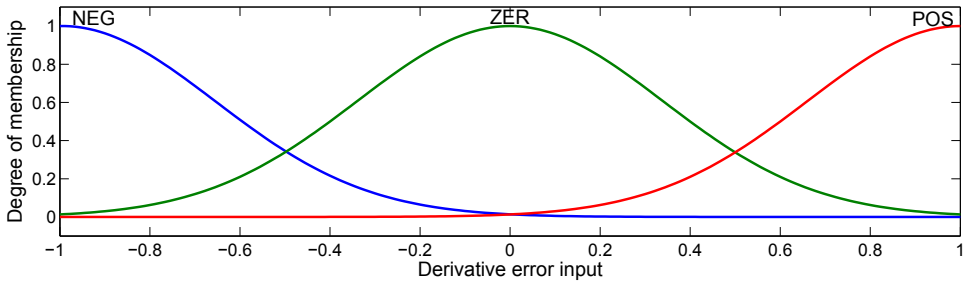

(b)

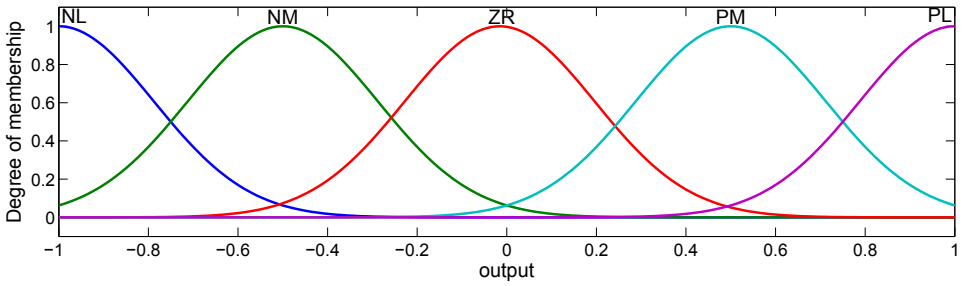

(c)

Figure 3.6: MFs for type-1 FLC (a) Input1 (b) Input2 (c)Output

And the derivative of the error signals are represented as $\dot{u}_d$ and $\dot{u}_q$, the controller gains K_e and K_d are used for scaling the error signals and K_u is used for scaling the controller output. The final controller inputs after the scaling appeared as

$$u_{qi} = K_e u_q \tag{3.19}$$

$$\dot{u}_{qi} = K_d \dot{u}_q \tag{3.20}$$

The general structure of the controller algorithm is shown in Figure 2.3. At first the crisp input signal is converted to fuzzy input using various fuzzy membership functions. A set of rules is formed to map the input with the output together known as inference mechanism. The type-2 output sets cannot be directly used for converting to crisp value due to computational limitations. For this reason the type-2 sets are converted to type-1 sets which is known as type reduction operation, then the type reduced sets are converted back to crisp value using various defuzzification techniques.

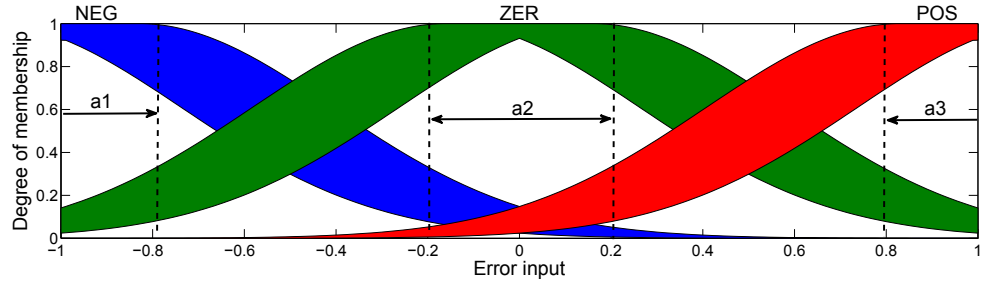

(a)

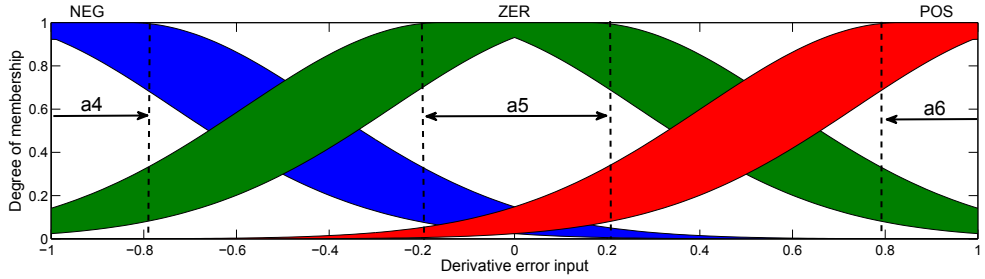

(b)

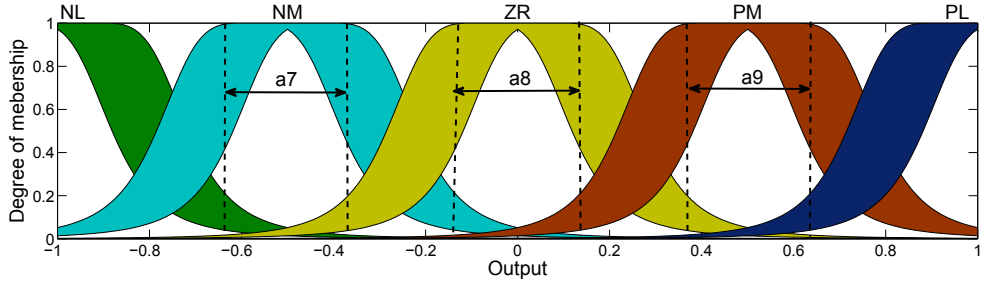

(c)

Figure 3.7: MFs for type-2 FLC (a) Input1 (b) Input2 (c)Output

The error inputs are fuzzified using three Gaussian membership functions and the output with five MFs; and the designed MFs for both type-1 and type-2 FLC are shown in Figures 3.6 and 3.7 respectively. The fuzzy sets have been defined as: NL-Negative Large, NM-Negative Medium, ZR-Zero, PL-Positive Large, PM -Positive Medium . The maximum and minimum values of the universe of discourse for all inputs and outputs are +1 to -1. The fuzzy mapping of the input variables to the output is formed with the help of IF-THEN rules and are framed as

$$If \quad u_d \quad is \quad x_1 \quad and \quad \dot{u}_d \quad is \quad y_1 \quad then \quad V_d \quad is \quad w_1$$

$$If \quad u_q \quad is \quad x_1 \quad and \quad \dot{u}_q \quad is \quad y_1 \quad then \quad V_q \quad is \quad w_2$$

In similar way, 9 rules are chosen for all the membership functions as shown in Table 3.1. The inference system uses min-method for Meet operation, max method for Join operation and Join aggregation, and min method for Meet implication. For type reduction operation that is, converting from type-2 output fuzzy sets to type-1 fuzzy sets, the height type

Table 3.1: Rules for type-2 FLC

$E/\Delta E$	NEG	ZER	POS
NEG	NL	NM	ZE
ZER	NM	ZE	PM
POS	ZE	PM	PL

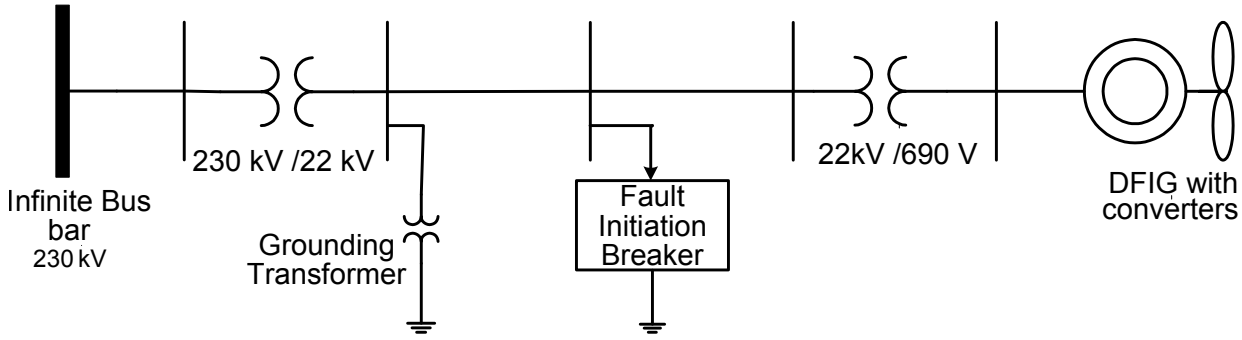

Figure 3.8: System model for real time simulations

reduction method is used. The centroid type defuzzification method is used for converting the output from fuzzy to crisp value.

The final output of the controller with the compensation is defined as

$$v_{dr}{}^{*} = v'_{dr} - (\omega_s - \omega_r)(\sigma L_r i_{qr}) \tag{3.21}$$

$$v_{qr}{}^{*} = v'_{qr} + (\omega_s - \omega_r)(L_m i_{ms} + \sigma L_r i_{dr}) \tag{3.22}$$

where the starred values are the final output, the prime terms are outputs of the type-2 fuzzy controllers and the terms in brackets are the compensation terms required to completely decouple the d and q axis voltages [136]. At last the controller outputs are converted from dq frame to ABC, and given to a pulse width modulator for generating the firing pulses to the switches.

The initial values of the controller parameters K_e, K_d, and K_u are tuned based on techniques described in [94]. To obtain the minimum variations in the control variables, several simulations are performed to tune the controller gains.

3.5 Simulations and results

To evaluate the performance of the type-2 FLC, simulations have been performed in a test system shown in Figure 3.8. The model consists of a 9 MW wind farm with six 1.5 MW

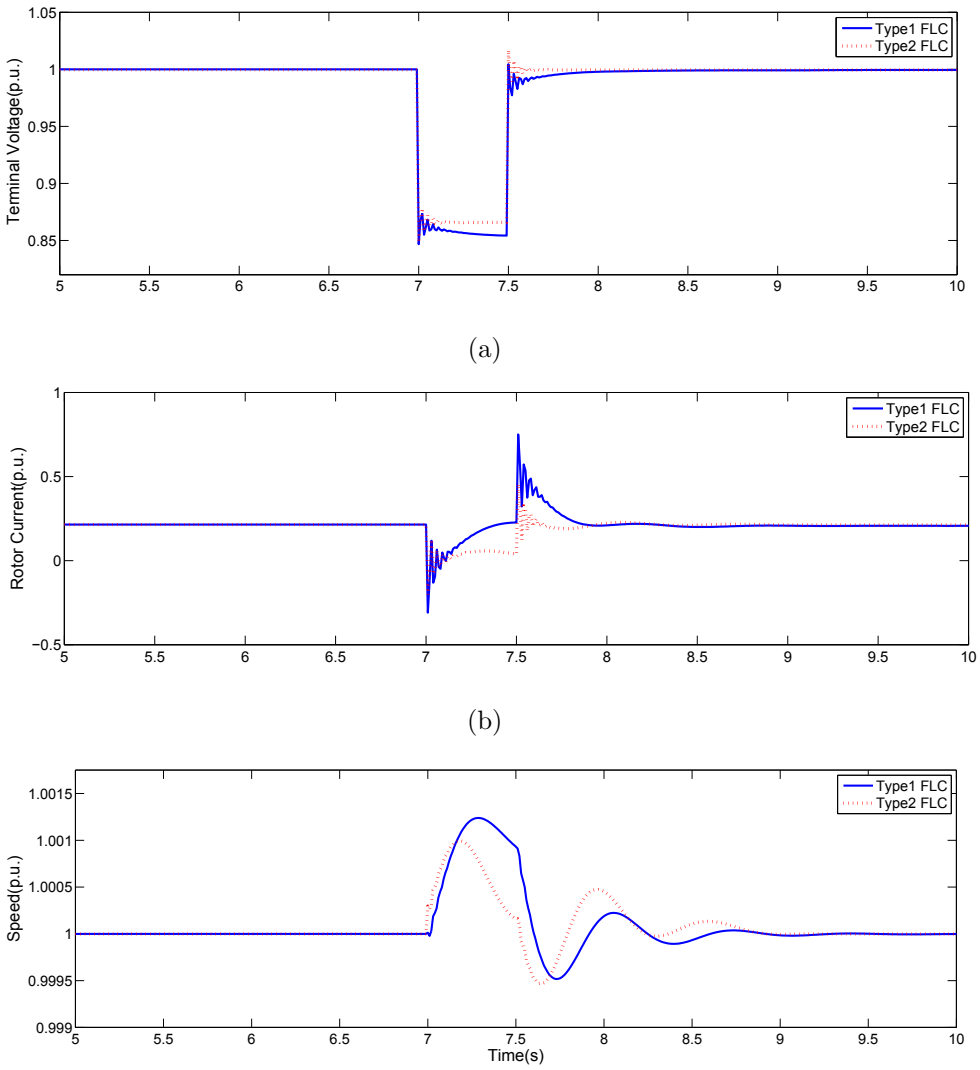

Figure 3.9: Responses for a remote fault

wind turbines connected to a 25-kV distribution system, and is extended to 120-kV grid through a 30-km, 25-kV feeder. The load is connected on the 25 kV feeders through a transformer. In order to simulate the network disturbances, a sudden load loss at 25-kV feeder and a voltage sag on 120kV system are programmed in the Simulink model. The performances of the system with the type-2 and type-1 FLC's are plotted and discussed. All the simulations in this work are performed with the following operating conditions; a constant wind speed of 12 m/s, reference terminal voltage and rotor speed at 1 p.u.

3.5.1 Fault on 120kV system

In order to analyze the impact of remote fault, a voltage drop of 0.15 p.u. lasting 0.5s is initiated at t= 7s on the 120 kV bus. The responses of terminal voltage, rotor current and rotor speed are plotted and discussed. As shown in Figure 3.9, at the instant of fault, with

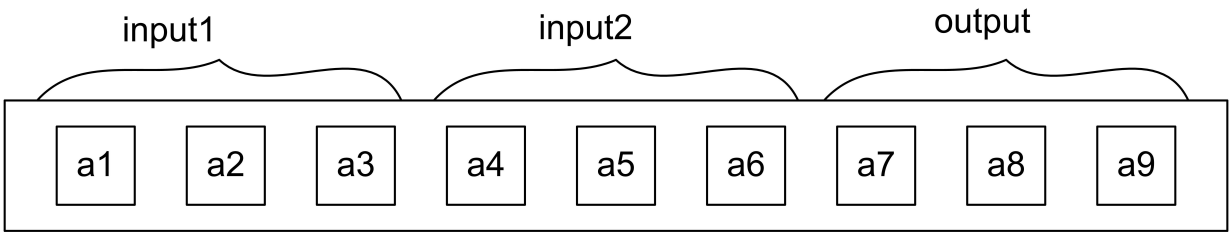

Figure 3.10: Structure of chromosome

type-1 FLC, the terminal voltage drops to 0.85 p.u; after clearing the fault the oscillations in the rotor current and speed are settled after 2s.

With the type-2 FLC, the fault voltage is maintained at 0.86 p.u. and quickly recovered to the steady state. The oscillations in the rotor speed and current are damped out much faster than that of type-1 FLC without degrading the transient performance. This shows that a properly optimized type-2 FLC may perform better than these results.

3.6 Optimization of type-2 FLC Parameters

Choosing the appropriate width of foot print of uncertainty (FOU) to represent the uncertainty in parameters, is a challenging task in designing the type-2 FLC. In the previous section, the controller parameters are chosen based on the experience and observations from the simulations results. It is observed that a large width of FOU is causing a computational delay and a small width leading to inappropriate representation of uncertainties. In order to relate the width of FOU and uncertainties representation, an optimization problem based on genetic algorithm is formulated for the acquisition of controller parameters. The main focus of this work is to verify whether the optimized setting of the FOU is improving the output response.

The mean of the Gaussian membership functions is chosen as the parameter to be optimized. Before the GA is applied, the optimization problem is converted to a suitably described function, called fitness function, which represents the performance of the solution to the problem. In this case, for simplicity, integral square error is chosen as the fitness function. Each set of variables for the given problem is encoded into a binary bit string, called chromosome. Such a string is made up of sub-strings, called genes, which correspond to each different variable. Several chromosomes representing different solutions comprise the population. In this case, 40 chromosomes each consisting of 9 genes are generated as the initial population, as depicted in Figure 3.7. As shown in Figure 3.10, the first 6 genes

Table 3.2: Parameters of GA

Elements of GA	Sselected value
Population Size	20
Elite Count	2
Crossover fraction	0.8
Migration direction	forward
Migration interval	20
Migration fraction	0.2
Generations	100

are parameters related to the input membership functions whereas the rest of the genes are related to the output.

The GA starts the evaluation of each chromosomes fitness. The repopulation of the next generation is done using three operators: reproduction, crossover, and mutation. Through reproduction, strings with high fitness (i.e., low value of the fitness function) receive multiple copies in the next generation while strings with low fitness receive fewer or even none at all. Crossover refers to taking a string, splitting it into two parts at a randomly generated crossover point and recombining it with another string which has also been split at the same crossover point. This procedure serves to promote change in the best strings which could give them even higher fitness. Mutation is the random alteration of a bit in the string which assists in keeping diversity in the population. Finally, the new population replaces the old (initial) one. This procedure continues until the specified termination condition is reached. The optimization parameters of the GA are shown in Table 3.2

3.6.1 Response for Remote fault

To evaluate the performance of the optimized type-2 FLC , simulations have been performed in the same test system used in previous section, shown in Figure3.8.

The remote fault is initiated with a voltage drop of 0.15 p.u. lasting 0.5s on the 120 kV bus. The responses of terminal voltage, rotor current and rotor speed are shown in Figure 3.11. With the optimized FLC, at the instant of fault, the terminal voltage drops to 0.87 p.u which is a significant improvement over the type-1 FLC; after clearing the fault, the oscillations in the rotor current and speed are damped out and recovered to steady state

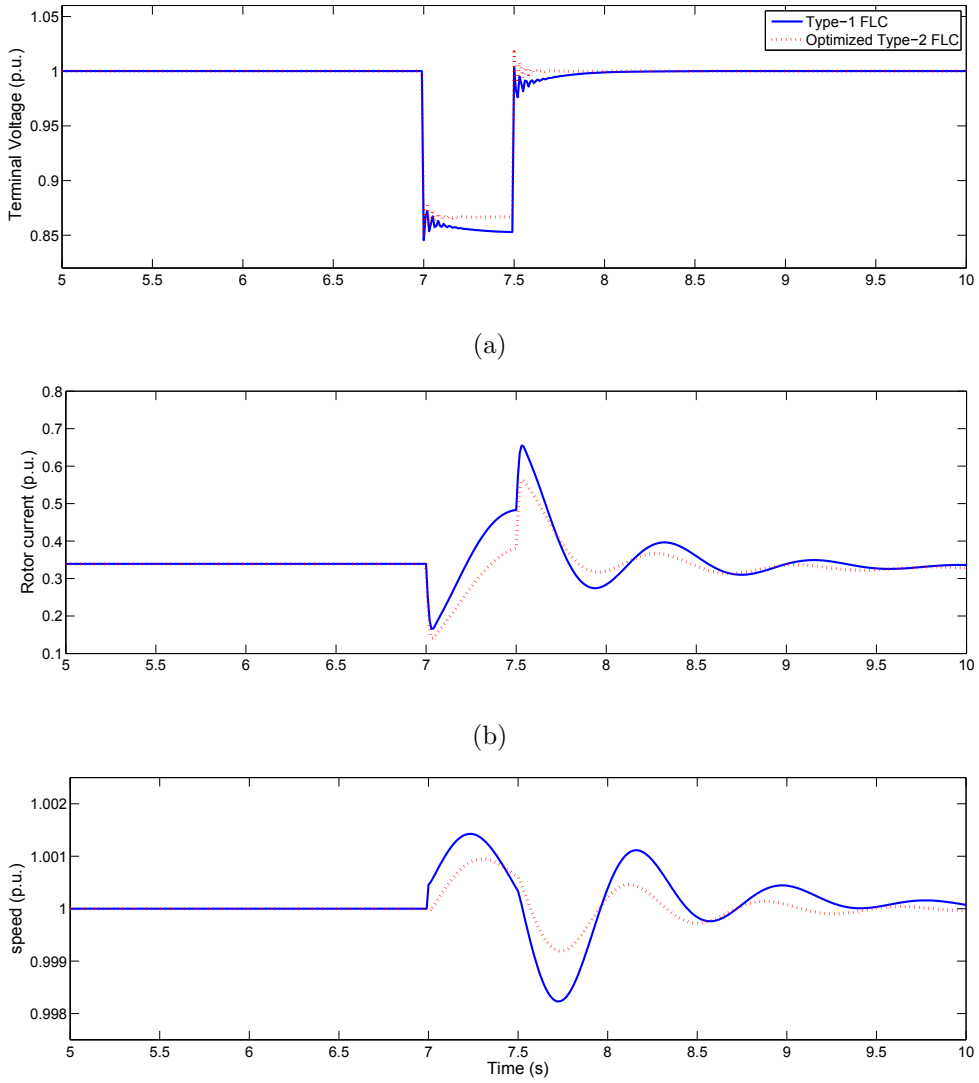

Figure 3.11: Responses for a remote fault

much faster compared to the unoptimized results. This result confirms that a properly designed type-2 FLC can perform better in the presence of uncertainties. To corroborate its applicability to practical applications, the controller needs to be tested in a real-time environment. For this purpose, the analysis done in the further sections and chapters are completely based on the real-time simulations.

3.7 Real time simulations

3.7.1 Controller Design

The controllers for MATLAB simulations are designed with minimum number of membership functions to avoid the computational delays. In this case, the controller is implemented

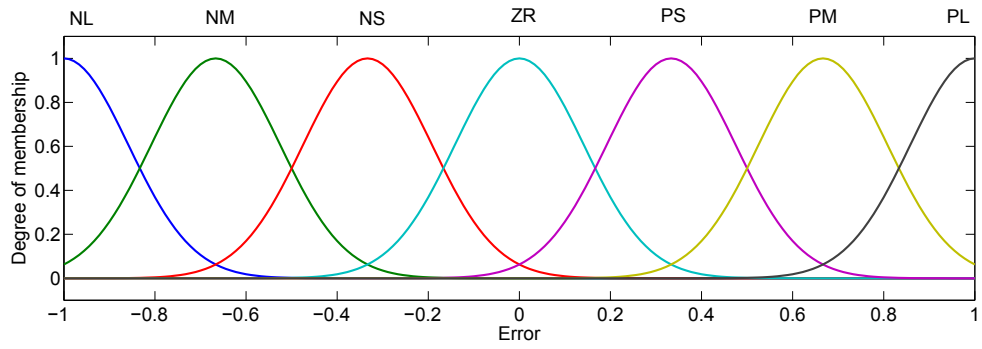

(a)

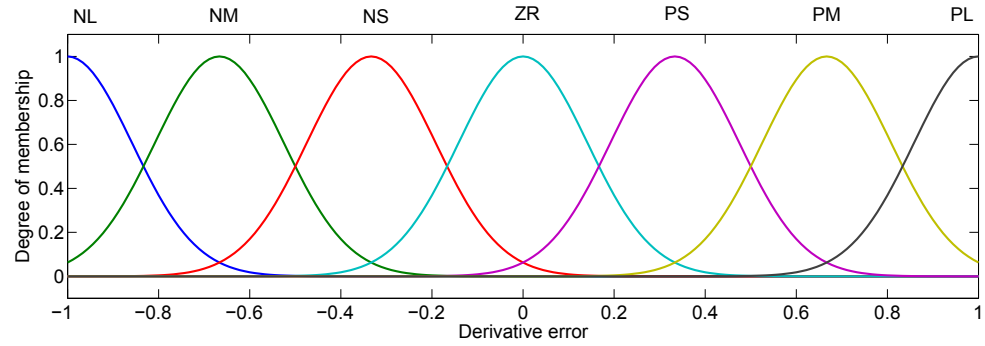

(b)

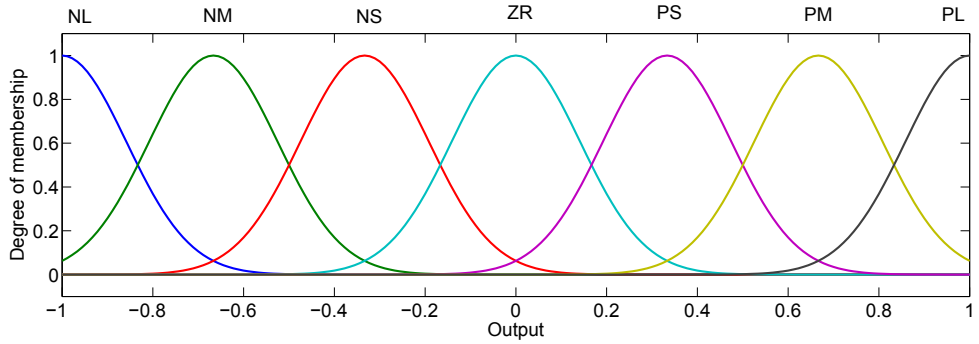

(c)

Figure 3.12: MFs for type-1 FLC (a) Input1 (b) Input2 (c)Output

on a dedicated Dspace module, which enables the choice to choose the desired number of membership functions. The designed MFs for both type-1 and type-2 FLC are shown in Figures 3.12 and 3.13 respectively. For both the inputs and output, seven Gaussian MFs are chosen with a normalized range from +1 to -1.

3.7.2 Results and Analysis

RTDS is a digital electromagnetic transient power system simulator that operates in real-time with hardware interfacing features. It facilitates real time simulation of complex power system models using parallel processors which allows simulations with a time step up to 250 ns. The RTDS platform is considered by many research laboratories as a real-time testing

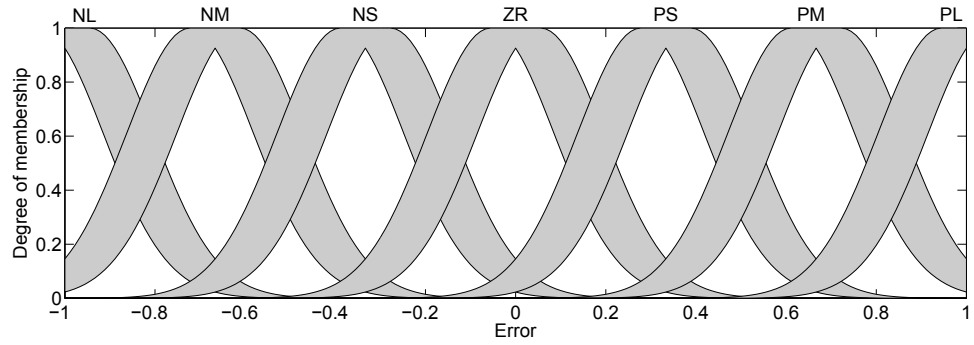

(a)

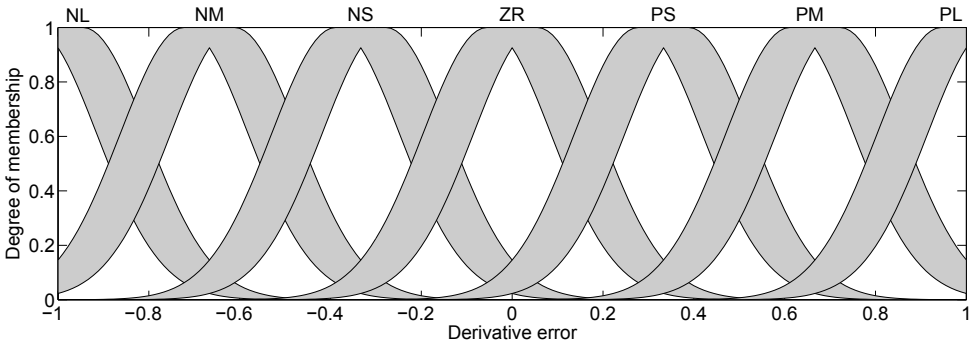

(b)

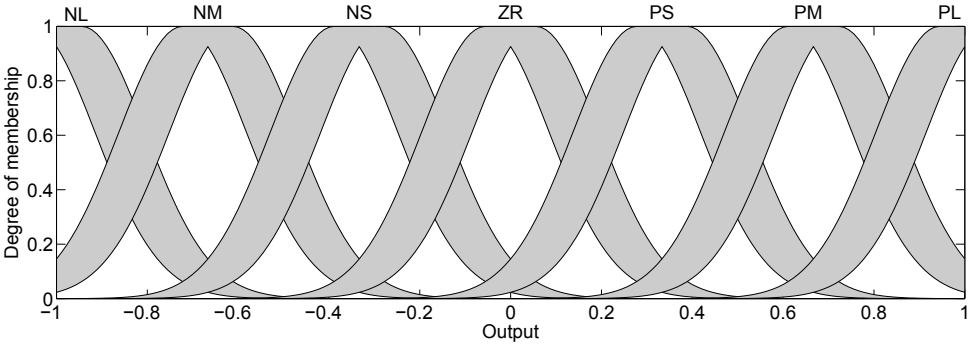

(c)

Figure 3.13: MFs for type-2 FLC (a) Input1 (b) Input2 (c)Output

module for controller prototyping and also for hardware in the loop (HIL) simulations with power system models [121, 134]. The designed system model in RSCAD is depicted in Figure 3.8. A DFIG rated 2MW, 0.69KV, 60Hz is connected to 230KV grid through a transformer. The fault initiation breaker is connected directly to the bus to initiate the fault and the crowbar circuit is connected to the rotor. To minimize losses, the power rating of the VSC is chosen to be 40% of the machine rating. Also, the rated DFIG speed is chosen to be 1.2 times synchronous speed in order to extract energy from both the rotor and the stator of the DFIG. This indicates that with the wind turbine operating at 1.0 p.u. speed, the DFIG is turning at 1.2 p.u. speed.

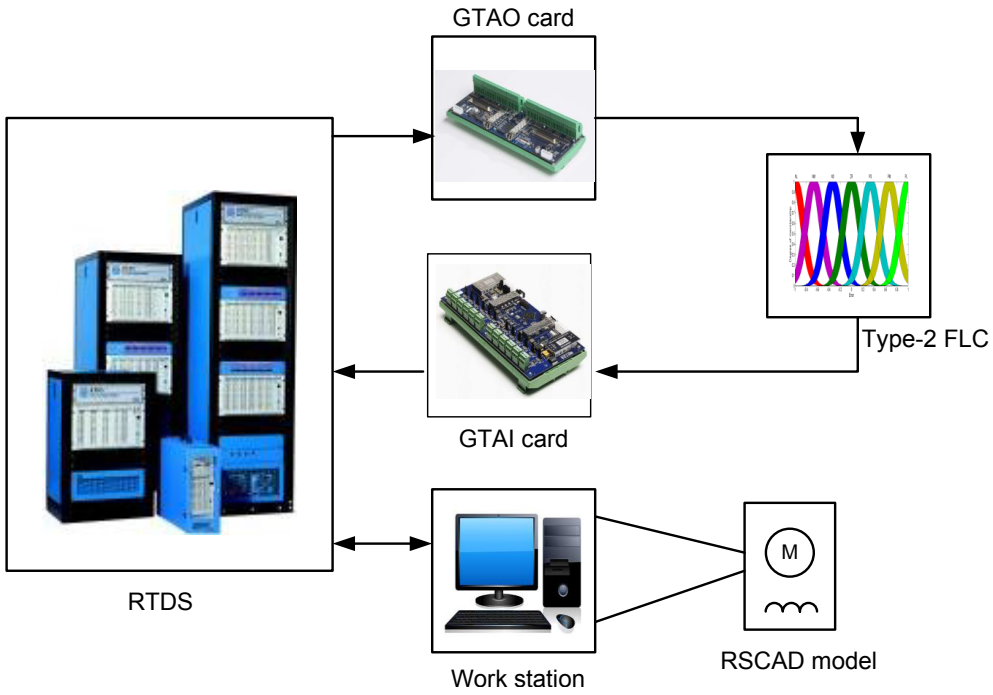

Figure 3.14: Schematic diagram of Real time simulation process

3.7.3 Hardware in loop (HIL) description

The HIL arrangement of the proposed control scheme is shown in Figure 3.14. The workstation computer compiles the RSCAD draft models and, interacts with the RTDS to execute it on the required number of processor modules. In this work, the entire plant model is implemented on a RSCAD draft model and the controller algorithm is made to execute on Dspace. After comparing the reference powers, the generated error signals in the RSCAD platform are converted to analogue signals using Gigabit transceiver analogue output (GTAO) card. GTAO facilitates scaling of digital signals to ±10V analogue output through a 16 bit Digital to Analog converter (DAC). The analogue error signals are normalized and sent to type-2 fuzzy controller algorithm which is processed through Dspace 1104 module. The controller output is fed back to RTDS through Gigabit transceiver analogue input (GTAI) card. The GTAI card comprises 16 bit A/D converters through 12 channels with a range of ±10V. The scaling factors are adjusted so that compatibility is maintained between GTAI card output and RSCAD. The experimental setup is shown in Figure 3.15.

In order to simulate the variations in parameters, the system is introduced with two different types of uncertainties in the operating conditions. Three phase faults are most common among various types of grid faults; so at first the performance of the controller is analyzed with a three phase short circuit fault. Secondly, the system is tested for unbalance fault and also variable wind speed conditions. The controller gains are tuned based on the

Table 3.3: Parameters of the controllers used in the simulations

Controller	K_e	K_d	K_u
Type-1 FLC	0.803	0.35	49.3
Type-2 FLC	0.9	0.02	51
PI controller	1.387(P)	0.02808(I)	-

Figure 3.15: Experimental setup for real time simulations

observations from the simulation results and the final values for both type-1 and type-2 FLC are listed in Table 3.3.

3.7.4 Three phase short circuit fault

The fault is applied for the duration of 0.08s, and the comparative performance of the PI and FLCs is shown in Table 3.4. The response of the system with PI controller is shown in Figure 3.16. It is observed that during the fault period the stator voltage drops to 0.1 p.u. , and settles with distorted magnitude after clearing the fault. In general, damping of current oscillations after clearing the fault, is an important factor, in maintaining the grid stability. In this case, the stator and rotor currents settles after 0.9s and 1s respectively. The oscillations in the current in turn lead to sustained oscillations in DC link voltage, and active and reactive powers.

The performance of the type-1 FLC is depicted in Figure 3.17. At the instant of fault

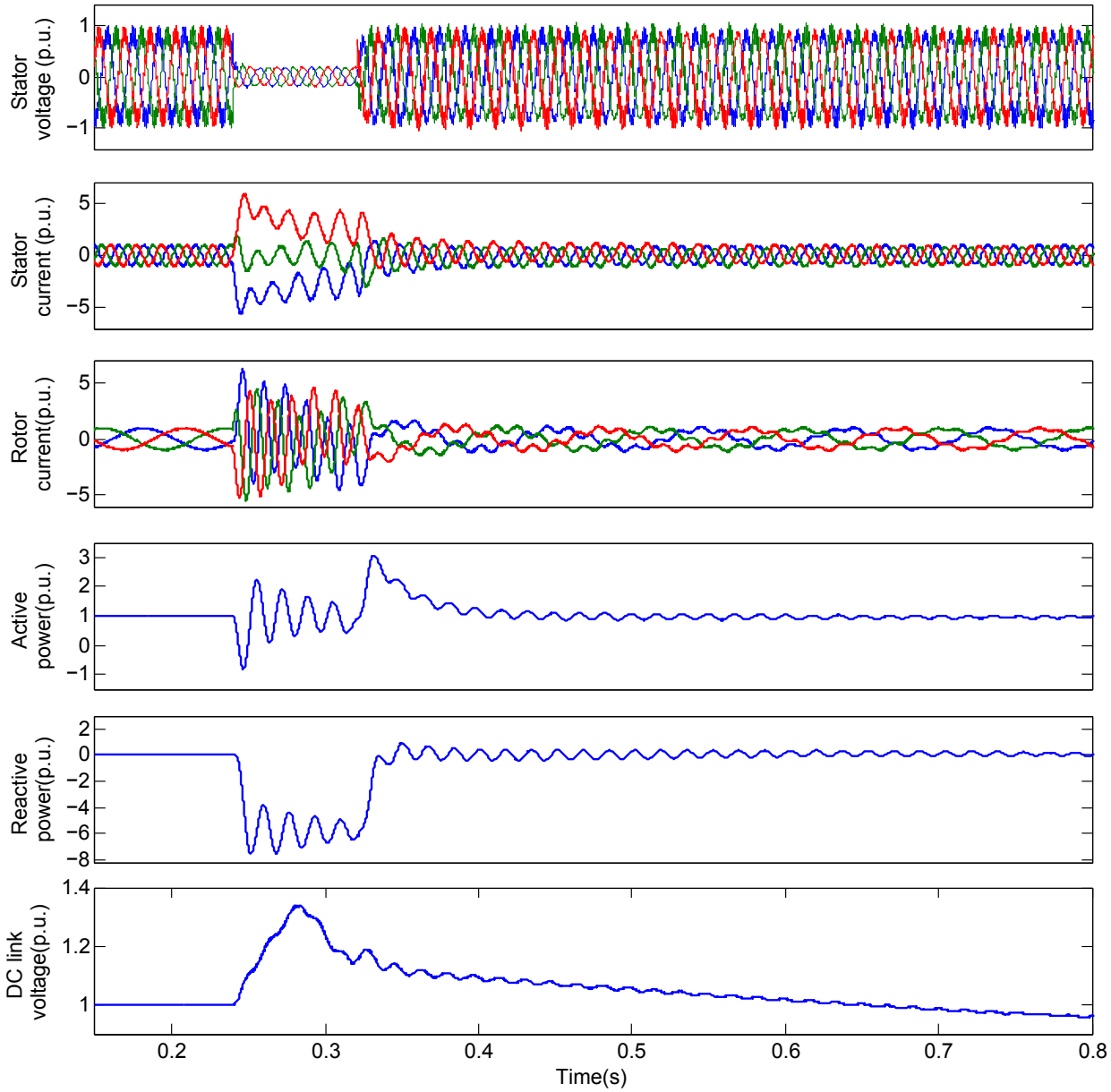

Figure 3.16: Responses for three phase short circuit fault with PI controller

the stator voltage drops to 0.15p.u., which causes the stator current to rise above its normal value, with small oscillations. The magnetic coupling between stator and rotor reflects the stator currents on rotor, leading to high currents of 5 p.u. in the rotor windings. The sudden drop in the voltage causes hindrance to the grid side converter to transfer the excess power to the grid from the rotor side converter. So, during the fault period, the excess power in the rotor side converter causes a rise in the dc link capacitor voltage to 1.341 p.u., however it has been brought down to normal value before reaching the fault clearing time. Crowbar circuit is implemented to protect the system from higher DC link voltage. The protection logic is implemented according to the standard grid codes. The active power reaches a peak value of 3.9 p.u. with damped oscillations. The reactive power

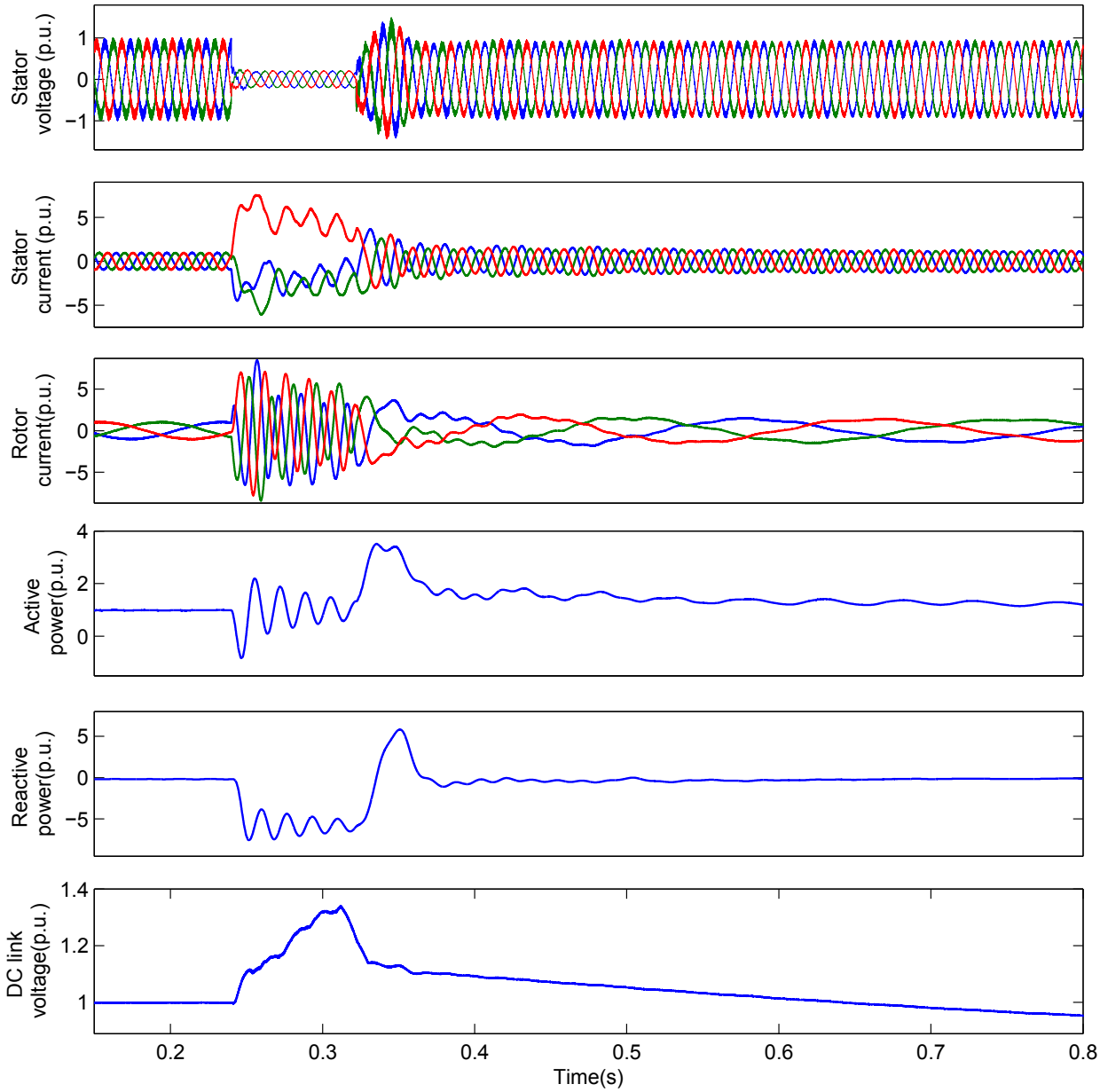

Figure 3.17: Responses for three phase short circuit fault with type-1 FLC

reaches a negative peak of 6.1p.u. during the fault period and recovered with a positive peak of 5.1 p.u.

Figure 3.18. depicts the performance of type-2 FLC for three phase fault. During the fault period the rise in stator currents is reduced by 0.85% with a small improvement in the settling time. In the PI case, the rotor current in gets distorted after clearing the fault, in contrast, the with the proposed strategy it settles within 0.2s. An improvement in terms of oscillations is also observed for dc link voltage. It is observed that the controller was able to damp out the current oscillations very fast avoiding the tripping of the protection system.

The oscillations in the active and reactive power are damped out with in 0.2s, helping

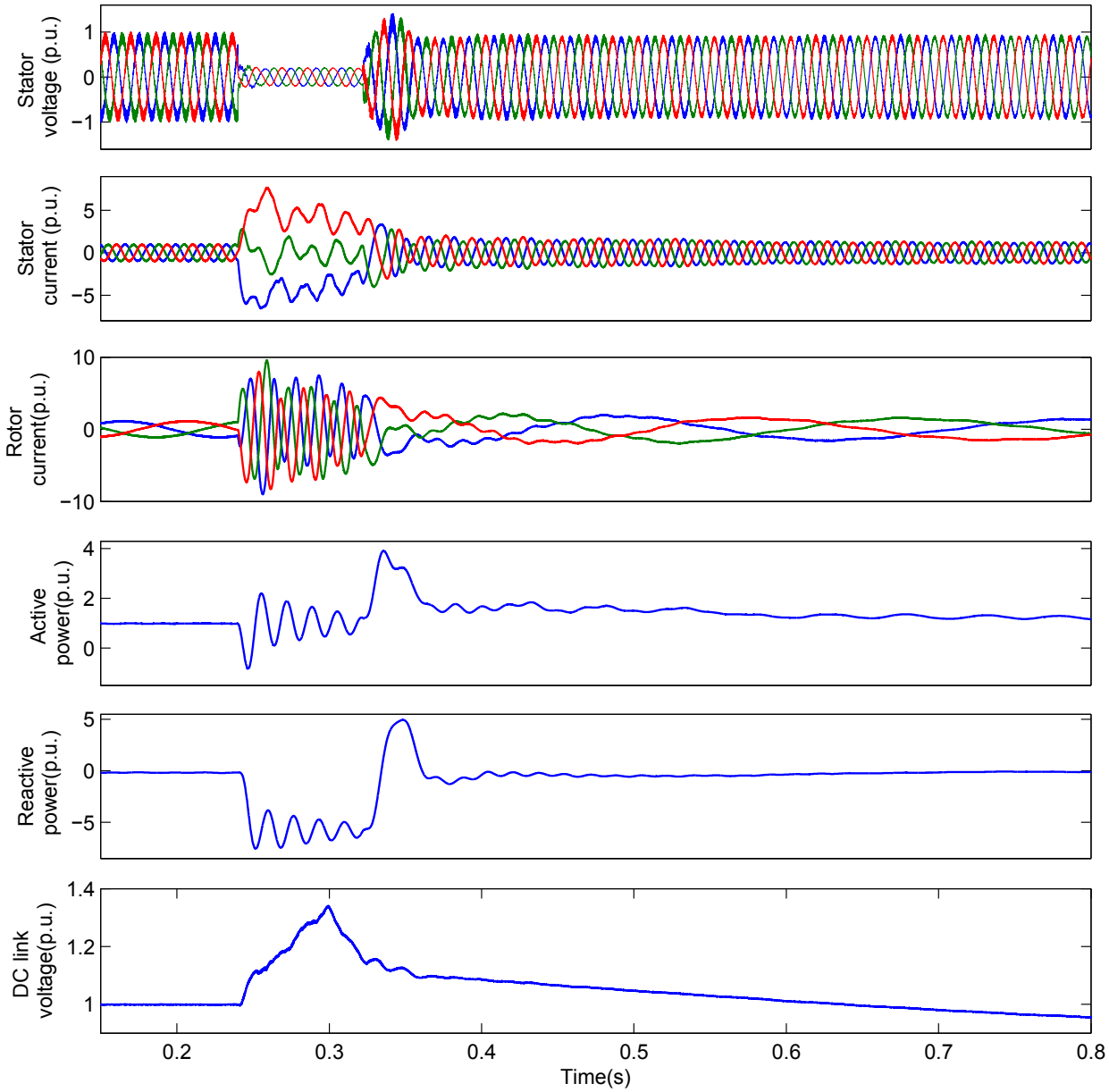

Figure 3.18: Responses for three phase short circuit fault with type-2 FLC

Table 3.4: System performance after clearing the fault

Controller	Voltage drop during fault (p.u.)	Magnitude of DC voltage (p.u.)	Stator current settling time (s)	Rotor current settling time (s)
PI	0.1	1.342	0.66	0.76
Type-1 FLC	0.13	1.341	0.36	0.46
Type-2 FLC	0.15	1.34	0.18	0.26

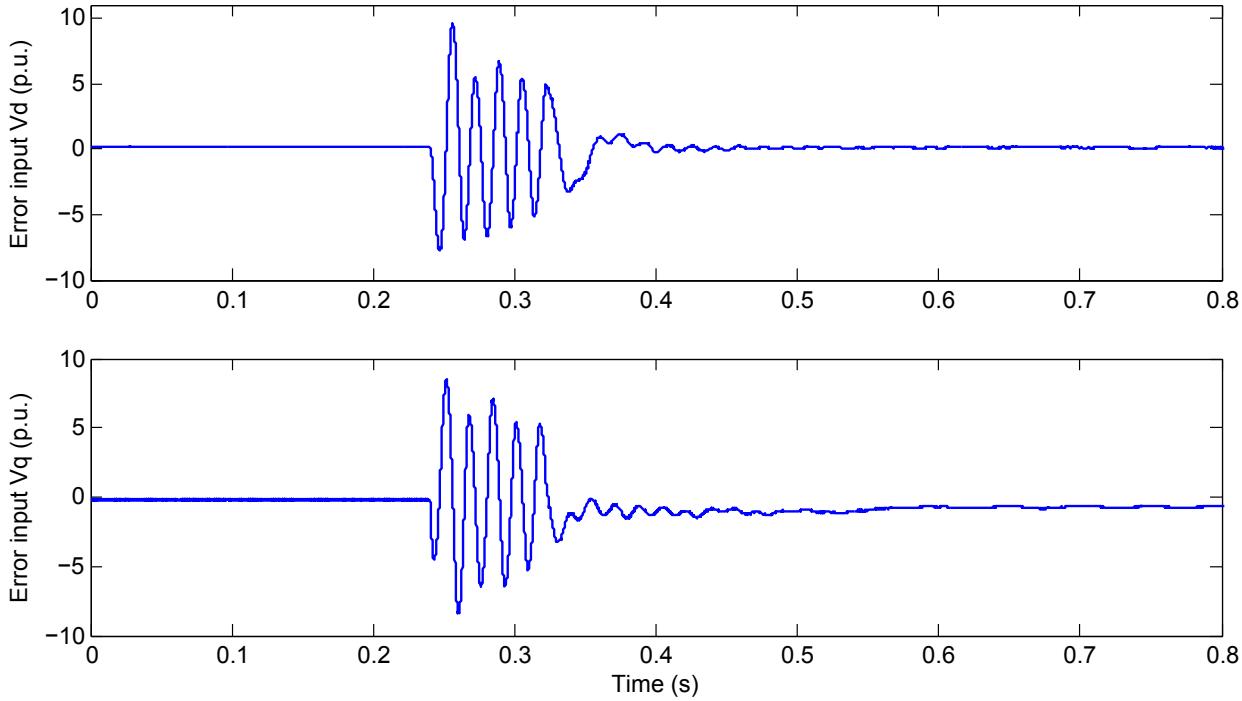

Figure 3.19: Error inputs of type-2 FLC for three phase fault

the voltage recovery much faster compared to that of PI and type-1 FLC. Figure 3.19 shows the error inputs of V_d and V_q which are used as analogue inputs for the type-2 FLC. At the instant of fault the magnitude of the error rises to 5 p.u. from normal value of 0.1p.u; the scaling gains are adjusted in such a way that the analogue error signal doesnt get saturated during the fault period.

3.7.5 Performance for variable wind speed

In this section the controller performance is analysed for variable wind speed conditions. As stated in the previous section, the optimal power algorithm decides the power output reference for a given wind speed. The controller has to track the variable reference, irrespective of operating conditions that are assumed while designing the controller parameters. In this simulation, the initial controller gains are tuned for an operating rotor speed of 1.2 p.u. at a wind speed of 12 m/s. Figure 3.20 depicts the tracking performance of the controller for wind speeds of 12 m/s and 10 m/s. When the speed is reduced to 10 m/s , the active power has reduced to 0.6 p.u. In order to capture the transition from higher reference to lower, the simulations are executed for 10s.

The change in reactive power consumption from -0.17 p.u. to -0.015 p.u. for a change in wind speed signifies the sub-synchronous operation of DFIG. The change in rotor current magnitude from 1 to 0.72 p.u. with a change in phase sequence, shows the interaction of

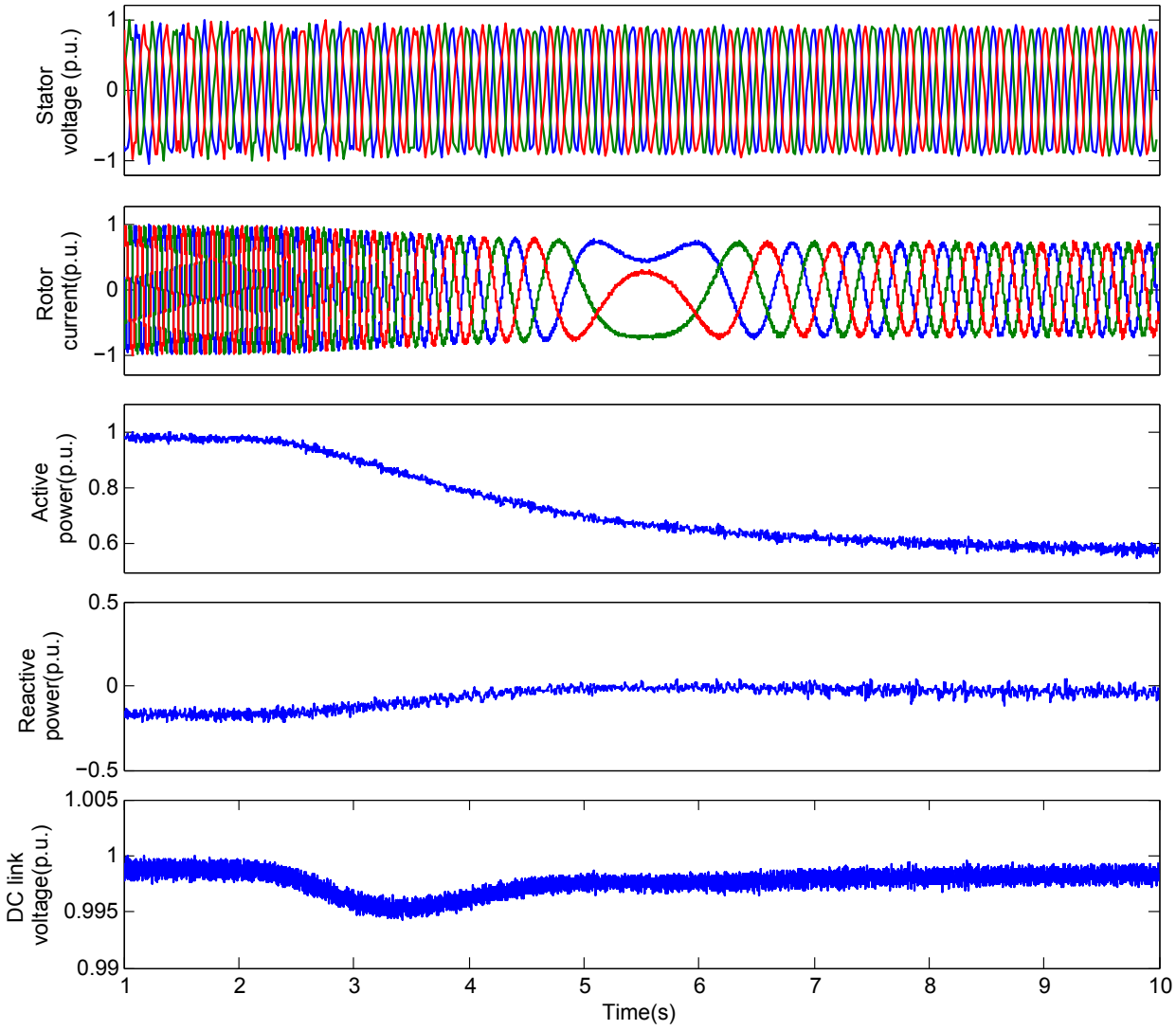

Figure 3.20: Responses with type-2 FLC for change in wind speed

RSC for super and sub synchronous rotor speeds. A small dip in the dc link voltage is observed and is recovered very fast without any oscillations. Furthermore, the constant stator voltage and frequency shows the effectiveness of the controller for uncertainties in system parameters.

3.7.6 Performance for single line to ground fault

In order to check the robustness, the controller is tested for single line to ground short circuit fault and the performance is compared with PI controller. The performance of the PI and type-2 FLC are shown in Figure 3.21 and 3.22 respectively. In PI case, after clearing the fault sustained oscillations were present in active and reactive powers for more than 0.6s. The stator voltage gets distorted after clearing the fault and settles after 1.2s. The peak amplitude of dc link voltage has reached to 1.09 p.u. and settles with small oscillations

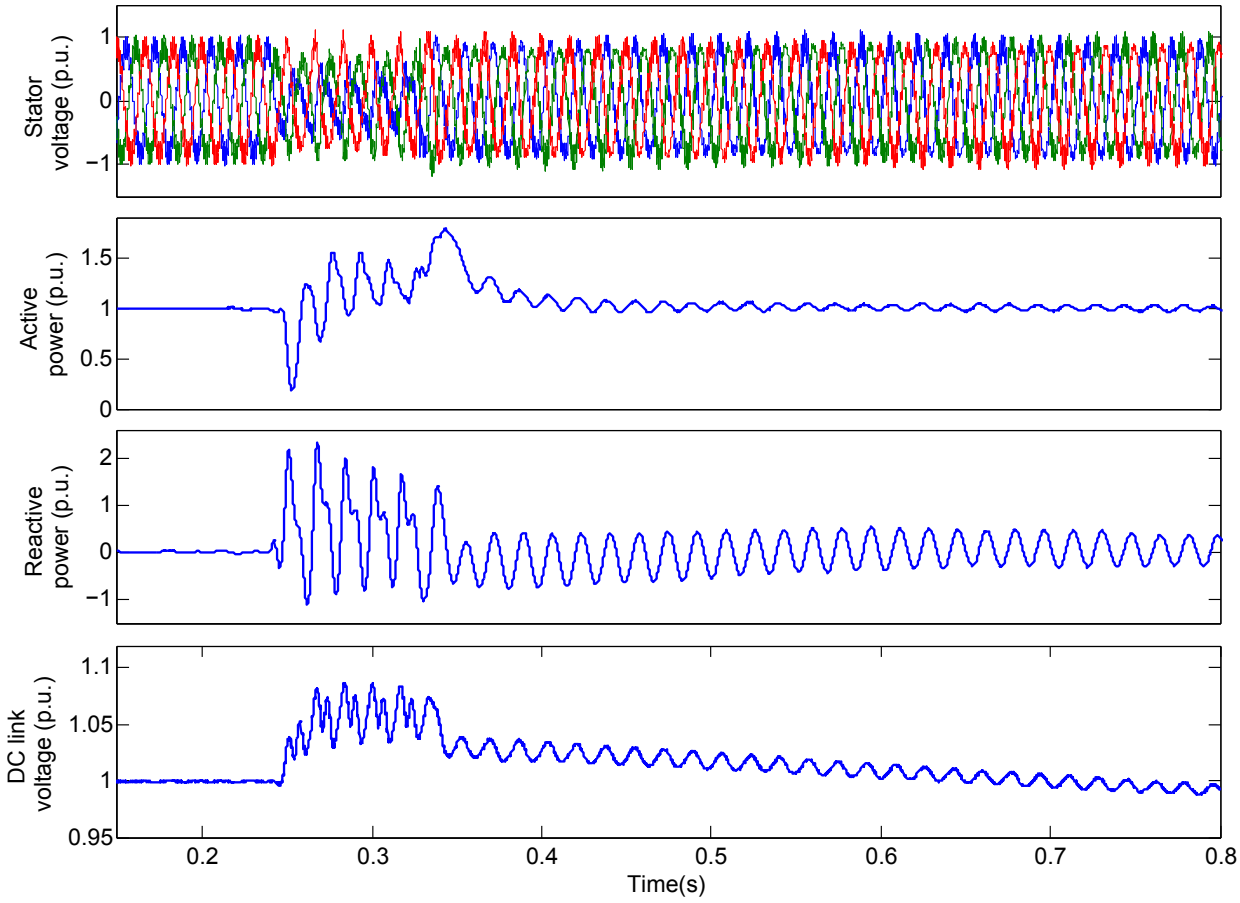

Figure 3.21: Responses for single phase fault with PI controller

in its steady state value.

With the proposed case, the oscillations in the powers are damped out within 0.2s and the stator voltages remain steady without any distortion. The peak amplitude of dc link voltage has reached only 1.035 p.u. marking an improvement of 5.5% over the PI case. Moreover, the type-2 FLC is tuned for initial operating condition, with that, it is able to sustain all the testing conditions without the need of retuning the control parameters. The control surface of the type-2 FLC uses the KarnikMendel type reduction algorithm, results in very smooth surface by aggregating the outputs of large number of embedded type-1 fuzzy sets [167]. This smooth surface will consequently make it less sensitive to uncertainties in parameters and disturbances, giving a very good control performance. As illustrated in Figure 3.23, the designed control surface of the type-2 controller is much smoother compared to that of type-1 controller, which further supports the claim that the performance of the proposed scheme is superior to that of PI and type-1 FLC. Furthermore, the consideration of huge computational delays of the controllers and process delays in the conversion process makes the results more realistic and useful for real time analysis.

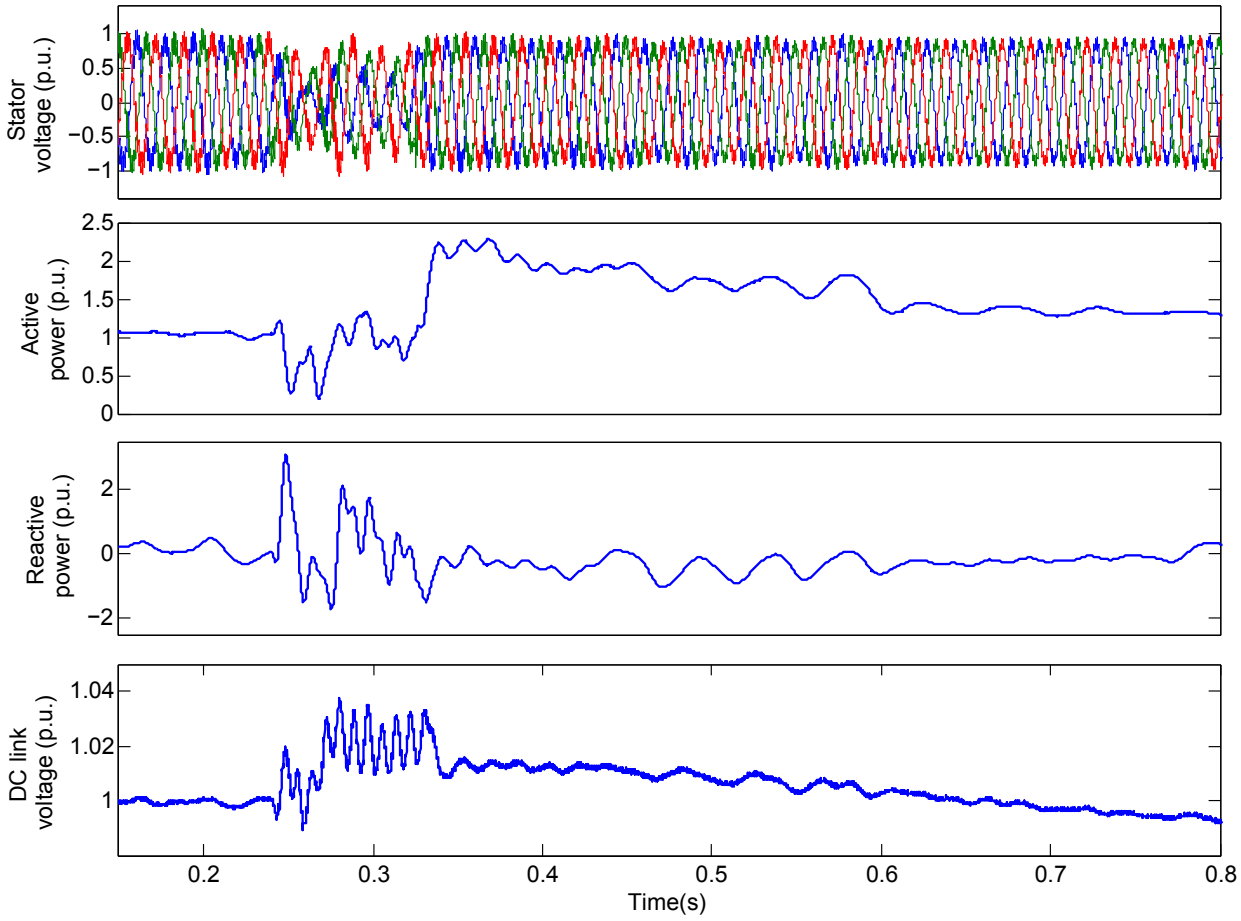

Figure 3.22: Responses for single phase fault with type-2 FLC

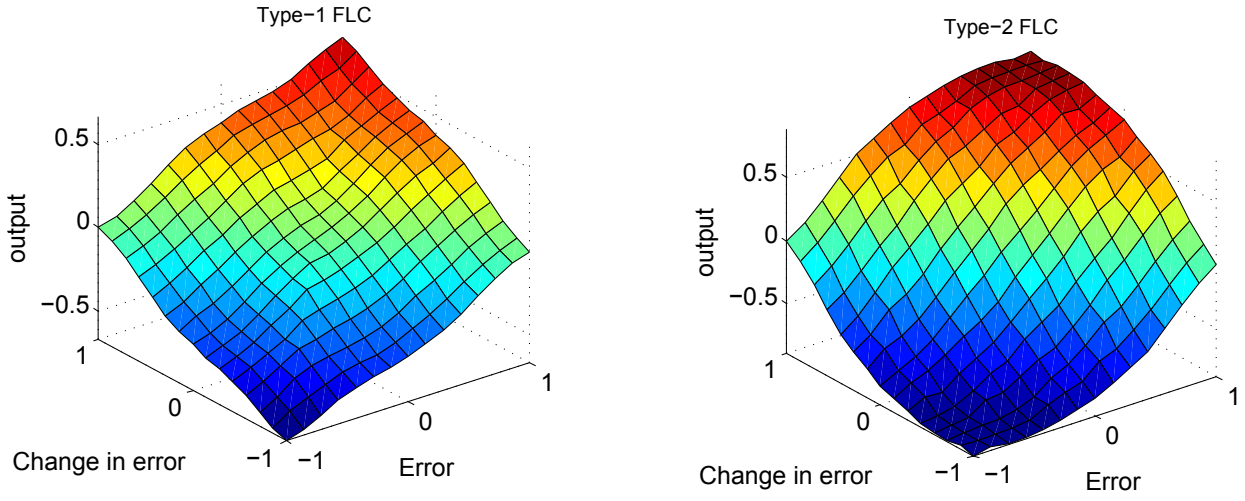

Figure 3.23: Control surfaces for type-1 and type-2 FLC

3.8 Conclusion

In this chapter, a new control strategy using type-2 FLC is proposed for the grid connected DFIG. The performance of the designed controllers for RSC is evaluated by comparing with that of PI and type1 FLC subjected to a three phase short circuit fault. The designed controller is implemented on Dspace 1104, and interfaced with the RTDS/RSCAD for real time simulations. The HIL test is carried out using analogue signals of error and actuating output. The Simulation results showed a significant improvement in the grid interaction of DFIG under network fault conditions. The proposed strategy is able to give a satisfactory performance, in variable wind speed conditions, without the need of retuning the controller parameters. Furthermore, the whole system turns out to be significantly robust against parameter deviations, fulfilling the LVRT requirements of standard grid codes. Although the type-1 FLC is able to handle the non-linearity present in the system, type-2 FLC is more effective in handling the uncertainties present in the system parameters. The results presented in this work are more realistic, since the computational delays and signal conversion delays are taken into account.

Chapter 4

Design and Implementation of Type-2 Fuzzy Logic Controller for DFIG-Based Wind Energy Systems in Distribution Networks

4.1 Introduction

In chapter 3, the type-2 FLC is designed for DFIG directly connected to the grid and the performance is verified with the network uncertainties like three phase fault and unbalanced fault. In general, the wind generators are operated with distribution networks, which encounters various uncertainties like unbalance voltages, load changes etc. The goal of this chapter is to verify the effectiveness of the proposed controller for various issues, particularly to the uncertainties in the distribution network. The work that has been done in the previous chapter is extended with enhanced analysis.

Over the last few years, the use of doubly fed induction generators (DFIGs) in wind power generation has received an increasing attention because of its ability to control active and reactive powers and also support variable speed operation with reduced mechanical stresses. Moreover, DFIG topology requires converters of only 20% to 30% of the generator rating with an efficient power capture capability [91]. The drawback is, the DFIG based wind generator is sensitive to voltage variations which are caused by disturbances such as grid faults and other load changes. The network faults cause a voltage dip at the generator connection point, which leads to an increased current in the stator windings. The magnetic coupling between stator and rotor reflects the stator current in the rotor windings which may further leads to damage of the rotor side converter and DC link capacitor [51]. In earlier stages of grid integration, for the safety of the converter system, the wind generators were allowed to get disconnected from the grid if a grid fault causes a large voltage drop. However, recently, the transmission system operators require that during the faults, the wind generators should remain connected to the grid, for reliable and stable operation of the grid [173]. The power oscillations in the distributed network after clearing the fault, is a matter of concern when the penetration levels of wind farms are very high.

In general the wind turbines are located in remote areas where the feeders are long,

and operated with unbalanced voltages with low short circuit levels commonly known as weak network. The uncertainty in the wind speed causes fluctuations in the output powers, which poses another challenge to maintain the steady state voltage levels [148]. Therefore, for reliable grid operation, the wind generators must be able to withstand network disturbances that are successfully eliminated. The recent grid codes also demand low voltage ride through capability (LVRT) from wind turbines to export power to the grid. This chapter addresses the uncertainty issues in distribution networks, as an extension to the designs proposed in the chapter 3.

4.1.1 Problem description

In the existing literature, distinct control schemes are suggested for grid integrated operation of variable speed wind generators and most of those schemes are based on conventional PI controllers [27, 169]. For reliable grid operation, the converters are controlled by employing direct feedback of torque and power in the cascaded control loops [28]. The problem of reactive power control during grid faults is addressed using different energy storage devices by varying the number of control loop parameters [174]. For enhancing the LVRT capability, a new technique with the application of FACTS devices has been investigated in [43]. Most of these control schemes are based on voltage and stator flux linkage oriented control, uses the traditional PI controllers accessing, the references from stator and rotor variables.

The challenging task in the above methods is in tuning the PI gains because the plant is highly nonlinear with uncertainty in operating conditions. The PI controller with fixed gains for a determined operating point provides an acceptable performance, but poor transient performance is often obtained when the converter operation point varies continuously because of changing dynamics of the plant. Operating points of the grid interactive inverters vary with the natural conditions such as solar radiation or wind speed. Moreover grid specifications such as grid voltage, frequency and impedance might change during operation of inverter [144]. To address the operating point issues, many variations for PI have been proposed in the power electronics literature including the addition of a grid voltage feedforward path, multiple-state feedback and increasing the proportional gain. Generally, these variations can expand the PI controller bandwidth but, unfortunately, they also push the systems towards their stability limits [153].

For transient studies of power system networks, the difficulty in controller design lies in modelling the network, which is highly nonlinear and in most of the literatures linearized plant models are used for the analysis. For severe disturbances such as three phase short

circuit fault and sudden change in wind speed, the linearized models does not predict the behavior of the system correctly [158].

The fuzzy logic controllers (FLCs) circumvent the problem of modelling, with the help of inference system and knowledge of field experts. Further, the control surface of the FLC can be shaped to define appropriate sensitivity for each operating point [61]. Recent review studies on DFIG shows that type-1 fuzzy logic controllers present a better performance in tracking the references compared to that of traditional PI controllers [62, 123, 126]. In general, the rules and membership functions (MFs) of FLC are chosen based on experience and knowledge of experts. However, the type-1 fuzzy logic sets (FLSs) cannot consider the uncertainty in the rules and MFs because it depends on the designer choice which varies from case to case.

Acknowledging the limitations of type-1 FLC and PI controller, in this chapter a novel control strategy with type-2 FSs is proposed to address the issues of uncertainties in the distribution networks. The interval type-2 FLC is generally more robust than its type-1 counterparts and can avoid frequent retuning of the controller parameters [109]. It has also been reported that the type-2 FLC behaves like a variable gain PI controller and has a smoother control surface around the steady state in comparison with its type-1 and conventional PI counterparts. Thus, tuning the FOUs of type-2 FLC might potentially result in more robust controllers since a smooth control surface might be generated [89]. In the previous chapter, it has already been proved that type-2 FLC is more immune to the network uncertainties compared to the other counterparts. In this work, by systematically varying the FOU, an attempt has been made to improve the grid interaction capability of DFIG considering the disturbances in the distribution network as parameter uncertainties similar to that of rules and membership functions.

At first, the plant model with DFIG and IEEE 34-bus test system is implemented in RSCAD for the analysis with real time simulations. The main objective of this chapter lies in designing a type-2 fuzzy logic controller for the rotor side converter (RSC) of the DFIG, to realize the effect of FOU to compensate the parameter uncertainties in the distribution network. To evaluate the feasibility of the controller for real-time applications, the control error signals in RSCAD model are converted to analog signals as controller input, then processed through type-2 FLC in HIL configuration, and fed back to the RTDS as an actuating input. Secondly, a type-1 FLC with suitable control parameters is also designed for comparative performance analysis. The performance of both the controllers is analyzed for a three phase short circuit fault and a sudden load disconnection. Furthermore, the

transient performance and the damping of power oscillations in the distributed network are analyzed for variable wind speed conditions.

4.2 Modelling of the system

The schematic diagram of wind turbine coupled to DFIG is shown in Figure 3.1. The stator windings of DFIG are directly connected to the grid and the rotor windings through a back-to back converters. The mathematical modelling equations expressed in the space vector form, referring to synchronous reference frame are used for implementing the DFIG [136]. The details about mathematical modeling equations are given in chapter 3.

4.2.1 Distribution network model

The IEEE 34-bus test system is a three phase radial distribution system with unbalanced distributed and spot loads. It operates at two different voltage levels 4.16 kV and 24.9 kV with two separate voltage regulators. The connected load is 1.769MW, 1.044 MVar with a grid loss of 0.27 MW. The bus 800 is connected to the external grid and a transformer is connected between bus 832 and bus 888 to supply the low voltage line. Further, the network comprises two capacitor banks at bus 844 and 848, so it makes sense to test the wind turbine by connecting it at bus 848 to avoid additional reactive power compensation devices [44].

4.3 Controller Design for RSC

The steps involved in the controller algorithm are shown in Figure 2.3. At first the crisp input signal is converted to fuzzy input with the help of various membership functions. A set of rules is formed using logical operators to aggregate the output fuzzy sets into a single set known as inference mechanism. The inferred output is converted to type-1 set known as type reduction operation, and then the type reduced sets are converted back to crisp value using various defuzzification techniques.

4.3.1 Type-2 FLC Design

At first the rotor currents are converted to per unit values and then converted from rotating reference frame to quasi DC quantities. The rotating reference frame in this case, is computed from the difference between the position of the stator flux vector and the physical

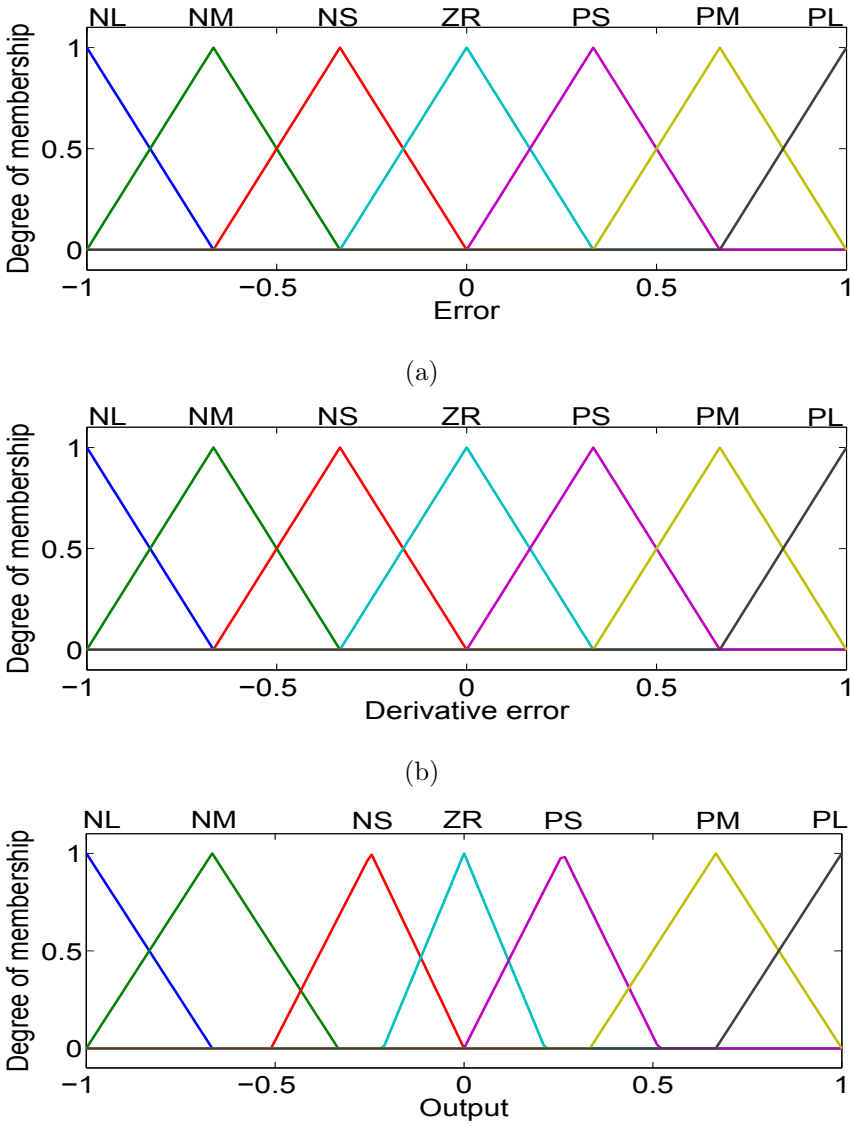

Figure 4.1: MFs for type-1 FLC (a) Input1 (b) Input2 (c)Output

rotor direct axis. This difference is generally changing and is referred to as the slip angle. By decoupling the d and q rotor currents, the electrical torque and rotor excitation current can be controlled independently. In order to describe the rotor voltages as a function of rotor currents the rotor voltage equations in [136] can be rearranged as

$$\begin{cases} v_{dr} = R_r i_{dr} - (\omega_s - \omega_r)\sigma L_r i_{qr} + \sigma L_r \frac{di_{dr}}{dt} \\ v_{qr} = R_r i_{qr} + (\omega_s - \omega_r)(L_m i_{ms} + \sigma L_r i_{dr}) + \sigma L_r \frac{di_{qr}}{dt} \end{cases} \tag{4.1}$$

where $\sigma = 1 - ({L_o}^2/L_s L_r)$, v_r and i_r are the rotor voltages and currents; ω_s and ω_r are the frequencies of stator and rotor; L_r and L_m are the rotor and mutual inductances; d and q are the direct and quadrature axis respectively. The reference value for V_q is generated from the optimal power reference algorithm, which decides the optimal power output for the turbine from available wind speed, and the same for V_d is defined from the set point value

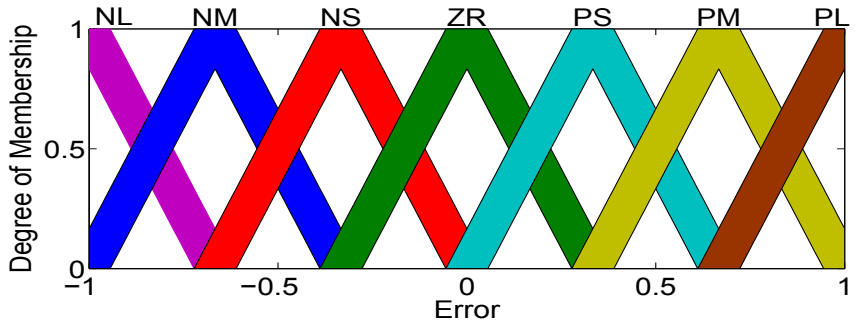

(a)

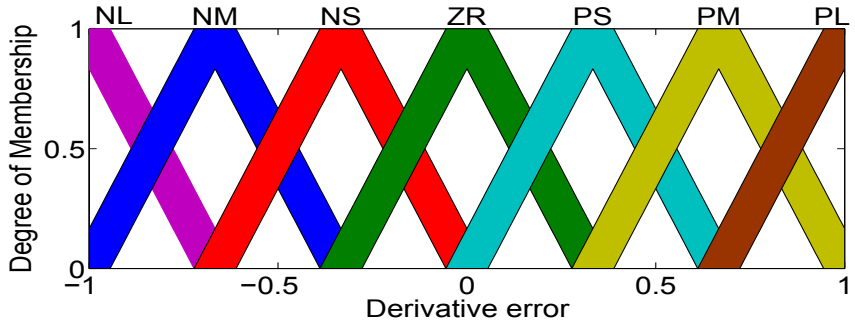

(b)

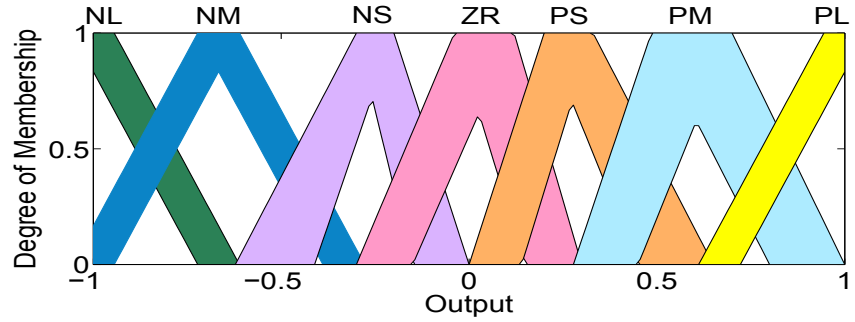

(c)

Figure 4.2: MFs for type-1 FLC (a) Input1 (b) Input2 (c)Output

of the reactive power. The structure shown in Figure 3.5 is considered for implementation of both type-1 and type-2 FLC.

Fuzzification

Schematic diagram of the controller structure is shown in Figure 3.5. The error signals are fuzzified using seven traingular MFs. The fuzzy sets have been defined as: NL-Negative Large, NM-Negative Medium, NS - Negative Small, ZR-Zero, PL-Positive Large, PM - Positive Medium, and PS- Positive Small. The designed MFs for type-1 and type-2 FLCs are shown in Figure 4.1 and 4.2, respectively. Most researchers choose the MFs with equal span and equal width of FOU which do not guarantee best performance. In this work, the MFs are chosen based on prior knowledge and observations from the various simulation

results. The width of the FOU is adjusted based on the observations from the output responses.The maximum and minimum values of the universe of discourse for all inputs and outputs are chosen as +1 to -1.

Inference Engine

The main operations in inference engine are the rule implication, aggregation and type reduction. The fuzzy mapping of the input variables to the output is formed with the help of IF-THEN rules and are framed as

$$If \quad e_d \quad is \quad x_1 \quad and \quad \dot{e}_d \quad is \quad y_1 \quad then \quad V_d \quad is \quad w_1$$
$$If \quad e_q \quad is \quad x_1 \quad and \quad \dot{e}_q \quad is \quad y_1 \quad then \quad V_q \quad is \quad w_2$$

In similar way, 49 rules are chosen for all the MFs as shown in Table I and equal weights are chosen for all the rules. The inference system uses min-method for Meet operation, max method for Join operation and Join aggregation, and min method for Meet implication. The Join and Meet operations are used in type-2 fuzzy sets to define the union and intersection operation for mapping the input and output sets with the fired rules. The general union operation applied on type-1 fuzzy sets cannot be used here, since the primary MF is also a type-1 fuzzy set. The detailed mathematical relations between union and join operations are explained in [122] using the Extension principle. In the aggregation process, a single output fuzzy set is derived by aggregating all the fired rules. Due to computational limitations, the type-2 output sets cannot be directly used for converting to crisp value. For this reason, the type reduction operation that is, converting from type-2 output fuzzy sets to type-1 fuzzy sets is done so that the normal techniques of defuzzification could be applied. Center-of-sets, height, modified-height and center-of-sums are some of the popular type reducing methods, in which centroids of the embedded type-2 sets are calculated. Computational time is the factor that needs to be considered while choosing the width of FOU. Because for a larger width of FOU, the number of embedded fuzzy sets increases this in turn increases the computational time of type reduction operation. In this design height type-reduction method is used for calculating the centroid of type-2 fuzzy sets.

Defuzzification

The centroid of the type-2 fuzzy set is the collection of centroids of all of its embedded sets. Using the Karnik-Mendel algorithm the smallest and largest elements among the centroids are identified and centroid type defuzzification method is used for converting the fuzzy

Table 4.1: Rule base for type-2 FLC

E/ΔE	NL	NM	NS	ZR	PS	PM	PL
NL	NL	NL	NL	NL	NM	NS	ZR
NM	NL	NL	NL	NM	NS	ZR	PS
NS	NL	NL	NM	NS	ZR	PS	PM
ZR	NL	NL	NM	ZR	PM	PM	PB
PS	NM	NS	ZR	PS	PM	PB	PB
PM	NS	ZR	PS	PM	PB	PB	PB
PL	ZR	PS	PM	PB	PB	PB	PB

output space to crisp value. In general, the centroid of an IT-2 FS is characterized by its left (y_l) and right (y_r) end points. Hence computing the centroid of an IT-2 FS set requires computing, only those two end-points. Using representation theorem the centroid $C_{\tilde{B}}$ of fuzzy output space $\tilde{B}$ is defined as the collection of the centroids of all of its embedded IT-2 FSs.This means the centroids of all of the n_B embedded type-1 fuzzy sets contained within $FOU(\tilde{B})$ must be computed [116]. The results of doing this are a collection of n_B numbers that have both a smallest and largest element, $C_l(\tilde{B}) \equiv C_l$ and $C_r(\tilde{B}) \equiv C_r$, respectively, so that $C_{\tilde{B}} = 1/\{C_l, ..., C_r\}$. And in general we can write $C_{\tilde{B}}$ as $[C_l, C_r]$. Therefore centroid type reduction can be expressed as

$$Y_{TR}(x^{'}) = [y_l(x^{'}), y_r(x^{'})] \equiv [y_l, y_r] \tag{4.2}$$

$$= \int_{y^1 \in \left[y_l^1, y_r^1\right]} ... \int_{y^M \in \left[y_l^M, y_r^M\right]} \int_{f^1 \in \left[\underline{f}^1, \overline{f}^1\right]} ..... \int_{f^M \in \left[\underline{f}^M, \overline{f}^M\right]} 1 \Big/ \frac{\sum_{i=1}^{M} f^i y^i}{\sum_{i=1}^{M} f^i} \tag{4.3}$$

where the multiple integral signs denote the union operation and the detailed explanation on this can be found from [49]. Karnik and Mendel algorithm [75] is applied to compute y_l and y_r. The defuzzified output of the FLC is simply the average of y_l and y_r i.e. $Y = \frac{(y_l)+(y_r)}{2}$ [114]. The final output of the controller with the compensation is defined as

$$v_{dr}{}^* = v'_{dr} - (\omega_s - \omega_r)(\sigma L_r i_{qr}) \tag{4.4}$$

$$v_{qr}{}^* = v'_{qr} + (\omega_s - \omega_r)(L_m i_{ms} + \sigma L_r i_{dr}) \tag{4.5}$$

where the starred values are the final output, the prime terms are outputs of the type-2 fuzzy controllers and the terms in brackets are the compensation terms required to completely

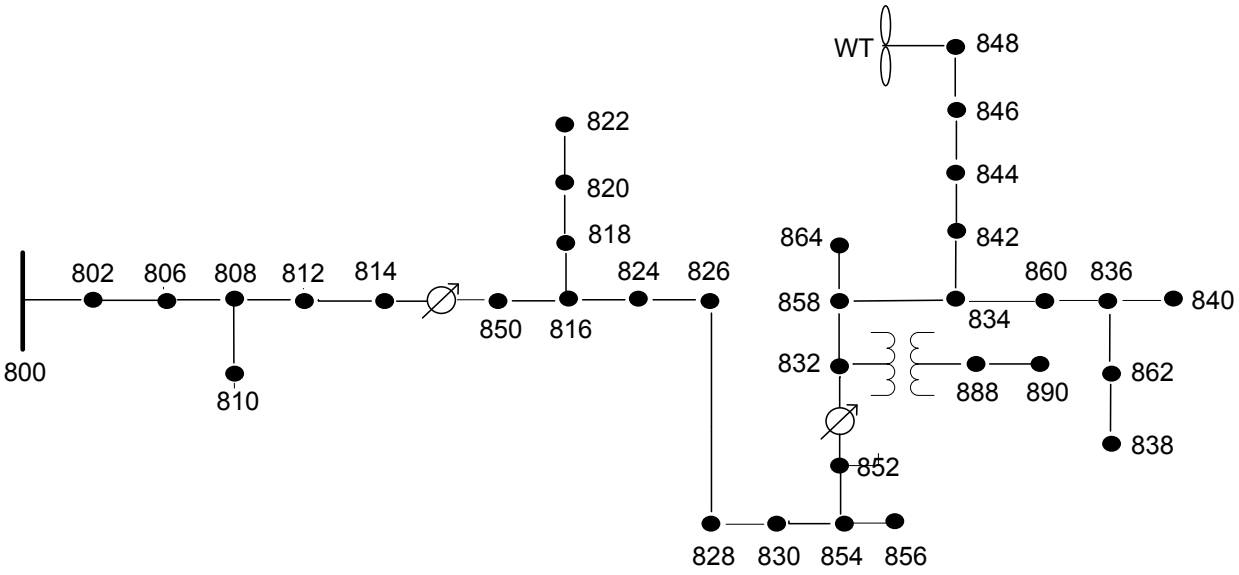

Figure 4.3: IEEE 34-bus system with Wind Turbine

Table 4.2: Parameters of the controllers used in the simulations

Model	Executed Module	Sampling time
Power system model	RTDS	$55\mu s$
Type-1 FLC	DS1104	$50\mu s$
Type-2 FLC	DS1104	$50\mu s$

decouple the d and q axis voltages. At last the controller outputs are converted from dq frame to ABC, and given to a pulse width modulator for generating the firing pulses to the switches. The initial values of the controller parameters K_e ,K_d and K_u are tuned based on techniques described in [94]. To obtain the minimum variations in the control variables, several simulations are performed to tune the controller gains.

4.4 RTDS Simulations and Results

RTDS is a digital electromagnetic transient power system simulator that operates in real-time with hardware interfacing features. It facilitates real time simulation of complex power system models using parallel processors which allows simulations with a time step up to 250 ns. The RTDS platform is considered by many research laboratories as a real-time testing module for controller prototyping and also for hardware in the loop (HIL) applications with power system models [36, 121, 134]. The IEEE 34-bus test system is a three phase radial distribution system with unbalanced distributed and spot loads. Two regulators are used to control the voltage and the connected unbalanced load is 1.769 MW and 1.044 MVar

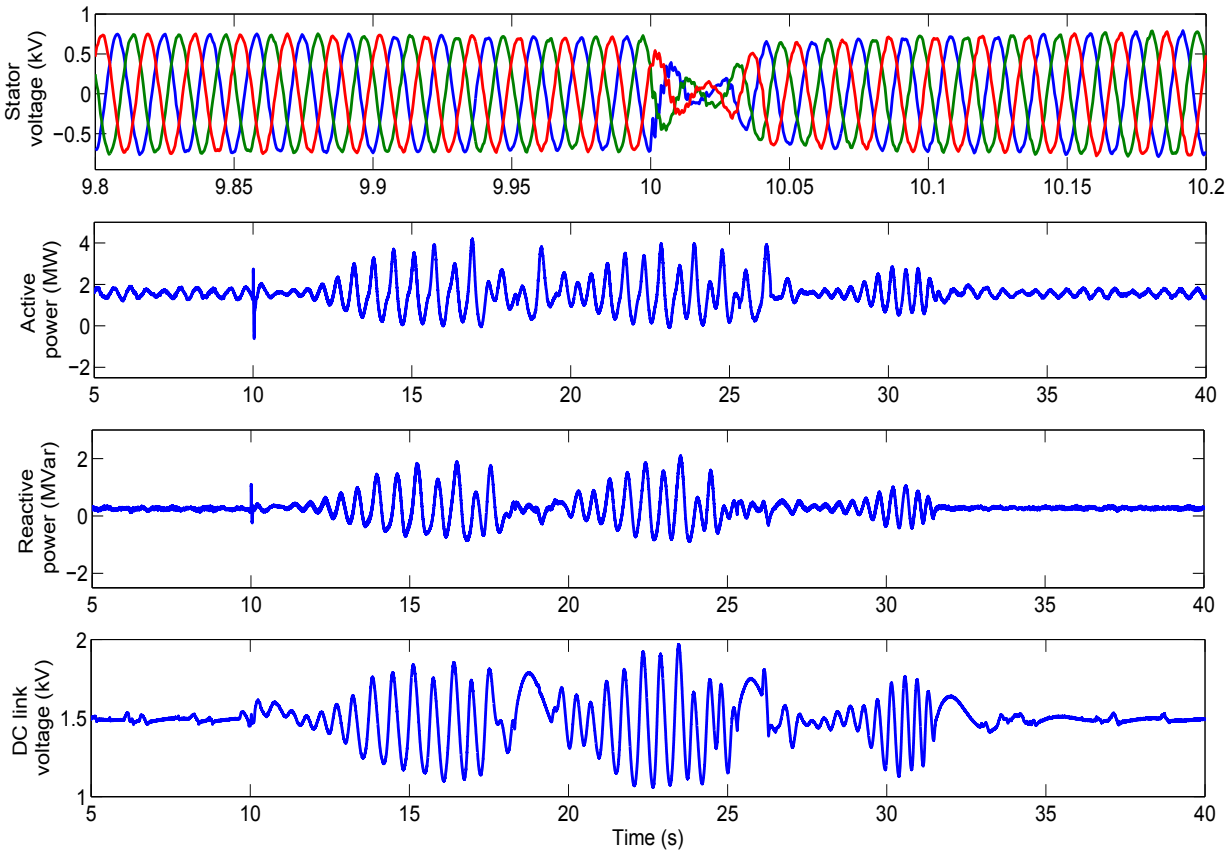

Figure 4.4: Responses at DFIG terminals for three phase fault(type-1 FLC)

with a grid loss of 0.27 MW. Using the bus data, the test system is designed in RSCAD as shown in Figure 4.3 . Due to node restrictions, the model is designed using four subsystems of RSCAD draft models and simulated using four racks of RTDS hardware with GPC/PB5 processors. Bus 890 and 844 are considered as load centers and bus 800 is connected to the grid. Further, the network comprises two capacitor banks at bus 844 and 848, so it makes sense to test the wind turbine by connecting it at bus 848 to avoid additional reactive power compensation devices.

A DFIG rated 1.5MW, 0.69 kV, 60Hz is connected to bus 848 through a 2 MVA, 4.16/0.69 kV transformer. To minimize losses, the power rating of the converter is chosen to be 40% of the machine rating. The rated rotor speed is chosen to be 1.02 times synchronous speed in order to extract energy from both the rotor and the stator ends of the DFIG. The grid side converter is controlled to maintain the dc link voltage at a constant level. The crowbar circuit is connected to the rotor to protect the converters and rotor windings, from high currents during fault conditions. For initiating the three phase fault, the initiation breaker is directly connected to the bus 890. The HIL arrangement of the proposed control scheme is shown in Figure 3.14. The workstation computer executes the RSCAD model

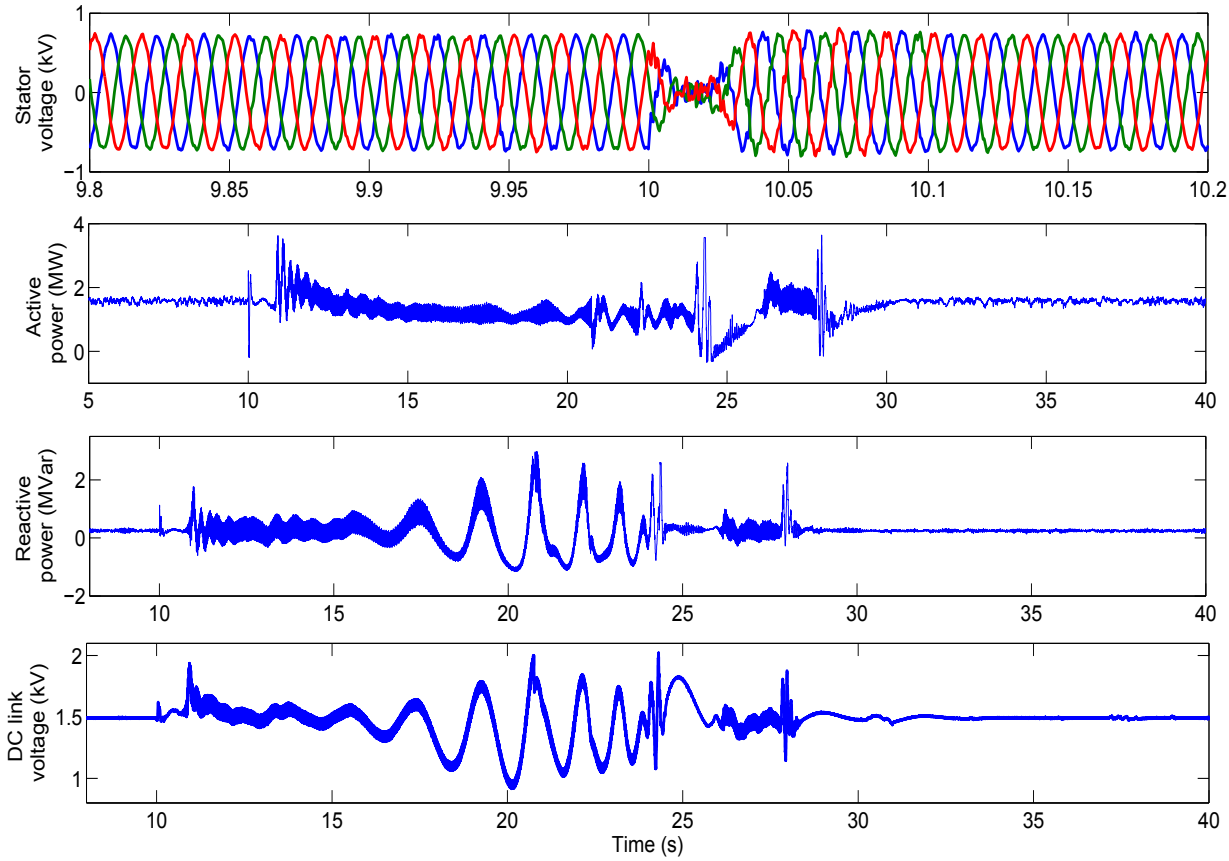

Figure 4.5: Responses at DFIG terminals for three phase fault(type-2 FLC)

and, interacts with the RTDS to generate real-time simulation results. The error signals generated for both v_d and v_q of RSC in the RSCAD platform are converted to analog signal using Gigabit transceiver analog output (GTAO) card. GTAO facilitates scaling down of high amplitude signals during fault conditions to 10V analog output through a multiplexed 16 bit Digital to Analog converter (DAC). The analog error signals are normalized and sent to type-2 fuzzy controller algorithm through a Dspace 1104 interface. The controller output is fed back to RTDS through Gigabit transceiver analog input (GTAI) card. The GTAI card comprises 16 bit A/D converters having 12 channels of a range $\pm 10V$. The scaling factors are adjusted so that compatibility is maintained between GTAI card output and RSCAD. The experimental setup is shown in Figure 3.15 and the details of HIL test are listed Table 4.2. The performance of the controller is tested for a three phase fault, sudden disconnection of load and sudden change in wind speed.

4.4.1 Three phase short circuit fault

A three phase fault is created at bus 890, 10s, which is cleared after 10.08s. The performance of the proposed method is compared with type-1 FLC. The initial reference signals for active

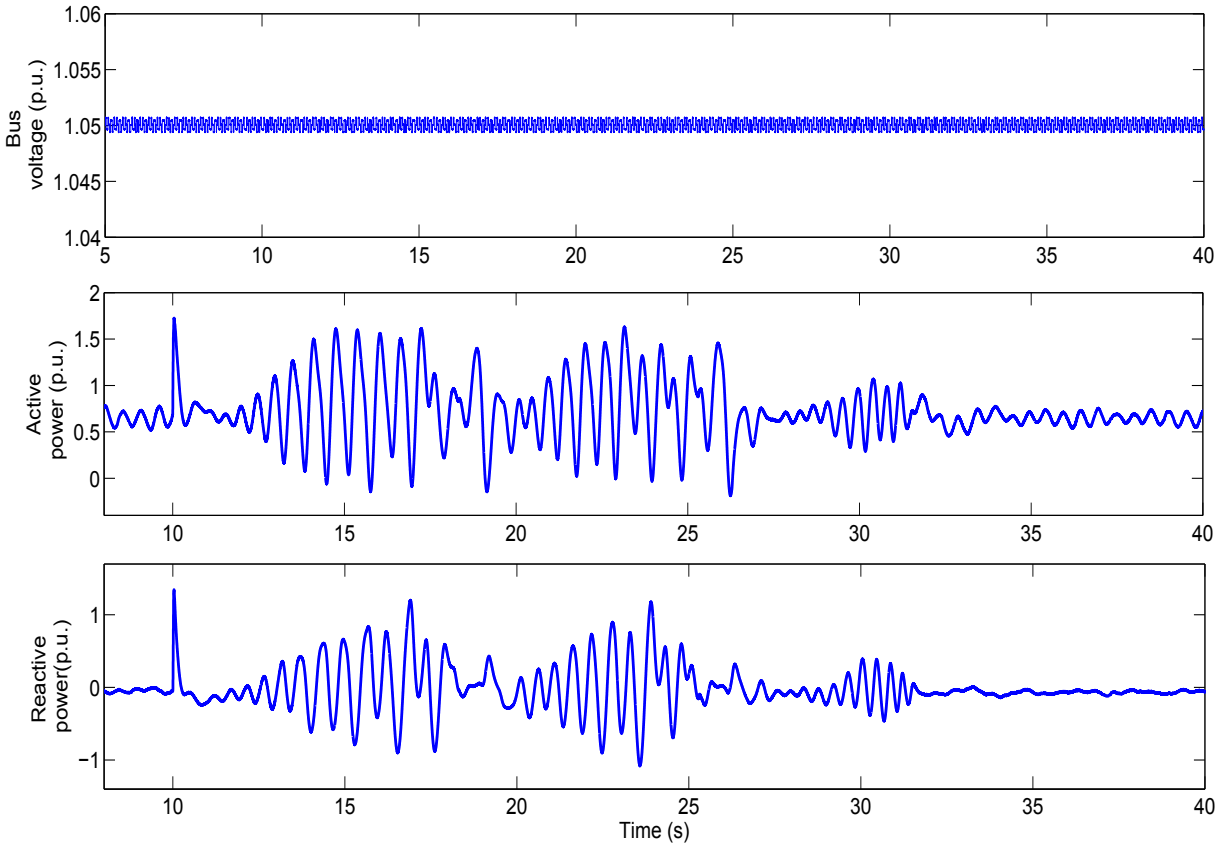

Figure 4.6: Responses at Bus 800 for three phase fault (type-1 FLC)

and reactive power are set at 1.5 MW and 0.3 MVar respectively. The response of the DFIG with type-1 FLC is shown in Figure 4.4. At the instant of fault the stator voltage drops close to zero, and causes the stator current to rise above its normal value. This results in high rotor current due to the magnetic coupling between stator and rotor. The sudden drop in the voltage causes hindrance to the grid side converter to transfer the excess power in the rotor to the grid. During the fault period, the excess power in the rotor side converter causes a rise in the dc link capacitor voltage to 1.73 kV that is 15.4% more than the steady state value; however it has been brought down to normal value avoiding the triggering of crowbar circuit. The oscillations in active and reactive power lasted more than 23 seconds. The response of the DFIG with the proposed controller is shown in Figure 4.5. It can be seen that with introduction of FOU in the membership functions, system damping has been significantly enhanced. As a result, the oscillations in the output powers are lasted only for 17 seconds. The dc link voltage has risen to only 1.65 kV marking an improvement of 4.6% in the peak magnitude over type-1 FLC. The power oscillations and the voltage behavior at bus 800 and 890 of the distribution network are monitored.

The responses at bus 800 and 890 with type-1 FLC are shown in Figure 4.6 and 4.8

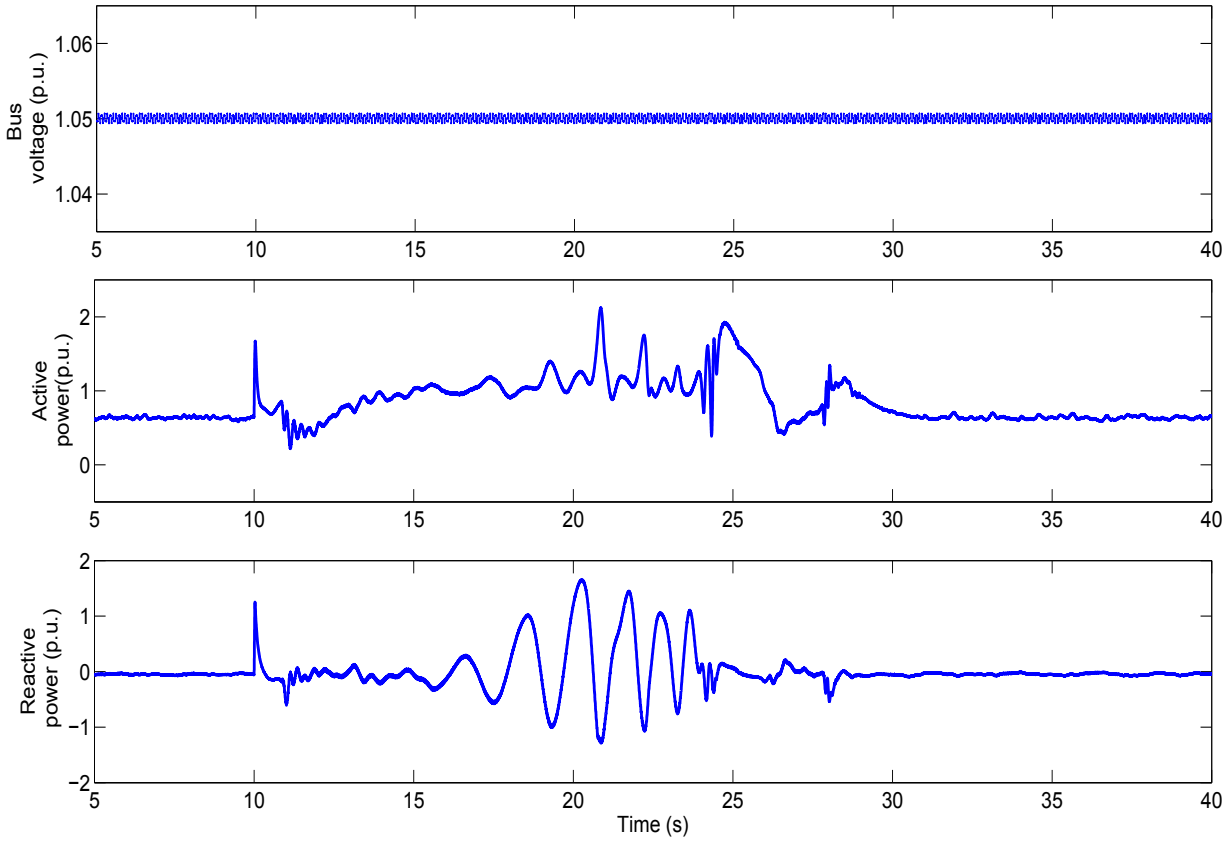

Figure 4.7: Responses at Bus 800 for three phase fault (type-2 FLC)

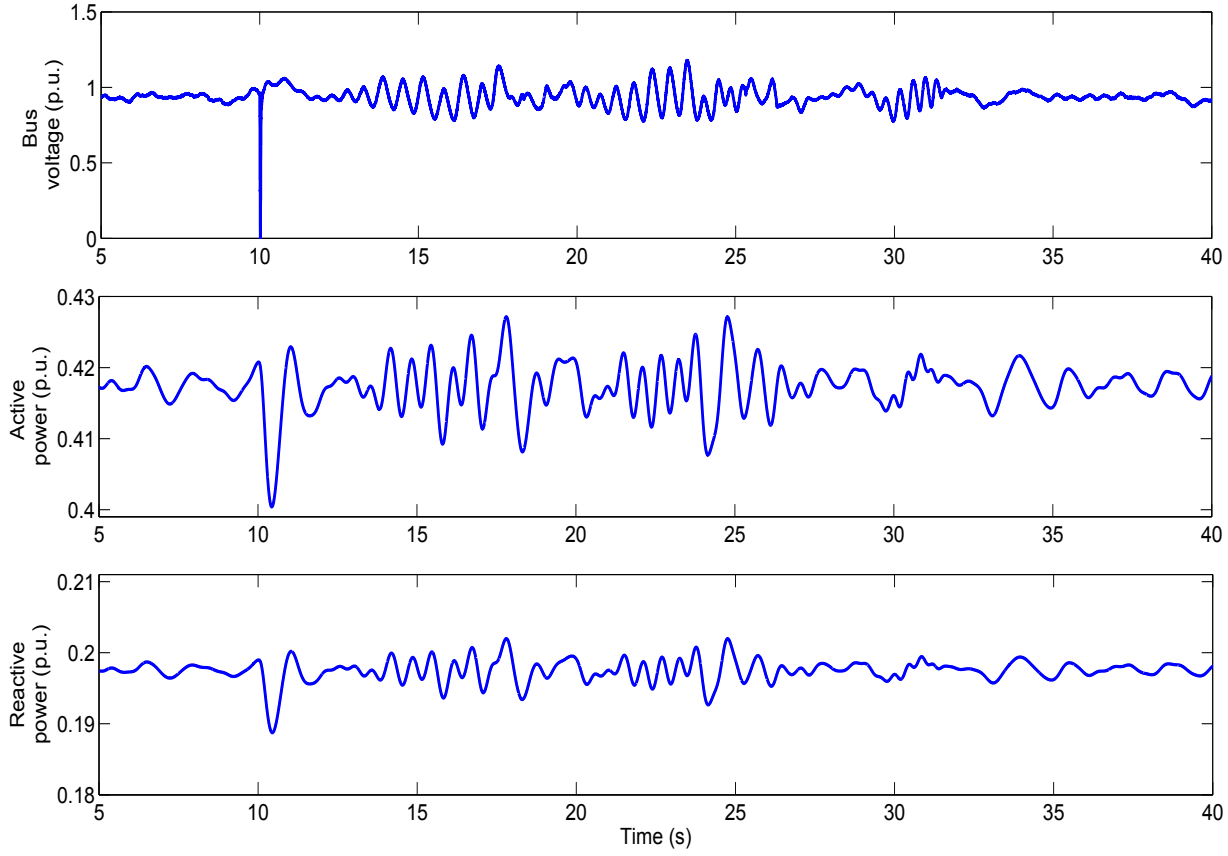

Figure 4.8: Responses at Bus 890 for three phase fault (type-1 FLC)

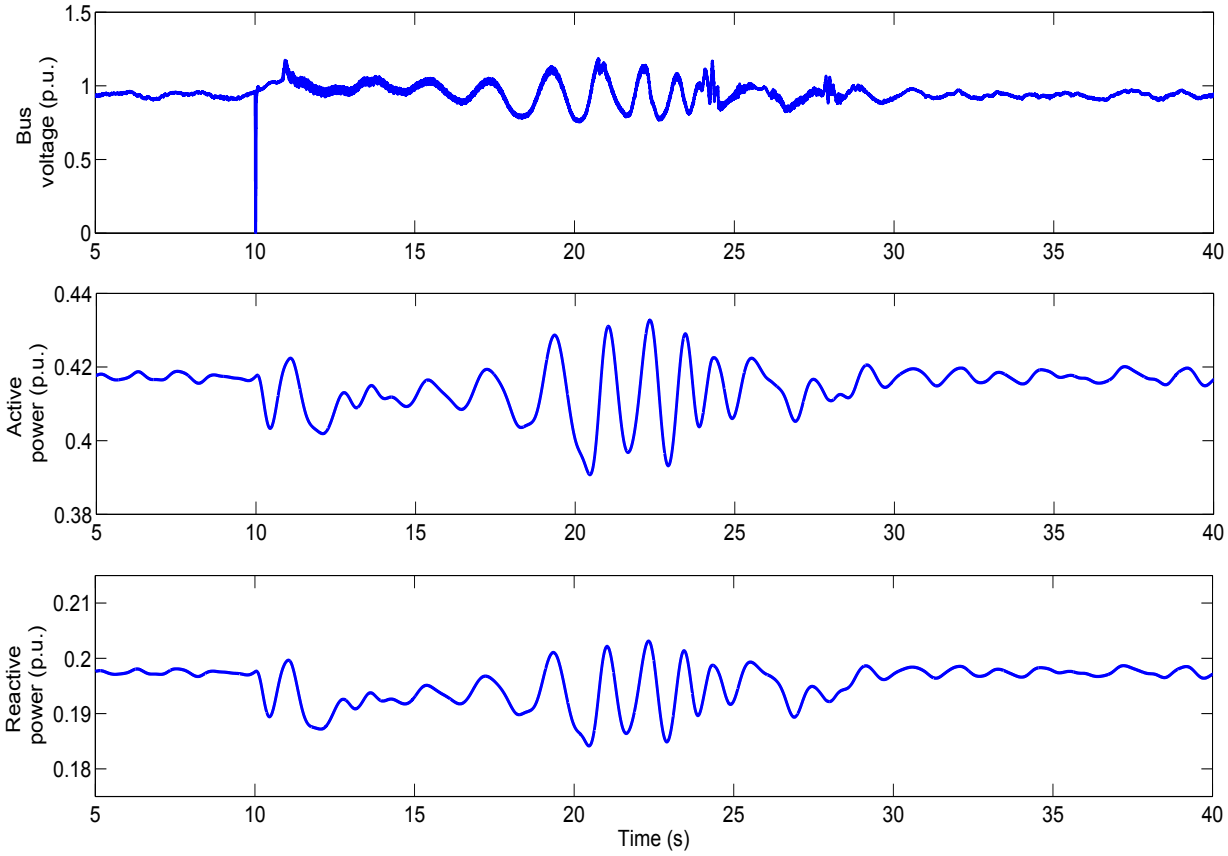

Figure 4.9: Responses at Bus 890 for three phase fault (type-2 FLC)

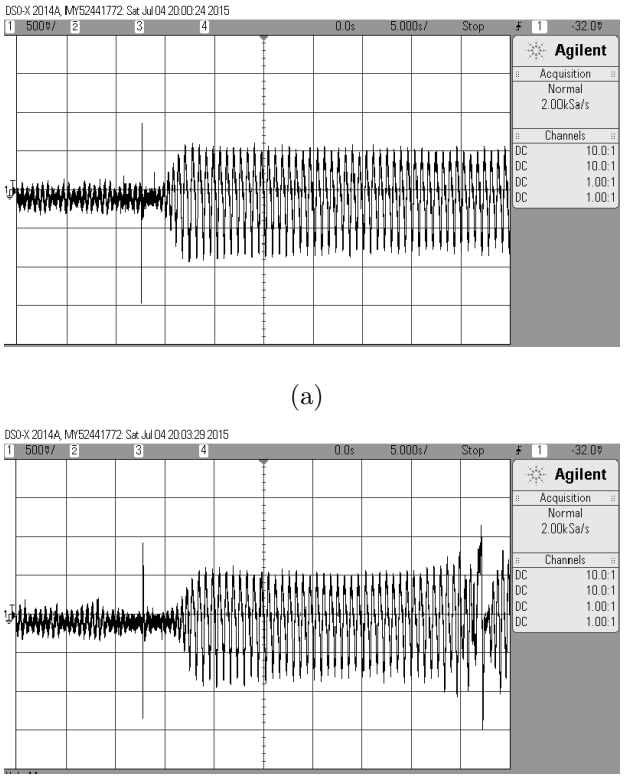

(a)

(b)

Figure 4.10: Control error with type-1 FLC (a) active power (b) reactive power

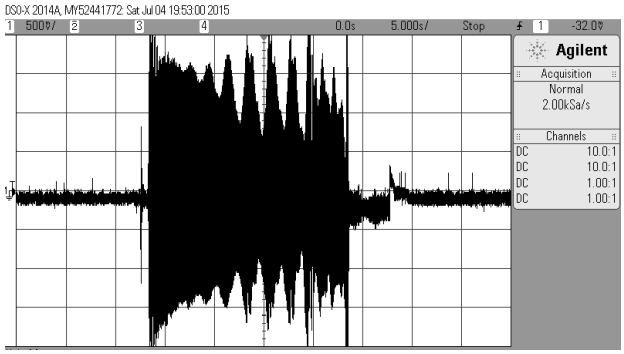

(a)

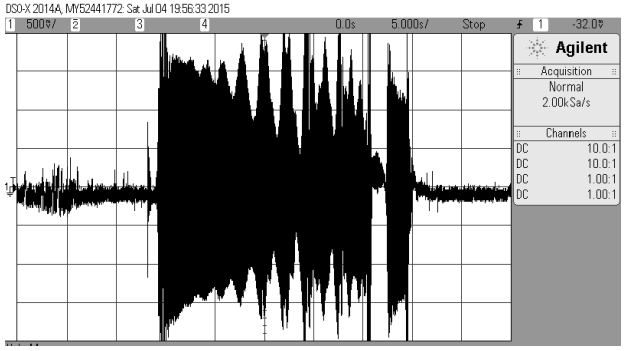

(b)

Figure 4.11: Control error with type-2 FLC (a) active power (b) reactive power

respectively and the same for type-2 FLC are shown in Figure 4.7 and 4.9 respectively. Since bus 800 is located near to the grid, with type-1 FLC, the voltage at bus 800 is maintained at its specified level 1.05 p.u. during the fault period and also after clearing the fault. Severe oscillations are observed in the active and reactive powers at bus 800 , which lasted 23s after clearing the fault. On other hand, the type-2 FLC responded with reduced oscillations in the active and reactive powers which are damped out completely after 17s as shown in Figure 4.7. The voltage level at the grid connection point is maintained at 1.05 p.u. and not distorted although there is a rise in active power. Although the rules and shape of membership functions are same for both the controllers, the presence of FOU in the type-2 membership functions, showing a clear improvement in this case.

In the case of bus 890, the voltage is maintained at specified level 0.91 p.u. with both type-1 and type-2 FLCs; however, the response with proposed controller settles much faster compared to that of type-1 FLC (Figure 4.9) . The case clearly shows that the proposed controller is able to damp out the power oscillations much faster than that of type-1 FLC without affecting the rated bus parameters. The error signals of active and reactive powers for both type 1 and type 2 FLCs are captured in digital oscilloscope and depicted in Figures 4.10 and 4.11 respectively.The scaling gains of GTAO and GTAI cards are adjusted in such

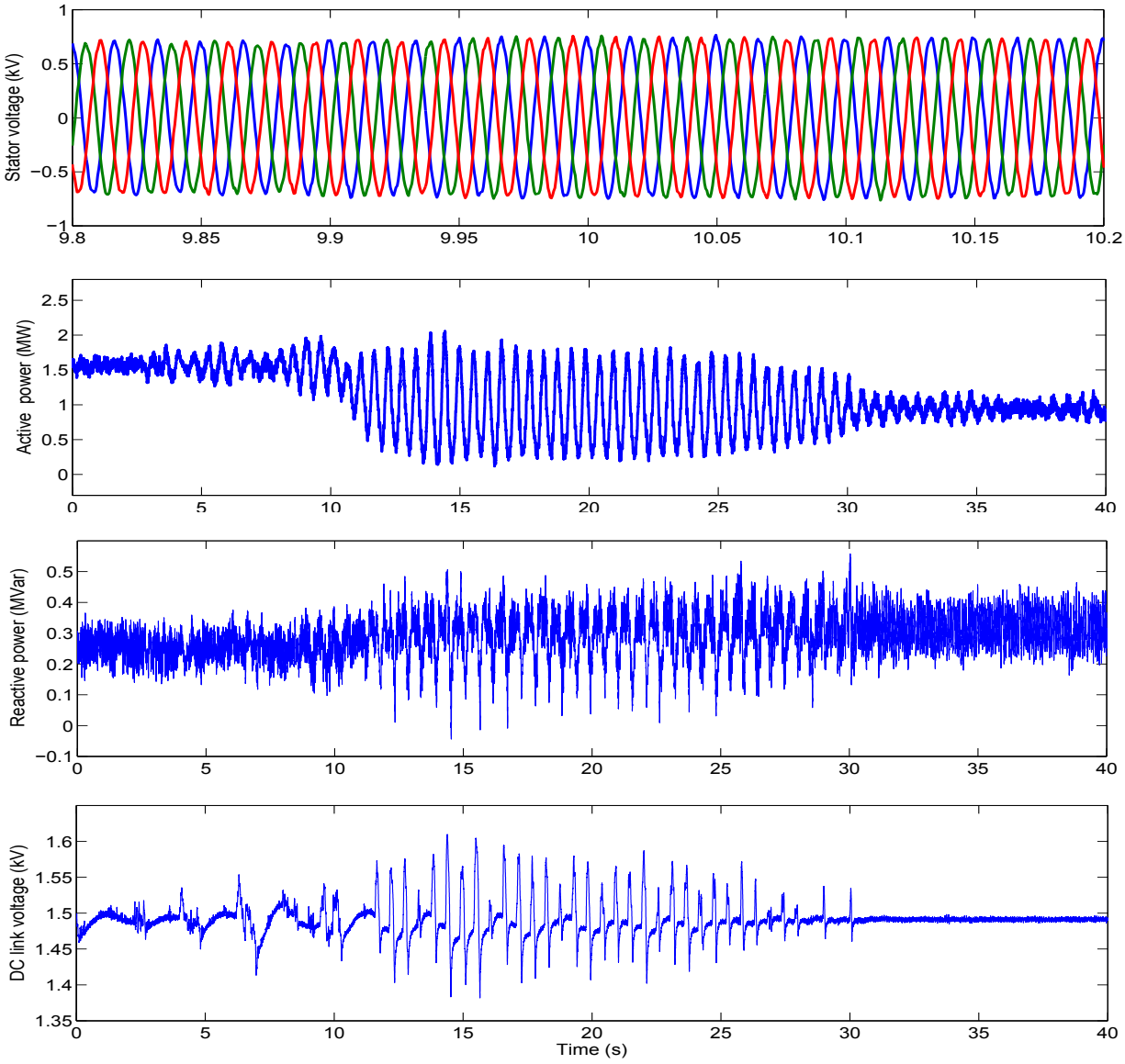

Figure 4.12: Responses of DFIG for change in wind speed (type-1 FLC)

a way that the error signal during the fault doesn't get saturated. The controller error output increases at the time of fault to bring the generator parameters at normal level. It is observed that the error signal generated by the proposed method is lasted few seconds compared to that of type-1 FLC and able to improve the performance during the transients generated by the fault. This shows that the proposed controller is very effective, in handling the sudden changes in the operating conditions.

4.4.2 Variable wind speed

In this section the controller performance is analyzed for variable wind speed conditions. As stated in the previous section, the optimal power algorithm decides reference output

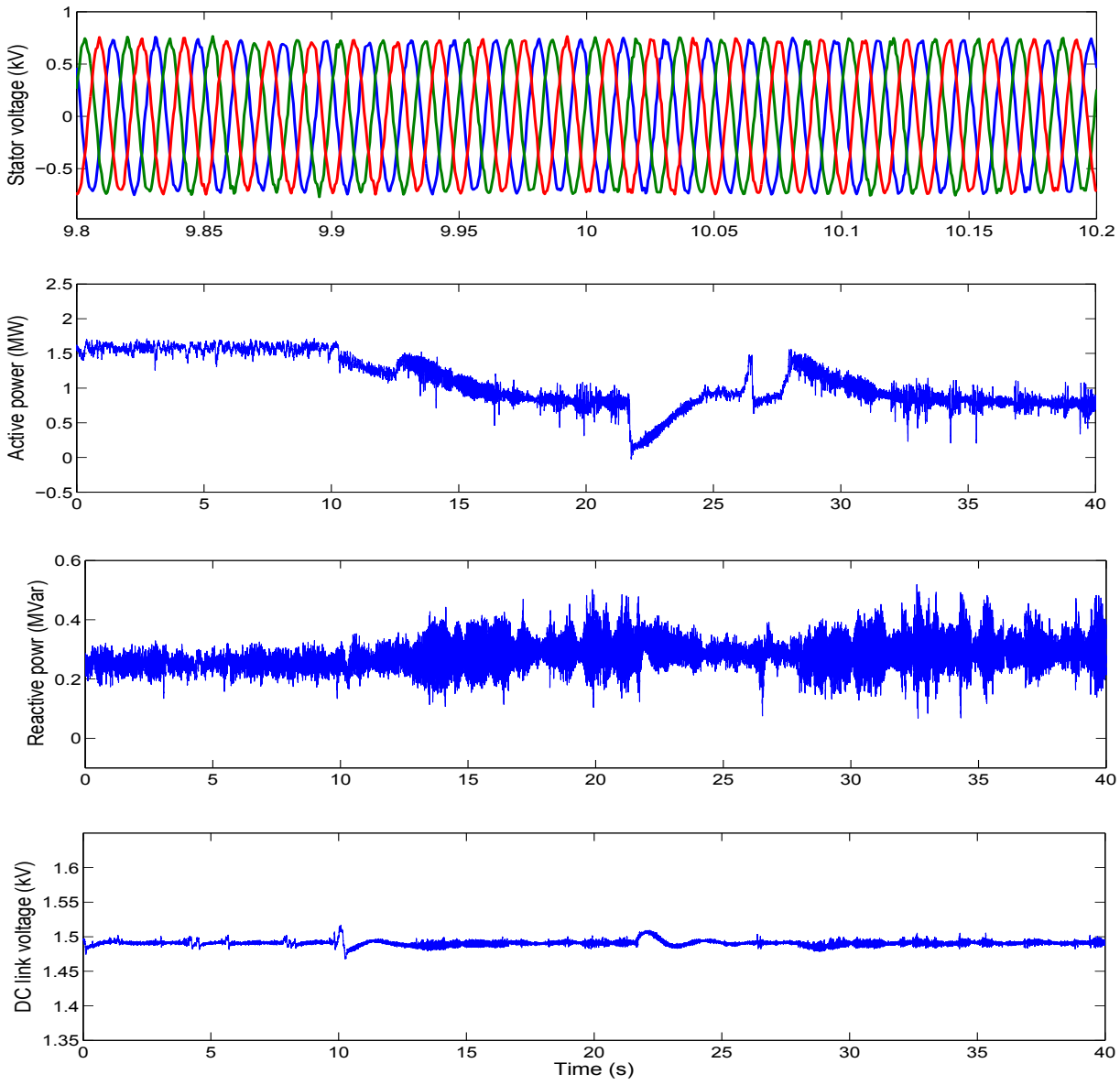

Figure 4.13: Responses of DFIG for change in wind speed (type-2 FLC)

for a given wind speed. The controller has to track the variable reference, irrespective of operating conditions that are assumed while designing the controller parameters. In this simulation, the initial controller gains are tuned for an operating rotor speed of 1.2 p.u. at a wind speed of 12 m/s. Figure 4.12 depicts the tracking performance of the type-1 FLC for wind speeds from 12 m/s to 10 m/s. When the speed is changed to 10 m/s, the active power has reduced to 0.95 MW. In order to capture the transition from higher reference to lower, the simulations are executed for 50s. In the type-1 FLC case, the transition of powers to the new steady state, is reached 20s after initiation of speed, with sustained oscillations. Sudden spikes in the dc link voltage is observed throughout the period of power oscillations, which has been monitored by the crowbar system. Further, the power

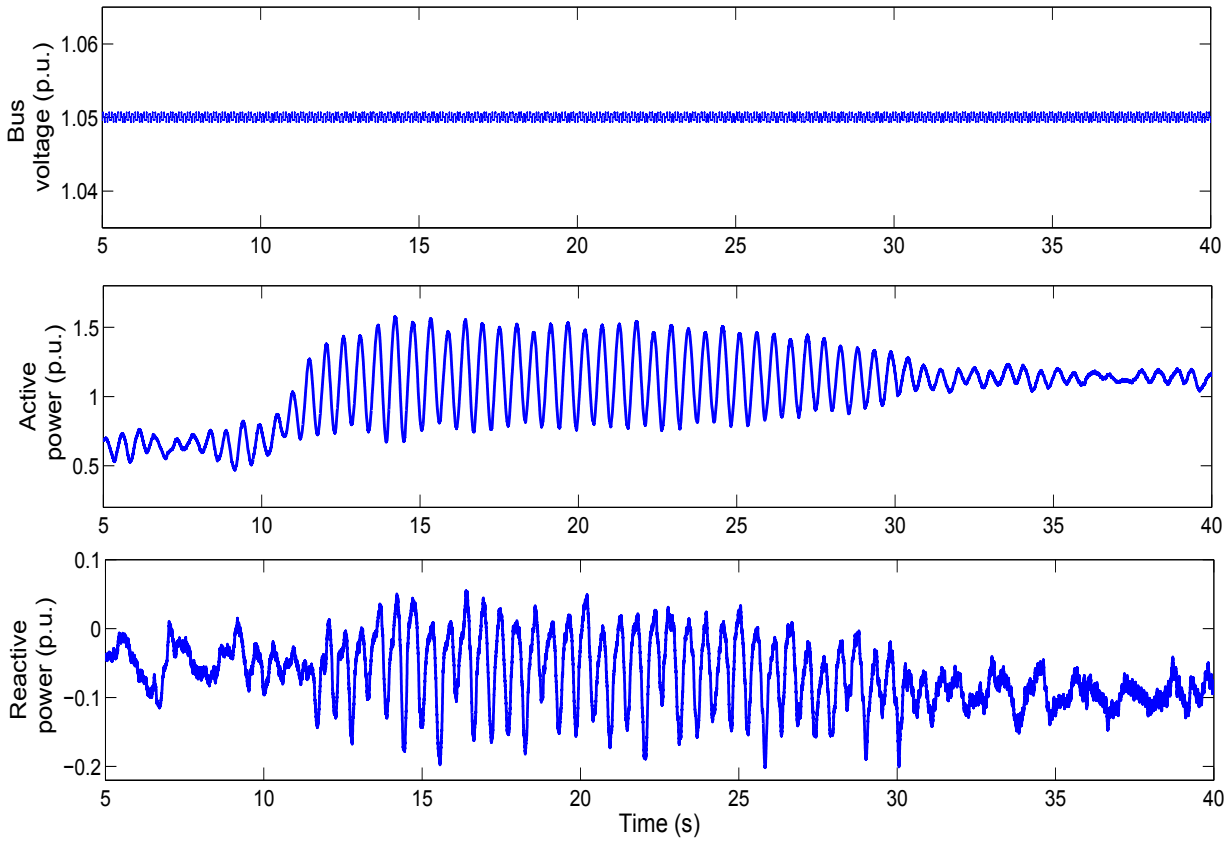

Figure 4.14: Responses for change in wind speed at Bus 800 (type-1 FLC)

oscillations are reflected in the stator voltage, in terms of rise in the voltage level; and the frequency is maintained constant irrespective of the available wind speed. The responses with type-2 FLC are shown in Figure 4.13. In the type-2 case, the new steady state of active power has reached within 15s, after initiation of speed; the oscillations in the active and reactive power are completely damped out. The constant dc link voltage shows the effectiveness of the controller for uncertainties in wind speed. Further, excellent response of stator voltage and frequency is achieved without any distortion.

The response at bus 800 reflects the impact of change in wind speed on the grid performance. The performance of type-1 and type-2 FLC are shown in Figures 4.14 and 4.15 respectively. The bus voltage maintains its normal level at 1.05p.u. The changes in the active and reactive powers at the bus are approximately equal to the amount of power that is lost due to change in wind speed at the turbine input. With type-1 FLC, severe oscillations are developed in both active and reactive powers for more than 20s that may have an impact on the grid stability. The response of both the powers with type-2 case is very smooth and settles with in 10s after initiation of the speed. The bus voltage in both type-1 and type-2 cases remains stable, because the bus 800 represents the grid voltage

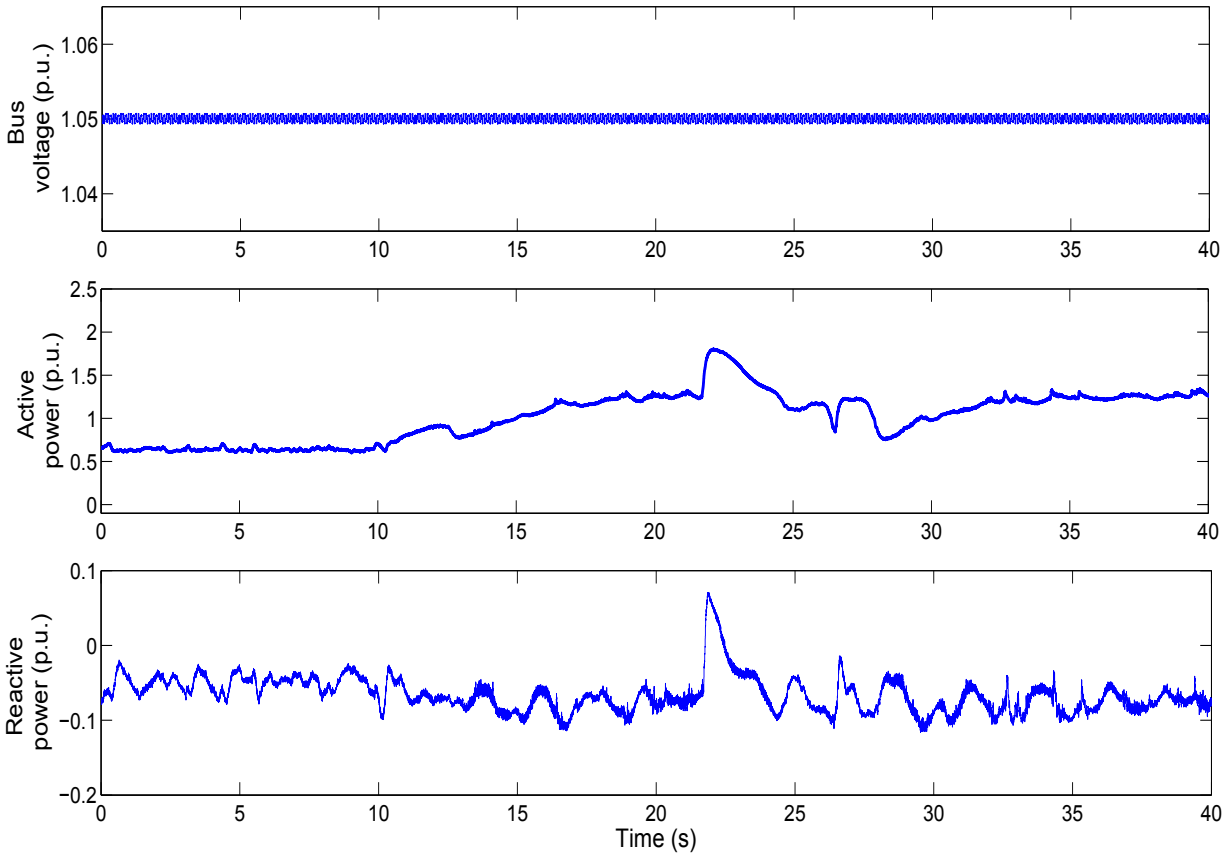

Figure 4.15: Responses for change in wind speed at Bus 800 (type-2 FLC)

which is unaffected by the small disturbances in the distribution side.

The responses at bus 890 are shown in Figures 4.16 and 4.17 for type-1 and type-2 FLC respectively. Similar to previous case, the power oscillations in type-1 case is much sever compared to that of type-2 case. Low frequency oscillations are observed in the bus voltage, which are subsequently damped out much faster in type-2 case.

4.4.3 Load loss

Load loss and load variations are quite uncertain in distribution network and stable operation is expected from the wind generator under these conditions. In order to verify this, the load at bus 890 (450 kW, 225 kVar) is disconnected from the bus at 10s and the response of the DFIG with both type-1 and type-2 FLC are shown in Figures 4.18 and 4.19 respectively. A small voltage dip is observed in stator voltage of the DFIG due to sudden disconnection of load with remaining parameters in intact.

The response at bus 800 for both type-1 and type-2 FLC are shown in Figures 4.20 and 4.21 respectively. Since the DFIG is supplying a constant output, the power exported to the grid has changed to 0.63MW and 0.1 MVar which is approximately equal to the

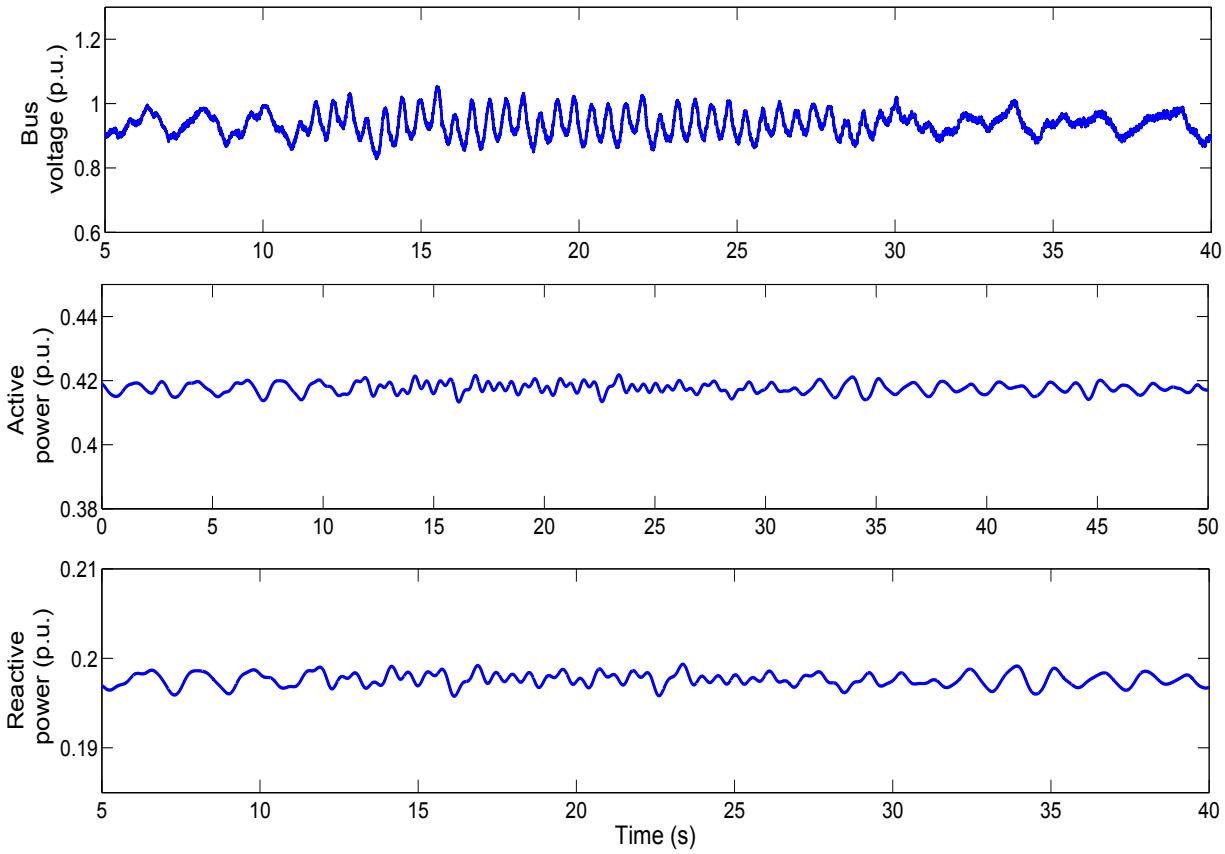

Figure 4.16: Responses for change in wind speed at Bus 890 (type-1 FLC)

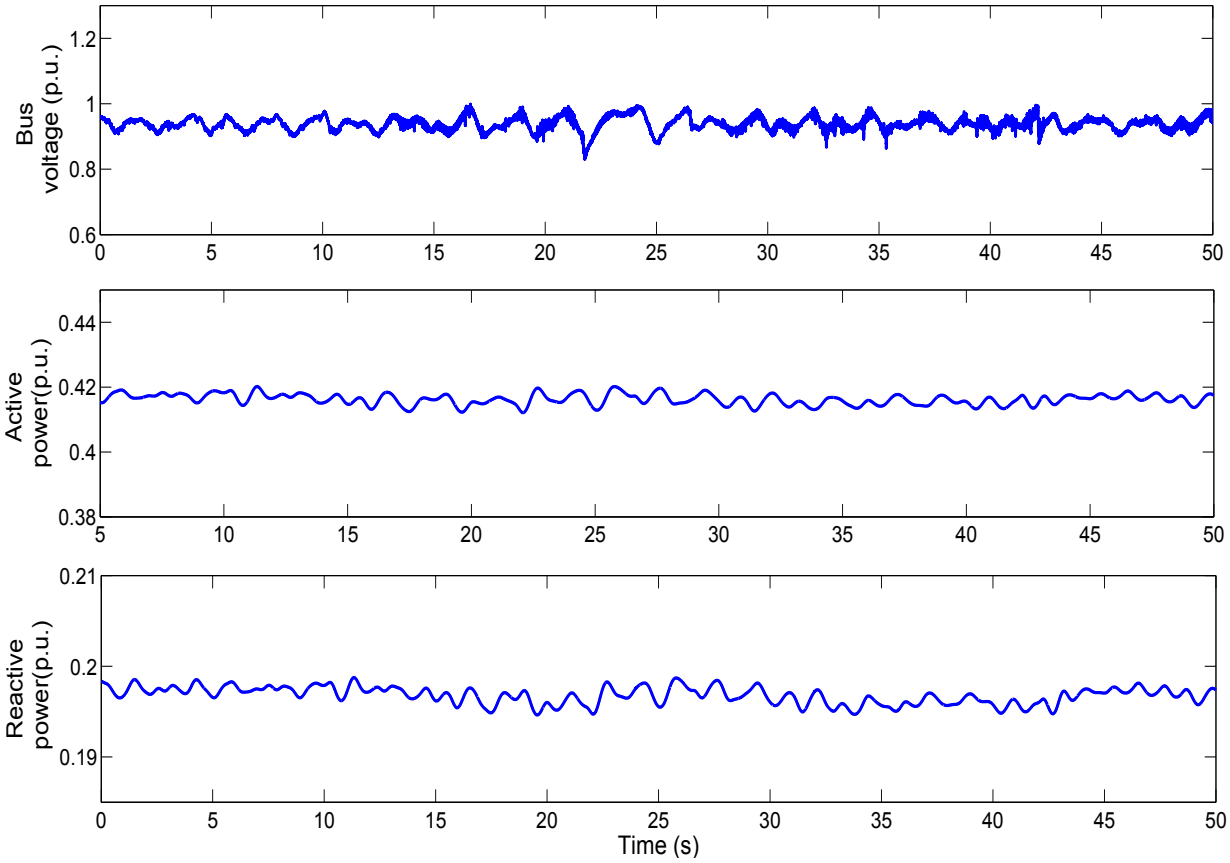

Figure 4.17: Responses for change in wind speed at Bus 890 (type-2 FLC)

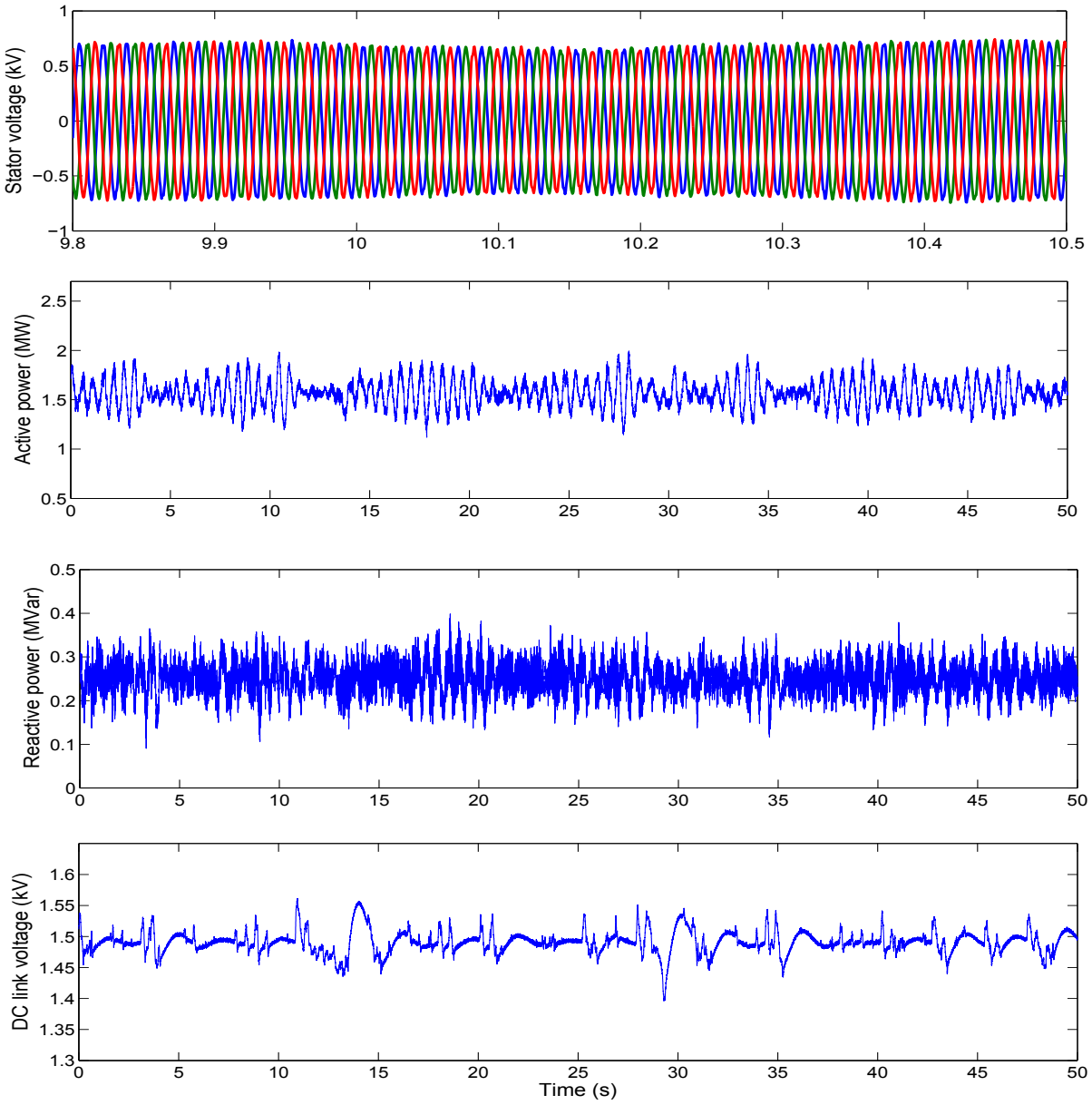

Figure 4.18: Response of DFIG for change in load (type-1 FLC)

amount of load that is disconnected. After the load disconnection, sustained oscillations in both active and reactive power are observed in type-1 case. An improved performance in the power oscillations has been observed with the proposed controller. Since the bus 800 is directly connected to the grid, the response at this bus represents the impact of load disturbances on the grid stability. It is observed that the type-2 FLC is successful in eliminating the effect of load disturbances on the grid stability.

The responses at bus 890 for both type-1 and type-2 FLC are shown in Figures 4.22 and 4.23 respectively. In both the cases, the bus voltage has dropped to 0.9 p.u. with sustained oscillations. With the proposed strategy, the control surface formed with large number of embedded type-1 FSs is very smooth compared to type-1 FLC as depicted in Figure 4.24.

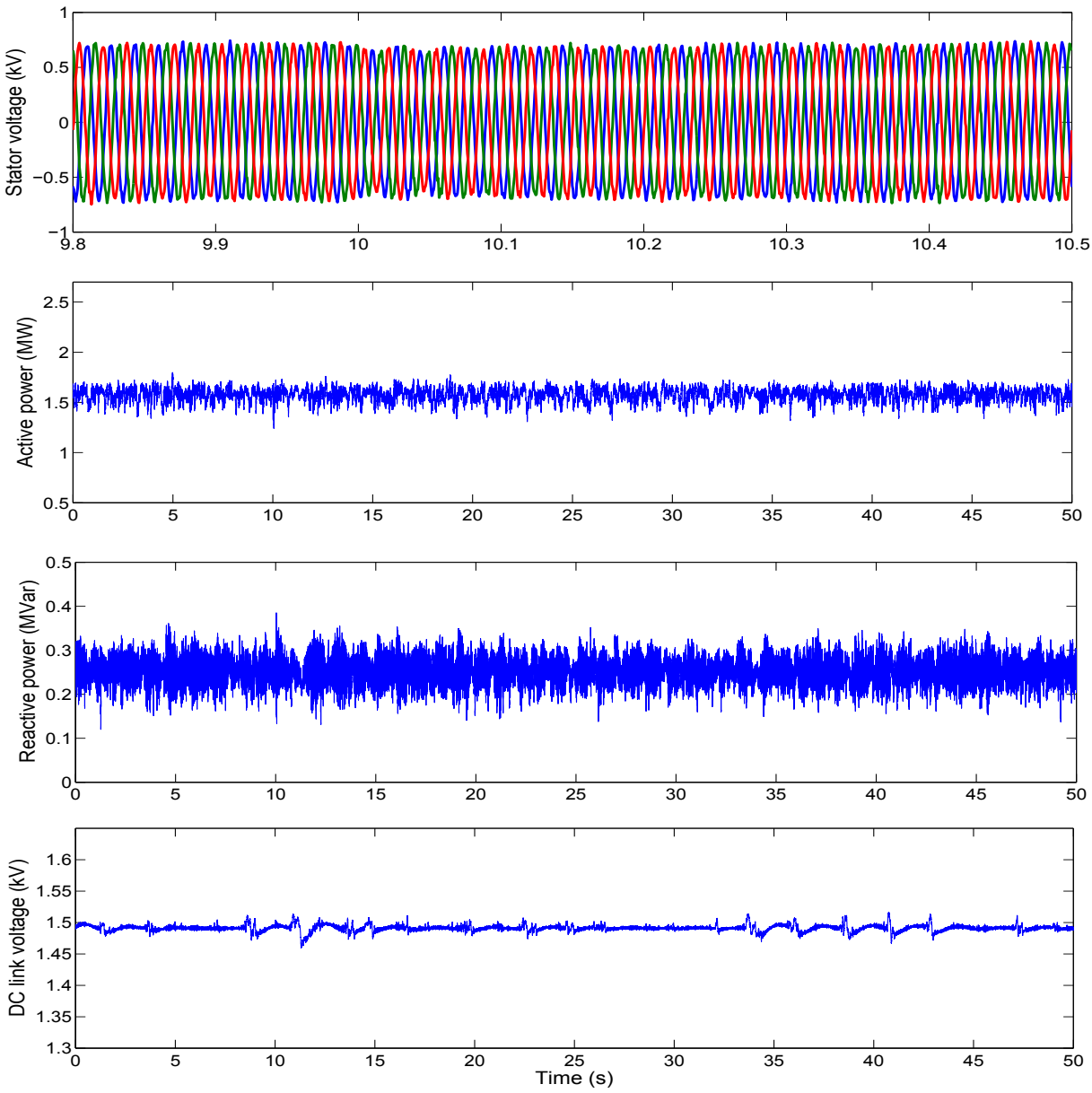

Figure 4.19: Response of DFIG for change in load (type-2 FLC)

This smooth surface will consequently make it less sensitive to uncertainties in parameters and disturbances and the result is clearly visible from the above responses. Since the controller is implemented in hardware-in-loop environment, the huge computational delays of the controllers and process delays in the conversion process makes the results more realistic and useful for real time analysis. This shows that the proposed controller is able to regulate the sudden changes in the system operating conditions without the need of retuning the controller parameters.

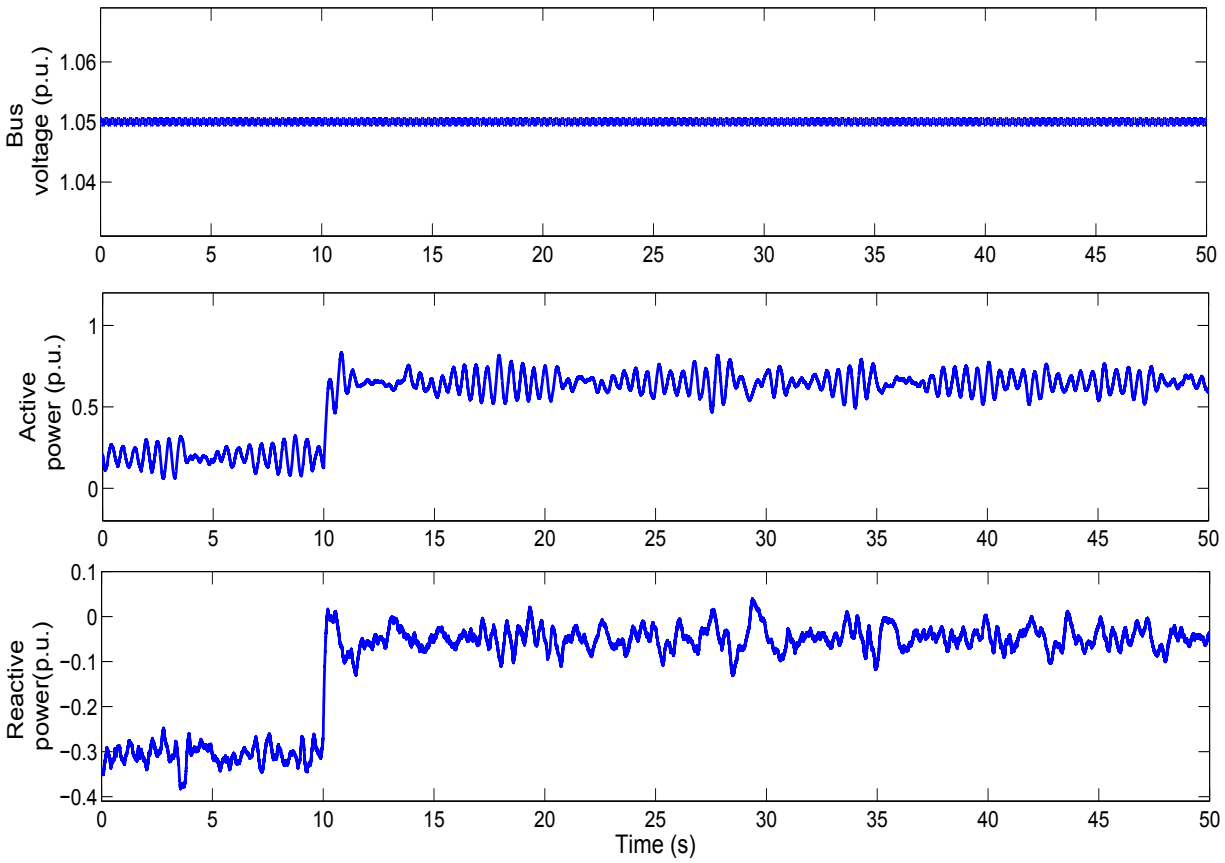

Figure 4.20: Responses at Bus 800 for change in load (type-1 FLC)

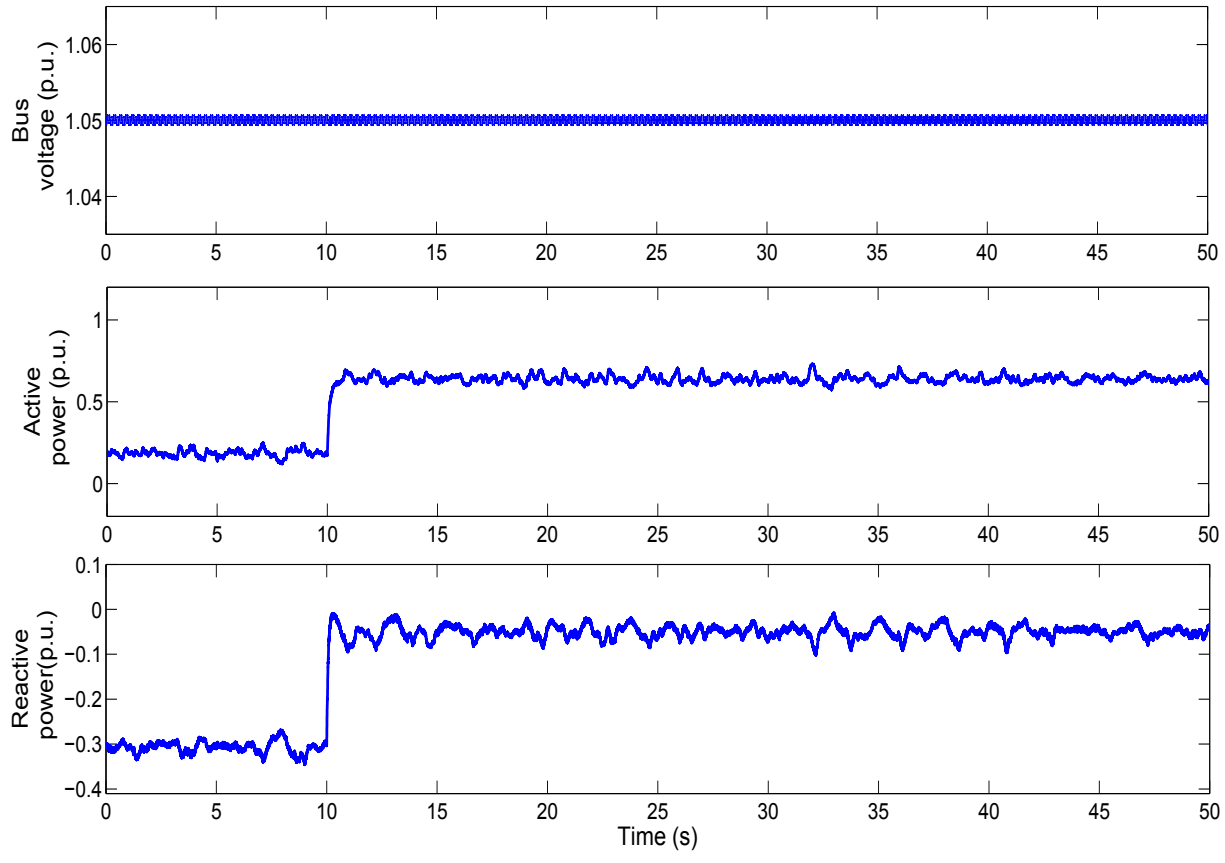

Figure 4.21: Responses at Bus 800 for change in load (type-2 FLC)

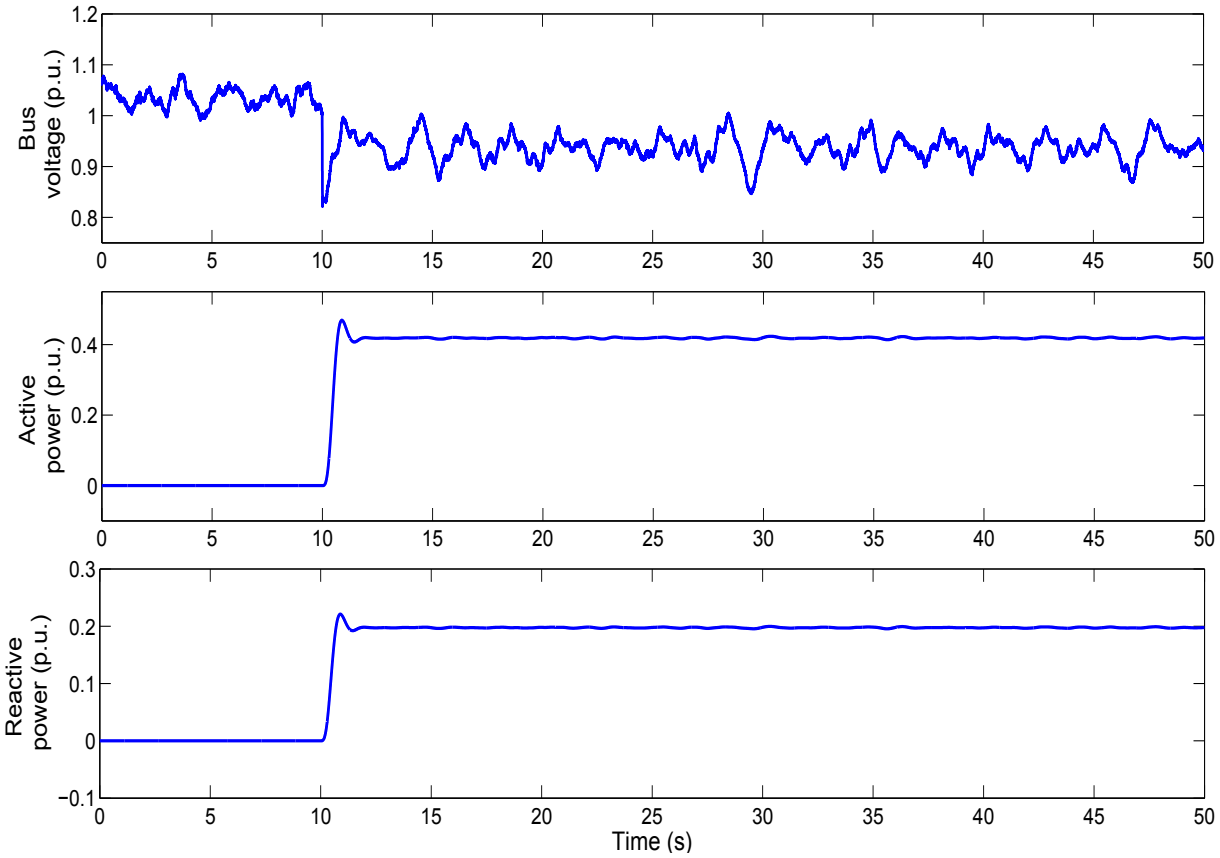

Figure 4.22: Responses at Bus 890 for change in load (type-1 FLC)

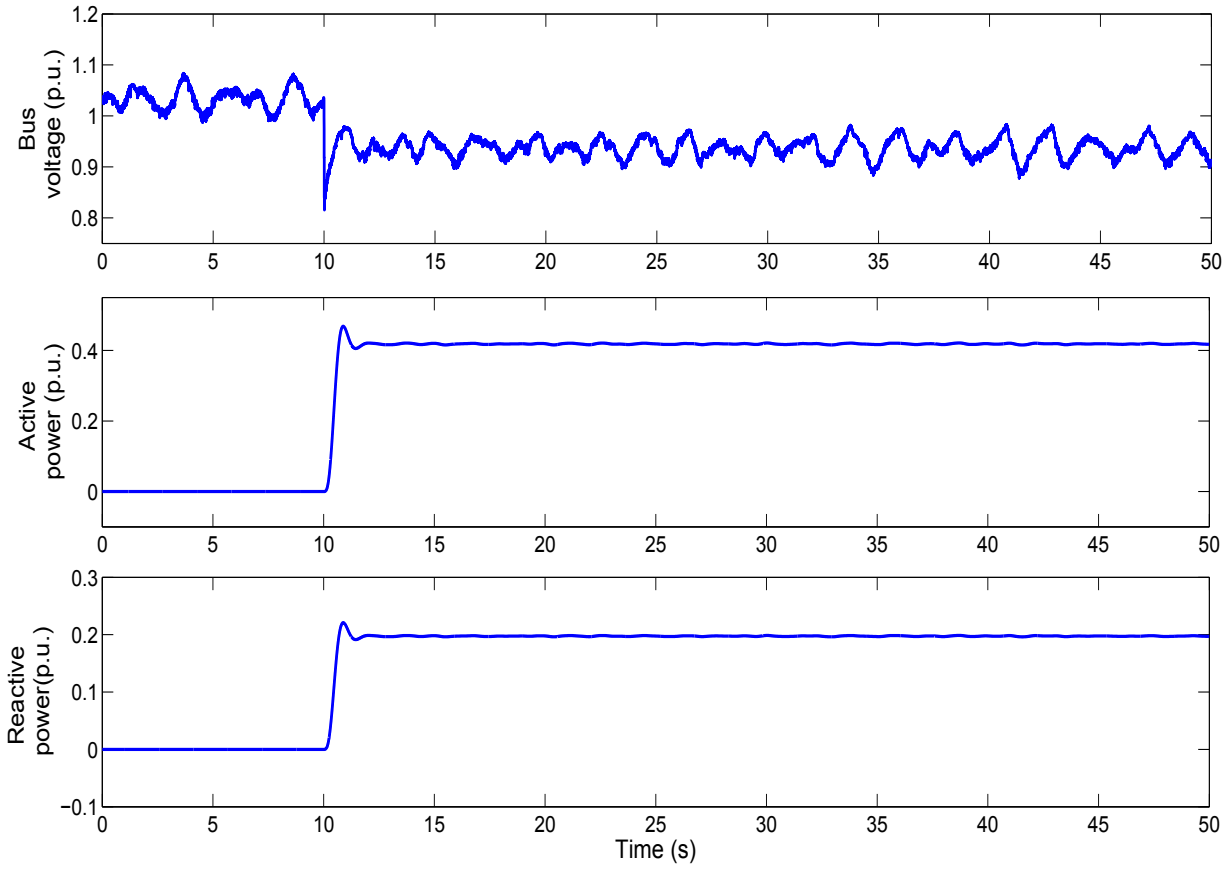

Figure 4.23: Responses at Bus 890 for change in load (type-2 FLC)

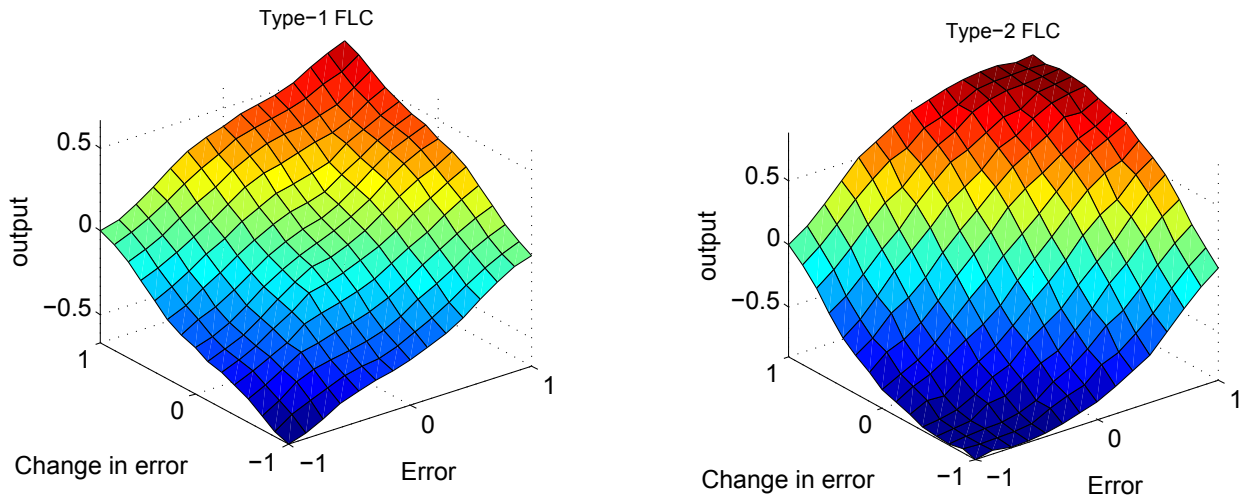

Figure 4.24: Control surfaces for type-1 and type-2 FLC

4.5 Conclusions

In this chapter, a novel control strategy using type-2 FLC is proposed for a DFIG based wind turbine connected to a distributed network. The controllers are designed for the converters of DFIG to examine the effect of FOU in the membership function for handling the system uncertainties. The designed controller is implemented for real time simulations and interfaced with the RTDS/RSCAD in HIL configuration using analog signals of control error. The performance is evaluated on IEEE-34 bus test system for steady state and dynamic behavior under three phase fault, load loss and variable wind speed conditions. The simulation results showed a significant improvement in the power oscillation damping and voltage profile of the distributed network compared to that of type-1 FLC. The proposed strategy is able to give a satisfactory performance, in variable wind speed conditions, without the need of retuning the controller parameters. Furthermore, the whole system turns out to be significantly robust against deviations in operating conditions, fulfilling requirements of standard grid codes. Although the type-1 FLC is able to handle the non-linearity present in the system, type-2 FLC is more effective in handling system uncertainties. The results presented in this work are more realistic, since the computational delays and signal conversion delays are taken into account.

Chapter 5

Type-2 Fuzzy Logic based Robust Control Strategy for Power Sharing in Microgrids

5.1 Introduction

The increasing energy demand, safety of environment and depletion of fossil fuels are the major concerns drawing the worlds attention towards alternative energy sources. The features like environment friendly and bulk energy production have made the renewable energy sources very popular in recent times. The increasing penetration of renewable sources in utility grids gave rise to the concept of microgrid(MG). A typical microgrid can be viewed as a cluster of distribution generation (DG) units capable of operating in either islanded or grid connected mode.

Among the renewable energy sources, wind and solar energy are the two important sources that have largest utilization in the recent times [15]. Besides the uncertainty in solar radiation and wind speed, grid integration, controllability, reliability and power quality are the main challenges to incorporate the renewable sources in microgrid [44]. Further, the DG units are low inertia sources and highly sensitive to disturbances. The power system networks with such sources are prone to various uncertainties which affects the network operating conditions, stability and reliability, leading to frequent islandings. Therefore, for effective power sharing the designed control schemes should be capable of handling the disturbances that arise as a result of uncertainties in the operating conditions.

For reliable islanding operation of microgrid, the power electronic converters associated with the DGs must share the power demand regardless of the network disturbances and in achieving this, the control schemes plays a crucial role. Many control schemes based on droop control techniques are presented in the literature for accurate power sharing [104, 107]. The conventional droop control methods are presented based on power flow theory which states that if the line impedance is highly inductive and power/torque angles are small enough, then the active and reactive powers can be controlled by power angle and voltage amplitude respectively. However, these methods suffer from mismatched line impedance between the loads and sources [140]. Recently, a few modified droop control methods are presented in [46], which addresses the drawbacks of the conventional droop

method. Nevertheless, the switching actions of droop curves may lead to stability problems caused by the uncertainty in bus frequency in MGs. In [26], a voltage/frequency or power sharing control strategy for both islanded and grid-connected mode shows effective coordination between inverter PQ controls. Pre-planned and unplanned switching incidents and subsequent islanding analysis are illustrated in [9]. The work presented in [80] deals with the upstream grid faults when the microgrid is in the grid-connected mode, and fails to address the faults in the islanded mode.

Most of the control strategies mentioned above uses conventional PI controllers with centralized as well as local control schemes. The fixed gain PI controller provides an acceptable performance under normal operating conditions, but poor transient performance is often obtained under changes in the network parameters and dynamics of the plant. In addition, the operating conditions of the microgrid may vary with uncertainty in wind speed, solar radiation, grid faults and other network disturbances. In such cases, the PI controller may require frequent re-tunning to cope with the change in network parameters. Further, an accurate and linear mathematical model of the plant is required to design an effective PI controller whereas modelling of the MG is complex and highly nonlinear in nature. Most of the existing literature used linearized models for the analysis that may not predict the behaviour of the system properly for severe disturbances in the network [15]. This chapter discusses about the other control schemes and their applicability to improve the operational performance of microgrid.

5.1.1 Problem description

Recent review studies on MG shows that existing fuzzy logic (type-1) controllers present a better performance in both grid connected and islanded mode compared to that of conventional PI controllers [13, 37]. The fuzzy logic controllers (FLCs) can be designed with proper rules and membership functions, and it offers some benefits such as independency from the MG model and structure. Further, the control surface of the FLC can be shaped to define appropriate sensitivity for each operating point [61]. The authors in [14] proposed a droop control strategy based on fuzzy logic that removes its dependency on line parameters. To enhance the performance in islanded mode, fuzzy based pitch angle controller and energy storage ultra-capacitor are used in [71].

In general, type-1 FLC is designed based on the rules and membership functions (MFs), mostly decided by the knowledge and experience of field experts. The uncertainty is always present in the rules and MFs because the number of MFs, its width and rules depends on

the designer choice which varies from case to case. However, the type-1 fuzzy logic sets (FLSs) cannot consider this uncertainty due to its two dimensional structure of MFs. With this drawback, the controller may not perform optimally and requires re-definition of rules and membership functions to counter the uncertainties [74].

This chapter addresses the robustness issue of PI and uncertainty issues of type-1 FLSs with a new control strategy based on interval type-2 fuzzy sets (IT-2 FSs). Unlike the type-1 sets, the type-2 FLSs are described with a three dimensional fuzzy MF that includes a footprint of uncertainty (FOU). The third dimension of MFs and FOU, together provide an additional degree of freedom in the controller design that makes it possible to directly model and handle the uncertainties associated with the rules and membership functions [89]. The above special features of the type-2 fuzzy sets can avoid frequent retuning of the controller parameters and provide a desirable performance over a wide range of operating conditions [118].

In this work, a robust type-2 FLC is designed for power sharing and implemented in real-time for hardware in loop simulations. The IEEE-34 bus system with a DFIG based wind energy system, PV system, and a storage battery together considered as a microgrid and tested for both grid connected and islanding operations. The IEEE 34-bus system and the DGs are implemented in RSCAD for the analysis with real-time simulations. Performance is verified based on digitally implemented control algorithm in DS1104 module and real time simulations through hardware-in-loop tests in RTDS environment. The controller performance is analyzed for transients during grid connected to islanding operation and also a three phase short circuit fault in microgrid. Further, to ascertain the robustness of the proposed strategy, sudden loss of DG source and load disturbances are also considered; the performance of the system in grid connected mode is compared with the results of PI controller. An attempt has been made to investigate, whether the uncertainty modelling capabilities of type-2 FLSs could be exploited to deal with the microgrid uncertainties.

5.2 Microgrid components

This section presents the dynamic models of DGs under consideration. To analyze the performance of the proposed control strategy, a standard IEEE-34 bus system is adopted as microgrid as shown in Figure 5.1. The original system is rated at 24.9 kV, 60Hz, 12 MVA supplying unbalanced spot and distributed loads and without any renewable sources. The rating of the DFIG and PV system are chosen in such a way to maintain compatibility

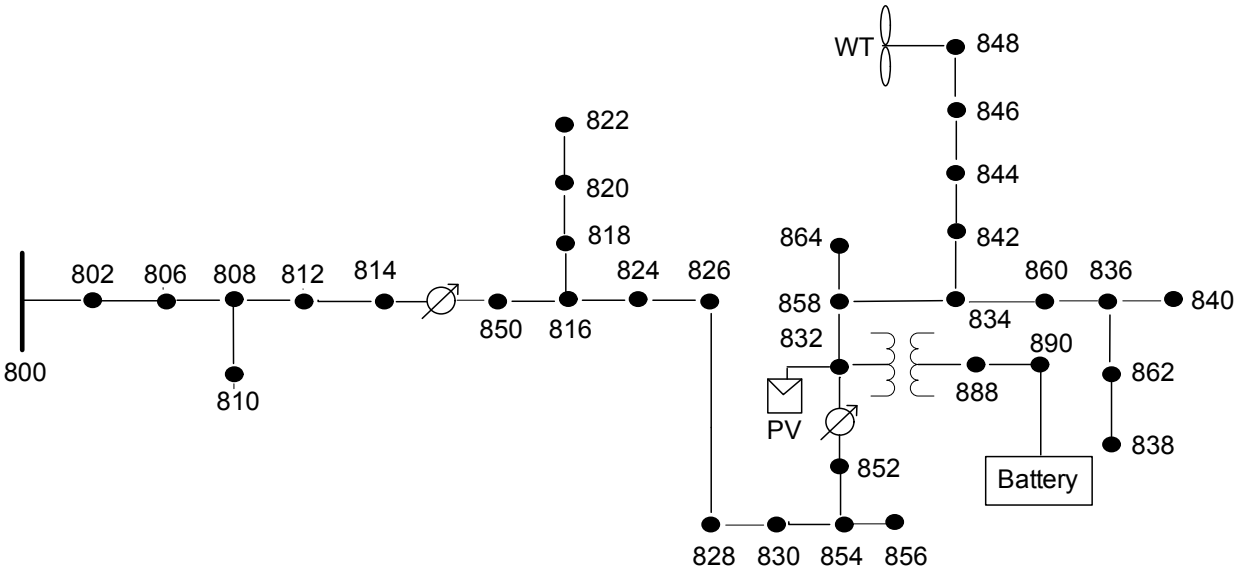

Figure 5.1: Schematic diagram of IEEE-34 bus system as a microgrid

with the original network. The network consists of two regulators for voltage control, two capacitor banks at bus 844 and 848 for reactive power compensation; and the bus 800 for connecting to the utility mains. The test microgrid is connected with a variable speed DFIG at bus 848, PV system at bus 832 and a battery storage system at bus 890 [44]. The modelling equations of DFIG are derived in chapter 3.

5.2.1 Mathematical modeling of the solar cell

An initial understanding of the performance of a solar cell may be obtained by considering it as a diode in which the light energy, in form of photons with the appropriate energy level, falls on the cell and generates electron-hole pairs. The electrons and holes are separated by the electric field established at the junction of the diode and are then driven around an external circuit by this junction potential. There are losses associated with the series and shunt resistance of the cell as well as leakage of some of the current back across the p-n junction [68]. An ideal solar cell is electrically represented as a current source in parallel with a single diode, however practical solar cell models require additional elements to accurately represent their nonlinear current-voltage characteristics. A commonly used practical model extends the ideal solar cell by including a series and shunt resistance as shown in Figure 5.2. The current-voltage relationship of the single diode, five parameter model is derived as follows:

The output-terminal current I is equal to the light-generated current I_{ph}, less than the

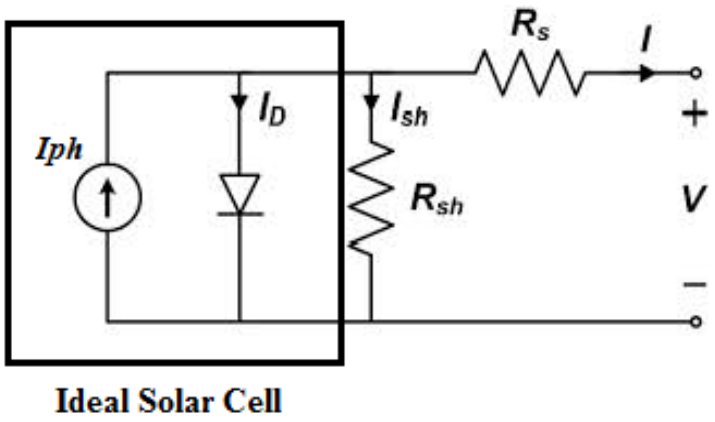

Figure 5.2: Equivalent circuit of a PV cell

diode current I_D and the shunt-leakage current I_{sh}.

$$I = I_{ph} - I_D - I_{sh} \tag{5.1}$$

The series resistance R_s represents the internal resistance to the current flow, and depends on the p-n junction depth, the impurities and the contact resistance. The shunt resistance R_{sh} is inversely related to the leakage current to the ground. In an ideal PV cell, $R_s = 0$ (no series loss), and R_{sh}=1(no leakage to ground). The PV cell conversion efficiency is sensitive to small variations in R_s , but is insensitive to variations in R_{sh} . A small increase in R_s can decrease the PV output significantly. In the equivalent circuit, the current delivered to the external load equals the current I_{ph} generated by the illumination, less than the diode current I_D and the ground-shunt current I_{sh} . The open circuit voltage V_{oc} of the cell is obtained when the load current is zero, i.e., when $I = 0$, and is given by the following:

$$V_{oc} = V + IR_s \tag{5.2}$$

where V is the terminal voltage of the cell (V). The diode current is given by the classical diode current expression [54]:

$$I_D = I_d \left[\frac{qV_{oc}}{A_{cf} K_B T} - 1 \right] \tag{5.3}$$

where,

I_D = the saturation current of the diode

q = the electron charge = $1.6 * 10^{-19}$ Coulombs

A_{cf} = curve fitting constant

K_B = Boltzmann constant = $1.38 * 10^{-23}$ Joule/^0KT

T = temperature [^0K].

The load current is given by the expression:

$$I = I_{ph} - I_{os} \left\{ \exp \left[\frac{qV_{oc}}{AKT} \right] - 1 \right\} - \frac{V_{oc}}{R_{sh}} \tag{5.4}$$

where

$$I_{ph} = \frac{G}{100}[I_{SCR} + K_I(T - 25)] \tag{5.5}$$

$$I_{os} = I_{or}\left(\frac{T}{T_r}\right)^3 \exp\left[\frac{qE_{GO}}{BK}\left(\frac{1}{T_r} - \frac{1}{T}\right)\right] \tag{5.6}$$

and

I, V = cell output current and voltage

I_{os} = cell reverse saturation current

A, B = ideality factor of p-n junction

K = Bolzmann constant

T = cell temperature $[^0C]$

K_I = short circuit current temperature coefficient at I_{SCR}, K_I= 0.0017 A/^0C

G = solar irradiation in W/m^2

I_{SCR} = short circuit current at 25^0C and 1000W/m^2

I_{ph} = light generated current

E_{GO} = band gap for silicon

T_r = reference temperature, $T_r = 301.180K$

I_{or} = cell saturation current at T_r

R_{sh} = shunt resistance

R_s = series resistance

The $I-V$ characteristics define the operating point of the PV array for a given insolation and temperature as shown in Figure 5.3. The curves range from the short circuit current (I_{sc},0) to the open circuit voltage (0,V_{oc}) with a knee point (I_m, V_m) defined as the maximum power point where the PV array generates maximum electrical power P_{max}. The $I - V$ characteristic of the solar cell depends on the variation of the solar parameters, insolation G (solar intensityW/m^2) and temperature $T(K)$.

5.2.2 Modelling of grid connected PV system

The three phase single stage PV system is connected to the grid and the schematic diagram of the system is shown in Figure 5.4 . The PV system mainly consists of PV panels, a three-phase voltage source converter (VSC), and an output LCL filter. The PV panels are connected in parallel to the dc-link capacitor C and the dc-side terminals of the VSC. The VSC is connected to the point of common coupling (PCC) through an LCL filter. The

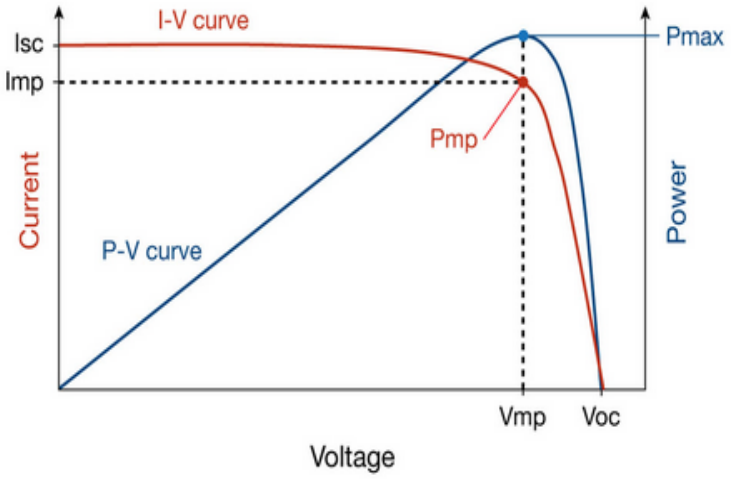

Figure 5.3: $I - V$ characteristics of a PV cell

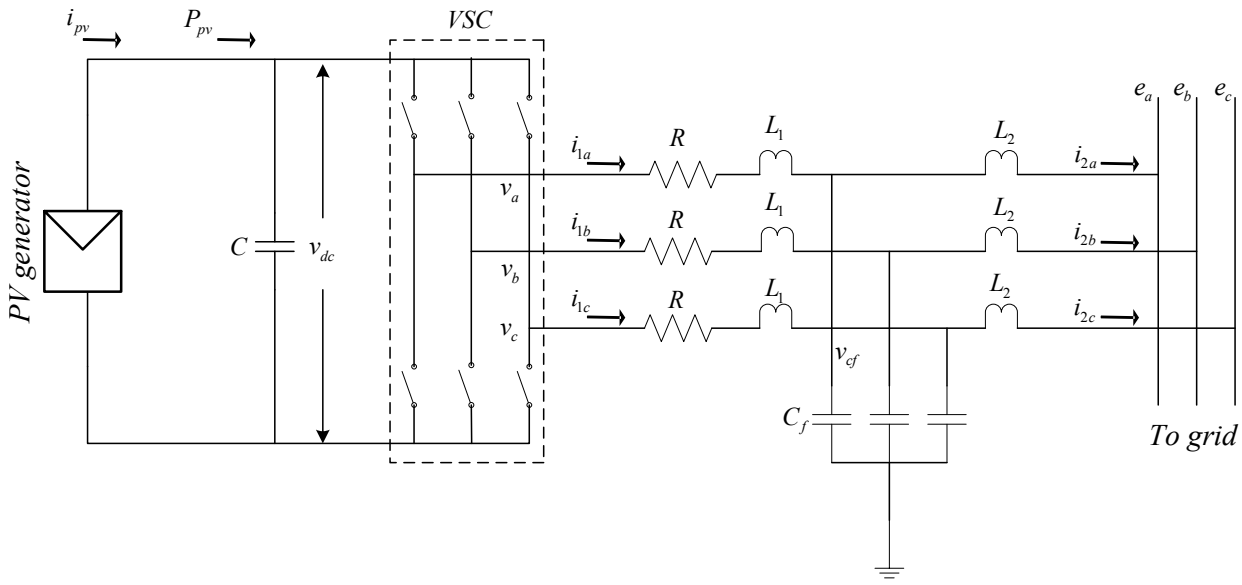

Figure 5.4: Three phase single stage grid connected PV system

nonlinear model of a three-phase grid-connected PV system can be obtained in dq frame using the angular frequency ω of the grid [54]:

$$L_1\dot{i}_{1d} = -Ri_{1d} - \omega L_1 i_{1q} + Ri_{2d} - v_{cfd} + v_{pv}K_{d1} \tag{5.7}$$

$$L_1\dot{i}_{1q} = -Ri_{1q} + \omega L_1 i_{1d} + i_{2q} - v_{cfq} + v_{pv}K_{q1} \tag{5.8}$$

$$L_2\dot{i}_{2d} = Ri_{1d} - Ri_{2d} - \omega L_2 i_{2q} + v_{cfd} - E_d \tag{5.9}$$

$$L_2\dot{i}_{2q} = Ri_{1q} - Ri_{2q} + \omega L_2 i_{2d} + v_{cfd} - E_q \tag{5.10}$$

$$C_f\dot{v}_{cfd} = -\omega C_f v_{cfq} + C_f(i_{1d} - i_{2d}) \tag{5.11}$$

$$C_f\dot{v}_{cfq} = \omega C_f v_{cfd} + C_f(i_{1q} - i_{2q}) \tag{5.12}$$

$$C\dot{v}_{pv} = i_{pv} + i_{1d}K_d - i_{1q}K_q) \tag{5.13}$$

Table 5.1: Parameters of PI controller

Parameters	PV system	DFIG
P	0.055	1.4387
I	0.52525	0.3898

Table 5.2: Parameters of type-2 FLC

Parameters	PV system	DFIG
K_e	0.9103	0.203
K_d	0.52525	0.03
K_u	0.47596	45

where R is the resistance, L_1 and L_2 are the inductances of the filter, C is the dc capacitance, C_f is the filter capacitance, v_{pv} is the voltage across the dc-link capacitor, V_{cf} is the voltage across the filter capacitor, i_1 and i_2 are the output currents of the inverter and filter, respectively, ω is the angular frequency, i_{pv} is the output current of PV array, and K_{d1} and K_{q1} are the binary input switching signals respectively. The subscripts d and q stand for direct and quadrature component and f for filter.

5.3 Control strategy

Depending on the mode of operation wide variety of control strategies are proposed in the literature for both interconnected and islanded microgrids [81]. Most of these control schemes comprises centralised controller that generates the references and the localised controllers for tracking the references. The reference signals are generated based on the power -voltage or power-frequency droop control techniques [98]. In general, the droop method requires the details of line parameters for accurate sharing of powers. In the proposed strategy, it is assumed that both wind and PV system are set to supply a constant power output. Since, the main objective of this work is to analyse the performance of the type-2 FLC in the presence of multiple DG sources, the detailed analysis of droop method and its performance analysis is not discussed in this work.

At first a PI controller is designed based on the control structure shown in Figure 5.5(a). The feed forward compensation is added to the controller output to take the grid disturbances into consideration. The PI parameters are tunned based on the observations from the output responses and the resulted parameters are shown in Table 5.1.

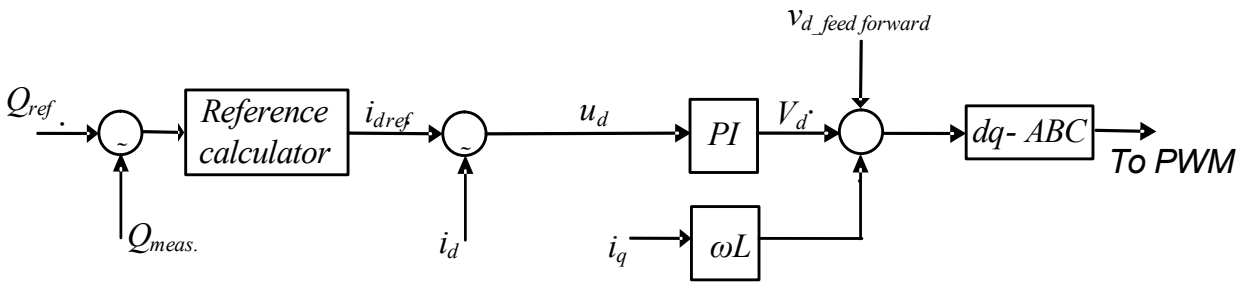

(a)

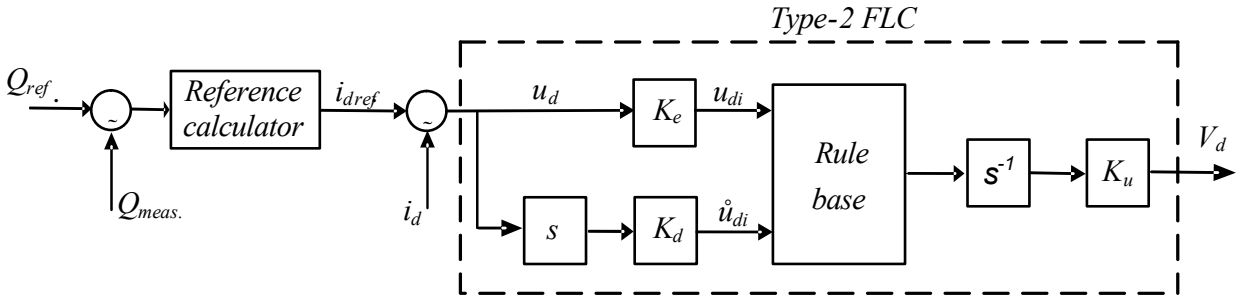

(b)

Figure 5.5: Block diagram of the control strategies with (a) PI controller, (b) type-2 FLC

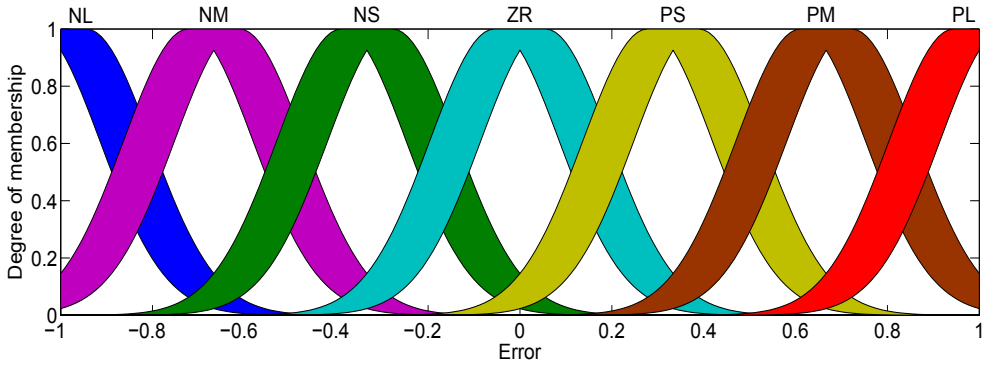

(a)

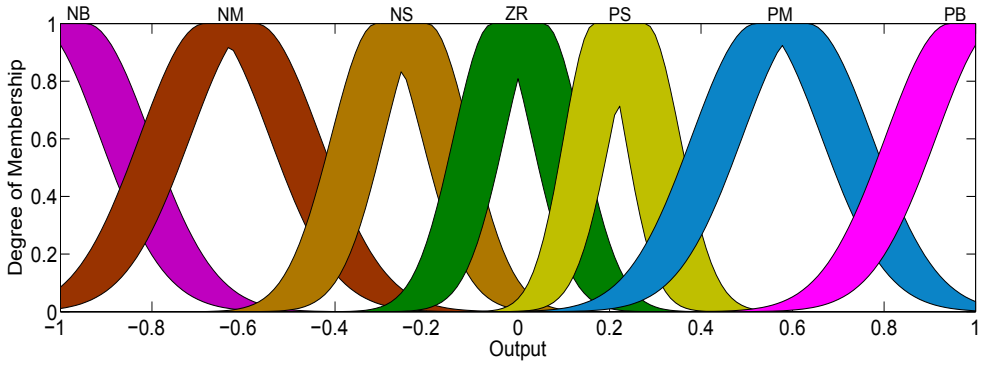

(b)

Figure 5.6: MFs for type-2 FLC (a) Input (b) Output

The proposed strategy with type-2 FLC is shown in Figure 5.5(b). Seven Gaussian membership functions are chosen for the fuzzification of input and output space and the designed membership functions are shown in Figure 5.6. The initial values of the controller parameters are determined by assessing the extensive simulations results in various operating conditions and the final tuned values are shown in Table 5.2.

5.4 Hardware-in-loop Simulations and Results

The real-time simulation setup based on the concept of HIL is shown in Figure 3.14, the setup comprises 1) six RTDS racks to execute microgrid model with 186 electrical nodes, 2) Gigabit transceiver analog output (GTAO) card and Gigabit transceiver analog input (GTAI) card for interfacing the simulator with control platform, 3) a DSP based Dspace 1104 module for processing the controller algorithm, and 4) a computer to run the RSCAD software and communicate with RTDS through Ethernet. RTDS is a digital electromagnetic transient simulator that can simulate any modern power grid configurations in real-time with various scenarios like physical damage, breaker and relay failures, cyber intrusion etc. It allows simulation time step up to 250ns and is considered by many researchers as a testing platform for controller prototyping and HIL tests [66].

In the simulation process, at first, the IEEE-34 bus system is modelled using RSCAD; a variable speed DFIG rated 1MW, 0.69 kV, 60Hz , is connected to bus 848 through a 2 MVA, 4.16/0.69 kV transformer. The PV system with rating of 1.2MW and the battery system of 1MWh are connected at bus 832 and 890 respectively. The workstation computer executes the RSCAD model and, interacts with the RTDS to generate real-time simulation results. The power error signals generated for both PV and DFIG converters on RSCAD platform are converted to analog signals using GTAO card. GTAO converts the digital signals in the range of $\pm$10V, through a multiplexed 16 bit Digital to Analog converter (DAC). The analog error signals are normalized and forwarded to type-2 FLC algorithm in Dspace 1104. The controller output is fed back to RTDS through GTAI card that has a 12 channel analog to digital converter (ADC) with the range of $\pm$10V. The sampling time and amplitude of the signals are adjusted to maintain compatibility between the simulator and controller. The controller with HIL setup is shown in Figure 3.15. To run the microgrid model on RTDS, the sampling time is set at 55μs and for the controller at 50μs.

In order to test and verify the effectiveness of the proposed control strategy, at first an intentional islanding has been simulated by disconnecting the utility grid; then a three

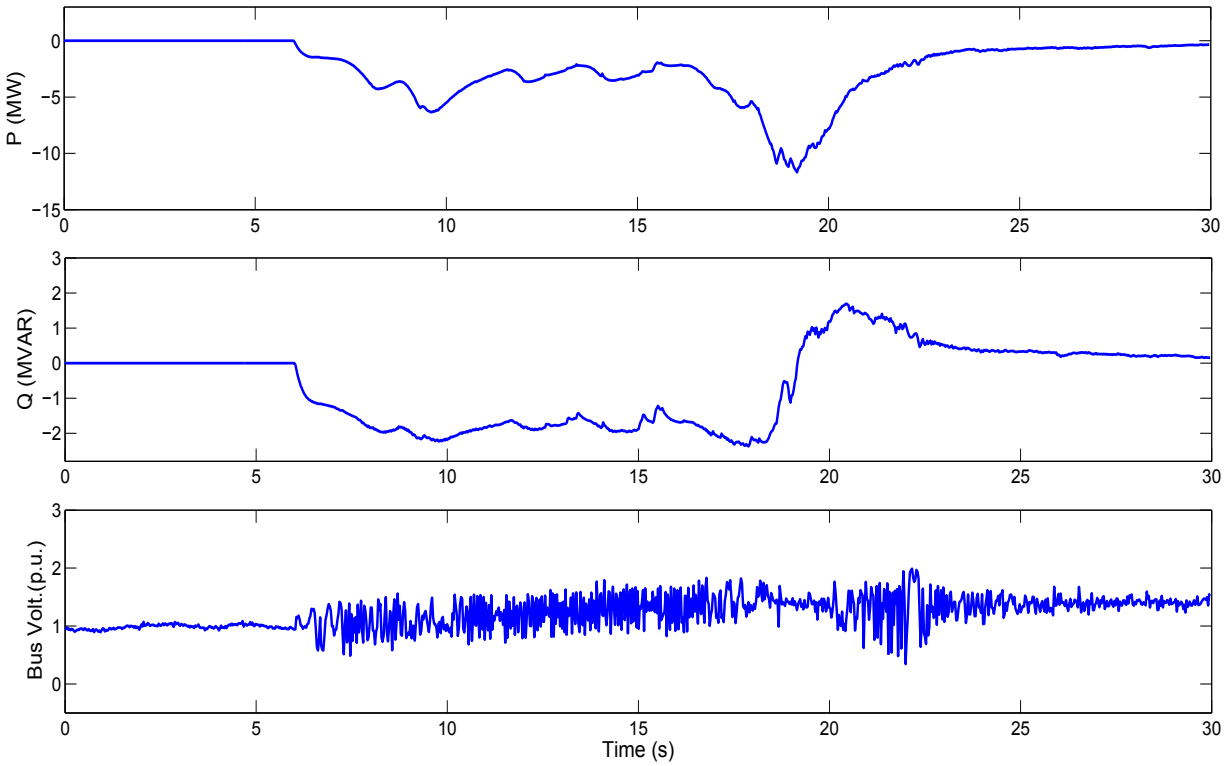

Figure 5.7: Responses of battery system for islanding with PI controller

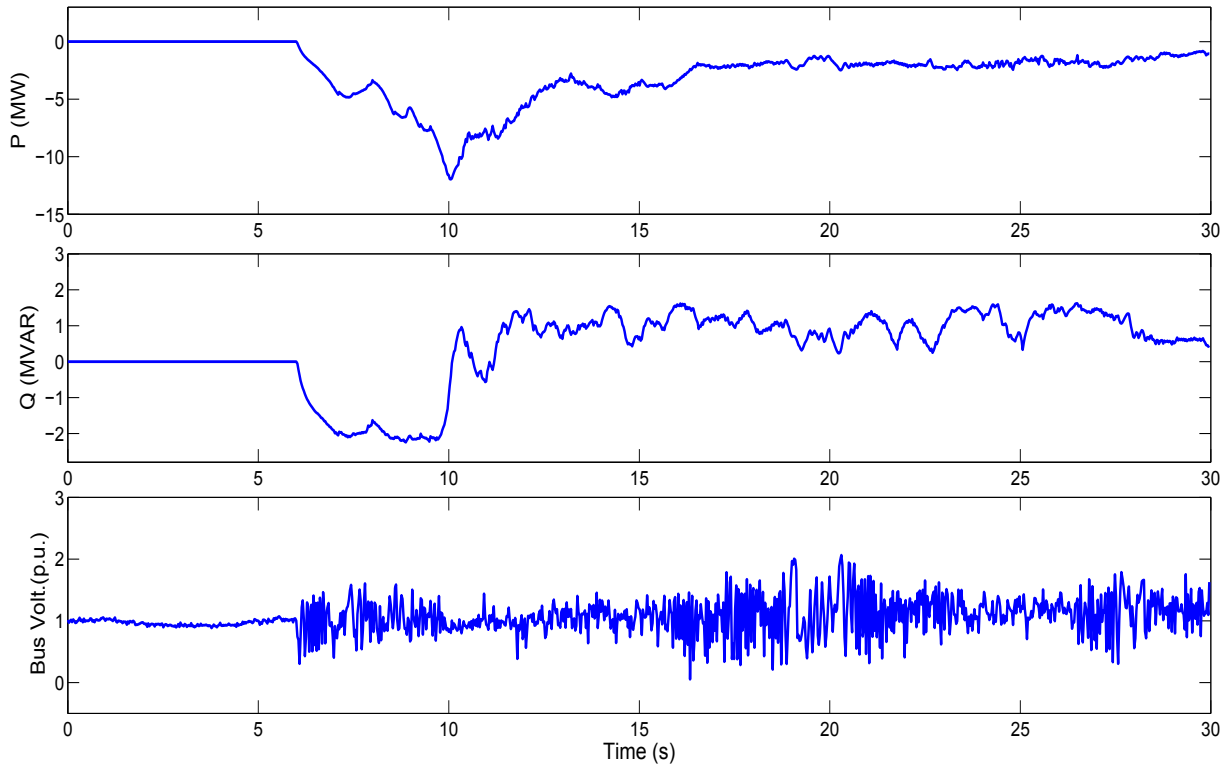

Figure 5.8: Responses of battery system for islanding with type-2 FLC

phase short circuit fault is applied in the MG, and the performances of bus voltages and power outputs of the DGs are analysed. Further to ascertain the robustness of the controller, the responses for PV outage and sudden load changes are also analysed keeping the network in grid connected mode.

5.4.1 Intentional Islanding

In this study the controller performance is analysed for islanding transients. An intentional islanding is implemented at 6s by tripping the grid breaker to disconnect the utility grid; the performance of the proposed method is compared with the PI controller. Initially, in the grid connected mode, the PV and DFIG were supplying 1 MW each, and utility grid at 0.5 MW to balance the supply and load. The battery system remains in floating condition. After the islanding, the battery is switched to discharge mode, compensating the power shared by utility grid. The responses of battery, utility grid, PV system and DFIG for both PI and type-2 FLC are shown in from Figure 5.7 to 5.10 .

As shown in Figure 5.7, with PI strategy, the transients in battery output powers settle after 17s, this in turn leads to severe oscillations in the bus voltage with peak amplitude of 0.5 p.u.. Whereas with the proposed case, a significant improvement has been visible in all the responses as shown in Figure 5.8. Both active and reactive powers are settled within 6s after the initiation of islanding.

Reactive power control is an important one in maintaining the voltage stability. The PV system with PI controller, low frequency oscillations are observed in the reactive power, consequently the bus voltage (Bus Volt.) is settled at 1.5 p.u. shown in Figure 5.9. The responses with FLC shows significant improvement in the power oscillations and also maintained the bus voltage 1.1 p.u. marking an improvement of 40% over the pi case. In this analysis, bus voltage means the voltage at the connection point that is bus 832, similarly for battery and DFIG it is at bus 890 and 848 respectively. This results shows a clear improvement in the performance of type-2 FLC.

The responses of the DFIG are shown in Figure 5.10 and 5.11. After the islanding, oscillations are observed in the output powers of DFIG, however the FLC is able to damp out them before reaching the steady state. Further, the type-2 FLC has maintained the bus voltage comparatively better than that of PI case. Since the DFIG is continued to supply the rated powers, so in this case , there is no much effect on its output performance.

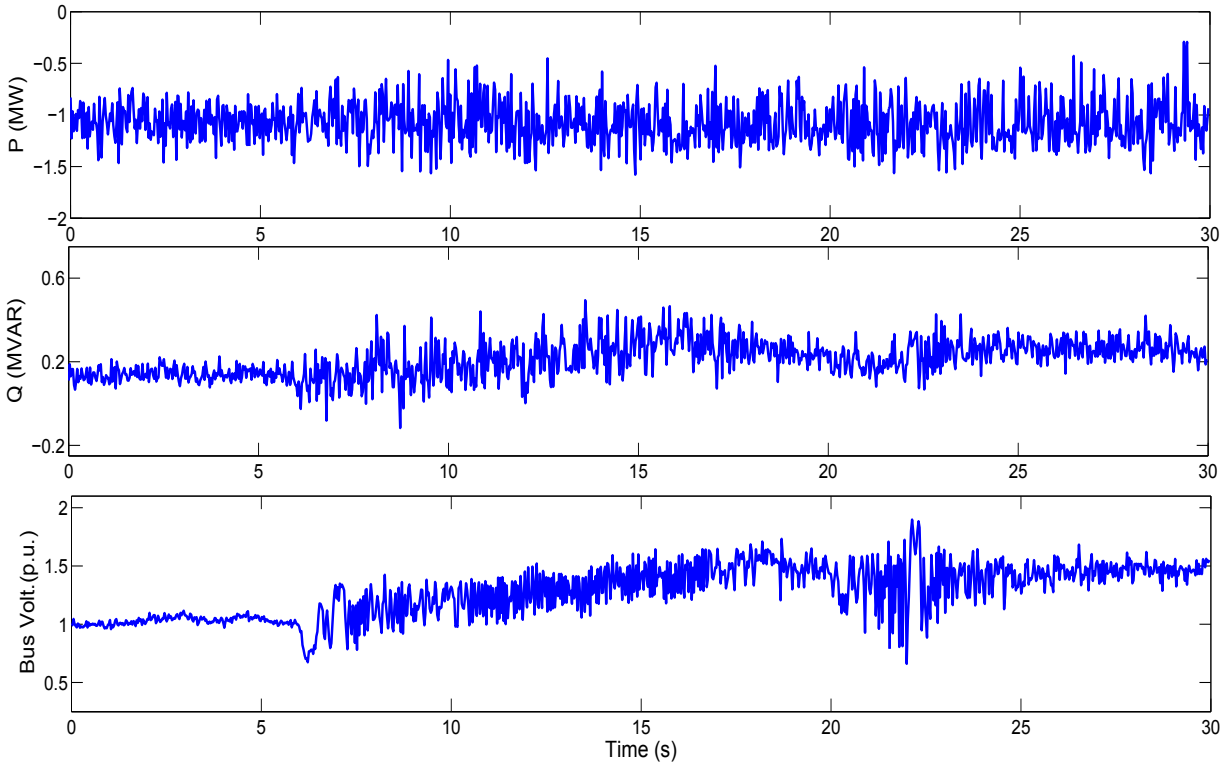

Figure 5.9: Responses of PV system for islanding with PI controller

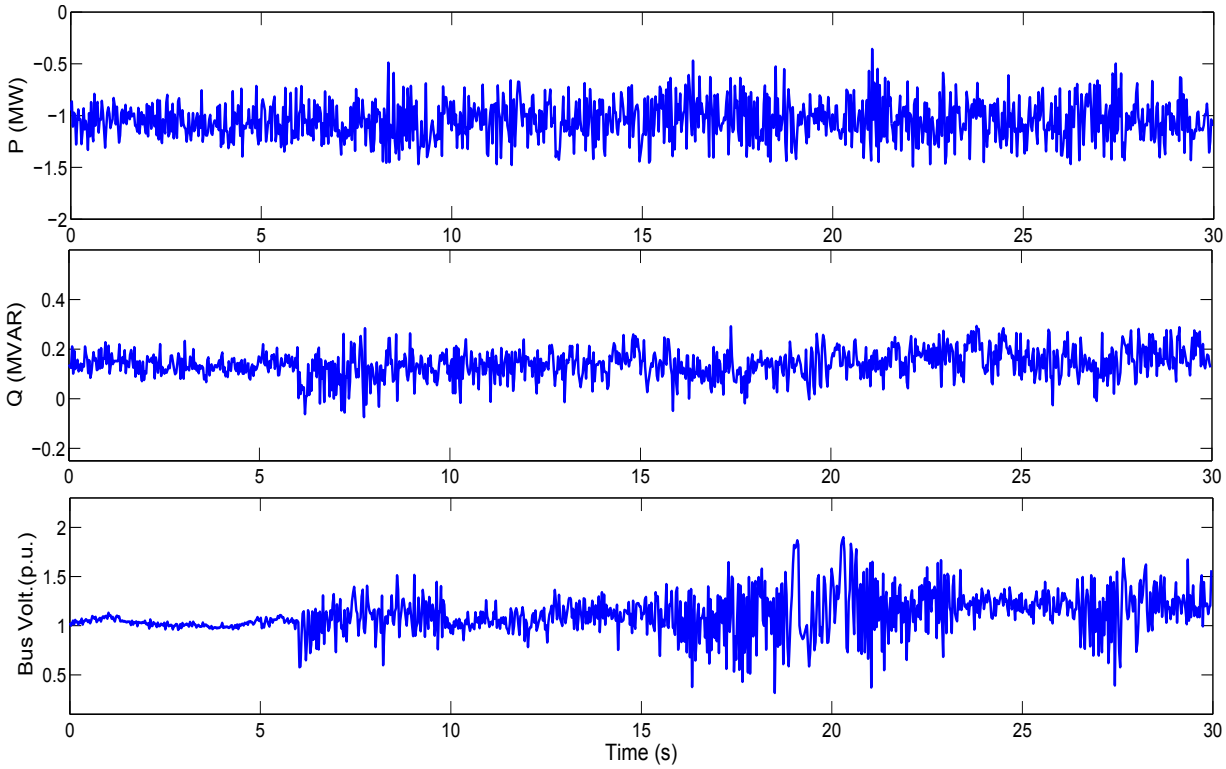

Figure 5.10: Responses of PV system for islanding with type-2 FLC

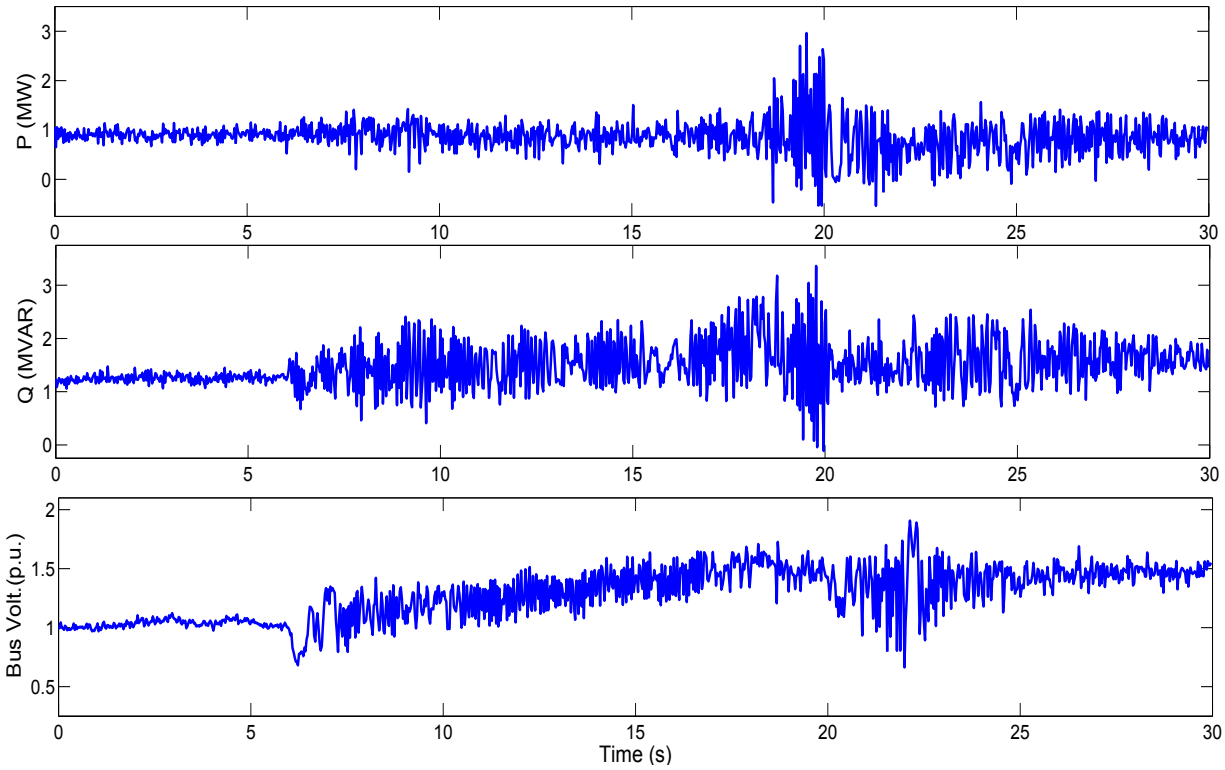

Figure 5.11: Responses of DFIG system for islanding with PI controller

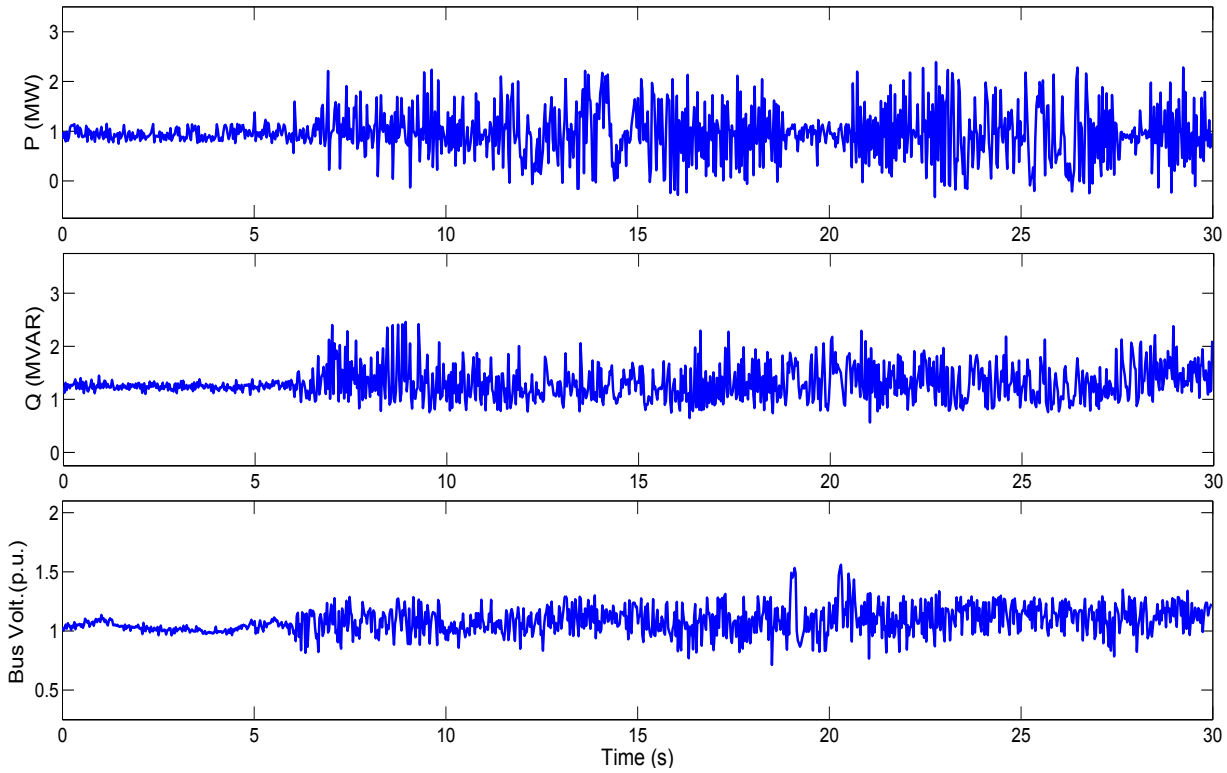

Figure 5.12: Responses of DFIG system for islanding with type-2 FLC

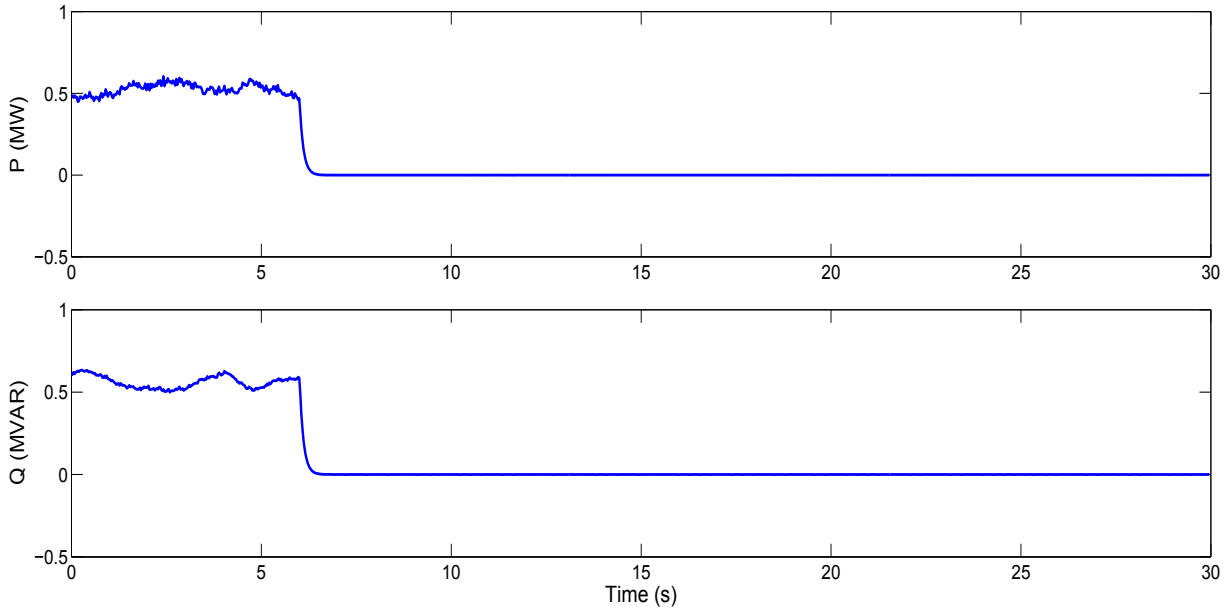

Figure 5.13: Responses of utility grid for islanding with PI controller

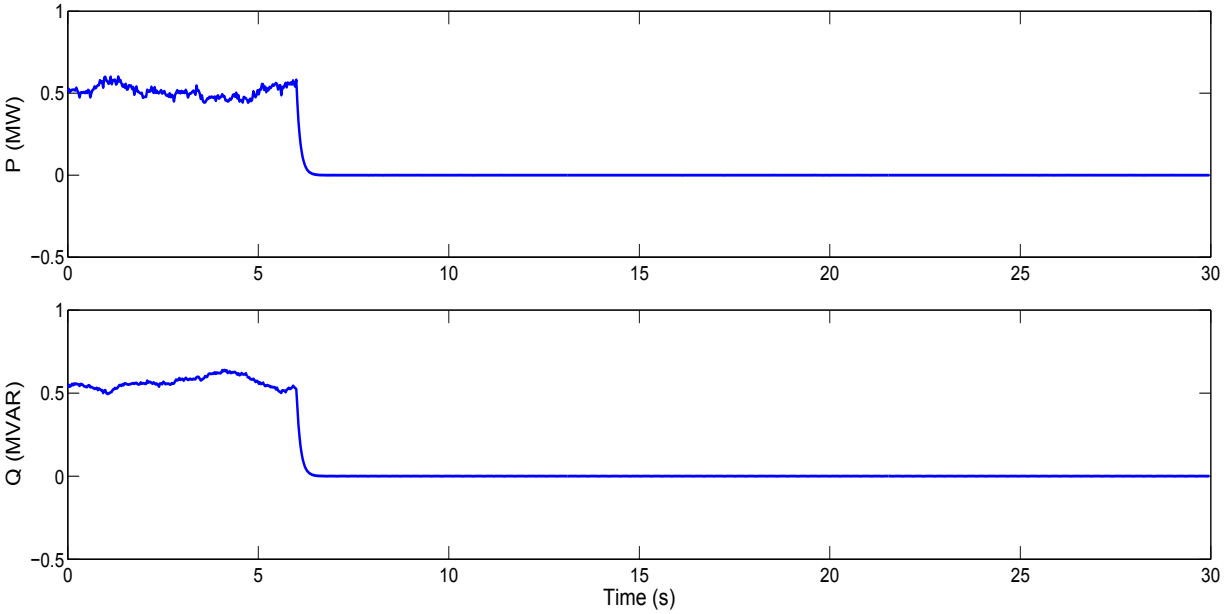

Figure 5.14: Responses of utility grid for islanding with type-2 FLC

Figures 5.13 and 5.14 shows the performance of the utility grid, it is obvious that the power supplied by the grid should be zero after the islanding. The captured digital oscilloscope images of error inputs to the controller are shown in Figure 5.15. The images show the change in magnitude for both PV and DFIG after initiation of the islanding operation. This analysis shows that type-2 FLC is better in handling the network uncertainties.

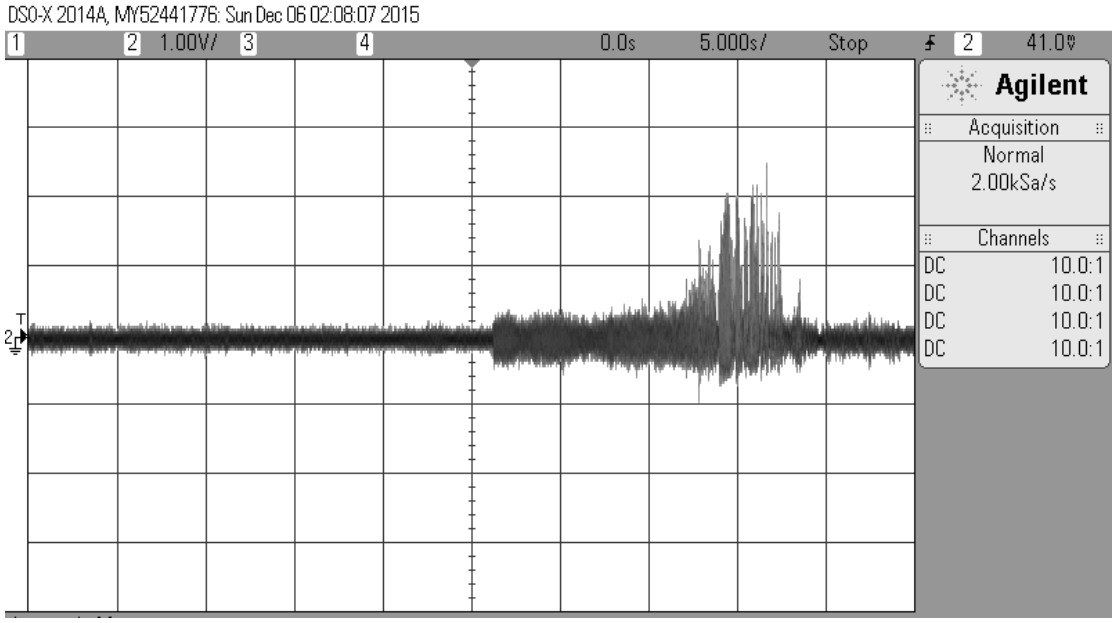

(a)

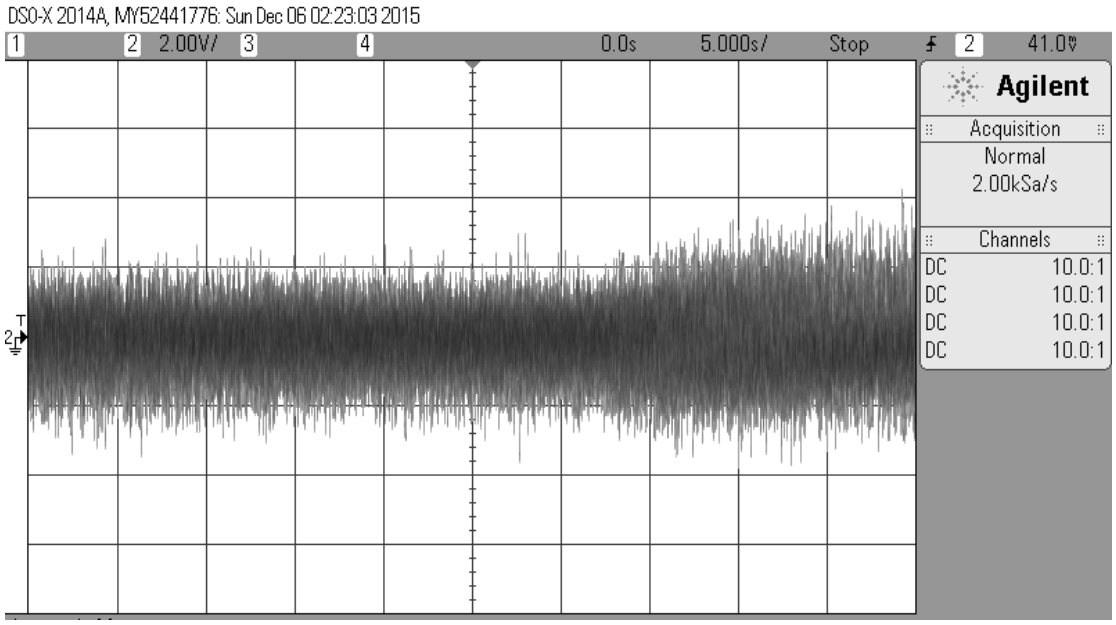

(b)

Figure 5.15: Error inputs during islanding operation (a) DFIG (b) PV system

5.4.2 Three phase fault

In general, the PI controller is designed for a specific operating condition of the plant and often observed a degraded performance with change in operating conditions. To verify the performance of proposed strategy in the above condition, a severe three phase fault is implemented at a feeder near to bus 832. Fault is initiated at 6s; the responses of PV system with PI and type-2 FLC are shown in Figure 5.16 and 5.17 respectively. With PI

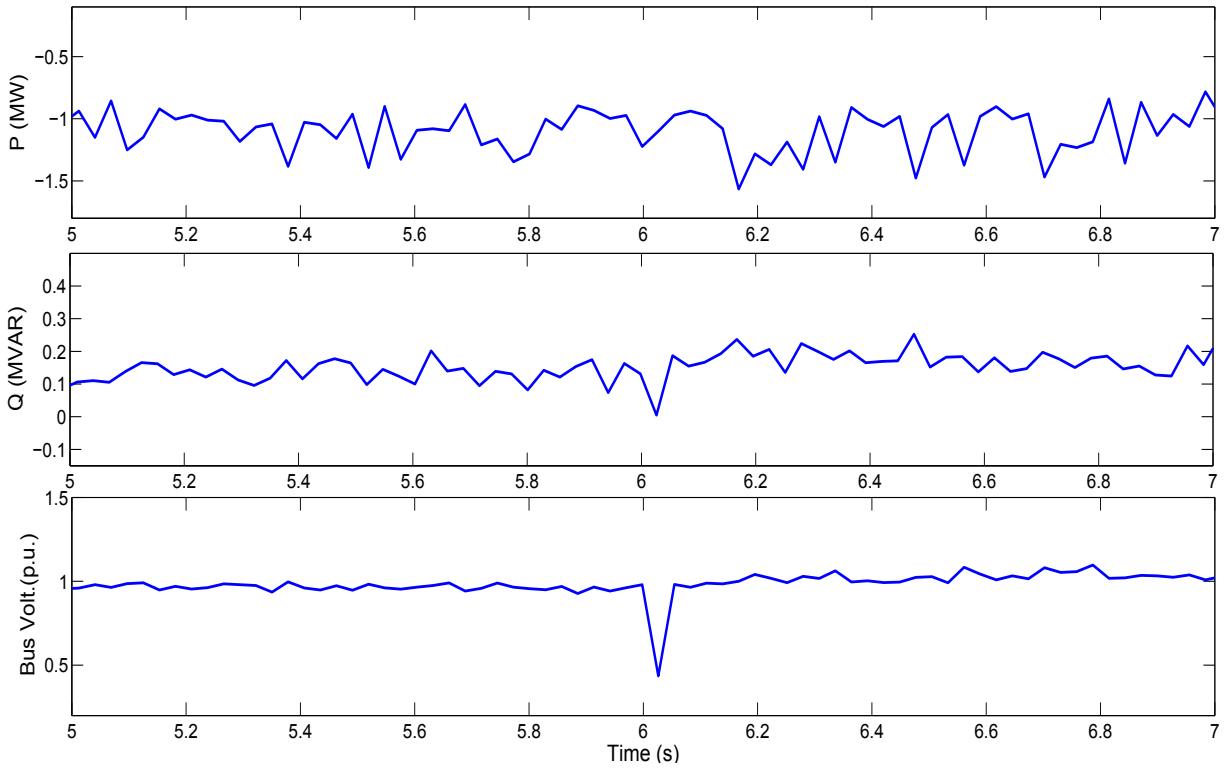

Figure 5.16: Responses of PV system for three phase fault with PI controller

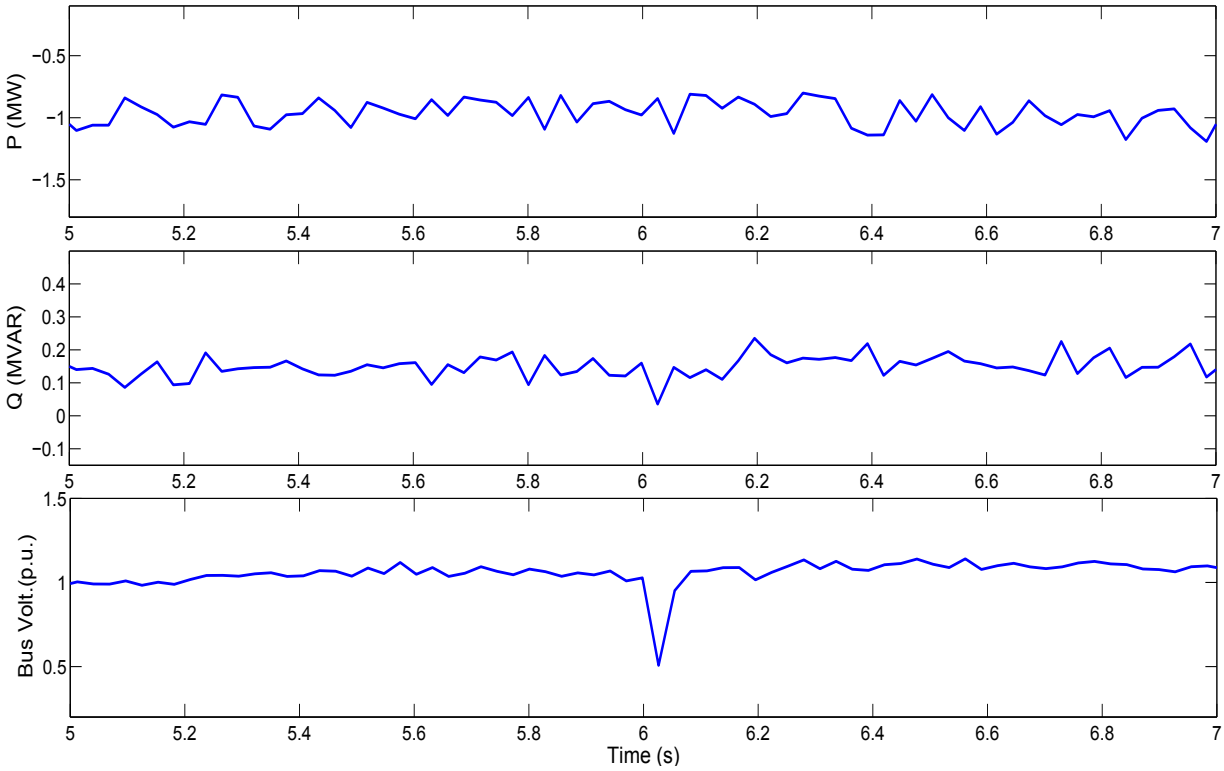

Figure 5.17: Responses of PV system for three phase fault with type-2 FLC

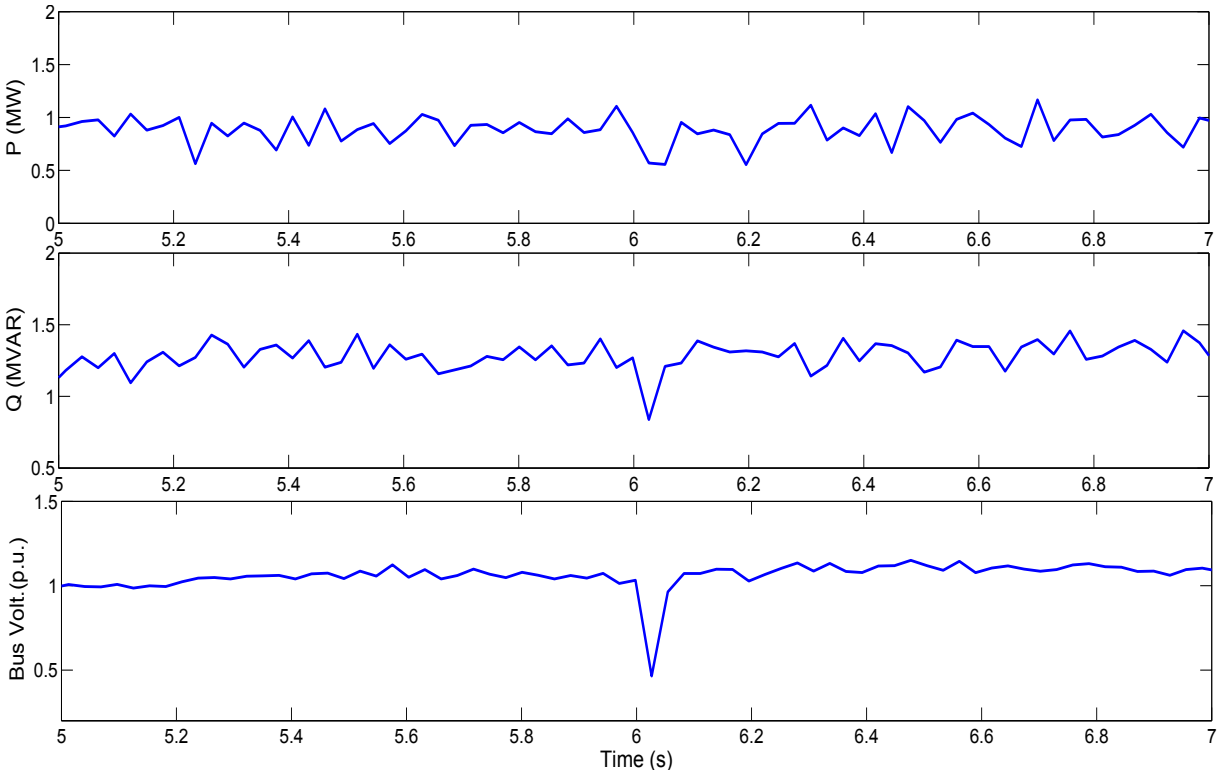

Figure 5.18: Responses of DFIG system for three phase fault with PI controller

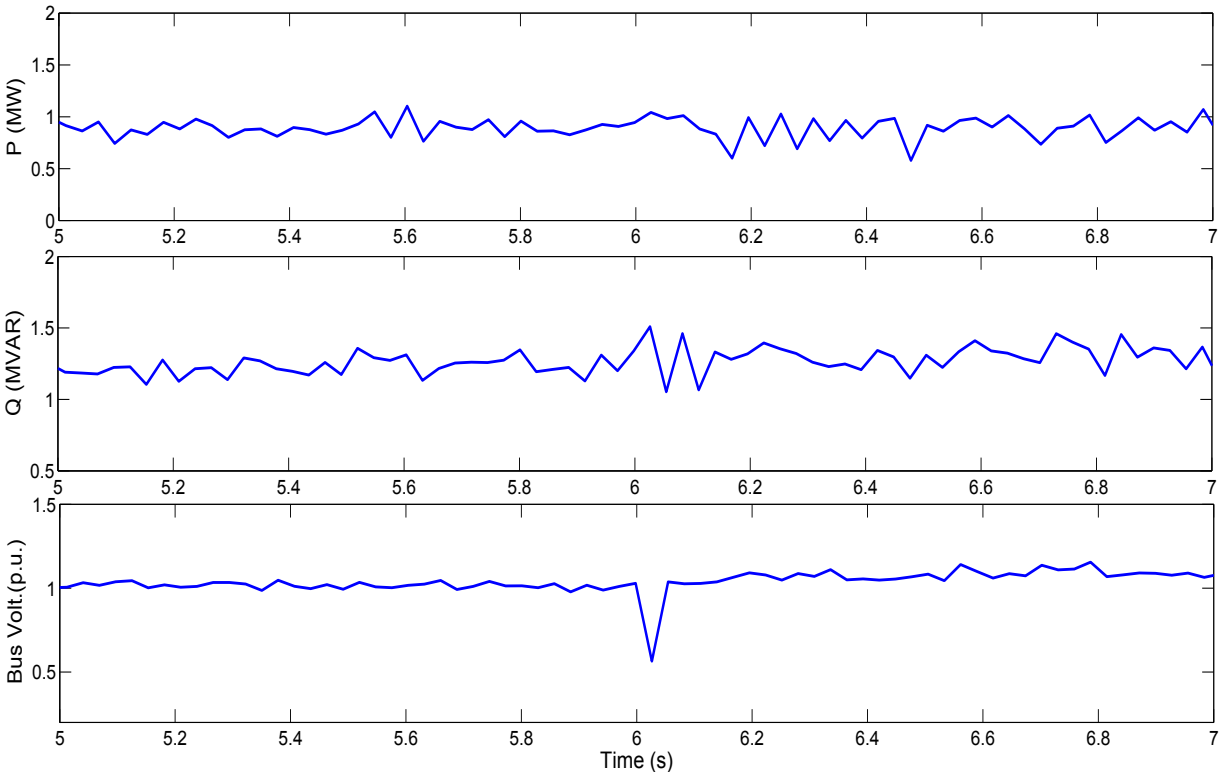

Figure 5.19: Responses of DFIG system for three phase fault with type-2 FLC

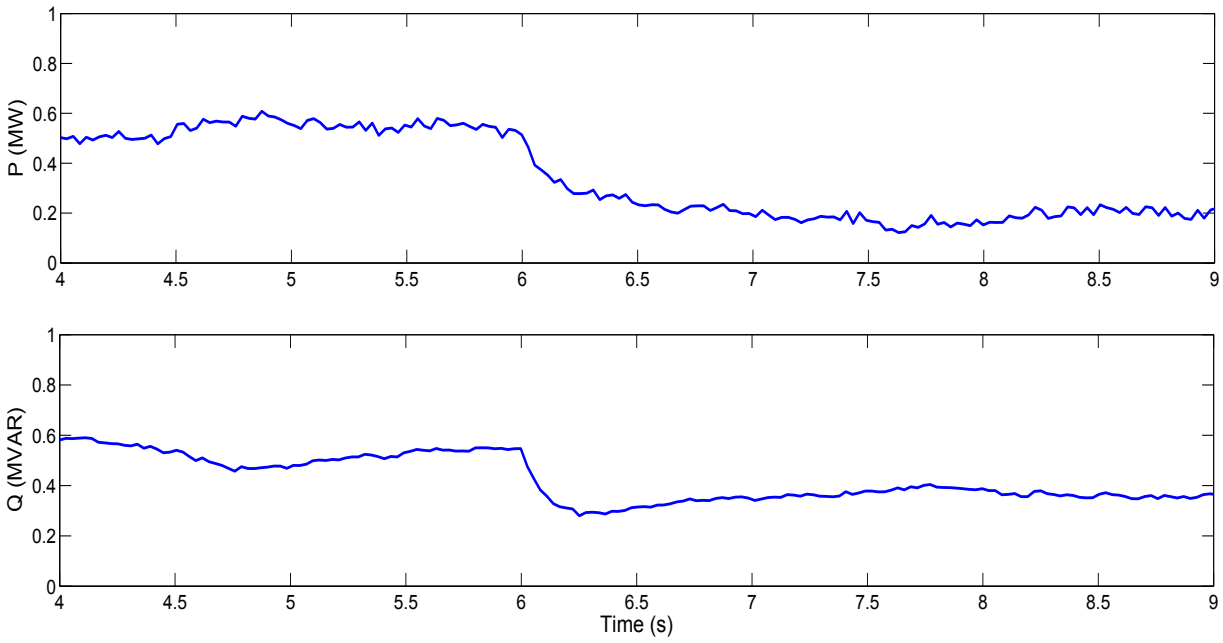

Figure 5.20: Responses of grid for Load loss (PI controller)

case(PV), at the instant of fault, the bus voltage drops to 0.43 p.u., and after clearing the fault,the power oscillations lasted more than 5s, whereas with the proposed case the oscillations are settled within 3s with the bus voltage maintaining at 0.5 p.u..

The responses of the DFIG are shown in Figures 5.18 and 5.19 for PI and type-2 FLC respectively. The low voltage ride through capability is an important requirement for wind generators for satisfactory grid operation. Fault condition is a typical case for the analysis of uncertainty in operating conditions. In this case, the performance of PI controller was suboptimal in dealing with the uncertainties consequently the bus voltage drops to 0.46 p.u. with sustained oscillations in the output powers.

Above all, the proposed case managed to maintain the bus voltage at 0.57 p.u., marking an improvement of 11%, with damped oscillations in the output powers. This shows the effectiveness of the FOU in maintaining the performance under uncertainties in operating conditions.

5.4.3 Load disturbance

Load loss and variations are quite common in distribution network which is an important factor to be considered while designing the controller. In order to prove that the proposed strategy is robust enough to handle the load disturbances, the load at bus 890 that is 450 kW, 225 kVAR is disconnected at 6s and the comparative analysis is done with PI case. The responses of grid with PI and type-2 FLC are shown in Figures 5.20 and 5.21 respectively.

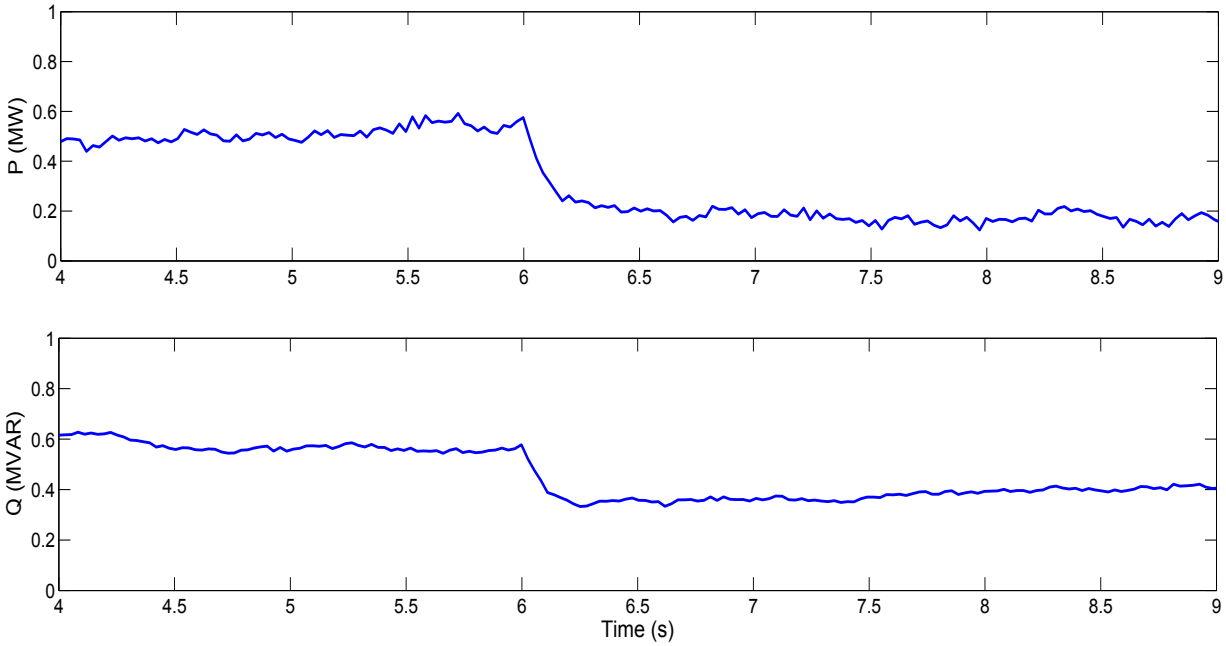

Figure 5.21: Responses of grid for Load loss (type-2 FLC)

After disconnecting the load, both PV and DFIG continued to supply the rated powers and grid power has been decreased to 0.2 MW . In response to the disturbance, the output power with PI, has reached the steady state in 1.5s and the same for type-2 FLC has reached within 0.5s, making a significant improvement over PI case. The bus voltage responses are shown in Figures 5.22 and 5.23. With PI case, the voltage at bus 890 rises to 1.15 p.u. that causes the other buses 832 and 848 to settle at 1.08 p.u.. The type-2 FLC,showing an immunity to the disturbance, maintains the voltage at bus 890 at 1.05 p.u. keeping the other bus voltages intact. This shows that the presence of FOU in type-2 MFs makes a difference in countering the uncertainties.

5.4.4 PV OUTAGE IN GRID CONNECTED MODE

Initially, the controllers are designed to generate 1.2 MW from PV and 1 MW from DFIG, assuming that the remaining load will be supplied from the the utility grid. The main objective of this study is to analyze the effect of a common disturbance in the microgrid i.e. outage of DG sources. In order to check the performance of the system in the absence of one of the DG sources, the PV system is disconnected at 6s and the corresponding responses of utility grid and DFIG are analyzed.

The response of the grid for PI and type-2 FLC are shown in Figures 5.24 and 5.25 respectively. The initial active power of the grid is at 0.5 MW, after the disconnection of PV, the grid output has changed to 1.7 MW to compensate the PV output. The DFIG

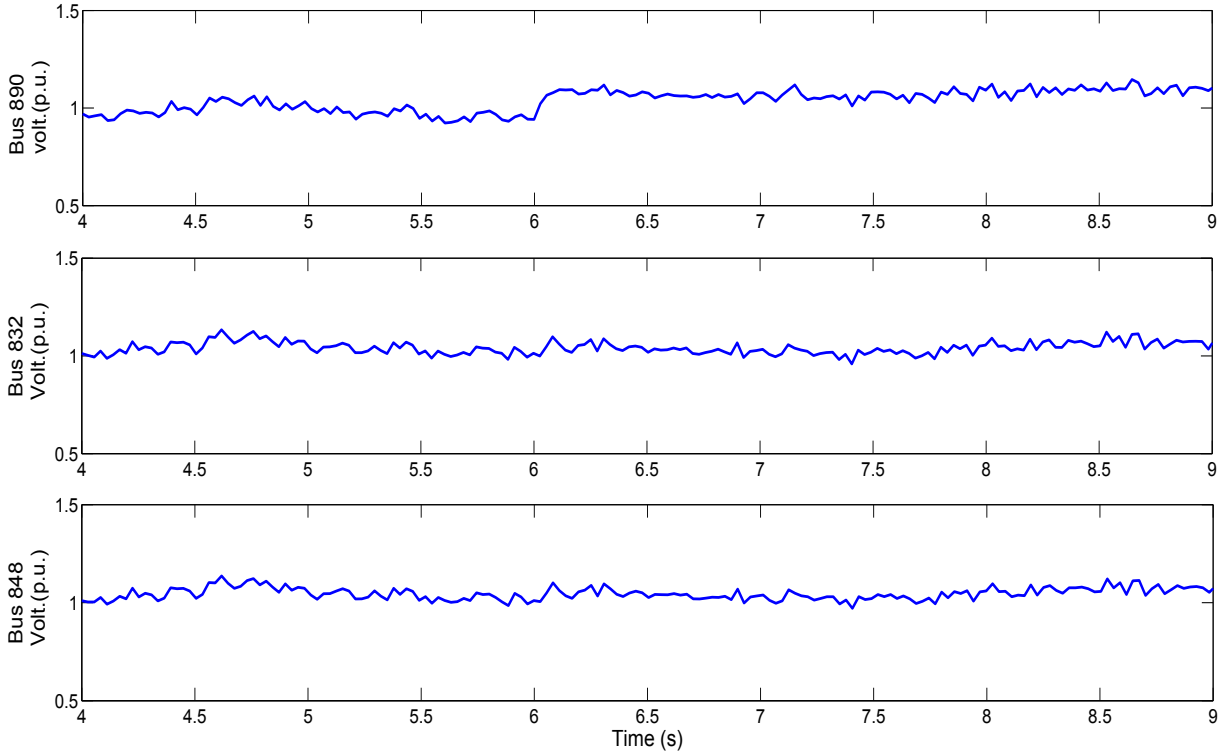

Figure 5.22: Responses of bus voltages for Load loss (PI controller)

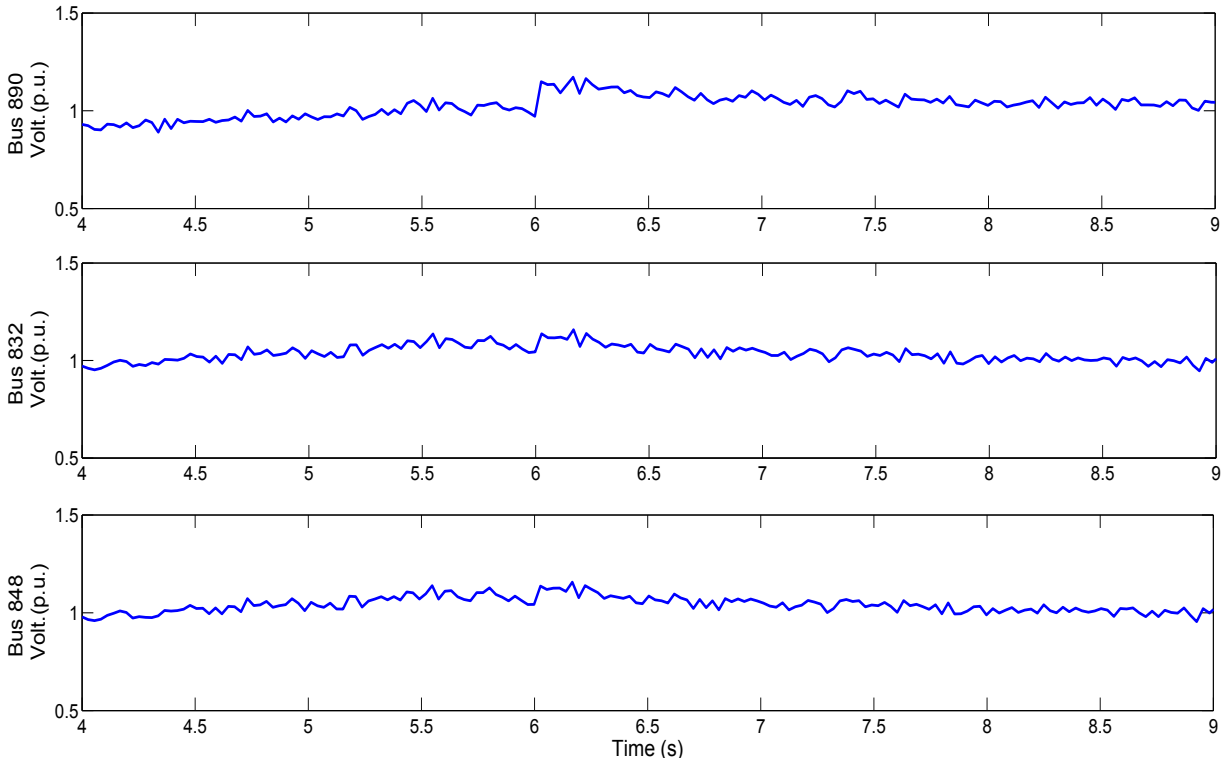

Figure 5.23: Responses of bus voltages for Load loss (type-2 FLC)

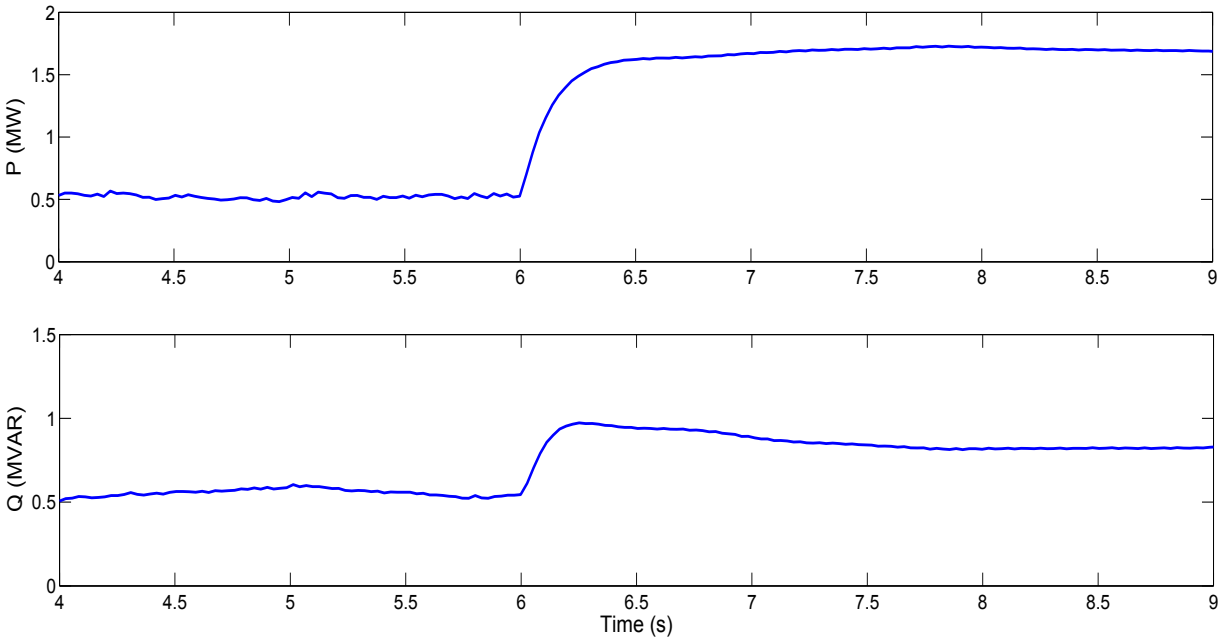

Figure 5.24: Responses of grid for PV outage (PI controller)

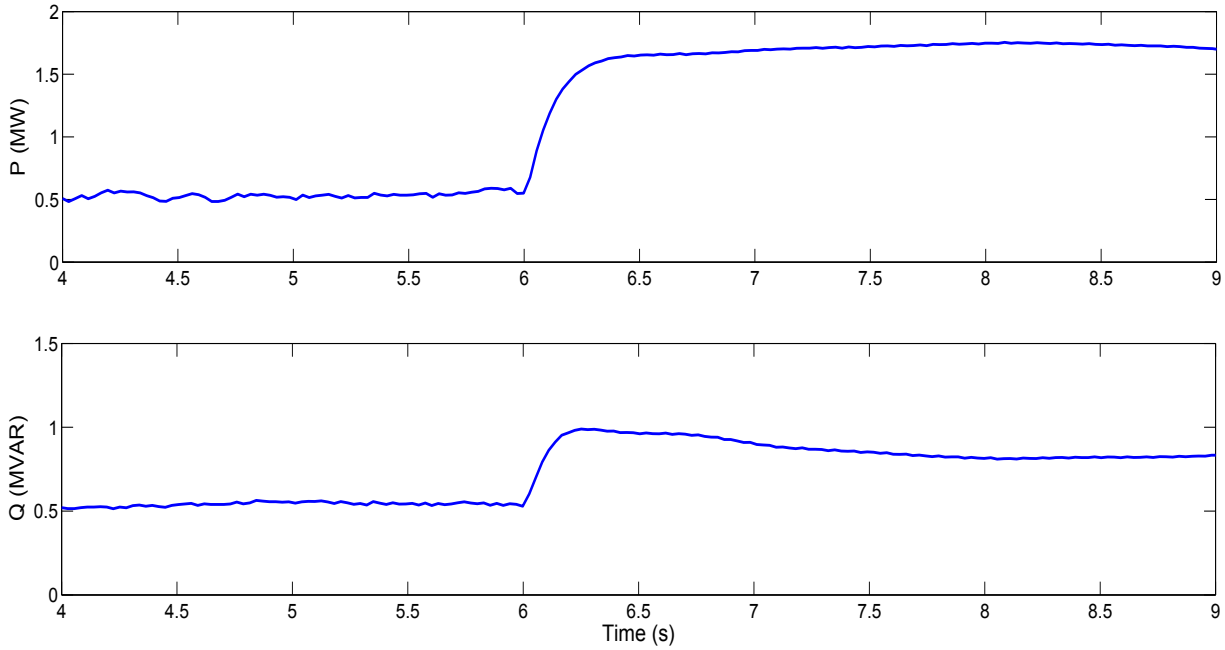

Figure 5.25: Responses of grid for PV outage (type-2 FLC)

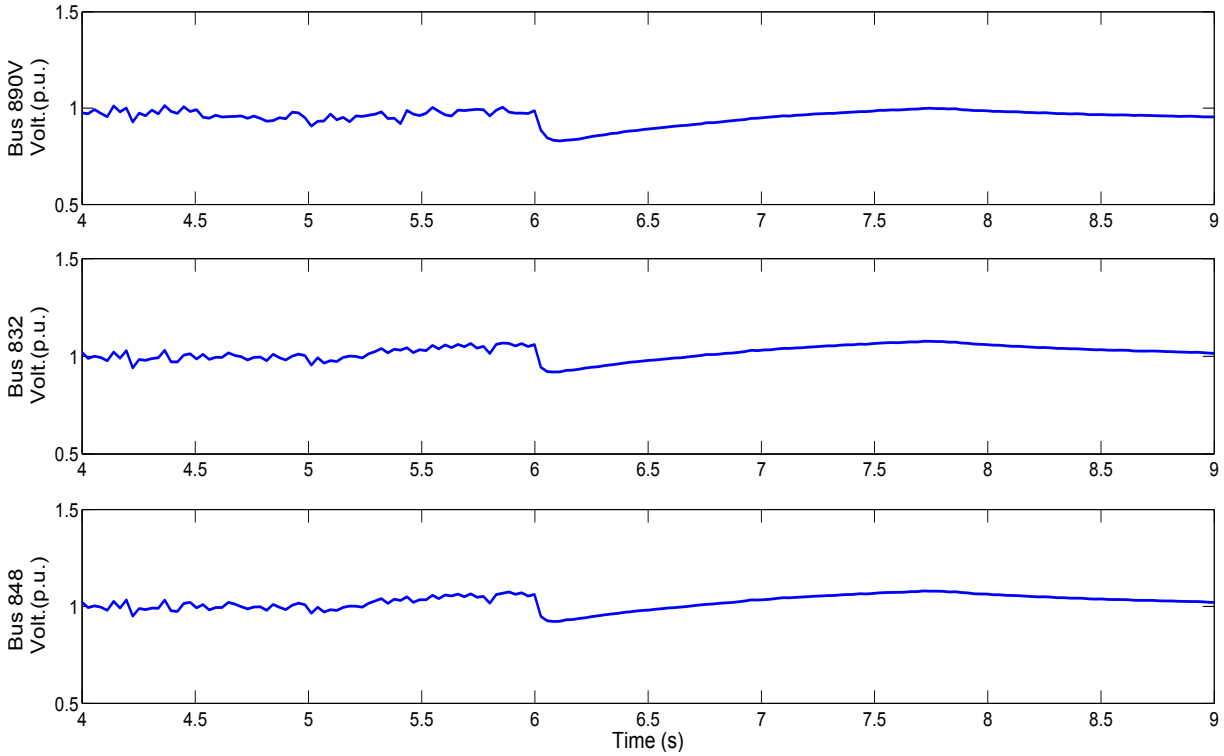

Figure 5.26: Responses of bus voltages for PV outage (PI controller)

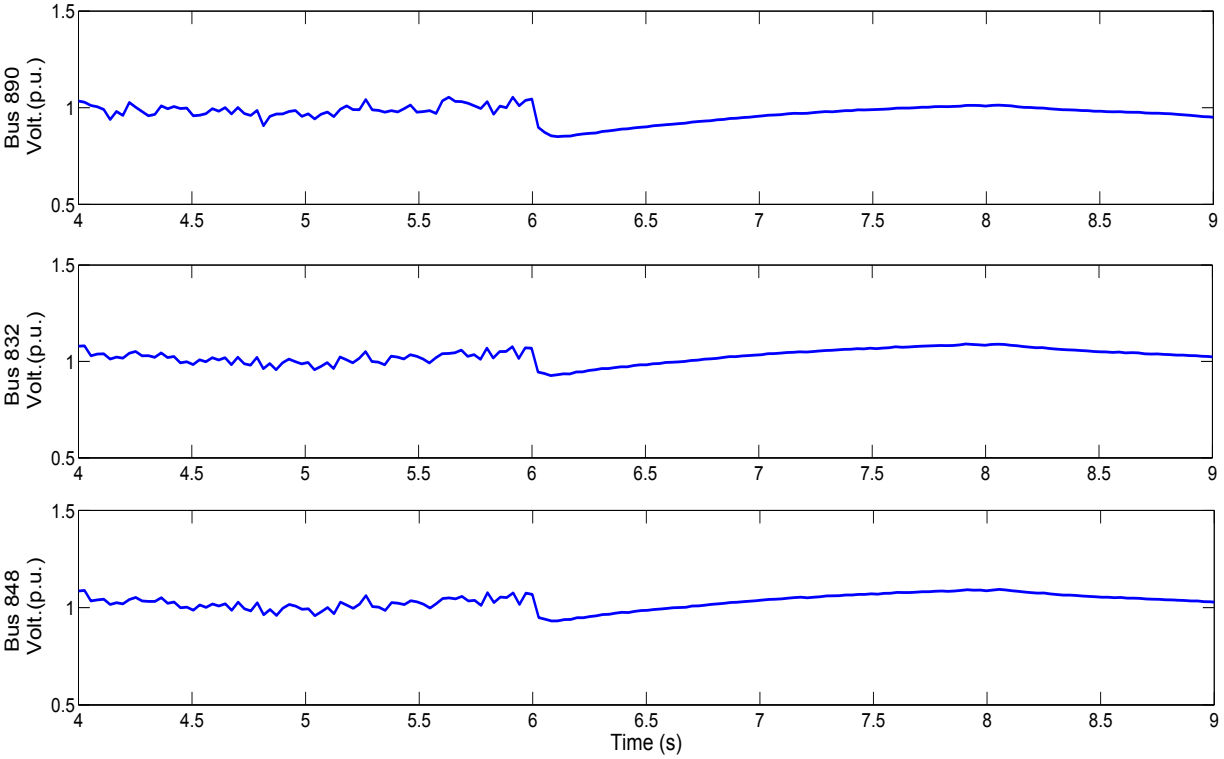

Figure 5.27: Responses of bus voltages for PV outage (type-2 FLC)

remains steady in maintaining the rated powers without any deviations. The bus voltage responses are shown in Figure 5.26 and 5.27 for PI and type-2 FLC respectively. During the transition period a small dip in the bus voltage is observed at the connection points of the DGs. Although the proposed strategy is not making a significant improvement in this case, it maintains same performance as that of PI controller, because the disturbance considered here is having insignificant impact on bus voltages and DFIG operation.

5.5 Conclusions

This chapter presents a novel control strategy for effective power sharing in a microgrid under various uncertainties in operating conditions. A standard IEEE 34 bus system is adapted as a microgrid with DG sources DFIG, PV and battery for the analysis in grid connected as well as islanded operations. A type-2 FLC is designed for power sharing in grid connected mode, and tested for various uncertainties like intentional islanding, three phase fault, PV outage and load loss. To verify the performance, real-time simulations are carried out with hardware-in-loop (HIL) configuration in RTDS environment. The performance of the proposed control strategy is analysed by comparing the results with that of conventional PI controller. The type-2 FLC has shown an improved performance in handling the transients especially during the islanding and three phase fault. Further, it was able to maintain a satisfactory performance under uncertainties in load changes and PV outage. The proposed strategy can provide desired performance over a wide range of operating conditions, without the need of re-tuning its parameters. The above results confirms that type-2 FLC is able to perform better than PI even in the presence of multiple DG sources.

Chapter 6

Conclusions and scope for Future work

6.1 Conclusions

The work presented in this thesis mainly focused on the feasibility study of interval type-2 fuzzy logic controllers and its application to Renewable energy systems. A special focus on DFIG based grid connected wind energy systems is concentrated to address the issues related with uncertainty in operating conditions of the network. The concept of type-2 fuzzy logic is introduced and its special features to handle the system uncertainties are discussed.

An effort has been made to design type-2 FLC by exploring the properties of interval type-2 fuzzy sets, for power electronic converters of the DFIG. The controller is implemented on a real-time platform for hardware in loop simulations.

The following conclusions are drawn on the accomplishments of this thesis:

- The fundamentals of fuzzy logic do not change from type-1 to type-2 fuzzy sets. In general, it will not change for any type-n. A higher type number just indicates a higher degree of fuzziness. A higher type fuzzy logic system only changes the nature of the membership functions. Therefore the operations that depend on the membership functions change. However the basic principles of fuzzy logic are independent of the nature of the membership functions and hence do not change. Since the membership functions of a type-2 FLS are fuzzy and also contain a footprint of uncertainty, which is nothing but the area covered between the lower and upper membership functions and represents the capacity to handle the degree of uncertainty, they can model and handle both linguistic and numerical uncertainties associated with the input and output of the fuzzy logic controller (FLC). Due to this reason the FLCs based on type-2 FSs will have the potential to give better performance than the type-1 FLC with respect to uncertainty.

- Embedding large number of type-1 fuzzy sets results in a type-2 fuzzy set. The use of such a large number of type-1 fuzzy sets to describe the input and output variables allows for a full description of the analytical control surface because the addition of

extra levels of classification gives a smoother control surface and response.

- Due to the extra degree of freedom provided by the footprint of uncertainty, it enables a type-2 FLS to produce outputs that cant be achieved by type-1 FLS with the same number of membership functions. It has been shown that a type-2 fuzzy set may give rise to an equivalent type-1 membership grade i.e. negative or larger than unity. Thus a type-2 FLS is able to model more complex input-output relationships than its type-1 counterparts. Thus it can give better control response. Using type-2 fuzzy sets to represent the FLC inputs and outputs will result in the reduction of the FLC rule base compared to type-1 fuzzy sets.

- As a preliminary study, a simple grid connected DFIG plant model is implemented in MATLAB platform and a type-2 FLC is designed for the power electronic converters to control the output powers. The controller is tested for various possible contingencies by comparing the performance with that of type-1 FLC. It is envisaged that a properly tuned type-2 FLC may result in better performance compared to other counterparts. Further, to realize the effect of foot print of uncertainty (FOU) on the output performance, an optimization problem is formed to choose the optimal width of FOU. The performance of the optimized controller is compared with that of other counter parts and found an improvement in the transient response. Varying the foot print of uncertainty which is achieved by varying the width of the membership function, affects the performance of the type-2 FLC. Therefore the FOU width should not be very high or very low, it should be an optimal value to satisfy the best performance of the controller.

- Real time digital simulator(RTDS) is a suitable platform for real-time analysis of power electronics and power systems and also for controller prototyping, real time simulations and hardware in loop tests. The parallel processing feature of RTDS enables it to model the large power system networks for electro magnetic transient simulations.

- The DFIG model is implemented in RSCAD for real time simulations using RTDS. The type-2 FLC is designed and implemented on a DSP based Dspace 1104 module for hardware-in-loop tests. The controller performance for tracking the active and reactive power references is evaluated with real-time simulations. Further, a comparative performance analysis is done with type-1 FLC and PI counterparts under three

phase fault and variable wind speed conditions. The tracking performance of type-2 FLC has been highly effective, especially during variable wind speed conditions. The presence of FOU has shown a significant improvement in the transients during the fault period.

- To evaluate the controller performance under unbalanced voltages and other uncertainties in the distributed networks, the IEEE-34 bus system with DFIG is considered as the plant model. The type-2 FLC is designed and the parameters are tuned based on the observations from extensive simulation results. The robustness of the controller is verified with all possible uncertainties in the distributed networks like three phase fault, load variations and changes in wind speed. In all the testing conditions, the type-2 FLC has shown a significant improvement in the transient response compared to that of PI controller. Further, the type-2 FLC is implemented in the hardware-in-loop environment. The conversion delays of analog to digital converters(ADCs) and digital to analog converters(DACs), and the computational time delay of the controller algorithm are the key factors that needs to be considered while designing the stable control loops. The three dimensional MF of type-2 FLC is capable of accommodating all the loop delays.

- In order to verify the performance of the proposed controller in the presence of multiple DG sources, the IEEE-34 bus system with PV system, battery and DFIG is considered as microgrid. The type-2 FLCs are designed to track the respective power references of the DG sources. Due to the node limitations the overall microgrid model cannot be implemented in a single rack of the RTDS. The system model is distributed among six racks of RTDS and designed in RSCAD to execute the real-time simulations. The system is tested for grid connected as well as islanding conditions. The performance of the proposed strategy is evaluated by comparing with that of PI controller under various possible contingencies. The controllers are implemented in Dsapce, in hardware-in-loop,and its excellent performance signifies its applicability to real-time applications of power system networks. In all the cases, the type-2 FLC has become immune to the uncertainties, performing better, without the need of retuning the controller parameters. With these observations and analysis, it is concluded that a properly designed type-2 FLC can handle the uncertainties, associated with renewable energy systems, much better than the type-1 FLC and PI controllers.

6.2 Suggestions For Future Development

Research and development is a non-stopping process. For any research work carried out, there is always a possibility for better chances of improvement and lot many avenues opened for further work. As a result of the investigations carried out in the area of application of type-2 fuzzy logic controllers for renewable energy systems, following aspects are identified for future scope of research work.

- Computational time is the major limitation for wide spread use of type-2 FLCs. A new type reduction algorithm can be developed and studied for comparative analysis with wind energy problems deliberated in this thesis.
- The microgrid considered in this work comprises only PV, battery and DFIG system. Type-2 FLC can be designed for microgrid by considering the other sources like fuel cells, diesel generators and non-linear loads etc..
- Analytical methods can be developed to study the relation between robustness and footprint of uncertainty.
- The optimization problem of foot print of uncertainty can be developed with more appropriate cost functions considering the sensitive parameters of the DFIG system.

Bibliography

[1] Abad, G., Lopez, J., Rodríguez, M., Marroyo, L., and Iwanski, G. (2011). *Doubly fed induction machine: modeling and control for wind energy generation*, volume 85. John Wiley & Sons.

[2] Aisbett, J. and Rickard, J. T. (2014). Centroids of Type-1 and Type-2 Fuzzy Sets When Membership Functions Have Spikes. *IEEE Transactions on Fuzzy Systems*, 22(3):685–692.

[3] Alawieh, A., Ortega, R., Pillai, H., Astolfi, A., and Berthelot, E. (2013). Voltage Regulation of a Boost Converter in Discontinuous Conduction Mode: A Simple Robust Adaptive Feedback Controller. *IEEE Control Systems*, 33(3):55–65.

[4] Angelov, P. (2006). Evolving fuzzy rule-based systems for modelling of non-linear non-stationary processes. In *Energy Saving Control*, volume 1, pages 43–50.

[5] Angelov, P. and Yager, R. (2011). Simplified fuzzy rule-based systems using non-parametric antecedents and relative data density. In *2011 IEEE Workshop on Evolving and Adaptive Intelligent Systems (EAIS)*, pages 62–69. IEEE.

[6] Angelov, P., Zhang, Y., and Wright, J. A. (2005). Automatic design generation of component-based systems using GA and fuzzy optimisation.

[7] Azzouz, M. A., Elshafei, A.-L., and Emara, H. (2011). Evaluation of fuzzy-based maximum power-tracking in wind energy conversion systems. *IET Renewable Power Generation*, 5(6):422–430.

[8] Bajpai, P. and Singh, S. N. (2007). Fuzzy Adaptive Particle Swarm Optimization for Bidding Strategy in Uniform Price Spot Market. *IEEE Transactions on Power Systems*, 22(4):2152–2160.

[9] Barklund, E., Pogaku, N., Prodanović, M., Hernandez-Aramburo, C., and Green, T. C. (2008). Energy management in autonomous microgrid using stability-constrained droop control of inverters. *IEEE Transactions on Power Electronics*, 23(5):2346–2352.

[10] Baruah, R. D., Angelov, P., and Baruah, D. (2014). Dynamically evolving fuzzy classifier for real-time classification of data streams. In *IEEE International Conference on Fuzzy Systems (FUZZ-IEEE) 2014*, pages 383–389. IEEE.

[11] Behera, L. and Kar, I. (2010). *Intelligent Systems and control principles and applications*. Oxford University Press, Inc.

[12] Bevrani, H., Ghosh, A., and Ledwich, G. (2010). Renewable energy sources and frequency regulation: survey and new perspectives. *IET Renewable Power Generation*, 4(5):438.

[13] Bevrani, H., Habibi, F., Babahajyani, P., Watanabe, M., and Mitani, Y. (2012). Intelligent frequency control in an ac microgrid: online pso-based fuzzy tuning approach. *IEEE Transactions on Smart Grid*, 3(4):1935–1944.

[14] Bevrani, H. and Shokoohi, S. (2013). An intelligent droop control for simultaneous voltage and frequency regulation in islanded microgrids. *IEEE Transactions on Smart Grid*, 4(3):1505–1513.

[15] Blaabjerg, F., Teodorescu, R., Liserre, M., and Timbus, A. V. (2006). Overview of Control and Grid Synchronization for Distributed Power Generation Systems. *IEEE Transactions on Industrial Electronics,*, 53(5):1398–1409.

[16] Byeon, G.-S., Park, I.-K., and Jang, G.-S. (2010). Modeling and control of a doubly-fed induction generator (dfig) wind power generation system for real-time simulations. *Journal of Electrical Engineering and Technology*, 5(1):61–69.

[17] Carvalho, P., Correia, P. F., and Ferreira, L. A. (2008). Distributed reactive power generation control for voltage rise mitigation in distribution networks. *IEEE transactions on Power Systems*, 23(2):766–772.

[18] Castillo, O. and Melin, P. (2008). Intelligent systems with interval type-2 fuzzy logic. *International Journal of Innovative Computing, Information and Control*, 4(4):771–783.

[19] Castillo, O. and Melin, P. (2012). A review on the design and optimization of interval type-2 fuzzy controllers. *Applied Soft Computing*, 12(4):1267–1278.

[20] Castro, J. R., Castillo, O., and Melin, P. (2007). An interval type-2 fuzzy logic toolbox for control applications. In *IEEE International Fuzzy Systems Conference, 2007. FUZZ-IEEE 2007.*, pages 1–6.

[21] Celikyilmaz, A. and Turksen, I. B. (2009). Modeling uncertainty with fuzzy logic. *Studies in fuzziness and soft computing*, 240.

[22] Chan, T.-F. and Shi, K. (2011). *Applied intelligent control of induction motor drives*. John Wiley & Sons.

[23] Chanhome, A., Phichaisawat, S., and Chaitusaney, S. (2012). Voltage regulation in distribution system by considering uncertainty from renewable energy. In *IEEE 9th International Conference on Electrical Engineering/Electronics, Computer, Telecommunications and Information Technology (ECTI-CON), 2012*, pages 1–4.

[24] Chanhome, A., Phichaisawat, S., and Chaitusaney, S. (2013). Minimization of voltage fluctuation by considering uncertainty from renewable energy resources. In *IEEE 10th International Conference on Electrical Engineering/Electronics, Computer, Telecommunications and Information Technology (ECTI-CON), 2013*, pages 1–6.

[25] Chaudhari, M. A., Suryawanshi, H. M., Kulwal, A., and Mishra, M. K. (2008). Three-Phase AC-to-DC Resonant Converter Operating in High Power Factor Mode in High-Voltage Applications. *Journal of Power Electronics*, 8(1):60–73.

[26] Chen, L. and Mei, S. (2015). An integrated control and protection system for photovoltaic microgrids. *CSEE Journal of Power and Energy Systems*, 1(1):36–42.

[27] Chen, M., Yu, L., Wade, N. S., Liu, X., Liu, Q., and Yang, F. (2011a). Investigation on the Faulty State of DFIG in a Microgrid. *IEEE Transactions on Power Electronics,*, 26(7):1913–1919.

[28] Chen, S. Z., Cheung, N. C., Wong, K. C., and Wu, J. (2011b). Integral variable structure direct torque control of doubly fed induction generator. *IET Renewable Power Generation,*, 5(1):18–25.

[29] Chowdhury, B. H. and Chellapilla, S. (2006). Double-fed induction generator control for variable speed wind power generation. *Electric Power Systems Research*, 76(9):786–800.

[30] Chowdhury, M., Hosseinzadeh, N., and Shen, W. (2012). Smoothing wind power fluctuations by fuzzy logic pitch angle controller. *Renewable Energy*, 38(1):224–233.

[31] D. Kumar and S. K. Nagar (2014). Order Reduction of Power System Models using Square-Root Balanced Approach. *Eighteenth National Power Systems Conference (NPSC), 2014*, (21):1–6.

[32] Das, D. (2006). A Fuzzy Multiobjective Approach for Network Reconfiguration of Distribution Systems. *IEEE Transactions on Power Delivery*, 21(1):202–209.

[33] Das, D., Aditya, S., and Kothari, D. (1999). Dynamics of diesel and wind turbine generators on an isolated power system. *International Journal of Electrical Power & Energy Systems*, 21(3):183–189.

[34] Das, S. Ghosh, D. K. Srinivas, D. (1999). Fuzzy Distribution Load Flow. *Electric Machines & Power Systems*, 27(11):1215–1226.

[35] de Almeida, R. G., Peas Lopes, J. A., and Barreiros, J. A. L. (2004). Improving power system dynamic behavior through doubly fed induction machines controlled by static converter using fuzzy control. *IEEE Transactions on Power Systems,*, 19(4):1942–1950.

[36] Deng, J., Li, C., and Zhang, X.-P. (2015). Coordinated Design of Multiple Robust FACTS Damping Controllers: A BMI-Based Sequential Approach With Multi-Model Systems. *IEEE Transactions on Power Systems,*, 30(6):3150–3159.

[37] Diaz, N. L., Dragicevic, T., Vasquez, J. C., and Guerrero, J. M. (2014). Intelligent distributed generation and storage units for dc microgridsa new concept on cooperative control without communications beyond droop control. *Smart Grid, IEEE Transactions on*, 5(5):2476–2485.

[38] Dong, B., Asgarpoor, S., and Qiao, W. (2009). Voltage analysis of distribution systems with dfig wind turbines. In *IEEE Power Electronics and Machines in Wind Applications, 2009. PEMWA 2009.*, pages 1–5.

[39] Dugan, R. and Kersting, W. (2006). Induction machine test case for the 34-bus test feeder-description. In *IEEE Power Engineering Society General Meeting, 2006.*, pages 4–pp.

[40] El Khateb, A., Abd Rahim, N., Selvaraj, J., and Uddin, M. N. (2014). Fuzzy-Logic-Controller-Based SEPIC Converter for Maximum Power Point Tracking. *IEEE Transactions on Industry Applications,*, 50(4):2349–2358.

[41] Erlich, I., Wrede, H., and Feltes, C. (2007). Dynamic behavior of dfig-based wind turbines during grid faults. In *Power Conversion Conference-Nagoya, 2007. PCC'07*, pages 1195–1200.

[42] Etemadi, A. H., Davison, E. J., and Iravani, R. (2014). A generalized decentralized robust control of islanded microgrids. *IEEE Transactions on Power Systems*, 29(6):3102–3113.

[43] Fan, L. and Miao, Z. (2012). Mitigating SSR Using DFIG-Based Wind Generation. *IEEE Transactions on Sustainable Energy,*, 3(3):349–358.

[44] Fu, Q., Montoya, L. F., Solanki, A., Nasiri, A., Bhavaraju, V., Abdallah, T., and Yu, D. C. (2012). Microgrid Generation Capacity Design With Renewables and Energy Storage Addressing Power Quality and Surety. *IEEE Transactions on Smart Grid*, 3(4):2019–2027.

[45] GEORGE J, K. and Bo, Y. (2008). Fuzzy sets and fuzzy logic, theory and applications. -.

[46] Gomes de Matos, J., de Souza Ribeiro, L. A., and de Carvalho Gomes, E. (2013). Power control in ac autonomous and isolated microgrids with renewable energy sources and energy storage systems. In *IECON 2013-39th Annual Conference of the IEEE Industrial Electronics Society*, pages 1827–1832. IEEE.

[47] Hachicha, F. and Krichen, L. (2012). Rotor power control in doubly fed induction generator wind turbine under grid faults. *Energy*, 44(1):853–861.

[48] Hagras, H. (2007). Type-2 FLCs: A New Generation of Fuzzy Controllers. *IEEE Computational Intelligence Magazine*, 2(1):30–43.

[49] Hagras, H. and Wagner, C. (2012). Towards the Wide Spread Use of Type-2 Fuzzy Logic Systems in Real World Applications. *IEEE Computational Intelligence Magazine*, 7(3):14–24.

[50] Hamane, B., Benghanemm, M., Bouzid, A., Belabbes, A., Bouhamida, M., and Draou, A. (2012). Control for variable speed wind turbine driving a doubly fed induction generator using fuzzy-pi control. *Energy Procedia*, 18:476–485.

[51] Hansen, A. D. and Michalke, G. (2007). Fault ride-through capability of DFIG wind turbines. *Renewable Energy*, 32(9):1594–1610.

[52] Hilloowala, R. M. and Sharaf, A. M. (1996). A rule-based fuzzy logic controller for a PWM inverter in a stand alone wind energy conversion scheme. *IEEE Transactions on Industry Applications,*, 32(1):57–65.

[53] Hisdal, E. (1981). The if then else statement and interval-valued fuzzy sets of higher type. *International Journal of Man-Machine Studies*, 15(4):385–455.

[54] Hossain, M., Pota, H. R., Mahmud, M. A., and Aldeen, M. (2015). Robust control for power sharing in microgrids with low-inertia wind and pv generators. *IEEE Transactions on Sustainable Energy*, 6(3):1067–1077.

[55] Hsiao, M.-Y., Li, T.-H. S., Lee, J.-Z., Chao, C.-H., and Tsai, S.-H. (2008). Design of interval type-2 fuzzy sliding-mode controller. *Information Sciences*, 178(6):1696–1716.

[56] Hu, J., He, Y., Xu, L., and Williams, B. W. (2009). Improved control of dfig systems during network unbalance using pi–r current regulators. *IEEE Transactions on Industrial Electronics*, 56(2):439–451.

[57] Huang, S.-H. and Chen, Y.-R. (2005). Vlsi implementation of type-2 fuzzy inference processor. In *IEEE International Symposium on Circuits and Systems, 2005. ISCAS 2005.*, pages 3307–3310. IEEE.

[58] Hughes, F. M., Anaya-Lara, O., Jenkins, N., and Strbac, G. (2005a). Control of DFIG-based wind generation for power network support. *IEEE Transactions on Power Systems,*, 20(4):1958–1966.

[59] Hughes, F. M., Anaya-Lara, O., Jenkins, N., and Strbac, G. (2005b). Control of dfig-based wind generation for power network support. *IEEE Transactions on Power Systems*, 20(4):1958–1966.

[60] Hwang, C. and Rhee, F. C.-H. (2007). Uncertain fuzzy clustering: interval type-2 fuzzy approach to c-means. *IEEE Transactions on Fuzzy Systems*, 15(1):107–120.

[61] Irwin, J., Kazmierkowski, M. P., Krishnan, R., and Blaabjerg, F. (2002). *Control in power electronics: selected problems*. Academic press.

[62] Jabr, H. M., Lu, D., and Kar, N. C. (2011). Design and Implementation of Neuro-Fuzzy Vector Control for Wind-Driven Doubly-Fed Induction Generator. *IEEE Transactions on Sustainable Energy,*, 2(4):404–413.

[63] Jacomini, R. V., Franca, A. P., and Bim, E. (2009). Simulation and experimental studies on double-fed induction generator power control at subsynchronous operating speed. In *International Conference on Power Electronics and Drive Systems (PEDS)2009*, pages 1421–1424.

[64] Jafarzadeh, S., Fadali, M. S., and Etezadi-Amoli, M. (2012). Fuzzy type-1 and type-2 tsk modeling with application to solar power prediction. In *IEEE Power and Energy Society General Meeting, 2012*, pages 1–6.

[65] Jazaeri, M. and Samadi, A. A. (2015). Self-tuning fuzzy pi-based controller of dfig wind turbine for transient conditions enhancement. *International Transactions on Electrical Energy Systems*, 25(11):2657–2673.

[66] Jeon, J.-H., Kim, J.-Y., Kim, H.-M., Kim, S.-K., Cho, C., Kim, J.-M., Ahn, J.-B., and Nam, K.-Y. (2010). Development of hardware in-the-loop simulation system for testing operation and control functions of microgrid. *Power Electronics, IEEE Transactions on*, 25(12):2919–2929.

[67] Johnson, D. and Turner, C. (2015). *European business*. Routledge.

[68] Joyce, A., Rodrigues, C., and Manso, R. (2001). Modelling a pv system. *Renewable energy*, 22(1):275–280.

[69] Kamal, E. and Aitouche, A. (2013). Robust fault tolerant control of dfig wind energy systems with unknown inputs. *Renewable energy*, 56:2–15.

[70] Kamel, R. M., Chaouachi, A., and Nagasaka, K. (2010). Wind power smoothing using fuzzy logic pitch controller and energy capacitor system for improvement Micro-Grid performance in islanding mode. *Energy*, 35(5):2119–2129.

[71] Kamel, R. M., Chaouachi, A., and Nagasaka, K. (2013). Three control strategies to improve the microgrid transient dynamic response during isolated mode: A comparative study. *Industrial Electronics, IEEE Transactions on*, 60(4):1314–1322.

[72] Kang, C., Feng, X., Yongjie, F., and Yuehai, Y. (2010). Comparative simulation of dynamic characteristics of wind turbine doubly-fed induction generator based on rtds and matlab. In *IEEE International Conference on Power System Technology (POWERCON), 2010*, pages 1–8.

[73] Karnik, N. and Mendel, J. (1999). Type-2 fuzzy logic systems. *IEEE Transactions on Fuzzy Systems*, 7(6):643–658.

[74] Karnik, N. N. and Mendel, J. M. (1998). Introduction to type-2 fuzzy logic systems. In *The 1998 IEEE International Conference on Fuzzy Systems Proceedings, 1998. IEEE World Congress on Computational Intelligence*, volume 2, pages 915–920. IEEE.

[75] Karnik, N. N. and Mendel, J. M. (2001). Centroid of a type-2 fuzzy set. *Information Sciences*, 132(1):195–220.

[76] Kasztenny, B. and Rosolowski, a. L. M. (1998). Differential Transformer Protection with an Artificial Neuron Network Application. *Technical Electrodynamics*, (5):67–73.

[77] Kasztenny, B., Rosolowski, E., Izykowski, J., Saha, M., and Hillstrom, B. (1998). Fuzzy logic controller for on-load transformer tap changer. *IEEE Transactions on Power Delivery*, 13(1):164–170.

[78] Kasztenny, B., Rosolowski, E., Saha, M., and Hillstrom (1997a). Fuzzy sets and logic in power system protection. *Engineering Intelligent Systems For Electrical Engineering And Communications*, 5(4):193–203.

[79] Kasztenny, B., Rosolowski, E., Saha, M., and Hillstrom, B. (1997b). A self-organizing fuzzy logic based protective relay-an application to power transformer protection. *IEEE Transactions on Power Delivery*, 12(3):1119–1127.

[80] Katiraei, F., Iravani, M., and Lehn, P. W. (2005). Micro-grid autonomous operation during and subsequent to islanding process. *IEEE Transactions on Power Delivery*, 20(1):248–257.

[81] Katiraei, F. and Iravani, M. R. (2006). Power management strategies for a micro-grid with multiple distributed generation units. *IEEE Transactions on Power Systems*, 21(4):1821–1831.

[82] Kayacan, E. (2011). *Interval Type-2 Fuzzy Logic Systems: Theory and Design*. PhD thesis, Bogaziçi University.

[83] Kelly, J. G., Angelov, P. P., Walsh, M. J., Pollock, H. M., Pitt, M., Martin-Hirsch, P. L., and Martin, F. L. (2008). A self-learning fuzzy classifier with feature selection for intelligent interrogation of mid-ir spectroscopy data from exfoliative cervical cytology using selflearning classifier eclass. *International Journal of Computational Intelligence Research*, 4(4):392–401.

[84] Khosravi, A. and Nahavandi, S. (2014). Load forecasting using interval type-2 fuzzy logic systems: Optimal type reduction. *IEEE Transactions on Industrial Informatics*, 10(2):1055–1063.

[85] Kickert, W. J. and Mamdani, E. H. (1978). Analysis of a fuzzy logic controller. *Fuzzy sets and Systems*, 1(1):29–44.

[86] Kolla, S. (1997). Applying fuzzy logic to power system protective relays. *InTech*, 44(6).

[87] Kolla, S. and Farison, J. (1991). Reduced-order dynamic compensator design for stability robustness of linear discrete-time systems. *IEEE Transactions on Automatic Control*, 36(9):1077–1081.

[88] Kolla, S. R. (1996). Improved stability robustness bounds for digital control systems in state-space models. *International Journal of Control*, 64(5):991–994.

[89] Kumbasar, T. and Hagras, H. (2015). A Self-Tuning zSlices-Based General Type-2 Fuzzy PI Controller. *Fuzzy Systems, IEEE Transactions on*, 23(4):991–1013.

[90] Kundur, P., Balu, N. J., and Lauby, M. G. (1994). *Power system stability and control*, volume 7. McGraw-hill New York.

[91] Kyaw, M. M. and Ramachandaramurthy, V. (2011). Fault ride through and voltage regulation for grid connected wind turbine. *Renewable energy*, 36(1):206–215.

[92] Lee, C.-S., Wang, M.-H., and Hagras, H. (2010). A type-2 fuzzy ontology and its application to personal diabetic-diet recommendation. *IEEE Transactions on Fuzzy Systems*, 18(2):374–395.

[93] Leottau, L. and Melgarejo, M. (2011). *An Embedded Type-2 Fuzzy Controller for a Mobile Robot Application*. INTECH Open Access Publisher.

[94] Li, H. X. (1997). A comparative design and tuning for conventional fuzzy control. *IEEE transactions on systems, man, and cybernetics. Part B, Cybernetics : a publication of the IEEE Systems, Man, and Cybernetics Society*, 27(5):884–9.

[95] Li, L., Lin, W. H., and Liu, H. (2006). Type-2 fuzzy logic approach for short-term traffic forecasting. In *IEE Proceedings on Intelligent Transport Systems*, volume 153, pages 33–40.

[96] Li, S. and Haskew, T. A. (2008). Characteristic Study of Vector-controlled Doubly-fed Induction Generator in Stator-flux-oriented Frame. *Electric Power Components and Systems*, 36(9):990–1015.

[97] Li, X., Song, Y.-J., and Han, S.-B. (2008). Frequency control in micro-grid power system combined with electrolyzer system and fuzzy pi controller. *Journal of Power Sources*, 180(1):468–475.

[98] Li, Y. W. and Kao, C.-N. (2009). An accurate power control strategy for power-electronics-interfaced distributed generation units operating in a low-voltage multibus microgrid. *IEEE Transactions on Power Electronics*, 24(12):2977–2988.

[99] Liang, Q. and Mendel, J. M. (2000a). Equalization of nonlinear time-varying channels using type-2 fuzzy adaptive filters. *IEEE Transactions on Fuzzy Systems*, 8(5):551–563.

[100] Liang, Q. and Mendel, J. M. (2000b). Overcoming time-varying co-channel interference using type-2 fuzzy adaptive filters. *IEEE Transactions on Circuits and Systems II: Analog and Digital Signal Processing,*, 47(12):1419–1428.

[101] Lin, P.-Z., Lin, C.-M., Hsu, C.-F., and Lee, T.-T. (2005). Type-2 fuzzy controller design using a sliding-mode approach for application to dc-dc converters. In *IEE Proceedings- Electric Power Applications,*, volume 152, pages 1482–1488. IET.

[102] Liu, F. and Mendel, J. M. (2008). Encoding words into interval type-2 fuzzy sets using an interval approach. *IEEE Transactions on Fuzzy Systems*, 16(6):1503–1521.

[103] Mahabuba, A. and Khan, M. A. (2009). Small signal stability enhancement of a multi-machine power system using robust and adaptive fuzzy neural network-based power system stabilizer. *European Transactions on Electrical Power*, 19(7):978–1001.

[104] Majumder, R., Chaudhuri, B., Ghosh, A., Majumder, R., Ledwich, G., and Zare, F. (2010a). Improvement of Stability and Load Sharing in an Autonomous Microgrid Using Supplementary Droop Control Loop. *IEEE Transactions on Power Systems*, 25(2):796–808.

[105] Majumder, R., Ghosh, A., Ledwich, G., and Zare, F. (2009). Load sharing and power quality enhanced operation of a distributed microgrid. *IET Renewable Power Generation*, 3(2):109.

[106] Majumder, R., Ghosh, A., Ledwich, G., and Zare, F. (2010b). Power Management and Power Flow Control With Back-to-Back Converters in a Utility Connected Microgrid. *IEEE Transactions on Power Systems*, 25(2):821–834.

[107] Majumder, R., Ledwich, G., Ghosh, A., Chakrabarti, S., and Zare, F. (2010c). Droop Control of Converter-Interfaced Microsources in Rural Distributed Generation. *IEEE Transactions on Power Delivery*, 25(4):2768–2778.

[108] Martinez, M. I., Tapia, G., Susperregui, A., and Camblong, H. (2012). Sliding-mode control for dfig rotor-and grid-side converters under unbalanced and harmonically distorted grid voltage. *IEEE Transactions on Energy Conversion*, 27(2):328–339.

[109] Martínez, R., Castillo, O., and Aguilar, L. T. (2009). Optimization of interval type-2 fuzzy logic controllers for a perturbed autonomous wheeled mobile robot using genetic algorithms. *Information Sciences*, 179(13):2158–2174.

[110] Mary Lourde, R. (2010). Fuzzy Logic in a Low Speed Cruise Controlled Automobile. *International Journal of Computer Science and Information Security*, 8(4):68–77.

[111] Melgarejo, M. and Pena-Reyes, C. A. (2007). Implementing interval type-2 fuzzy processors [developmental tools]. *IEEE Computational Intelligence Magazine*, 1(2):63–71.

[112] Mendel, J. (2000). Interval type-2 fuzzy logic systems: theory and design. *IEEE Transactions on Fuzzy Systems*, 8(5):535–550.

[113] Mendel, J. M. (2004). Computing derivatives in interval type-2 fuzzy logic systems. *IEEE Transactions on Fuzzy Systems*, 12(1):84–98.

[114] Mendel, J. M., Hagras, H., and John, R. I. (2006a). Standard background material about interval type-2 fuzzy logic systems that can be used by all authors.

[115] Mendel, J. M., John, R. I., and Liu, F. (2006b). Interval Type-2 Fuzzy Logic Systems Made Simple. *IEEE Transactions on Fuzzy Systems,*, 14(6):808–821.

[116] Mendel, J. M. and John, R. I. B. (2002). Type-2 fuzzy sets made simple. *IEEE Transactions on Fuzzy Systems*, 10(2):117–127.

[117] Mendel, J. M. and Wu, H. (2007). New results about the centroid of an interval type-2 fuzzy set, including the centroid of a fuzzy granule. *Information Sciences*, 177(2):360–377.

[118] Mikkili, S. and Panda, A. K. (2014). Performance analysis and real-time implementation of shunt active filter Id-Iq control strategy with type-1 and type-2 FLC triangular M.F. *International Transactions on Electrical Energy Systems*, 24(3):347–362.

[119] Mikkili, S., Panda, A. K., and Prattipati, J. (2015). Review of real-time simulator and the steps involved for implementation of a model from matlab/simulink to real-time. *Journal of The Institution of Engineers (India): Series B*, 96(2):179–196.

[120] Mishra, M. K., Joshi, A., and Ghosh, A. (2001). A new compensation algorithm for balanced and unbalanced distribution systems using generalized instantaneous reactive power theory. *Electric Power Systems Research*, 60(1):29–37.

[121] Mitra, P., Zhang, L., and Harnefors, L. (2014). Offshore Wind Integration to a Weak Grid by VSC-HVDC Links Using Power-Synchronization Control: A Case Study. *Power Delivery, IEEE Transactions on*, 29(1):453–461.

[122] Mizumoto, M. and Tanaka, K. (1976). Some properties of fuzzy sets of type 2. *Information and Control*, 31(4):312–340.

[123] Mokryani, G., Siano, P., Piccolo, A., and Chen, Z. (2013). Improving fault ride-through capability of variable speed wind turbines in distribution networks. *IEEE Systems Journal*, 7(4):713–722.

[124] Molinas, M. and Undeland, T. (2008). Low Voltage Ride Through of Wind Farms With Cage Generators: STATCOM Versus SVC. *IEEE Transactions on Power Electronics*, 23(3):1104–1117.

[125] Muyeen, S., Takahashi, R., Murata, T., Tamura, J., Ali, M., Matsumura, Y., Kuwayama, A., and Matsumoto, T. (2009). Low voltage ride through capability enhancement of wind turbine generator system during network disturbance. *IET Renewable Power Generation*, 3(1):65.

[126] Muyeen, S. M. and Al-Durra, A. (2013). Modeling and Control Strategies of Fuzzy Logic Controlled Inverter System for Grid Interconnected Variable Speed Wind Generator. *IEEE Systems Journal,*, 7(4):817–824.

[127] Nagarajan, S. T. and Kumar, N. (2015). Fuzzy logic control of SVS for damping SSR in series compensated power system. *International Transactions on Electrical Energy Systems*, 25(9):1860–1874.

[128] Nagrath, I. (2006). *Control systems engineering*. New Age International.

[129] Nie, M. and Wan Tan, W. (2008). Towards an efficient type-reduction method for interval type-2 fuzzy logic systems. In *IEEE International Conference on Fuzzy Systems, 2008. FUZZ-IEEE 2008.*, pages 1425–1432.

[130] Ning, J., Gao, W., and Ojo, J. (2008). Decoupled control of doubly fed induction generator for wind power system. In *IEEE Power Symposium, 2008. NAPS'08. 40th North American*, pages 1–6.

[131] Ogata, K. (2001). *Modern control engineering*. Prentice Hall PTR.

[132] Omar Faruque, M. D. S. (2015). Real-Time Simulation Technologies for Power Systems Design, Testing, and Analysis. *IEEE Power and Energy Technology Systems Journal*, 2(2):63–73.

[133] Ostadi, A., Yazdani, A., and Varma, R. K. (2009). Modeling and Stability Analysis of a DFIG-Based Wind-Power Generator Interfaced With a Series-Compensated Line. *IEEE Transactions on Power Delivery*, 24(3):1504–1514.

[134] Ouhrouche, M. (2009). Transient analysis of a grid connected wind driven induction generator using a real-time simulation platform. *Renewable Energy*, 34(3):801–806.

[135] Park, D.-J., Kim, Y.-J., Ali, M. H., Park, M., and Yu, I.-K. (2007). A novel real time simulation method for grid-connected wind generator system by using rtds. In *IEEE International Conference on Electrical Machines and Systems, 2007. ICEMS.*, pages 1936–1941.

[136] Pena, R., Clare, J., and Asher, G. (1996). Doubly fed induction generator using back-to-back PWM converters and its application to variable-speed wind-energy generation. *IEE Proceedings - Electric Power Applications*, 143(3):231.

[137] Pendharkar, I. and Pillai, H. (2003). On dissipative SISO systems: a behavioral approach. In *42nd IEEE International Conference on Decision and Control (IEEE Cat. No.03CH37475)*, volume 2, pages 1616–1620. IEEE.

[138] Pichan, M., Rastegar, H., and Monfared, M. (2013). Two fuzzy-based direct power control strategies for doubly-fed induction generators in wind energy conversion systems. *Energy*, 51(0):154–162.

[139] Rajpathak, B., Pillai, H. K., and Bandyopadhyay, S. (2015). Analysis of unstable periodic orbits and chaotic orbits in the one-dimensional linear piecewise-smooth discontinuous map. *Chaos (Woodbury, N.Y.)*, 25(10):103101.

[140] Rokrok, E. and Golshan, M. E. H. (2010). Adaptive voltage droop scheme for voltage source converters in an islanded multibus microgrid. *IET Generation, Transmission & Distribution,*, 4(5):562–578.

[141] Saad, N. H., Sattar, A. A., and Mansour, A. E.-A. M. (2015). Low voltage ride through of doubly-fed induction generator connected to the grid using sliding mode control strategy. *Renewable Energy*, 80(0):583–594.

[142] Saha, M., Hillstroem, B., Kasztenny, B., and Rosolowski, E. (1998). A fuzzy logic based relay for power transformer protection. *ABB REVIEW*, pages 41–48.

[143] Satpathy, P., Das, D., and Dutta Gupta, P. (2004). A fuzzy approach to handle parameter uncertainties in Hopf bifurcation analysis of electric power systems. *International Journal of Electrical Power & Energy Systems*, 26(7):527–534.

[144] Sefa, I., Altin, N., Ozdemir, S., and Kaplan, O. (2015). Fuzzy PI controlled inverter for grid interactive renewable energy systems. *IET Renewable Power Generation,*, 9(7):729–738.

[145] Shekhar Yadav and S. K. Nagar (2012). Digital control of magnetic levitation system using fuzzy logic controller. *International Journal of Computer Applications*, 41(21):1–6.

[146] Singh, B. and Singh, S. (2009). Wind Power Interconnection into the Power System: A Review of Grid Code Requirements. *The Electricity Journal*, 22(5):54–63.

[147] Singh, J. G., Tripathy, P., Singh, S. N., and Srivastava, S. C. (2009). Development of a fuzzy rule based generalized unified power flow controller. *European Transactions on Electrical Power*, 19(5):702–717.

[148] Singh, M., Khadkikar, V., Chandra, A., and Varma, R. K. (2011). Grid Interconnection of Renewable Energy Sources at the Distribution Level With Power-Quality Improvement Features. *IEEE Transactions on Power Delivery*, 26(1):307–315.

[149] Subbaraj, P. and Manickavasagam, K. (2008). Automatic generation control of multi-area power system using fuzzy logic controller. *European Transactions on Electrical Power*, 18(3):266–280.

[150] Sugeno, M. (1999). On stability of fuzzy systems expressed by fuzzy rules with singleton consequents. *IEEE Transactions on Fuzzy Systems*, 7(2):201–224.

[151] Surinkaew, T. and Ngamroo, I. (2014). Robust power oscillation damper design for dfig-based wind turbine based on specified structure mixed h2 h infinte control. *Renewable Energy*, 66:15–24.

[152] Tavakoli, A., Negnevitsky, M., Lyden, S., and Haruni, O. (2014). A decentralized control strategy for multiple distributed generation in islanded mode. In *IEEE PES General Meeting— Conference & Exposition, 2014*, pages 1–5.

[153] Teodorescu, R., Blaabjerg, F., Liserre, M., and Loh, P. C. (2006). Proportional-resonant controllers and filters for grid-connected voltage-source converters. *IEE Proceedings on Electric Power Applications,*, 153(5):750–762.

[154] Tremblay, E., Atayde, S., and Chandra, A. (2011). Comparative Study of Control Strategies for the Doubly Fed Induction Generator in Wind Energy Conversion Systems: A DSP-Based Implementation Approach. *IEEE Transactions on Sustainable Energy,*, 2(3):288–299.

[155] Vargas-Martínez, A., Minchala Avila, L. I., Zhang, Y., Garza-Castañón, L. E., and Badihi, H. (2015). Hybrid adaptive fault-tolerant control algorithms for voltage and frequency regulation of an islanded microgrid. *International Transactions on Electrical Energy Systems*, 25(5):827–844.

[156] Varma, R. K., Auddy, S., and Semsedini, Y. (2008). Mitigation of Subsynchronous Resonance in a Series-Compensated Wind Farm Using FACTS Controllers. *IEEE Transactions on Power Delivery*, 23(3):1645–1654.

[157] Verij Kazemi, M., Sadeghi Yazdankhah, A., and Madadi Kojabadi, H. (2010). Direct power control of DFIG based on discrete space vector modulation. *Renewable Energy*, 35(5):1033–1042.

[158] Vrionis, T. D., Koutiva, X. I., and Vovos, N. A. (2014). A genetic algorithm-based low voltage ride-through control strategy for grid connected doubly fed induction wind generators. *IEEE Transactions on Power Systems*, 29(3):1325–1334.

[159] Wei, W. and Mendel, J. M. (1999). A fuzzy logic method for modulation classification in nonideal environments. *IEEE Transactions on Fuzzy Systems*, 7(3):333–344.

[160] Weng, Z., Shi, L., Xu, Z., Lu, Q., Yao, L., and Ni, Y. (2015). Fuzzy power flow solution considering wind power variability and uncertainty. *International Transactions on Electrical Energy Systems*, 25(3):547–572.

[161] Wilch, M., Pappala, V. S., Singh, S. N., and Erlich, I. (2007). Reactive Power Generation by DFIG Based Wind Farms with AC Grid Connection. In *2007 IEEE Lausanne Power Tech*, pages 626–632. IEEE.

[162] Wu, B., Lang, Y., Zargari, N., and Kouro, S. (2011). *Power conversion and control of wind energy systems*. John Wiley & Sons.

[163] Wu, D. (2013). Approaches for reducing the computational cost of interval type-2 fuzzy logic systems: overview and comparisons. *IEEE Transactions on Fuzzy Systems*, 21(1):80–99.

[164] Wu, D. and Mendel, J. M. (2007). Aggregation using the linguistic weighted average and interval type-2 fuzzy sets. *IEEE Transactions on Fuzzy Systems*, 15(6):1145–1161.

[165] Wu, D. and Mendel, J. M. (2009). A comparative study of ranking methods, similarity measures and uncertainty measures for interval type-2 fuzzy sets. *Information Sciences*, 179(8):1169–1192.

[166] Wu, D. and Tan, W. W. (2006). Genetic learning and performance evaluation of interval type-2 fuzzy logic controllers. *Engineering Applications of Artificial Intelligence*, 19(8):829–841.

[167] Wu, D. and Tan, W. W. (2010). Interval type-2 fuzzy pi controllers: Why they are more robust. In *IEEE International Conference on Granular Computing (GrC), 2010*, pages 802–807.

[168] Wu, H. and Mendel, J. M. (2002). Uncertainty bounds and their use in the design of interval type-2 fuzzy logic systems. *IEEE Transactions on Fuzzy Systems*, 10(5):622–639.

[169] Xie, D., Xu, Z., Yang, L., Ostergaard, J., Xue, Y., and Wong, K. P. (2013). A Comprehensive LVRT Control Strategy for DFIG Wind Turbines With Enhanced Reactive Power Support. *IEEE Transactions on Power Systems,*, 28(3):3302–3310.

[170] Yamamoto, M. and Motoyoshi, O. (1991). Active and reactive power control for doubly-fed wound rotor induction generator. *IEEE Transactions on Power Electronics*, 6(4):624–629.

[171] Yao, J., Li, H., Chen, Z., Xia, X., Chen, X., Li, Q., and Liao, Y. (2013). Enhanced Control of a DFIG-Based Wind-Power Generation System With Series Grid-Side Converter Under Unbalanced Grid Voltage Conditions.

[172] Yazdani, A. and Iravani, R. (2010). *Voltage-sourced converters in power systems: modeling, control, and applications*. John Wiley & Sons.

[173] Yunus, A. M. S., Abu-Siada, A., and Masoum, M. A. S. (2011). Improvement of LVRT capability of variable speed wind turbine generators using SMES unit. *IEEE PES Innovative Smart Grid Technologies Asia (ISGT), 2011,*, pages 1–7.

[174] Yunus, A. M. S., Masoum, M. A. S., and Abu-Siada, A. (2012). Application of SMES to Enhance the Dynamic Performance of DFIG During Voltage Sag and Swell. *IEEE Transactions on Applied Superconductivity,*, 22(4):5702009.

[175] Zadeh, L. (1975). The concept of a linguistic variable and its application to approximate reasoningI. *Information Sciences*, 8(3):199–249.

[176] Zhang, Y., Zhu, J., Zhao, Z., Xu, W., and Dorrell, D. G. (2012). An Improved Direct Torque Control for Three-Level Inverter-Fed Induction Motor Sensorless Drive. *IEEE Transactions on Power Electronics,*, 27(3):1502–1513.

[177] Zhao, P., Yao, W., Wang, S., Wen, J., and Cheng, S. (2014). Decentralized nonlinear synergetic power system stabilizers design for power system stability enhancement. *International Transactions on Electrical Energy Systems*, 24(9):1356–1368.

[178] Zhi, D. and Xu, L. (2007). Direct Power Control of DFIG With Constant Switching Frequency and Improved Transient Performance. *IEEE Transactions on Energy Conversion*, 22(1):110–118.

[179] Zhou, T. and François, B. (2011). Energy management and power control of a hybrid active wind generator for distributed power generation and grid integration. *IEEE Transactions on Industrial Electronics*, 58(1):95–104.

Author's Research Publications

[1] S Krishnama Raju and GN Pillai, "Design and Implementation of Type-2 Fuzzy Logic Controller for DFIG based Wind Energy Systems in Distribution Networks," *IEEE Transaction on Sustainable Energy*, vol.7, no.1, pp. 345 - 353, 2016.

[2] S Krishnama Raju and GN Pillai,"Design and real-time implementation of type-2 fuzzy vector control for DFIG based wind generators", *Renewable Energy*, vol.88, pp. 40 - 50, Apr. 2016.

[3] S Krishnama Raju and GN Pillai, "Enhancing LVRT capability of DFIG based wind power plants by Interval Type-2 Fuzzy logic controller", *International Journal of Applied Engineering Research*, vol. 10, no. 44, 2015.

[4] S Krishnama Raju and GN Pillai, Type-2 Fuzzy Logic based Robust Control Strategy for Power Sharing in Microgrids with Uncertainties in Operating conditions, *International Transaction on Electrical Energy Systems.* (Under Review)

Appendix

Real time Digital Simulator

The RTDS simulator consists of custom hardware and software, specifically designed to perform real time Electro Magnetic Transient (EMT) simulations. It operates continuously in real time while providing accurate results over a frequency range from DC to 3 kHz. This range provides a greater depth of analysis on power systems than traditional stability or load flow programs which study phenomenon within a very limited frequency range.

The RTDS simulator's fully digital parallel processing hardware is capable of simulating complex networks using a typical time step of $50\mu s$. The simulator also allows for small time step subnetworks that operate with time steps in the range of 1-4 μs for simulation of fast switching power electronic devices. The hardware is bundled into modular units called racks that allow easy expansion of the simulator's computing capability as required. Using the RTDS simulator, analytical studies can be performed much faster than with offline EMT simulation programs.

The parallel processing required by the RTDS simulator is carried out by processor cards. These cards are mounted in card cages, knows as racks, which are housed in cubicles. As the simulation demands of a user increase, processor cards can be added to the racks. As the racks are filled, more cubicles can be acquired, and many different racks can be involved in a given simulation. RTDS simulator cubicles include standard DIN rails for the installation of I/O cards and other components. The I/O cards are used for closed loop testing of protective relay and control systems, power hardware in the loop studies, and much more.

RTDS Technologies proprietary software, designed specifically for interfacing to the RTDS simulator hardware, is called RSCASD. RSCAD is a user friendly interface, intended to create a working environment familiar to the power system engineer. RSCAD is an all-in-one package, containing all facilities that the user needs to prepare and run simulations, and to view and analyze results. Since the RTDS simulator operates in continuous real time, the simulated power system can be operated in a manner similar to a real power system. As simulation parameters are modified and contingencies are applied, the user can watch the power system respond in real time.

RSCAD represents a family of software tools consisting of individual modules that

Figure i: Real-time Digital Simulator with Racks

accomplish the different tasks involved in operating the simulator. Through RSCAD, the user has the ability to organize and share simulation projects and cases; assemble circuit diagrams using predefined or user-defined power and control system component models; automate or interact with simulator operation; and analyze and post-process simulation results. A brief description about various hardware modules which are included in RTDS is appended as follows.

GT Workstation Interface Card (GTWIF)

Each RTDS rack includes either a WIF card or an improved version GTWIF card. The main functions of the GTWIF are

- **Communication between the RTDS rack and the computer workstation running the RSCAD software:** Communication is over an ethernet based LAN. RSCAD/RunTime software communicates with the GTWIF cards realtime O/S to send and receive messages associated with plot updates and user initiated events (eg.

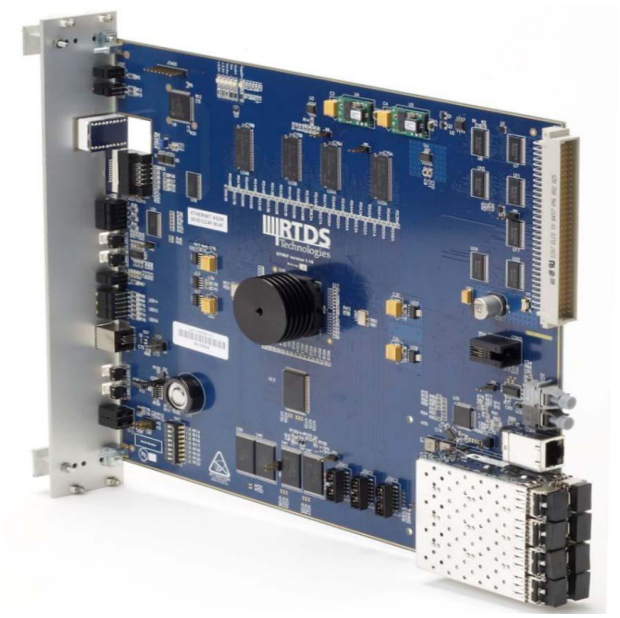

Figure ii: GTWIF Card

change of a setpoint via a Slider, Switch or other such RunTime component). The GTWIF card is also used for communication of data with the computer workstation in order to load new simulation cases, as well as, to start and stop the simulations.

- **Synchronization of racks for multirack simulation cases:** Each timestep, and the communication intervals within the timestep, are synchronized by the GTWIF installed in the first rack allocated for the simulation case. The first rack in the simulation case is designated as the master rack.

- **Communication with other racks participating in a simulation case:** Each GTWIF card uses its interrack communication channels to exchange data with up to six other racks while the simulation case is running.

- Communication of data between processors over the racks backplane is coordinated by the GTWIF.

- The GTWIF performs self tests and runs diagnostics on other cards installed in its rack. The diagnostics are automatically run at power up and may be initiated by the user. Results from the diagnostic tests are accessible from RSCAD.

The GTWIF IP address may be entered by using the SELECT and SET buttons located on the GTWIFs front panel. To set the IP address in this manner, the IP address must be entered in hexadecimal format.

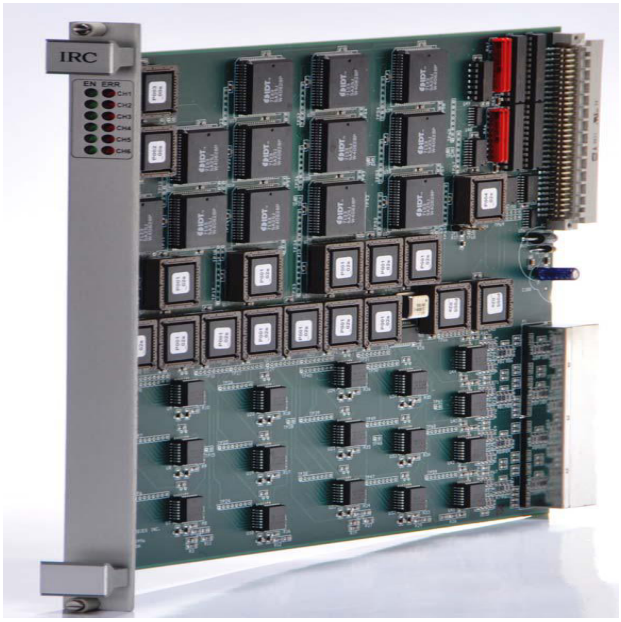

Figure iii: Inter rack communication card

Inter rack communication card (IRC)

The InterRack Communications Card (IRC) provides direct, bidirectional, data communication paths from one rack to at most six others. IRC cards are required for multirack RTDS systems which are equipped with WIF cards. RTDS systems equipped with GTWIF cards do not require IRC cards as the IRC function is included as part of the GTWIF. The six communication channels on an IRC card permit an RTDS comprised of seven racks to be fully interconnected. It is possible to include two IRC cards per rack in which case each rack is able to directly communicate with 12 others. In this case an RTDS simulator consisting of 13 racks can be fully interconnected. It should be noted that for most power system simulation cases it is not necessary to have full and complete communication between all RTDS racks. As such, RTDS simulators consisting of a large number of racks may be used to simulate power system models which include a large number of busses. Each IRC card consumes a maximum of 35 Watts.

Giga Processor card (GPC)

The GPC Card is the processor card used to solve the equations representing the power system and control system components modelled within the RTDS. An RTDS rack typically contains between 2 and 6 GPC cards. The GPC card may be installed in RTDS racks which also contains 3PC cards. Each GPC card includes two IBM Power PC 750GX processors

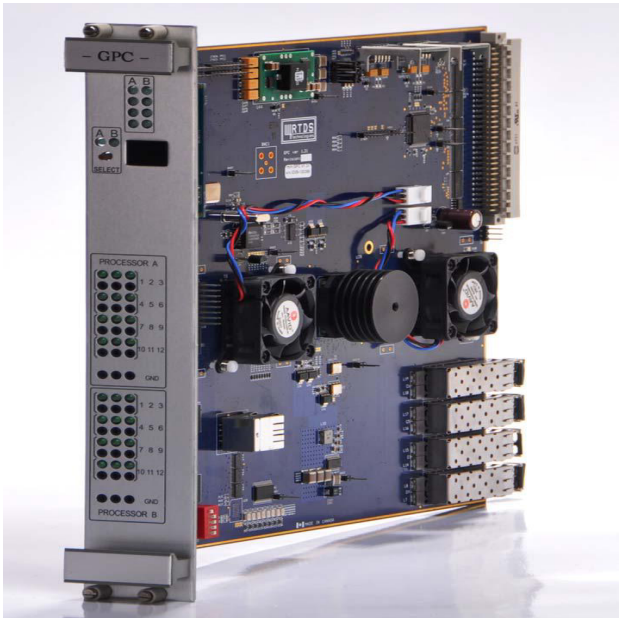

Figure iv: Giga Processor card

running at 1 GHz. The GPC Card is used for the following in the RTDS rack

- **Power system network solution:** 1 processor on a GPC card within an RTDS rack is generally assigned to the power system network (ie. computation of node voltages, passive branches etc.). For GTWIF based systems the network solution may be assigned up to 66 nodes. For WIF based systems the number of nodes is limited to 54.

- **Power System Components:** GPC processors are assigned to handle the various power system components (eg. machines, transmission lines, transformers . . .) comprising the power system model being simulated.

- **Control system components:** 1 processor on a GPC card within a rack is generally assigned to handling the control system components modelled within the RTDS. Simulation cases which have a large number of controllers modelled may allocate more than a single GPC processor may for the controls components. Control system components are also used to exchange data with GT I/O cards connected to the GPCs fiber ports.

- **Small timestep power electronic circuits:** GPC processors may be assigned to the simulation of power electronic circuits represented using small timestep (2 to 3 microsecond) components.

- **Connection to GT I/O Cards:** GPC processors include fiber ports which are

Figure v: Network Interface Card

used to connect various types of I/O cards (eg. GTAO (analogue output), GTAI (analogue input), GTDO (digital output), GTDI (digital input), GTFPI (front panel interface), GTNET (network interface card)). Each GPC card consumes a maximum of 55 Watts.

Network Interface Card (GTNETx2)

The GTNETx2 card is used to interface the RTDS to external equipment over a LANconnection using various standard network protocols. The following protocols are supported on the GTNETx2

- GSE/Goose IEC61850
- SV IEC6185092(sampled values)
- PMU IEEE C37.118
- DNP3 Distributed Network Protocol
- DNP104 IEC 608705104
- PLAYBACK playback of large data sets
- Socket TCP or UDP

Each GTNETx2 comes configured with Socket communication and one additional user selected protocol. Additional protocols may be optionally added to a GTNETx2 Card. Each GTNETx2 card is capable of running two network protocols simultaneously, one on its A processor and one on its B processor.

The GTNETx2 card can be thought of as a protocol converter accepting packets from the LAN, extracting data from the packets and sending the payload information to the processor card (PB5 orGPC) to which the GTNETx2 is connected via the GTfiber port. Data from the simulation running on the RTDS may also be sent from the processor card to the GTNETx2 where it is assembled into a packet and put out on the LAN where it will be picked up by the devices assigned to accept the data.

The GTNETx2 card resides within the standard RTDS rack and obtains its power signals from the racks backplane. Communication between a processor card and the GTNETx2 is, however, not over the backplane but rather using a GT port fiber cable connected between the GTNETx2 and processor card. Thus, a GTNETx2 card physically installed in one rack may be interconnected to processor cards installed in other racks.

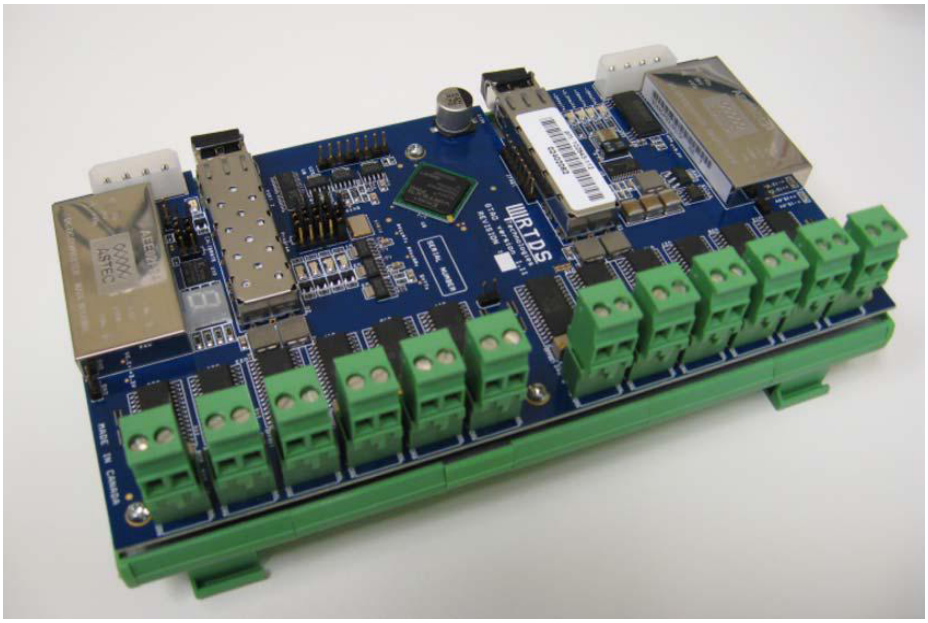

Figure vi: Analog output card (GTAO)

Analog output card (GTAO)

The Gigabit Transceiver Analogue Output Card (GTAO) is used to interface analogue signals from the RTDS to external devices. The GTAO card includes twelve, 16 bit analogue output channels with an output range of ±10 volts. The 16 bit DACs provide a wide

dynamic range. Such a wide dynamic range may be required when using the GTAO to send measured current signals to an external protection device. Under fault conditions the current may be some thirty times larger than the steadystate current. The GTAO outputs are oversampled at a rate of 1 microsecond and the cards output channels are updated synchronously. Each GTAO card is mounted on a DIN rail located in the rear of the RTDS cubicle and connects to an RTDS processor card (GPC or PB5) via a fiber cable. Power for the GTAO is provided by a DIN rail mounted power supply (+24Vdc) located in the rear of the RTDS cubicle. Analogue output signals connect to terminal blocks available on the GTAO card.

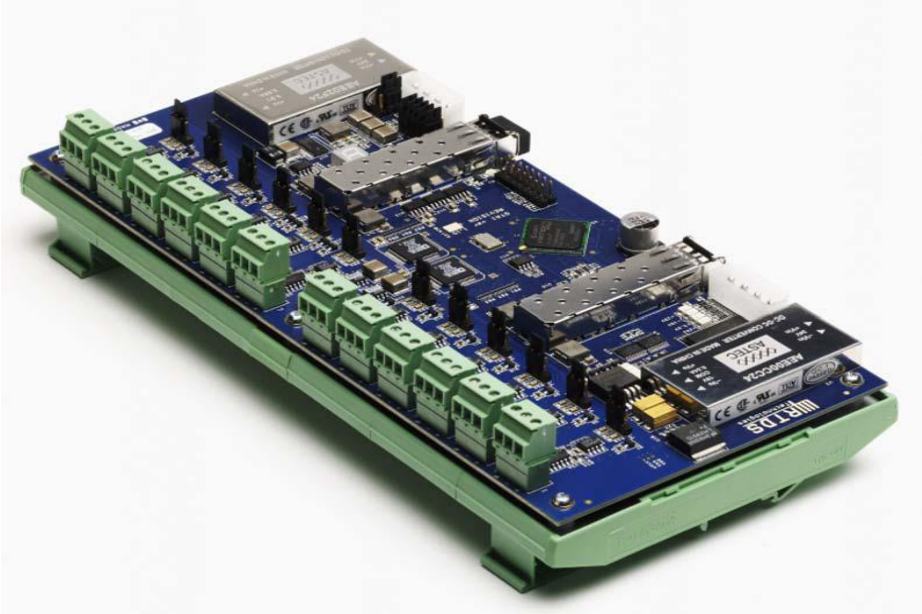

Figure vii: Analog input card (GTAI)

Analog input card (GTAI)

The Gigabit Transceiver Analogue Input Card (GTAI) is used to interface analogue signals from an external device to the RTDS. The GTAI card includes 12 analogue input channels with each channel configured as a differential input with an input range of ±10 volts. Sixteen bit A/D converters are used on the GTAI card. All 12 analogue channels are sampled synchronously with new samples sent to the GPC card every 6.0 microseconds. Each GTAI card is mounted on a DIN rail located in the rear of the RTDS cubicle and connects to a GPC processor card via an optical cable. A single +24 volt power supply signal is required to power the card. Analogue input signals connect to terminal blocks available on the GTAI card. GTAI cards can be daisy chained with other GTAI, GTDO(digital output),

GTDI (digital input), GTAO (analogue output) or GTFPI cards.

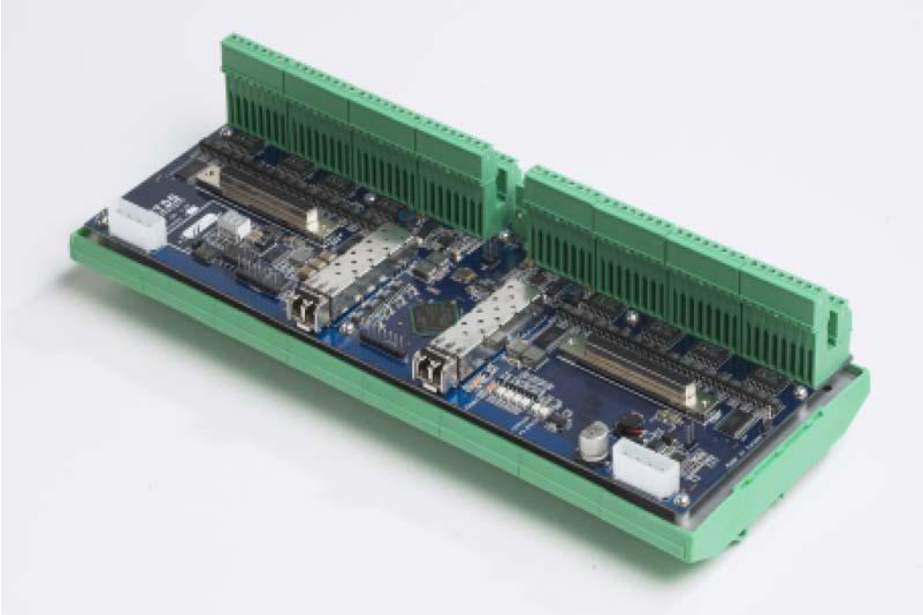

Figure viii: Digital Output card (GTDO)

Digital Output card (GTDO)

The Gigabit Transceiver Digital Output Card (GTDO) is used to interface digital signals from the RTDS to external equipment. The GTDO card includes 64 optically isolated digital output channels which are arranged into two banks of 32 channels each. Each bank of 32 channels may be operated at a different voltage level in the range of +5V to +24Vdc. External power supplies are required to provide the output voltage source. Each GTDO card is mounted on a DIN rail located in the rear of the RTDS cubicle and connects to a GPC card via an optical cable. A single +24 volt power supply signal is required to power the card. Output signals are open emitter type and as such an external power supply is required to drive the output signals. Digital output signals connect to terminal blocks available on the GTDO card. The GTDO card includes a digital output timestamp (DOTS) function which allows digital output signals to change at a given instant within a simulation timestep. The DOTS function can be used, for example, to accurately provide current zero pulses to an external HVDC controller. GTDO cards can only be used with GPC cards. GTDO cards can be daisy chained with other GTDO, GTDI (digital input), GTAI (analogue input), GTAO(analogue output) or GTFPI (Front Panel Interface) cards if required. Two optical connectors are available on the GTDO card. The first connector (port1) is used for connection to the GPCcard or a prior GTI/O card in the chain. The

second connector (port2) can be used for connection to a subsequent GT I/O card in the chain.

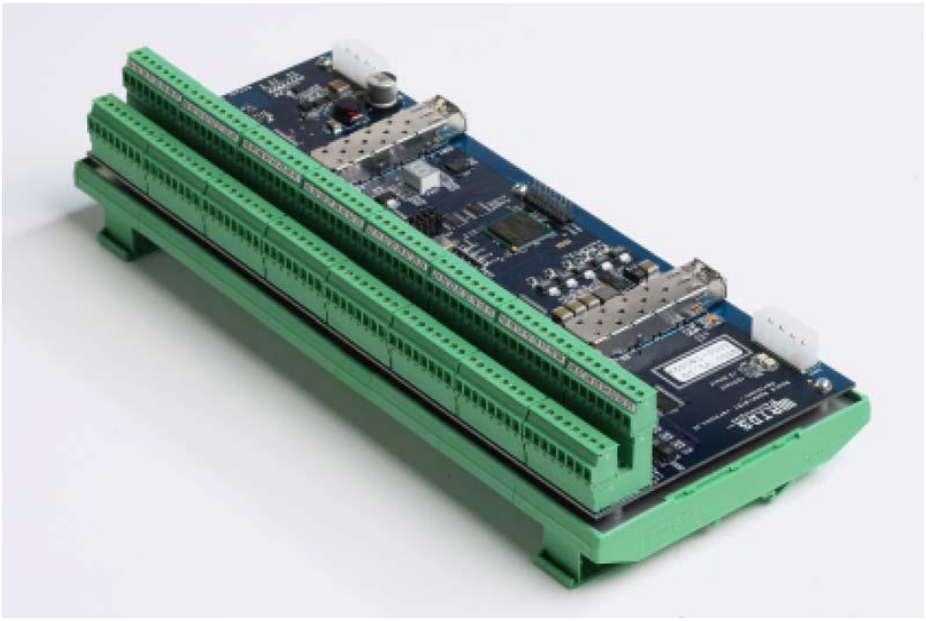

Figure ix: Digital Input card (GTDI)

Digital Input card (GTDI)

The Gigabit Transceiver Digital Input Card (GTDI) is used to interface digital signals from an external device to the RTDS. The GTDI card includes 64 optically isolated digital input channels. Each GTDI card is mounted on a DIN rail located in the rear of the RTDS cubicle and connects to a GPC card via an optical cable. A single +24 volt power supply signal is required to power the card. Digital input signals connect to terminal blocks available on the GTDI card. The GTDI card has also been designed to include all the functionality of a DITS card. Therefore the GTDI can be used to read time critical firing pulses from an external controller. The GTDI card will send the required timing information to the RTDS software. The first sixty channels of the GTDI card can be used in this manner, 10 groups of 6 channels. GTDI cards can only be used with GPC cards. GTDI cards can be daisy chained with other GTDI, GTDO (digital output), GTAI (analogue input), GTAO (analogue output) or GTFPI cards if required. Two optical connectors are available on the GTDI card. The first connector (port1) is used for connection to the GPC card or a prior GT I/O card in the chain. The second connector (port2) can be used for connection to a subsequent GT I/O card in the chain.

Figure x: Front panel interface card

Front panel interface card (GTFPI)

The GTFPI card forms the interface between the digital I/O panel and the GT port on the GPC card. The GTFPI also acts as the interface to the GPC card for systems which include an optional High Voltage interface panel. Connections between the GTFPI card and the I/O and HV panels are via ribbon cables as shown in Figure 6.10. These ribbon cables are preinstalled for RTDS units that are shipped with a GTFPI card. A GT fiber cable is used as the connection between the GTFPI card and the GPC card. One GTFPI card is able to interface to only one I/O panel and one HV Panel. For systems which include two I/O or HV panels mounted in a single cubicle, a second GTFPI card is required. The GTFPI card is mounted on the DINrail in the rear of the RTDS cubicle and is powered from a +5 volt power supply. A+5V power connector for the GTFPI is available near the top left side of the RTDS cubicle. For units with more than one GTFPI card in the cubicle a power supply jumper connector is provided.

Synchronization card (GTSYNC)

The clock used to generate the RTDS simulation timestep has an accuracy of ±100 ppm. As such, the phase of signals computed within the RTDS will drift relative to the phase of signals on external equipment that is synchronized to a high precision timereference. For applications such as phase measurement unit (PMU) testing it is important that signals

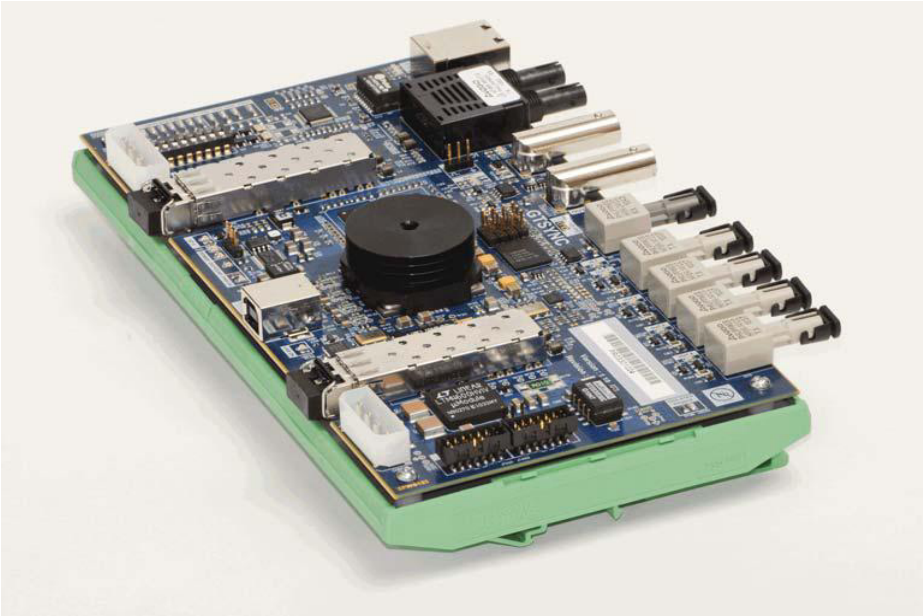

Figure xi: Synchronization card (GTSYNC)

computed on the RTDS do not drift relative to a high precision time reference. Similarly, when the RTDS is required to provide time stamped sampled signals when testing IEC6185092 enabled devices for example, the timestamp must be relative to a high precision reference. The GTSYNC card is used to ensure that the RTDS timestep clock remains locked to the timereference signal provided as input to the GTSYNC.

The GTSYNC uses either IEEE 1588 PTP, 1 PPS, or IRIGB unmodulated signals as the synchronization source. Figure 6.11 shows the connections required for testing an IEC6185092SV enabled protective relay using an RTDS with a GTSYNC card. In the example, the GTSYNC is used to synchronize the RTDS Sampled Values output from the GTNET with a GPS clock via a 1 PPS signal. The external device also uses 1 PPS to synchronize to the GPS clock.

Inter rack communication switch (IRC switch)

The IRC Switch is a high speed communications switch used to replace GTWIF to GTWIF IRC connections for inter rack communication. RTDS Simulators consisting of seven or fewer racks can be fully interconnected using direct connection of IRC channels between GTWIF Cards and as such an IRC Switch is usually not included in RTDS simulators consisting of fewer than 8 racks. RTDS simulators consisting of eight or more racks require an IRC Switch if full IRC interconnection of all racks is required.

If an IRC Switch is present, each RTDS racks GTWIF is connected to a port on the

Figure xii: Inter rack communication switch

IRC Switch via a fiber optic cable. The IRC Switch routes data from each rack to all racks requiring the particular data. Full connectivity between all racks in a system of up to 60 racks is possible. The IRC Switch has a scalable architecture with up to 5 IRC Switch cards installed in a single chassis. Each IRC Switch card has 12 ports so that with 5 cards installed in the chassis a maximum of 60 RTDS racks may be fully interconnected. The IRC Switch chassis is usually installed in its own midsize cubicle along with the Global Bus Hub (GBH) and ethernet LAN switch.

Dspace

Dspace offers a complete and integrated development environment for embedded control software. Dspace prototyping systems are flexible development platforms that let us develope and optimize the control designs without manual programming. With comprehensive and reliable software support, including first-rate MATLAB/Simulink integration, it is ready-to-use and easy-to-run. Design faults are found immediately and corrections can be carried out on the spot. It is completed by a full range of signal conditioning and power stage modules to connect the prototyping system to sensors and actuators. The production code TargetLink generates highly efficient C code straight from MATLAB/Simulink Stateflow and allows early verification through built-in simulation and testing. This drastically reduces the time need for implementation, and results in systematic consistency between the specification and the production code. Changes on the model level are quickly

Figure xiii: Dspace module

transferred to code.

HIL Testing

When the model is programmed in a Electronic control unit (ECU), its functions can be tested quickly and automatically by using DSPACE simulator hardware. It replaces the real environment, and one can execute the tests in any conceivable test scenario. The comprehensive software support includes proven-in-practice " Automatic Simulation models"(ASM) and convenient test automation support to increase the productivity in test development and test execution. The data management software SYNECT with its test management module is ideal for managing test data and monitoring, analyzing and visulizing test results.